

Real-Time Optimal Controls for Active Distribution Networks: From Concepts to Applications

THÈSE N° 6795 (2015)

PRÉSENTÉE LE 11 DÉCEMBRE 2015

À LA FACULTÉ INFORMATIQUE ET COMMUNICATIONS

LABORATOIRE POUR LES COMMUNICATIONS INFORMATIQUES ET LEURS APPLICATIONS 2

PROGRAMME DOCTORAL EN INFORMATIQUE ET COMMUNICATIONS

ÉCOLE POLYTECHNIQUE FÉDÉRALE DE LAUSANNE

POUR L'OBTENTION DU GRADE DE DOCTEUR ÈS SCIENCES

PAR

Konstantina CHRISTAKOU

acceptée sur proposition du jury:

Prof. P. Thiran, président du jury
Prof. J.-Y. Le Boudec, Prof. M. Paolone, directeurs de thèse
Prof. M. Shahidehpour, rapporteur
Prof. A. Abur, rapporteur
Dr R. Cherkaoui, rapporteur



ÉCOLE POLYTECHNIQUE
FÉDÉRALE DE LAUSANNE

Suisse
2015

On the mountains of truth you can never climb in vain:
either you will reach a point higher up today, or
you will be training your powers so that you
will be able to climb higher tomorrow.
— Friedrich Nietzsche

To my mother...

Acknowledgements

First and foremost, I would like to thank my thesis directors, Professors Jean-Yves Le Boudec and Mario Paolone for giving me the opportunity to do my PhD thesis under their supervision. Their excellent guidance and constant support, both on a scientific and a personal level, made the PhD a wonderful experience. It was truly an honor to work with them during the past few years.

My sincere gratitude goes to Professors Patrick Thiran, Mohammad Shahidehpour, Ali Abur and to Dr. Rachid Cherkaoui for accepting to serve in my PhD exam committee and for their feedback and interesting discussions. Special thanks go to Professor Ali Abur for the opportunity to do an internship in his lab at Northeastern University, in Boston.

During my PhD at EPFL, I was very fortunate to collaborate with many brilliant colleagues in joint research papers, teaching or supervision of students. I am particularly grateful to Dan for contributing to this thesis and for his endless patience and constant motivation. Working with him was a truly enriching experience. Furthermore, I would like to thank Tech for the numerous hours we spent together studying Performance Evaluation and exploring BGP during TCP/IP. I would also like to thank Mostafa and Marco for the wonderful collaboration and for their always optimistic approach to research.

During the last 4 years, I was very lucky to be a member of both the LCA2 and the DESL lab. I would like to express my gratitude to all my colleagues in both labs for the warm atmosphere inside and outside the lab and for making me feel at home all these years. Special thanks go to Miroslav, Tech and Maaz for all the fun times, the outings and the support. They have been like a second family to me during the course of the PhD. I would also like to thank Paolo, Stela, Lorenzo and Marco for all the dinners, the aperos, the drinks and the great times we had together.

I also owe thanks to our secretaries, Patricia, Holly, Sophie and Andrée, as well as to our system administrators, Marc-André, Yves and Jean-Michel for their constant availability and support.

In addition to my colleagues, I am particularly grateful to a number of people who were always around both at the good and the bad moments. In particular, I would like to thank Javier and Iraklis, who helped me survive through the very first years of the PhD. Special thanks go to Vasilis, for all the patience, and the support, both personally and academically. Many thanks go to my Greek friends Afroditi, Tolis, Giannis and Sila,

Acknowledgements

as well as my cousins Efi and Kostas, for being by my side throughout the course of my PhD and for the nice and refreshing times we spent together whenever I visited Greece.

I would also like to thank Michele for making the last year of my PhD life special.

Finally, I am enormously grateful to my mother who, even though not familiar with all the bells and whistles of the PhD life, was there to support me through every deadline and every joy or sorrow related to my life as a doctoral student.

Abstract

In the last few years, the entire power industry is undergoing profound changes towards a smarter electrical grid. Decentralized generation, distributed energy storage systems and active participation of end-users in the lower level of the electrical infrastructure, intelligently managed to provide support to the grid, define the notion of Active Distribution Networks (ADNs). The increased connection of distributed generation in ADNs, essentially composed of renewable energy resources, incurs severe impacts on planning and operational procedures of both transmission and distribution systems and calls for application of intelligent control techniques in order to achieve specific operation objectives. In this respect, this thesis focuses on the compelling problem of optimal operation and control of ADNs, with particular reference to the design of real-time control algorithms for voltage regulation and lines congestion management.

In the first part of this thesis, we adopt a centralized control architecture for voltage regulation and lines congestion management in ADNs. The goal of the proposed controller is to schedule both the active and reactive power injections of a set of controllable resources, in coordination with other traditional resources, in order to achieve an optimal grid operation. The proposed online controller is based on a linearized approach that links control variables (e.g., power injections, transformers tap positions) and controlled quantities (e.g., voltages, current flows) by means of sensitivity coefficients. We first provide a straightforward analytical derivation of node-voltages and line-currents sensitivity coefficients as a function of the power injections and transformers' tap-changers positions that allows us to significantly reduce the computational time compared to traditional approaches. The proposed centralized scheme is suitable for the real-time control of a limited number of distributed energy resources, (e.g., medium-sized dispersed generation units) as it relies on a point-to-point communication from the distribution network operator (DNO) to each controllable resource. Once the proposed control algorithm is validated, as a further step, we relax the assumption that the DNO has an accurate knowledge of the system model, i.e., a correct network admittance matrix $[Y]$ and we adapt the proposed centralized control architecture to such a scenario. To this end, we formulate the optimal control problem of interest as an uncertain mixed integer linear programming (MILP) one and we use a robust optimization framework to immunize the solution against the uncertainty in the system model. Additionally, we propose a methodology for the computation of voltage sensitivity coefficients for a multi-phase unbalanced grid without relying on

Acknowledgements

the knowledge of the system model and its state. We validate the proposed methods and assess their performances by making reference to typical IEEE 13- and 34-nodes balanced and unbalanced distribution test feeders and using load profiles inferred from real measurements coming from two Italian low voltage (LV) networks.

In cases where the available controllable resources are heterogeneous and large in number, control mechanisms that rely on two-way communication between the controllable entity and the DNO can quickly result in algorithms that cannot scale in the number of network buses and controllable resources. Additionally, the adoption of completely different architectures for the control of different energy resources, renders the problem difficult when heterogeneous energy resources need to be coordinated to achieve a common goal. The distributed and heterogeneous nature of the available controllable resources, as well as their large number and small individual impact motivates the need for unified scalable control mechanisms. In this direction, in the second part of this thesis, we propose as a possible solution, to keep the system tractable, the use of broadcast-based control schemes that rely on state estimation for the feedback channel. In particular, we propose a low-overhead broadcast-based control mechanism, called Grid Explicit Congestion Notification (GECN), intended for deployment by DNOs to provide grid ancillary services by a seamless control of large populations of distributed, heterogeneous energy resources. GECN is a decentralized control scheme, conceived to provide primary voltage control in a scalable way by broadcasting low bit-rate control signals to large populations of distributed energy resources (DERs) in order to manage the variations of the nodal power injections in the network. Two very promising candidates in terms of controllable resources, expected to be deployed for grid ancillary services, are energy storage systems (ESSs) and elastic loads. Therefore, we choose to apply and validate GECN in the case of large aggregations of thermostatically controlled loads, as well as of distributed electrochemical-based storage systems. Similar to the aforementioned centralized control scheme, the GECN mechanism relies on an approximation/linearization of the power flow equations by means of sensitivity coefficients. In order to estimate the benefits and assess the performances of the GECN mechanism, the evaluation of the algorithm is carried out by using typical IEEE 13- and 34-nodes test feeders equipped with loads and generation units. Real measurements are used both for the active and reactive load profiles and for the non-dispatchable generation of photovoltaic units coming from low voltage and medium voltage (MV) distribution feeders in Italy and Switzerland.

In the last part of the thesis, we go one step further and we formulate the voltage control and lines congestion management problem as a non-approximated AC optimal power flow problem (OPF). Whilst the category of OPF problems represents the main set of problems for the optimal operation of power systems, the AC-OPF problem is known to be non-convex, thus difficult to solve efficiently. A recent approach that focuses on the branch-flow convexification of the OPF problem is claimed to be exact for the case of radial distribution systems under specific assumptions, despite the absence of apparent approximations. We show that this claim, in fact, does not hold,

as it leads to an incorrect system model and therefore, there is a need to develop algorithms for the solution of the non-approximated OPF problem that remains inherently non-convex. To overcome the aforementioned limitations we propose an algorithm for the solution of the non-approximated, non-convex AC OPF problem in radial networks. Our proposed solution uses an augmented Lagrangian approach, relies on the method of multipliers and does not require that the problem be convex. In particular, we first design a centralized OPF algorithm that is proven to converge to a local minimum of the original non-approximated OPF problem. With respect to the case of controlling multiple dispersed energy resources, it is of interest to also define a distributed solution method that is formally equivalent to the centralized formulation. We investigate the application of the alternating direction method of multipliers (ADMM) for the distributed solution of the original non-approximated OPF problem and we show, through practical examples, cases for which the ADMM-based decomposition of the non-relaxed OPF problem fails to converge. As a solution we present a distributed version of the proposed OPF algorithm that, unlike ADMM, is based on a primal decomposition and does not require that the problem be convex. We evaluate the performance of the proposed algorithms using both small-scale electrical networks, where typical values of medium-voltage underground cables are considered for the resistance, reactance and shunt capacitances of the lines, taken from manufacturers' data, as well as a modified balanced IEEE 13-nodes test feeder.

Key words: Active distribution network, alternating direction method of multipliers, ancillary services, asynchronous algorithms, broadcast signals, convex relaxation, decomposition methods, demand response, distributed algorithms, distributed generation, elastic demand, electrical distribution networks, energy storage systems, congestion management, method of multipliers, optimal control, optimal power flow, power systems, real-time, robust optimization, smart grids, unbalanced distribution networks, primary voltage control, voltage/current sensitivity coefficients.

Résumé

Au cours des dernières années, l'industrie de l'énergie a connu de profonds changements, évoluant vers des réseaux électriques intelligents. La production décentralisée de l'énergie, les systèmes de stockage d'énergie distribués et la participation active des utilisateurs dans les réseaux électriques moyenne et basse tension, gérés de façon intelligente afin de fournir des services auxiliaires au réseau, définissent la notion de "réseaux actifs de distribution". La connexion croissante de la production distribuée de l'énergie dans les réseaux de distribution, composée essentiellement de ressources énergétiques renouvelables, entraîne de graves conséquences sur la planification et l'opération des systèmes de transmission et de distribution et exige des techniques intelligentes de contrôle afin d'atteindre des objectifs opérationnels spécifiques. À cet égard, dans cette thèse, nous nous concentrons sur le problème d'opération optimale et de contrôle en temps-réel des réseaux actifs de distribution. En particulier, nous concevons des algorithmes pour le contrôle de la tension et la gestion de la congestion des lignes.

Dans la première partie de cette thèse, nous adoptons une architecture de contrôle centralisée pour la régulation de la tension et la gestion de la congestion des lignes dans les réseaux actifs de distribution. Le but du contrôleur proposé est le calcul des injections de puissance active et réactive de ressources contrôlables qui permettront, en coordination avec des ressources traditionnelles, une opération optimale du réseau. Le contrôleur proposé est basé sur une approche linéarisée qui relie les variables de contrôle (par exemple, les injections de puissance, les changeurs de prises) et les quantités contrôlées (par exemple, la tension, les flux de puissance) en utilisant des coefficients de sensibilité. Nous proposons d'abord une dérivation analytique de coefficients de sensibilité de la tension et des courants de ligne en fonction des injections de puissance et des changeurs de prises des transformateurs. Cette méthode nous permet de réduire considérablement le temps de calcul des coefficients de sensibilité par rapport aux méthodes traditionnelles. Le contrôleur proposé est adapté au contrôle, en temps réel, d'un nombre limité de ressources énergétiques distribuées (par exemple, des unités de production dispersées de capacité moyenne), car il est basé sur une communication point-à-point entre l'opérateur de réseau de distribution et chaque ressource contrôlable. Une fois que l'algorithme de contrôle proposé est validé, nous détendons l'hypothèse que l'opérateur de réseau a une connaissance exacte du modèle du système, i.e., une matrice d'admittance correcte, et nous adaptons l'architecture

Acknowledgements

de contrôle centralisé à un tel scénario. À cette fin, nous formulons le problème de contrôle optimal comme un programme linéaire incertain et nous utilisons un cadre d'optimisation robuste pour immuniser la solution contre l'incertitude dans le modèle du système. En plus, nous proposons une méthode pour le calcul des coefficients de sensibilité de tension pour un réseau polyphasé et asymétrique quand le modèle du système et l'état du réseau ne sont pas connus. Nous validons les méthodes proposées et nous évaluons leur performance en faisant référence aux réseaux de distribution IEEE, symétriques et asymétriques, composés de 13 et 34 nœuds. Les profils de charge utilisés sont déduits des mesures réelles provenant de deux réseaux basse tension italiens.

Dans les cas où les ressources contrôlables sont hétérogènes et nombreuses, les mécanismes de contrôle qui utilisent une communication bidirectionnelle entre l'entité contrôlable et l'opérateur de réseau ne sont pas capables de traiter un très grand nombre de nœuds de réseau et de ressources contrôlables. En plus, l'adoption d'architectures complètement différentes pour le contrôle des ressources énergétiques rend le problème difficile lorsque des ressources hétérogènes doivent être coordonnées pour atteindre un objectif commun. La nature distribuée et hétérogène des ressources contrôlables disponibles dans les réseaux actifs de distribution, ainsi que leur grand nombre et leur impact individuel négligeable motive le développement de mécanismes de contrôle unifiés. Pour cette raison, dans la deuxième partie de cette thèse, nous proposons comme solution possible l'utilisation des stratégies de contrôle basées sur la diffusion de signaux de contrôle qui utilisent l'estimation d'état pour le retour d'information. En particulier, nous proposons un mécanisme de contrôle basé sur la diffusion de signaux, appelé Grid Explicit Congestion notification (GECN), conçu pour fournir des services auxiliaires au réseau par un contrôle transparent de grandes populations de ressources énergétiques distribuées et hétérogènes. GECN est un système de contrôle décentralisé, conçu pour fournir un contrôle primaire de la tension en diffusant des signaux de commande de faible débit binaire à de grandes populations de ressources énergétiques distribuées afin de gérer les variations des injections de puissance dans les nœuds du réseau. Deux candidats très prometteurs, en termes de ressources contrôlables, qui vont être déployés pour des services auxiliaires, sont les systèmes de stockage d'énergie et les charges élastiques. Pour cette raison, nous appliquons et validons GECN dans le cas de larges groupes de charges thermostatiques contrôlables, ainsi que de systèmes de stockage distribués, à base électrochimique. GECN, comme le système de contrôle centralisé susmentionné, est basé sur une approximation / linéarisation des équations de flux de puissance en utilisant des coefficients de sensibilité. Afin d'estimer les avantages et d'évaluer la performance de GECN, la validation de l'algorithme est réalisée en utilisant des réseaux typiques IEEE, composés de 13 et de 34 nœuds, équipés avec des charges et des unités de production. Des mesures réelles sont utilisées pour les profils de charge active et réactive ainsi que pour la génération non contrôlable d'unités photovoltaïques, provenant de réseaux de distribution basse et moyenne tension en Italie et en Suisse.

Dans la dernière partie de la thèse, nous formulons le problème du contrôle de la tension et de la congestion des lignes comme un problème non approximé de flux de puissance optimal en régime alternatif (AC-OPF). Alors que la catégorie des problèmes OPF est très importante pour l'opération optimale des systèmes de puissance, le problème AC-OPF est connu pour être non-convexe, donc difficile à résoudre de manière efficace. Une méthode récente, basée sur la convexification du problème OPF en utilisant le modèle de flux de branche (BFM), est présentée comme exacte pour le cas des réseaux de distribution radiaux sous des hypothèses spécifiques, malgré l'absence d'approximations apparentes. Nous montrons que cette allégation, en fait, ne tient pas, car cette méthode repose sur un système erroné. Il est donc, il est nécessaire de développer des algorithmes pour la solution du problème OPF non approximé, qui reste intrinsèquement non-convexe. Pour adresser les limitations susmentionnées, nous proposons un algorithme pour la solution du problème AC OPF non approximé et non-convexe dans les réseaux électriques radiaux. Notre solution proposée utilise une méthode de Lagrangien augmenté. Elle est basée sur la méthode des multiplicateurs et ne nécessite pas que le problème soit convexe. En particulier, nous concevons d'abord un algorithme OPF centralisé, dont nous prouvons la convergence vers un minimum local du problème OPF original. En ce qui concerne le cas de contrôle de plusieurs ressources énergétiques dispersées, il est intéressant de définir également un algorithme distribué qui est équivalent à la formulation centralisée. Nous étudions l'application de la méthode des directions alternées (ADMM) pour la solution distribuée du problème OPF original non-approximé et nous montrons, à travers des exemples concrets, des cas pour lesquels la décomposition du problème OPF basé sur ADMM n'arrive pas à converger. Comme solution, nous présentons une version distribuée de l'algorithme OPF proposé. Cette version, contrairement à l'ADMM, est basée sur une décomposition primale et ne nécessite pas que le problème soit convexe. Nous évaluons la performance des algorithmes OPF proposés en utilisant des modèles des réseaux électriques à petite échelle, où des valeurs typiques des câbles souterrains moyenne tension sont considérés pour la résistance, la réactance et les capacités des lignes, provenant des données des fabricants, ainsi qu'un réseau IEEE composé de 13 nœuds.

Mots clefs : Réseau de distribution actif, méthode des directions alternées, services auxiliaires, algorithmes asynchrones, signaux de diffusion, relaxation convexe, méthodes de décomposition, gestion de charge, algorithmes distribués, production distribuée, charge élastique, réseaux électriques de distribution, systèmes de stockage d'énergie, gestion de la congestion, méthode des multiplicateurs, contrôle optimal, flux de puissance optimal, systèmes de puissance, temps réel, optimisation robuste, réseaux intelligents, réseaux de distribution asymétriques, contrôle primaire de la tension, coefficients de sensibilité de tension/courant.

List of Abbreviations

ADMM	Alternating Direction Method of Multipliers
ADN	Active Distribution Network
BFM	Branch Flow Model
CHP	Combined Heat and Power
DER	Distributed Energy Resource
DG	Distributed Generation
DMS	Distribution Management System
DNO	Distribution Network Operator
DR	Demand Response
ENTSO-E	European Network of Transmission System Operators for Electricity
ESS	Energy Storage System
FACTS	Flexible AC Transmission Systems
GECON	Grid Explicit Congestion Notification
HV	High Voltage
ICT	Information and Communication Technologies
LV	Low Voltage
MILP	Mixed-Integer Linear Programming
MV	Medium Voltage
OLTC	On-Load Tap Changer
OPF	Optimal Power Flow
PMU	Phasor Measurement Unit
PV	Photovoltaic
PVC	Primary Voltage Control
RER	Renewable Energy Resource
RO	Robust Optimization
RT	Real-Time
SC	Supercapacitor
SCUC	Security Constraint Unit Commitment
SDP	Semi-Definite Programming
SE	State Estimation
SoC	State of Charge
SOCP	Second Order Cone Programming
SVC	Secondary Voltage Control
TCL	Thermostatically Controlled Load
TVC	Tertiary Voltage Control
TSO	Transmission System Operator

Contents

Acknowledgements	i
Abstract (English, French)	iii
List of Abbreviations	xii
1 Introduction	1
1.1 Motivation	1
1.2 Dissertation Outline	5
1.3 Contributions	6
2 Active Distribution Networks: Control Needs and Current Practices	9
2.1 Operational Limits of ADNs with Respect to Maximum DG Penetration and Impact on the Quality of Service	9
2.2 Current Practices and Future Opportunities for DNOs	13
2.3 Perspective Control Functionalities and Corresponding Time Frames	14
3 Centralized and Linearized Control Strategies in ADNs	17
3.1 Introduction	17
3.2 Related work	19
3.3 Centralized Online Controller for Voltage Control and Lines Congestion Management in ADNs	22
3.3.1 Control Architecture	22
3.3.2 Controller's Actions	23
3.4 Efficient Computation of Sensitivity Coefficients of Node Voltages and Line Currents in Unbalanced Radial Electrical Distribution Networks	25
3.4.1 Classic Computation of Sensitivity Coefficients in Power Networks	25
3.4.2 Analytical Derivation of Sensitivity Coefficients with respect to Nodal Power Injections	26
3.4.3 Sensitivity Coefficients with respect to Transformers OLTC	31
3.4.4 Computational Cost Analysis	32
3.4.5 Numerical Validation	33
3.5 Application Examples	36

Contents

3.6	A Robust Optimization Approach to ADNs Control with Uncertain Feeder Parameters	48
3.6.1	The Nominal Control Problem and the Sources of Data Uncertainty	48
3.6.2	Robust Formulation of Uncertain Linear Programming Problems	50
3.6.3	Robust Counterpart of the Optimal Control Problem	51
3.6.4	Evaluation	52
3.7	Measurement-based Computation of Voltage Sensitivities in Unbalanced Electrical Distribution Networks	60
3.7.1	Problem Statement	61
3.7.2	Numerical Validation	63
3.8	Conclusions	66
4	A Unified Broadcast-based Control Strategy for ADNs	69
4.1	Introduction	69
4.2	Related Work	71
4.3	The Grid Explicit Congestion Notification Mechanism: Hypotheses and Architecture	73
4.4	GECN Central Network Controller	75
4.5	GECN Local Resources Controllers	78
4.5.1	The Case of Thermostatically Controlled Loads	78
4.5.2	The Case of Distributed Energy Storage Systems	81
4.6	GECN Performance Evaluation and Application Examples: Primary Voltage Control via Demand Response and Distributed Storage Management	86
4.6.1	Primary Voltage Control via Real-time Demand Response	87
4.6.2	Primary Voltage Control via Distributed ESSs Management	98
4.6.3	Coordination of Heterogeneous Populations for Primary Voltage Control	102
4.6.4	On the Adequacy of volt/var Control in ADNs	105
4.6.5	Application of GECN to Compensate Fast Voltage Variations: The Case of Load Inrush	107
4.6.6	Computational Performances of the GECN Network Controller	109
4.7	Hardware-in-the-Loop Validation of the GECN Mechanism	109
4.7.1	HIL Setup and Experiment Design	110
4.7.2	Regression Testing	111
4.7.3	Demonstration Example and Performance Assessment	115
4.8	Discussion on the Applicability of GECN in a Real ADN Context and its Comparison with respect to Traditional Control Means	119
4.9	Conclusions	123
5	Centralized and Distributed AC OPF Algorithms	125
5.1	Introduction	125
5.2	Related Work	127
5.3	Generic OPF Formulation	129

5.4	On the Limits of the Farivar-Low Approach for the Solution of the OPF Problem	130
5.4.1	The Farivar-Low Formulation of the OPF Problem	130
5.4.2	Misinterpretation of the Physical Network Model in the Farivar-Low OPF Formulation	132
5.4.3	On the Assumptions Required for the Exactness of the Farivar-Low Relaxation	135
5.4.4	On the Extension of the SOCP Relaxation to Networks with Lines Modeled as π -equivalents	137
5.5	On the Application of ADMM for the Solution of the OPF Problem . . .	139
5.5.1	ADMM-based Solution of the OPF Problem	139
5.5.2	Investigation of the Convergence of the ADMM-based Solution of the OPF Problem	141
5.6	AC OPF in Radial Distribution Systems	144
5.6.1	The Proposed Centralized OPF Algorithm	144
5.6.2	Distributed Solution of the OPF Problem	148
5.7	Performance Evaluation of the Centralized OPF Algorithm	151
5.7.1	Effect of the Line Length, Network Rated Value and Network State on the Convergence of the Centralized OPF Algorithm	152
5.7.2	Performance Evaluation of the Proposed Algorithm in the Presence of Shunt Capacitors in the Network	153
5.7.3	Performance Evaluation of the Proposed Algorithm under Different Initial Conditions of the Network State	156
5.8	Performance Evaluation of the Proposed Distributed Asynchronous OPF Algorithm	157
5.9	Comparison of the OPF Algorithms and the Linearized Control Algorithms	160
5.10	Conclusions	162
6	Conclusions	167
	Bibliography	187
	Curriculum Vitae	189

1 Introduction

1.1 Motivation

Increased connection of decentralized generation, distributed energy storage systems and active participation of end-users in the lower levels of the electrical infrastructure, intelligently managed to provide support to the grid, define the notion of active distribution networks (ADNs) [1].

Within the context of ADNs, the structure and operation of conventional electrical networks will undergo important changes. The integration of embedded generation into the lower voltage levels, essentially composed of renewable energy resources (RERs), as a first consequence, will result in bidirectional power flows between the transmission and distribution levels. These bidirectional power flows require the definition of appropriate dispatching strategies of ADNs with respect to transmission networks. Specifically, grid ancillary services¹, typically employed in the HV transmission networks, should be extended to distribution networks, according to the recent proposal by the European Network of Transmission System Operators for Electricity (ENTSO-E) [2]. As a second consequence, the distributed generation (DG) integration in distribution networks calls for a complete re-engineering of the control processes related to the local operation requirements of ADNs [3]. This thesis focuses on this second aspect of the DG integration related to the control needs of ADNs.

Several studies of the impact of the embedded generation in distribution systems have shown how the lack of controllability of highly volatile RERs causes frequent violations of operational constraints (e.g., [4, 5]). For example, Figure 1.1 (adapted from [4]) shows the simulation results of an analysis that was realized to determine the maximum amount of dispersed generation that can be hosted in the Italian MV system. It can be observed that, in the absence of generation, hardly any constraint is violated. However, with 10 MW of embedded generation the majority of network nodes face violations of operational constraints, such as line power flows and voltage limits.

¹By “grid ancillary services” we refer to frequency support, voltage support, black start and island-operation capabilities, system coordination and operational measurement. See, as a general reference, [2] for further details.

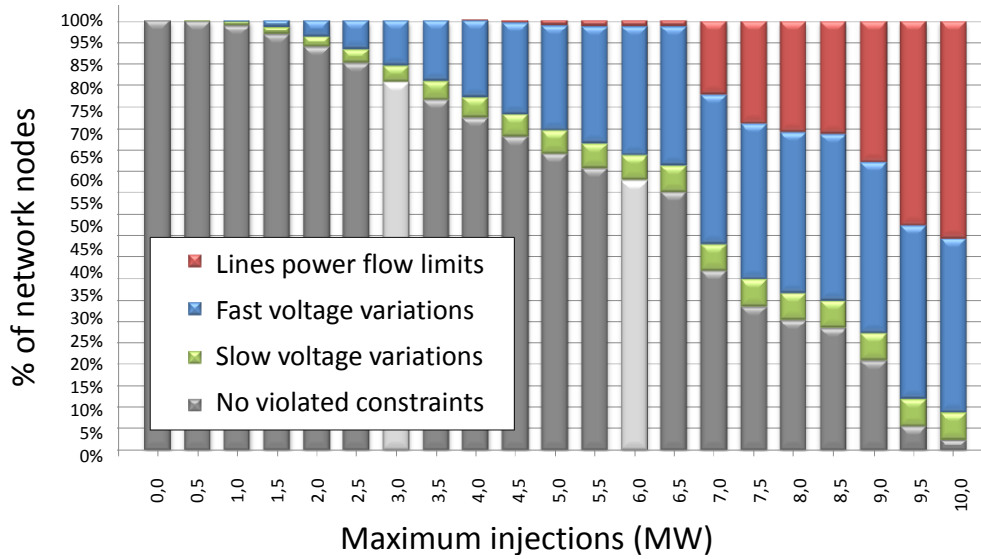


Figure 1.1: Percentage of network nodes exhibiting violations of operational constraints as a function of the amount of embedded generation (adapted from [4]).

It is clear that the “connect and forget” approach applied so far by the distribution network operators is no longer adequate. On the contrary, it is important to develop optimal control strategies specifically applied to the operation of these networks in order to achieve specific operation objectives (e.g., [6, 7, 8, 9, 10, 11]). Two of the most important control functionalities that have not yet been deployed in ADNs are voltage control and lines congestion management [3].

On the one hand, recent progress in information and communication technologies (ICT), the introduction of new generation of advanced metering devices such as phasor measurement units (PMUs) (e.g., [12, 13]) and the development of real-time state estimation algorithms (SE) (e.g., [14]) present new opportunities and will, eventually, enable the deployment of processes for voltage control and lines congestion management in distribution networks.

On the other hand, ADNs exhibit specific peculiarities that render the design of such control processes compelling. In particular, distribution networks are characterized by reduced line lengths with a non-negligible resistance over reactance (R/X) ratio of line longitudinal parameters, limited power-flow values, low inertia and high dynamics. These characteristics need to be properly taken into account in the design of control algorithms for distribution networks and, as discussed below, do not allow the direct adoption of control schemes that are established and well-performing in HV transmission networks. Additionally, the coordination of large numbers of dispersed energy resources in ADNs, in combination with their small size and heterogeneous nature, poses significant technical challenges requiring the design of scalable control

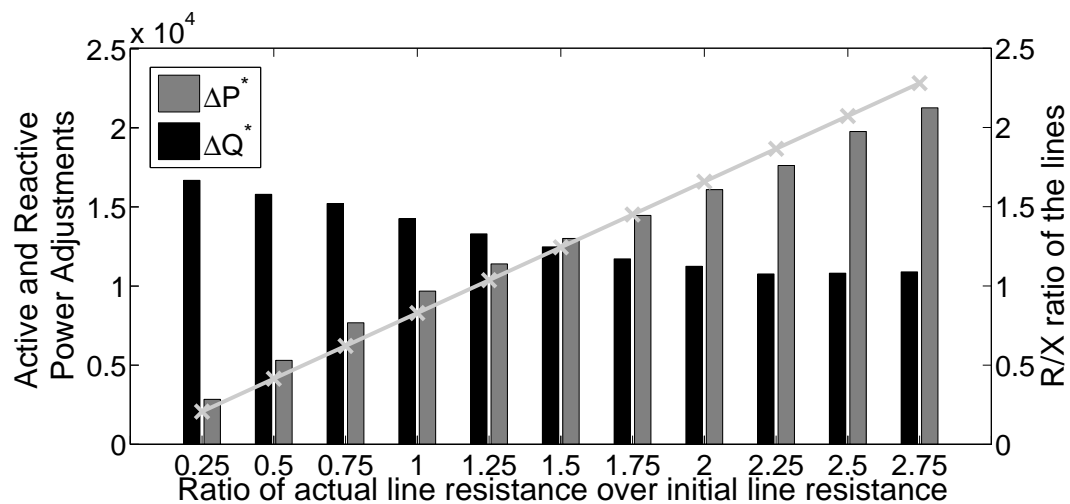


Figure 1.2: Optimal active and reactive power adjustments necessary to improve the voltage by 2% as a function of the line parameters (adapted from [16]).

mechanisms.

As far as voltage control is concerned, it is a well-known concept in the domain of high voltage (HV) transmission networks where, typically, it is related to reactive power management [15]. Although, this is true in HV transmission networks², such an assumption is no longer valid for distribution networks. Figure 1.2 (adapted from [16]) shows the optimal active and reactive power adjustments required to improve the voltage magnitude of a network bus by 2%, as a function of the R/X ratio of the network lines. As this ratio increases the active power requirements become, eventually, more important than the reactive power ones. As a consequence, the design of voltage control schemes for ADNs requires the control of both active and reactive power injections, in view of the non-negligible R/X ratio of longitudinal parameters of the medium and low voltage lines (e.g., [17, 18]).

Lines congestion management is also a well-explored area in the case of transmission networks. It constitutes one of the major tasks performed on a frequent basis by transmission system operators (TSOs) in order to ensure the operation of the system within safe limits, as overloading the lines can lead to severe deterioration of the conductors and even to cascading failures (e.g., [19, 20, 21, 22, 23, 24, 25]). Typically, this type of control in HV networks is incorporated in the market processes and is performed by dispatching generators through the market operations (e.g., [26]). Other means of dealing with congestion management is through flexible AC transmission systems devices (FACTS), via system reconfiguration or by curtailing excessive load-

²In general this holds for networks where the ratio of the longitudinal-line resistance versus reactance is small resulting in the decoupling of the active and reactive power injections on voltage angle differences and magnitudes.

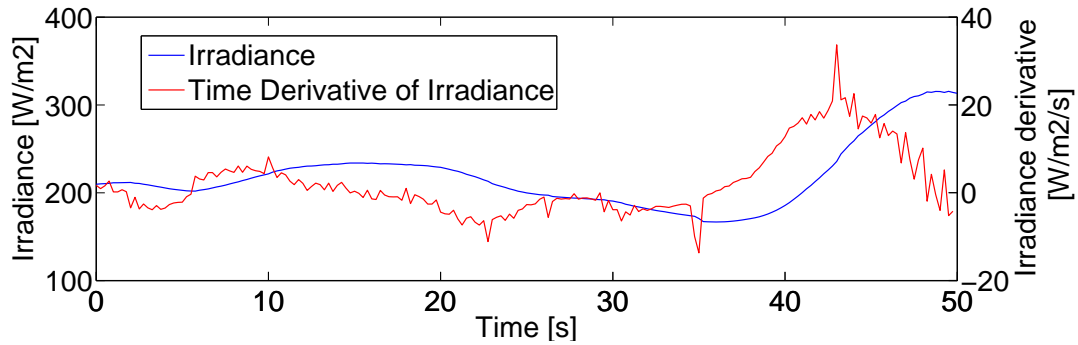


Figure 1.3: Example of the highest solar irradiance dynamics measured on March, 24th 2014 at location 46.518397-N, 6.565229-E (adapted from [34]).

/generation as a last resort (e.g., [27, 28, 29]). However, in the case of distribution systems, in the presence of line-ampacity violations, no optimal control solution has been established. The radial nature of these systems, the heterogeneity and small size of the available controllable resources in ADNs prohibits the application of the majority of the control schemes adopted in HV transmission systems. So far, to avoid congestion problems, distribution networks have been over-dimensioned [3]. However, within the context of ANDs, capacity expansion cannot constitute a viable solution to the problem, as reinforcement of the grid typically incurs prohibitive costs to the DNOs. Currently, when the network is overloaded, the DNOs curtail the active power in strategic points of the network until the current flows lie again within their allowed limits (e.g., [30, 31, 32, 33]). The aforementioned approach represents an extreme solution, however, when dealing with current-flows violations because it is not cost effective. Therefore, research efforts are required to deal with the congestion management of distribution systems.

Finally, a significant challenge related to ADNs operation, which affects the design of both voltage-control and lines-congestion management processes, is the high short-term dynamics of the non-dispatchable renewable energy resources. Real measurements of the power production of solar panels found in the literature (e.g., [34]) show that there can be variations in the power profiles of these resources in the order of more than 50% within a few seconds (e.g., Figure 1.3 (adapted from [34])). Within this context, the solution of optimal control problems becomes of interest, only if it meets the stringent time constraints imposed by the dynamics of distribution networks.

Taking into account the aforementioned challenges, in this thesis we focus on the design concepts and application of real-time control algorithms for voltage regulation and lines congestion management in ADNs. To this end, we develop a set of control schemes, ranging from centralized to fully decentralized solutions, that will allow to take advantage of the available DERs in ADNs, such as generators, loads and storage systems and engage them in local grid ancillary services.

1.2 Dissertation Outline

This thesis is organized as follows.

In Chapter 2, we provide the context, specifically we first identify the operational limits of ADNs with respect to the maximum amount of DG penetration, and we discuss the impact of the embedded DG on the quality of service. Then we describe the current practices used by DNOs, we identify their limitations and we discuss possible alternatives for the control of ADNs. Finally, we categorize the control functionalities expected to be deployed in ADNs with respect to their perspective time frame of application.

In Chapter 3, we adopt a centralized control architecture for voltage regulation and lines congestion management in ADNs; it relies on two-way point-to-point communication between the DNO and the controllable DERs. The goal of the proposed controller is to schedule both the active and reactive power injections of the controllable energy resources, in coordination with traditional resources, such as transformers' on load tap-changers, in order to achieve an optimal grid operation. The proposed real-time controller is based on a linearized approach that links control variables and controlled quantities by means of the known concept of sensitivity coefficients. We propose a formal analytical derivation of node-voltages and line-currents sensitivities with respect to the power injections and transformers' OLTC positions as a function of the system model and state. The proposed derivation is computationally efficient and is three times faster than traditional approaches. This approach requires the availability of both the grid model and the system state. In the last part of the chapter, we relax these assumptions and propose a robust optimization framework to formulate the voltage control problem in ADNs when the DNO has available information on the network admittance matrix but its entries are known with some level of uncertainty. Finally, we also propose a methodology for the computation of voltage sensitivity coefficients in a multi-phase unbalanced grid when there is no information on the system model and its state.

In Chapter 4, we are interested in designing a scalable control scheme for ADNs; it manages nodal power injections of the network buses where a large population of distributed, heterogeneous energy resources are connected and, at the same time, centralized resources such as transformers' OLTC. We propose a low-overhead broadcast-based control mechanism, called Grid Explicit Congestion Notification (GECN), intended for deployment by DNOs to provide grid ancillary services by a seamless control of large populations of distributed, heterogeneous energy resources. GECN is a decentralized control scheme that is conceived to provide primary voltage control in a scalable way by broadcasting low bit-rate control signals to large populations of distributed energy resources in order to manage the variations of the nodal power injections in the network. We assess the performances of GECN in the case of large aggregations of thermostatically controlled loads, as well as of distributed supercapacitor arrays.

In Chapter 5, we go one step-further in the problem formulation. In particular, we do not linearize the control problem of interest by means of sensitivity coefficients. Instead, we formulate the voltage control and lines congestion management problem as a non-approximated non-convex AC optimal power flow problem (OPF). First, we briefly review several OPF algorithms that are based on approximations in order to guarantee convergence; we focus on the branch-flow model (BFM) convexification of the OPF problem that has been recently proposed as an exact method for the OPF solution. We show that the BFM convexification of the OPF problem, in fact, is not exact, as it leads to an incorrect system model. Therefore, as an alternative solution, we propose a centralized algorithm for the non-approximated non-convex AC OPF problem in radial networks. Our proposed solution uses an augmented Lagrangian approach, relies on the method of multipliers, and does not require that the problem be convex. In an effort to provide also a fully distributed algorithm for the OPF problem, we investigate the application of ADMM for the solution of the original non-approximated OPF problem and we show cases for which the ADMM-based decomposition of the non-relaxed OPF problem fails to converge. As a solution, we present an asynchronous, distributed version of the proposed centralized algorithm that, unlike ADMM, is based on a primal decomposition and once more does not require that the problem be convex.

Finally, in Chapter 6 we conclude this thesis with a summary of the main findings and possible directions for future work.

1.3 Contributions

A detailed list of the contributions of this thesis can be found below.

1. We develop a method for the analytical computation of voltage and current sensitivities that (i) is generalized to account for a generic number of slack buses; (ii) enables the computation of sensitivities with respect to OLTC positions; (iii) for a given state of the system, is proved to admit a unique solution for the case of radial networks; (iv) supports the computation of the sensitivities for a generic unbalanced multi-phase electrical network by using the network admittance compound matrix that is suitable for distribution systems and (v) allows us to reduce the computational time by almost a factor of three compared to traditional approaches, thus enabling, in principle, its implementation in real-time optimal controllers.
2. By leveraging on (1), we propose a dedicated control scheme where each of the three phases of the DERs can be controlled independently of the others and we show that, when this possibility exists, the resulting optimal voltage and current profiles are better than those corresponding to the balanced control of the 3-phase output of the set-points of the DERs.
3. We relax the assumption that the DNO has an accurate knowledge of the system model, i.e., a correct network admittance matrix, which is a typical assumption

when designing control algorithms. In this direction, we formulate the optimal control problem of interest as an uncertain mixed integer linear programming (MILP) one, and we use a robust optimization framework to immunize the solution against the uncertainty in the system model. Additionally, we propose a methodology for the computation of voltage sensitivity coefficients for a multi-phase unbalanced grid, without relying on the knowledge of the system model and its state.

4. By leveraging on (1), we design and implement GECN, a new low-overhead broadcast-based decentralized control mechanism. We describe in depth the principles and operation of the GECN control mechanism and provide the detailed architecture of the GECN network controller.
5. We design a local GECN controller tailored to the characteristics of thermostatically controlled loads (TCLs). Furthermore, we investigate the potential of real-time demand response (DR) for providing grid ancillary services, and we indirectly reveal storage capabilities of end-customers. In the design of the load controller, we take into account the issue of limiting the frequency of cycles of the elastic appliances and avoid possible synchronization (i.e., cold load pick up after the DR actions).
6. We design a local GECN controller tailored to the characteristics of electrochemical-based energy storage systems. We evaluate the potential of distributed energy storage systems (ESSs) for providing primary voltage control via broadcast signals. In the case of ESSs control, we propose a method for estimating the energy reserve required for successfully performing voltage control depending on the characteristics of the network lines.
7. We show that without altering the GECN signal, a suitably designed controller implemented in the storage devices enables them to successfully contribute to primary voltage control, in addition to the elastic loads, and allows the successful use of the same broadcast signal for the control of heterogeneous energy resources.
8. We assess the performance of the proposed control mechanism in real-time using a hardware-in-the-loop (HIL) setup where all the chain including the models of the network and measurement devices, the real-time state-estimation and the control mechanism is presented. This allows us to assess the performance, in terms of accuracy and latencies, of the whole process.
9. We show that the BFM-based convexification of the OPF problem proposed in [35, 36], claimed to be exact for the case of radial distribution systems under specific assumptions, despite no apparent approximations, is in fact not exact.
10. We extend the BFM convexification of the OPF problem to account also for networks characterized by lines modeled accurately as π -equivalents. We show

Chapter 1. Introduction

that even in the case where the system model is correctly represented, the BFM-based convexification of the OPF problem might provide physically infeasible solutions.

11. We investigate ADMM for the distributed solution of the AC OPF problem and we highlight specific cases for which the ADMM-based solution of the non-relaxed OPF problem fails to converge.
12. We design a centralized algorithm for the solution of the non-approximated non-convex AC-OPF problem that is based on an augmented Lagrangian approach. We use a primal decomposition framework to extend the proposed algorithm to a fully decentralized asynchronous implementation.

2 Active Distribution Networks: Control Needs and Current Practices

2.1 Operational Limits of ADNs with Respect to Maximum DG Penetration and Impact on the Quality of Service

Within the context of ADNs, the supply mix is expected to evolve towards a carbon-constrained future where renewable energy resources and distributed storage systems will replace conventional generation. Moreover, the demand requirements are expected to change with the integration of new types of loads, such as plugged-in electric vehicles and intelligent appliances, leading to active participation of end-users in the grid ([1, 3]).

The first steps towards the evolution of conventional distribution systems into ADNs has already begun as evidenced by the continuously increasing penetration of distributed generation in the lower voltage levels of the electrical infrastructure. Both renewable technologies (e.g., solar, wind, geothermal, etc.) and conventional generation units (e.g., internal combustion engines, micro-turbines, fuel cells, etc.) are experiencing an unprecedented growth worldwide. In particular, at least 67 countries have renewable energy policy targets with many European countries having legally binding renewable energy targets (the baseline target is 20% by 2020 [37]). The USA also has a national target of 20% integration of renewables for the same horizon ([38]). Furthermore, recently G8 leaders called on countries to adopt instruments and measures to significantly increase the share of combined heat and power (CHP) in the generation of electricity [39].

This growth is driven by several different reasons (e.g., [40, 41, 42]). First, the green-house gas emissions are expected to be decreased and the construction of new large power plants could be avoided. Additionally, smaller DG units will represent less financial risks for stakeholders compared to the investment in large power stations. In the same direction, introduction of small DG units is expected to facilitate the competition in the electricity market which is an essential step towards achieving lower energy prices and improved quality of service. Finally, the increased penetration of DG, in combination with appropriate control schemes, can have beneficial impacts on

Chapter 2. Active Distribution Networks: Control Needs and Current Practices

power quality (e.g., voltage and power flows control), supply reliability (e.g., reductions in supply interruptions) and can contribute to the improvement of the energy security.

Despite the numerous benefits associated to DGs, severe impacts on the operation of distribution networks are expected when no control action is taken and challenges such as technical, commercial and regulatory will be non-negligible. In view of the scope of this thesis, we first briefly review the technical and operational requirements for distribution networks and then we focus on the impact of the DG on the operational constraints of distribution systems and on the quality of supply.

The quality requirements for electrical networks are intimately coupled with the supply voltage of the system. The reason is that for electrical equipment to operate correctly, electrical energy needs to be supplied at a voltage that is within a specified range around the rated value [43]. Depending on the country, several standards exist that define the main characteristics of the voltage at the customers' supply terminals (in particular in public LV and MV electricity distribution systems) under normal operating conditions¹. For instance, in Europe, it is the EN50160 standard [44] that describes the main voltage parameters and their permissible deviation ranges at the customer's point of common coupling in public LV (nominal voltage less than 1kV) and MV (nominal voltage between 1kV and 35kV) distribution systems, under normal operating conditions². In North America, the IEEE recommended practice for monitoring electric power quality [46] describes nominal conditions and deviations from these conditions that may originate within the source of supply or load equipment or from interactions between the source and the load. Finally, the NRS-048 standard [47] is assembled by representatives of the South African Electricity Supply Industry and covers voltage quality parameters that can affect the normal operation of the electricity dependent processes of customers.

Despite their differences, these standards classify the possible disturbances in electrical grids and provide the limits within which any customer can expect the voltage to remain. Despite the different admissible limits of the various grid codes, a generally approved classification of the grid disturbances is in periodic and aperiodic events. Below, we provide a short description of the possible disturbance events along with the corresponding limits found in the EN50160 standard.

- Periodic/recurring events
 - *Permanent variations of the voltage magnitude*: During pre-defined periods of time the mean rms values of the supply voltage shall be within a specified

¹With normal operating condition we refer to the condition of meeting load demand, system switching and clearing faults by automatic system protection in the absence of exceptional conditions due to external influences or major events [44].

²Even though the EN50160 is a European standard it is complemented in some countries by other rules or standards. For instance, in Germany the voltage parameters defined in EN50160 are taken into account but they are considered extreme situations in the network and not typical conditions, therefore national recommendations should be followed [45].

2.1. Operational Limits of ADNs with Respect to Maximum DG Penetration and Impact on the Quality of Service

range of the network nominal value. According to EN50160, both for LV and MV networks, each week 95% of 10min mean rms values of the supply voltage should remain with $\pm 10\%$ of the network rated value. For LV systems all 10min mean rms voltage values should not exceed $+10\%/ -15\%$ of the network voltage rated value.

- *Voltage imbalances*: Limits on the degree of asymmetry of the voltages of a three phase system. The ratio of direct and indirect sequence components of the voltages should be bounded. EN50160 states that under normal operating conditions, during each period of one week, 95% of the 10min mean rms values of the negative phase sequence component of the supply voltage shall be within the range $0-2\%$ of the positive phase sequence component.
- *Harmonic distortion*: Limits on the harmonic voltages, i.e., on the voltages with a frequency equal to an integer multiple of the fundamental frequency of the supply voltage. Under normal operating conditions, during each period of one week, 95% of the 10min mean rms values of each individual harmonic voltage should be less than or equal to a pre-specified value which is a function of the harmonic order h (e.g., for $h=19$ this value is 1.5%). Moreover, the total harmonic distortion of the supply voltage (including all harmonics up to the order 40) should be less than or equal to 8% .
- *Flicker*: The impression of unsteadiness of visual sensation induced by a light stimulus whose luminance or spectral distribution fluctuates with time. Caused by the modulation of the voltage magnitude. For both MV and LV networks, under normal operating conditions, in any period of one week the long-term flicker severity caused by voltage fluctuation should be less than 1 for 95% of the time.
- *Network frequency variations*: Frequency is allowed to vary around the nominal value (50Hz for Europe and 60Hz in the USA) for a specified limited amount of time. $\pm 1\%$ is allowed for 99.5% of a year, whereas the range $+4\%/ -6\%$ should never be exceeded.

- Aperiodic events

- *Voltage dips/swells*: Voltage magnitude 110% above the nominal value (swell), or 90% below the nominal value characterized by a duration (typically) less than 1sec. For LV systems $\pm 5\%$ is allowed normally and 10% infrequently, whereas for MV systems these limits are 4% and 6% respectively.
- *Interruptions of supply*: Absence of supply with duration between 1sec and 1min (very short-term), or between 1min and 60min (short-term). Few tens to few hundreds of very short-term interruptions per year are allowed for MV and LV grids, whereas short-term interruptions should be less than 10-50 a year.

In addition to the aforementioned limits on the voltage characteristics, ampacity limits on the current flows along the network branches apply. In general, network lines are over-sized according to the peak load of the system. Operation of the lines close to their ampacity limits should be avoided as overheating can have detrimental effects on the conductors. When the thermal limits of a line are exceeded a conductor can be severely damaged. For this reason it is necessary to calculate the line ampacity that keeps the temperature within allowed limits. Typically, the ampacity of the lines is calculated by solving a circuit that represents their thermal behavior. Several standards exist that provide ways to calculate the line ampacity limits as a function of the type of cable, i.e., its dimension and material, such as the IEC 60287 Standard, the IEEE 399-1997 Standard, the National Electric Code (NEC), and the IEEE 835-1994 Standard ([48, 49, 50, 51, 52, 53]).

Several studies found in the literature summarize the main impacts of DG on the aforementioned operational limits of ADNs and on the quality of supply (e.g., [41, 40, 54, 4, 55, 56]). The first aspect which is influenced by the connection of DG units is the voltage. In the absence of generation in distribution systems (passive networks), the voltage magnitude typically decreases as a function of the distance from the primary substation and as the load of the feeders increases. The impact of the DG on the network voltage profile is dependent on the power flows in the network. In particular, when the injected power by these units exceeds the network load, then, typically, there is a rise on the voltage magnitude.

The power quality is also affected by the integration of DG units. In particular, transient voltage variations may occur in addition to the steady-state voltage rise effect, for instance due to connection/disconnection of generators. DG may cause noticeable flicker as a consequence of starting a machine or due to changes in the DG output that result in a significant voltage change on the feeder. Finally, harmonic distortion of the network voltage may also occur, whose type and severity depends on the power converter technology and interconnection configuration.

As far as lines congestion is concerned, DG units can significantly alter the loading patterns in the network. It is likely that increased levels of DG will eventually increase the overall current flow in the network and can lead to the operation of overhead lines and/or cables closer to their thermal limits.

Further technical consequences of the penetration of DG units in distribution networks, that are outside the scope of this thesis, include changes in the losses pattern, increase of short-circuit levels, possible new fault events, stability issues, etc.

Overall, it is obvious that DG units can be beneficial for ADNs, but their integration in distribution systems cannot be realized in a “connect and forget” approach as their impact on the system operation cannot be neglected. In the following section we discuss what are the current practices of DNOs with respect to planning and operation of distribution networks and we identify the current limitations and possible future opportunities.

2.2 Current Practices and Future Opportunities for DNOs

As discussed in the previous section, DNOs are required to operate their networks in a way that ensures a given quality of supply of electricity and respects specific operational limits. So far, in the absence of DG, distribution networks have been oversized as a function of the peak load of the system in order to cope with the worst-case scenario in terms of voltage variations, lines congestion management and certain security constraints. As a consequence, minimal or no monitoring and active control actions were required for their everyday operation (e.g., [57, 41]).

Currently, even in cases where DG units are connected in distribution networks, essentially DNOs apply the “connect and forget” approach. This entails a planning phase during which it is assessed whether the network can actually host the connected DG while ensuring that operational constraints such as congestion, voltage rise and power flows, will be within acceptable limits. This planning study is mainly using maximum generation-minimum demand scenarios. In particular, in the case of medium-sized DG units DNOs currently accepts DG connections until operational limits are reached or, in some cases, the DNOs impose automatic tripping of DG units in case of limits violation to allow for an increased hosting capacity. In the case of smaller scale distributed generation, essentially composed of photovoltaic panels or CHP units little or no control actions take place from the DNO’s point of view. As a consequence, high penetrations of small-scale DG can quickly and more easily lead LV circuits to face technical issues similar to those of higher voltage levels [58].

In general, current practices in distribution networks essentially consist in proactive or passive approaches in compliance with the view that these systems have been designed to deal with the worst-case scenario. On the contrary, future practices are expected to include maximum exploitation of existing assets and expected DERs, with the operation of these systems closer to their physical limits and integration of monitoring and control procedures similar to the ones found in HV systems [3].

In particular, in the case of voltage rise or drop, so far, curtailment of loads and/or generation takes place (e.g., [59, 60]). Additional measures include generation tripping and use of capacitor banks. Within the context of ADNs, several efforts in the literature propose that the voltage variations be tackled by coordinated volt-var control, static var compensators, coordinated dispatch of DERs (DGs, ESSs, DR) or even on-line system reconfiguration.

In the case of limited hosting capacity, so far, network reinforcement in terms of new lines and transformers was proposed as a counter-measure (e.g., [61, 62]). In the future, advanced monitoring of the network will allow the real-time dynamic thermal rating of assets, which in combination with the dispatch of DERs or the reconfiguration of the system will provide a means of congestion alleviation.

The fault levels, i.e., short circuit currents are traditionally dealt with by upgrading the equipment (e.g., switchgears), by inserting higher impedance components in

the network (e.g., transformers) or by network reconfiguration. As part of the future smarter distribution networks, this technical issue can be addressed by managing actively the DG and load connections and, also, through deployment of fault-current limiters.

Overall it is worth observing that distribution systems operation currently is limited to passive network elements (e.g., OLTCs, capacitor banks, etc.). This passive way of planning and operating distribution networks has proven to be cost-effective and adequately performing until recently. However, as discussed in the previous section it might soon inhibit the increasing penetration of DG and, in general, non-conventional resources. As discussed in this section, distribution networks are expected to require also the control of active elements, namely demand and generation, in order to promote their evolution into ADNs. Consequently, the full deployment of ADNs, i.e., more observable and controllable networks, will lead to a future where DNOs will manage the networks in a very similar fashion to the TSOs for transmission systems [3].

For this to become reality, research efforts are required to bring new control concepts into application and development of dedicated control mechanisms is essential. This thesis constitutes an effort towards this direction with particular reference to voltage control and lines congestion management in ADNs.

2.3 Perspective Control Functionalities and Corresponding Time Frames

In this section we discuss the perspective control functionalities as a function of their time frame of application. In particular, first, we discuss the architectures and time-frames of voltage control processes within the context of transmission systems. Also we discuss the congestion management processes in transmission networks and their relevance in the context of ADNs. The reason is that, currently, no established control architectures exist for ADNs and the requirements of these networks in terms of categorization of controls as a function of time-frames need to be defined.

In general, the control processes adopted by each country and/or each utility is different from each other. The architecture of the control system can be centralized/decentralized or hierarchical, while the variety of the control operation changes from a completely manual solution to different kinds of automation [63].

To provide a concrete example, we refer to the known problem of voltage control in HV transmission systems. In many countries, hierarchical systems based on network area subdivision and automatic coordination of reactive power resources are adopted for network voltage control purposes (e.g., Italy [64, 63], France [65, 66], and Spain [67]). As a result of the deregulation of the energy markets, hierarchical voltage control systems are increasingly being adopted. In fact, system operators recognize that the hierarchy favors the simplification of automatic control of overall transmission network voltages and allows the potential contributions of different participants to the voltage

2.3. Perspective Control Functionalities and Corresponding Time Frames

ancillary service.

From a system perspective, the overall task of regulating the voltage is typically organized in a 3-level hierarchical fashion. It is important to note that the hierarchy levels are temporally and spatially independent as much as possible to avoid oscillatory behaviors and instability issues [68]. A brief description of the levels, their functionalities and time-frame of application is as follows.

- *Primary Voltage Control (PVC)*: This type of control maintains the generator stator voltages at their set-point values. It is an automatic control that is performed within a few seconds in order to compensate against rapid voltage variations. PVC is an immediate control that must operate continuously, as it maintains the voltage at its nominal value and ensures stability. It is mostly realized through actions of the generators' automatic voltage controllers (AVR), systems that monitor the output voltage and control the input voltage of the generator [64].
- *Secondary Voltage Control (SVC)*: The time constant of this control system is typically of a few minutes (1-15min) and the goal is to compensate voltage variations that are slower compared to the ones tackled by the PVC system. Essentially, this control is applied to network zones that are non-interacting and within which the voltage can be controlled independently. The control is typically performed through the generating units' reactive power which is already available in the field, low-cost and simple to control for network voltage support; Few main buses (pilot-nodes) in the system are suitably identified and considered in the voltage control action and the rest of the buses are forming control areas as a function of their electrical coupling. The control structure, based on the subdivision of the grid into control areas, automatically and, as much as possible, independently regulates each area's pilot node voltage [68].
- *Tertiary Voltage Control (TVC)*: This type of control is at the highest level of the hierarchy and its goal is to optimize the nationwide voltage map. The time frame of application of tertiary control is roughly 15mins to 1hr and it is typically a manual control. The basic idea of TVC comes from the need to increase the system's operating security and efficiency through centralized coordination of the decentralized SVC structure. Within the TVC context the pilot nodes' voltage set-points must be adequately updated and coordinated but with dynamics slower than the one of SVC, considering the real condition of the overall grid. In the same time conflicting inter-area control efforts should be avoided. Typically, the pilot nodes voltage set-points are optimized to minimize grid losses in addition to preserving control [69].

Within the context of distribution networks voltage control, secondary control is not of interest in view of the size and radiality of these systems and tertiary control is out of context. For this reason, in this thesis we focus on the design of primary control

Chapter 2. Active Distribution Networks: Control Needs and Current Practices

algorithms for ADNs, namely we are interested in real-time (RT) applications that have a time range of few seconds.

As far as line congestion management is concerned, it is a problem usually treated in transmission networks within the context of market operations and in particular as part of the problem of the security constraint unit commitment/dispatch (SCUC) [70, 26]. In conventional distribution systems, this problem cannot be easily expressed as a SCUC problem and is, traditionally, solved in the design/planning phase. As a consequence, the RERs' contribution cannot be easily taken into account in the lines congestion management problem. For this reason, in this thesis we propose that this problem be casted as a control problem with the same time-frames of voltage control. Therefore, we incorporate the congestion management functionality as a primary control application.

3 Centralized and Linearized Control Strategies in ADNs

3.1 Introduction

As seen in Chapter 2 the progressive penetration of distributed energy resources (DERs) in distribution systems poses significant challenges in terms of operation and control philosophies. With the view that the DERs can become an opportunity for the DNO rather than a problem, it is essential to develop optimal control strategies tailored to the characteristics of ADNs that will allow their participation in the network management (e.g., [6, 7, 8, 9, 10, 11]).

In particular, the solution of optimal control problems in ADNs becomes of interest only if it meets the stringent time constraints required by real-time controls and imposed by the stochasticity of RERs, in particular photovoltaic units (PVs), largely present in these networks. Moreover, control schemes are meaningful for implementation in real-time controllers only when convergence to an optimal solution is guaranteed. Finally, control processes for ADNs need to take into account the inherent multi-phase and unbalanced nature of these networks, as well as the non-negligible R/X ratio of longitudinal parameters of the medium and low voltage lines (e.g., [17, 18]) together with the influence of transverse capacitances¹. Taking into consideration the aforementioned requirements, the distribution management systems (DMSs) need to be updated accordingly in order to incorporate optimization processes for the scheduling of the distributed energy resources [71].

In this direction, in this chapter, we adopt a centralized control architecture for voltage regulation and lines congestion management in ADNs (e.g., [71, 72, 9, 73, 74]). The proposed centralized scheme is suitable for the real-time control of a limited number of distributed energy resources, such as medium-sized dispersed generation units. The goal of the proposed controller is to schedule both the active and reactive power injections of the controllable energy resources, in coordination with traditional resources, such as on load tap-changers (OLTCs), in order to achieve an optimal grid operation.

¹Note that line shunt parameters are non-negligible in case of networks characterized by the presence of coaxial cables. These types of components are typical in the context of urban distribution networks.

We consider that the distribution grid is equipped with a centralized distribution management system where all the operation and control functionalities are performed (e.g., [9]). Additionally, we assume availability of a monitoring infrastructure and a state estimation process that provides the DNO with the state of the grid, i.e., the phasors of the phase-to-ground voltages at all the network buses. The DMS comprises an online centralized controller that uses the knowledge of the network state to formulate an optimization problem in order to minimize the deviations of the voltage magnitudes from the network rated value while keeping the line current flows below their ampacity limit. The resulting solution of the control problem provides the DNO with the optimal nodal power set-points for the controllable energy resources and the optimal OLTC positions.

The formulation of the optimization problem of the proposed online controller is based on a linearized approach that links control variables (e.g., power injections, transformers tap positions) and controlled quantities (e.g., voltages, current flows) by means of sensitivity coefficients. The use of sensitivity coefficients for optimal control is a well-explored concept in the case of transmission systems (e.g., [75, 76, 77, 78, 79]). In order to increase the computational efficiency of this category of approaches, and to extend it to the inherent multi-phase unbalanced configuration of distribution networks, we provide a straightforward analytical derivation of node-voltages and line-currents sensitivities as a function of the power injections and transformers' tap-changers positions.

The proposed control architecture relies on the assumption that the DNO has an accurate up-to-date model of the network topology and a complete knowledge of the feeder parameters, i.e., a correct network admittance matrix $[Y]$. However, this assumption does not always hold in reality. In particular, the distribution network operator (DNO) might have wrong data for the feeder parameters, resulting in a non-accurate network admittance matrix (e.g., [80, 81]). Furthermore, there are factors, such as the temperature that can cause variations of the values of the resistances of the network branches along the day and are not taken into account in the computation of the admittance matrix (e.g., [82]). Such uncertainties, when not taken into account, can lead to control decisions that are meaningless for the grid operation.

To account for such scenarios, in the last part of this chapter, we assume that the DNO has limited or no information on the system model. We propose a robust optimization framework ([83]) to formulate the voltage control problem in ADNs when the DNO has available information on the network admittance matrix but its entries are known with some level of uncertainty. In detail, we assume that the feeder parameters are uncertain but bounded and that a monitoring infrastructure is available that allows the DNO to have information on the voltage phasors of the network buses. We consider uncertainty sets that are intervals and we formulate the robust counterpart of the control problem using the method proposed in [84]. In the same direction, we also propose a methodology for the computation of voltage sensitivity coefficients in a

multi-phase unbalanced grid when there is no information on the system model and its state. In particular, we assume availability of a monitoring infrastructure that provides measurements of power injections and voltage magnitudes only and we obtain the desired sensitivities as a solution to an over-determined system of linear equations.

The main contributions of this chapter can be summarized as follows. We develop a method for the analytical computation of voltage and current sensitivities that (i) is generalized to account for a generic number of slack buses; (ii) allows the computation of sensitivities with respect to OLTC positions; (iii) is proved to admit a unique solution for the case of radial networks; (iv) supports the computation of the sensitivities for a generic unbalanced multi-phase electrical network by using the $[\mathbf{Y}]$ compound matrix being, thus, suitable for distribution systems and (v) allows us to reduce the computational time by almost a factor of three compared to traditional approaches, thus enabling, in principle, its implementation in real-time network controllers. We verify that, in distribution systems, both active and reactive power for voltage control need to be taken into account as their impact on the voltage variations can be comparable. We propose a sophisticated control scheme where each of the three phases of the DERs can be controlled independently of the others and we show that, when there is this possibility, the optimal voltage and current profiles are better than the ones corresponding to the balanced control of the 3-phase output of the set-points of the DERs. Finally, we relax the assumption that the DNO has an accurate knowledge of the system model, i.e., a correct network admittance matrix $[\mathbf{Y}]$. We show that uncertainty in the network admittance matrix can have a significant effect on the solution of the optimal voltage control problem and that formulating the voltage control problem using a robust optimization framework can immunize the solution against the considered uncertainties in $[\mathbf{Y}]$ without significantly increasing the complexity of the problem. Additionally, we show that it is possible to compute voltage sensitivity coefficients for a multi-phase unbalanced grid and, consequently, perform voltage control without knowledge of the grid model and the system state.

3.2 Related work

Voltage control and lines congestion management are typical examples of optimal controls that are expected to be deployed in ADNs in the near future. This category of problems has been well investigated in the domain of HV transmission systems and, usually, it has been addressed in the literature by means of linear approaches applied to the dependency between voltages and power flows (both nodal and branch) as a function of the power injections (e.g., [9, 10, 85, 86]).

For the case of nodal voltage sensitivities with respect to nodal powers, the typical approach for the solution of this class of control problems is the use of the sensitivity coefficients through an updated Jacobian matrix derived from the load flow problem (e.g., [75, 76, 77, 78, 79]). However, from the computational point of view, the main disadvantage of such a category of methods is that, for every change in the operation

conditions of the network, an updated Jacobian matrix needs to be built on the basis of the network state and needs, then, to be inverted. This procedure involves non-trivial computation constraints for the implementation in real-time centralized or decentralized controllers.

In order to overcome the aforementioned limitations, the authors of [87] have proposed the direct computation of voltages and network-losses sensitivity coefficients, based on the Gauss-Seidel formulation of the load flow problem, by making use of the impedance matrix ($[Z]$) of a balanced network. Also, in [85] the use of the $[Z]$ matrix has been proposed along with the constant-current model for loads and generators. In [86] the sensitivity coefficients are proposed to be calculated starting from the network branch currents. Finally, the approach presented in [88, 89, 90, 91, 92] belongs to a class of methods typically derived from circuit theory and is based on the use of the so-called adjoint network.

Compared to [85] our approach for the computation of the sensitivities takes into account the whole admittance matrix of the network. On the other hand the analytical derivation of sensitivities in [85] was based on the approximated representation of the network lines where lines shunt parameters are neglected². The method presented in [86] always requires a base-case load flow solution and it relies on the assumption that all generators are PV nodes (i.e., with fixed voltage magnitude). Also, it does not account for the mutual coupling between different phase conductors.

Close to our work is the approach proposed in [87]. However, there are several significant differences. First, the method in [87] depends on a pseudo-load flow approach (i.e., it makes use of a Gauss-Seidel iterative process with a fixed number of iterations) which influences the accuracy of the computed coefficients. Furthermore, compared to [87] we are able to generalize the problem formulation for a generic number of slack buses and extend the computation of sensitivities to tap-changers positions (i.e., changes of slack-buses reference voltages). Moreover, we prove that the analytical computation of sensitivities admits a unique solution for the case of radial networks. Finally, we adopt the so-called $[Y]$ compound matrix, which has the advantage of being sparse. This allows us to take into account the inherent multi-phase and unbalanced nature of distribution networks and to reduce the computation time by almost a factor of three compared to traditional approaches, thus enabling, in principle, the implementation of the proposed method in real-time optimal controllers.

Despite their differences, all the aforementioned methods rely on the key assumption that an accurate knowledge of the system model, i.e., the $[Y]$ admittance matrix, is available for the computation of the desired sensitivities. However, this assumption does not always hold in reality. For this reason, recently, there has been an effort in the literature to compute sensitivity coefficients using measurements and, thus, avoiding

²It is important to note that line shunt parameters are non-negligible in case of networks characterized by the presence of coaxial cables. These types of components are typical in the context of urban distribution networks.

the use of the network admittance matrix. In particular, in [93, 94] a least squares method is proposed for the computation of injection shift factors in transmission networks where large sets of synchronized measurements of PMUs are available. In the same direction, in [95], availability of historical data coming from smart meters is assumed and voltage sensitivity coefficients are computed for a low voltage grid and for different loading scenarios in the network.

Compared to the work in [93, 94], we propose here a methodology for the computation of voltage sensitivity coefficients in low voltage 3-phase unbalanced grids without relying on the knowledge of the system model and its state. As availability of PMUs is still limited in low voltage grids, our proposed method does not require highly synchronized phasor measurements. Instead we assume availability of a monitoring infrastructure that provides us with measurements of power injections and voltage magnitudes only. Our work is closer to [95]. However, compared to [95] we consider the computation of sensitivities in the generic case of 3-phase unbalanced networks and we take into account noise in the available measurements. Furthermore, we perform the computation in an online fashion, thus enabling, in principle, the adoption of the method in real-time ADN controllers. Finally, we validate and benchmark the proposed method using real measurements coming from a real low voltage distribution feeder in Switzerland.

In cases when the DNO has some knowledge of the system model, but the available information is inaccurate, the voltage control problem can be formulated as an optimization problem with uncertain data. In this respect, a robust optimization (RO) framework can be adopted for its solution ([83]). RO is one possible way to handle optimization problems where a certain measure of robustness is sought against uncertainty of the problem data. Contrary to stochastic optimization, in the case of RO, there is no assumption on the distribution of the uncertain parameters and the uncertainty can be represented as deterministic variability in the value of the parameters of the problem. Within the context of the smart grid, RO has recently gained attention due to the increasing presence of uncertain sources in the grid. It has already been applied to the unit commitment problem in order to account for price uncertainty (e.g., [96]). Other problems that have been tackled in the literature, so far, by means of RO is the capacity expansion problem, the reactive power planning and the real-time demand response under uncertain energy prices (e.g., [97, 98, 99]). However, to the best of our knowledge RO has not yet been applied to the case of voltage control when there are uncertainties in the feeder parameters.

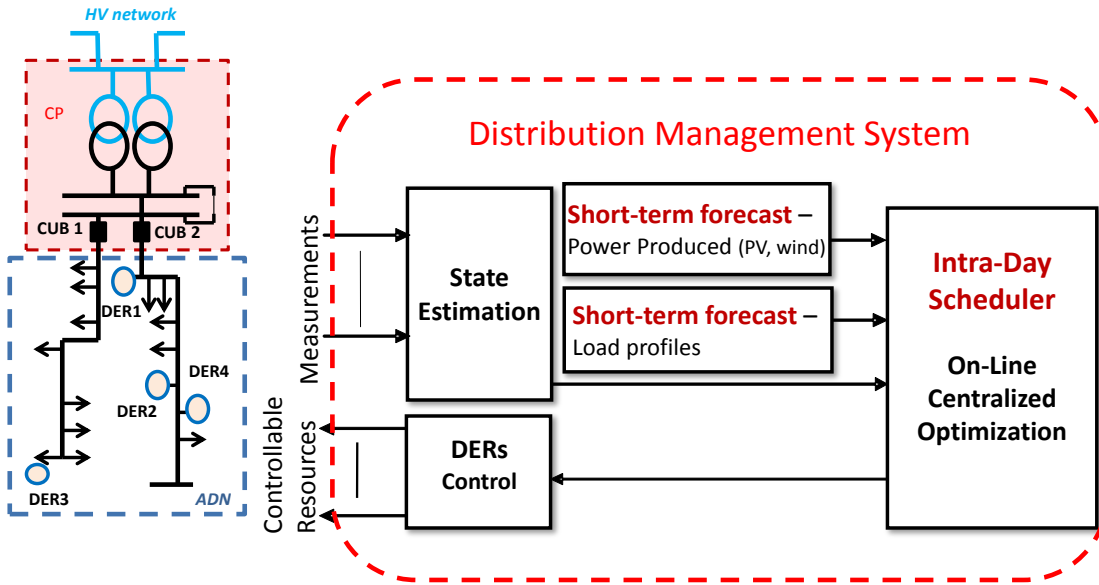


Figure 3.1: Distribution Management System adopted for the proposed centralized controller, adapted from [71].

3.3 Centralized Online Controller for Voltage Control and Lines Congestion Management in ADNs

3.3.1 Control Architecture

Throughout this chapter we consider an ADN equipped with a number of distributed controllable energy resources, a monitoring infrastructure that provides the DNO with field measurements and a centralized DMS adapted from [71]. The architecture of the considered DMS is shown in Figure 3.1. Its main modules are the following:

- State estimation:** The first step towards the development of control schemes for ADNs is the knowledge of the system state. To this end, the state estimation (SE) module involves algorithms that process field measurements and provide the DNO with the state of the grid, i.e., the voltage phasors at the network buses. It is worth noting, that control functionalities in distribution systems can be characterized by dynamics in the order of few seconds. In this respect, we consider a real-time state estimator (RTSE) that is capable of assessing the ADNs' state within few tens/hundreds of ms with relatively high levels of accuracy (e.g., [14]). Provided that the network admittance matrix is known, once the voltage phasors are obtained, the computation of the nodal power injections, as well as the flows of each line is straightforward.

3.3. Centralized Online Controller for Voltage Control and Lines Congestion Management in ADNs

- **Short-term forecasts:** This DMS module incorporates algorithms that are able to provide ultra short-term forecasts for both the loads' consumption and the RERs' production (e.g., [34]). ADNs are characterized by increased penetration of highly volatile renewable energy resources. Therefore, the possibility to forecast as accurately as possible their power production can play a fundamental role, especially in cases where the RERs are requested to contribute to grid ancillary services. In the same direction, load forecasting is crucial especially in cases when demand-response actions are included in the control functionalities. This module is also useful in cases where multi-horizon optimization is used for the grid control (e.g., model predictive control) or uncertainty in loads and RERs' production is included in the control via, for instance, a robust optimization framework.
- **Intra-day scheduler & DERs control:** The intra-day scheduler module essentially comprises the real-time controller that acts in short time intervals (in the order of few seconds to several minutes according to the control application). It uses the system state and the available short-term forecasts as inputs and formulates an optimization problem in order to obtain the optimal required power adjustments and the optimal variations in the OLTC positions which lead to the desired operation set-point. Depending on the control application that the DNO wishes to implement, the objective function is modified accordingly. Typical examples of controls include resistive losses minimization, voltage deviations minimization, lines congestion management or energy supply cost minimization. Once the optimal set-points are computed the DERs control module is responsible to communicate them to the controllable DERs.

In our case, the DNO is interested in minimizing the voltage deviations from the network rated value and in maintaining the line current flows below their ampacity limits. In the following section, we focus on the actions that the online centralized controller performs to achieve these objectives.

3.3.2 Controller's Actions

In what follows, the modules of state estimation, on-line centralized optimization and DERs control (Figure 3.1) are adopted to formulate the control problem.

A network is considered composed of K buses, L lines and N_{DER} controllable resources. The DNO wishes to compute the optimal DERs' active and reactive power variations ($\Delta P_i, \Delta Q_i, i = 1, \dots, N_{DER}$), and the optimal OLTC positions $\Delta \mathbf{n}$ in order to achieve primary voltage control and lines congestion management.

The first step towards this direction is to linearize the dependencies of the voltage and line currents with respect to the nodal power injections and OLTC positions. To this end, at each time step, t , the DNO uses the network state computed by the SE

module, i.e., the voltage phasors $\bar{E}_i(t)$ at each bus i (e.g., [100, 101])³. Also, we assume that the system model, namely the network admittance matrix, $[\mathbf{Y}]$ is known. Using this information, the DNO can compute, subsequently, the nominal values of the voltage and current sensitivity coefficients with respect to absorbed/injected power of a bus ℓ where a controllable resource is connected, as well as with respect to the transformer's OLTC positions⁴:

$$\begin{aligned} K_{P,il}(t) &:= \frac{\partial |\bar{E}_i|}{\partial P_\ell}, & K_{Q,il}(t) &:= \frac{\partial |\bar{E}_i|}{\partial Q_\ell} \\ H_{P,k\ell}(t) &:= \frac{\partial \bar{I}_k}{\partial P_\ell}, & H_{Q,k\ell}(t) &:= \frac{\partial \bar{I}_k}{\partial Q_\ell} \\ K_{n,i}(t) &:= \frac{\partial |\bar{E}_i|}{\partial E_0}, & H_{n,k}(t) &:= \frac{\partial \bar{I}_k}{\partial E_0} \end{aligned}$$

These sensitivities can be computed on-line by solving a linear system of equations ([17]). The details related to the computation of the sensitivities will be discussed in the following section.

Therefore, the following linear relations between variation in bus voltages, line currents and variations of active/reactive power $\Delta P_i, \Delta Q_i$ and OLTC $\Delta \mathbf{n}$ can be derived (e.g., [9]):

$$\begin{aligned} \Delta |\bar{E}|_i &\approx \mathbf{K}_{P_i} \Delta \mathbf{P} + \mathbf{K}_{Q_i} \Delta \mathbf{Q} + \mathbf{K}_n \Delta \mathbf{n} \triangleq (\mathbf{K}_{P,Q,n}(t) \Delta(\mathbf{P}, \mathbf{Q}, \mathbf{n}))_i \\ \Delta \bar{I}_k &\approx \mathbf{H}_{P_k} \Delta \mathbf{P} + \mathbf{H}_{Q_k} \Delta \mathbf{Q} + \mathbf{H}_n \Delta \mathbf{n} \triangleq (\mathbf{H}_{P,Q,n}(t) \Delta(\mathbf{P}, \mathbf{Q}, \mathbf{n}))_k \end{aligned}$$

where $\mathbf{K}_{P_i} = [K_{P_{i1}}, \dots, K_{P_{iN_{DER}}}]$, $\mathbf{K}_{Q_i} = [K_{Q_{i1}}, \dots, K_{Q_{iN_{DER}}}]$, $\mathbf{K}_n = [K_{n1}, \dots, K_{nB}]$, $\mathbf{H}_{P_k} = [H_{P_{k1}}, \dots, H_{P_{kN_{DER}}}]$, $\mathbf{H}_{Q_k} = [H_{Q_{k1}}, \dots, H_{Q_{kN_{DER}}}]$, $\mathbf{H}_n = [H_{n1}, \dots, H_{nL}]$.

At this stage, using the sensitivity coefficients $\mathbf{K}_{P,Q,n}$ and $\mathbf{H}_{P,Q,n}$ the DNO can compute the optimal required power adjustments in the buses and the optimal OLTC positions $\{\Delta(\mathbf{P}, \mathbf{Q}, \mathbf{n})^*\}$ which lead to the desired operation set-point for optimal grid control. Depending on the grid's needs, the DNO can formulate different objective functions. In this chapter, we assume that at a given time step t , the DNO wishes to minimize the deviations of the voltage magnitudes in the network buses from the network rated value, E_o , while keeping the line flows below the ampacity limits, via the following constrained optimization problem ([102]):

³In the rest of the thesis complex numbers are denoted with a bar above (e.g., \bar{E}) and complex conjugates with a bar below (e.g., \underline{E}).

⁴Note that we assume that transformers' tap-changers are located in correspondence of the slack buses of the network because for distribution networks these represent the connections to external transmission or sub-transmission networks.

3.4. Efficient Computation of Sensitivity Coefficients of Node Voltages and Line Currents in Unbalanced Radial Electrical Distribution Networks

$$\min_{\Delta(\mathbf{P}, \mathbf{Q}, \mathbf{n})} \sum_i \lambda_i [(|\bar{E}_i(t)| + (\mathbf{K}_{\mathbf{P}, \mathbf{Q}, \mathbf{n}}(t) \Delta(\mathbf{P}, \mathbf{Q}, \mathbf{n}))_i - |E_o|)^2 - \delta^2]^+ \quad (3.1)$$

$$+ \sum_k \mu_k [(|\bar{I}_k + (\mathbf{H}_{\mathbf{P}, \mathbf{Q}, \mathbf{n}}(t) \Delta(\mathbf{P}, \mathbf{Q}, \mathbf{n}))_k|)^2 - \epsilon^2]^+$$

$$\text{subject to: } (P_j, Q_j) \in \mathcal{H}_j, j = 1, \dots, N_{DER} \quad (3.2)$$

$$n_{min} \leq n \leq n_{max} \quad (3.3)$$

where we have used the notation $[a]^+ \triangleq \max(a, 0)$ and λ_i and μ_k are weighting the two terms of the objective function that correspond to voltage and current control respectively. The constants δ and ϵ represent the voltage and current thresholds which define the ranges outside of which the controller optimizes the voltage and the current flows. This avoids the minimization of the voltage deviations and the current flows when they are within acceptable limits imposed by the DNO. Constraints (3.2) represent the capability curves of the controllable resources. The last constraint (3.3) represents the minimum and maximum OLTC positions allowed.

Note that the formulation of the optimization problem in (3.1)-(3.3) is generic. According to the DNO's desire, the objective can be modified to account only for the voltage or the current flows control. Also, in case the OLTCs are included in the control the problem becomes a mixed integer one, otherwise the corresponding sensitivity coefficients can be set to zero and control is achieved only through the scheduling of the DERs. In all cases, the key element for the formulation and solution of the linearized control problem is the computation of the sensitivity coefficients. To this end, in the following section we recall the traditional way to compute sensitivity coefficients and we propose a method for the analytical derivation of these sensitivities, that is suitable for real-time network controllers.

3.4 Efficient Computation of Sensitivity Coefficients of Node Voltages and Line Currents in Unbalanced Radial Electrical Distribution Networks

3.4.1 Classic Computation of Sensitivity Coefficients in Power Networks

In this paragraph we make reference to a balanced network composed by K buses.

Traditionally, there are three proposed ways to calculate the sensitivity coefficients of our interest. The first method consists of estimating them by a series of load-flow calculations each performed for a small variation of a single control variable (i.e., nodal

power injections, P_l, Q_l) [9]:

$$\begin{aligned} \frac{\partial |\bar{E}_i|}{\partial P_l} &= \frac{\Delta |\bar{E}_i|}{\Delta P_l} \bigg|_{\substack{\Delta P_{i,i \neq l} = 0 \\ \Delta Q_{i,i \neq l} = 0}} & \frac{\partial |\bar{I}_{ij}|}{\partial P_l} &= \frac{\Delta |\bar{I}_{ij}|}{\Delta P_l} \bigg|_{\substack{\Delta P_{i,i \neq l} = 0 \\ \Delta Q_{i,i \neq l} = 0}} \\ \frac{\partial |\bar{E}_i|}{\partial Q_l} &= \frac{\Delta |\bar{E}_i|}{\Delta Q_l} \bigg|_{\substack{\Delta P_{i,i \neq l} = 0 \\ \Delta Q_{i,i \neq l} = 0}} & \frac{\partial |\bar{I}_{ij}|}{\partial Q_l} &= \frac{\Delta |\bar{I}_{ij}|}{\Delta Q_l} \bigg|_{\substack{\Delta P_{i,i \neq l} = 0 \\ \Delta Q_{i,i \neq l} = 0}} \end{aligned} \quad (3.4)$$

where \bar{E}_i is the direct sequence phase-to-ground voltage of node i and \bar{I}_{ij} is the direct sequence current flow between nodes i and j ($i, j \in \{1 \cdots K\}$).

The second method uses the Newton Raphson formulation of the load flow calculation to directly infer the voltage sensitivity coefficients as sub-matrices of the inverted Jacobian matrix (e.g., [75, 76, 77, 78, 79]):

$$J = \begin{bmatrix} \frac{\partial \mathbf{P}}{\partial |\bar{\mathbf{E}}|} & \frac{\partial \mathbf{P}}{\partial \boldsymbol{\theta}} \\ \frac{\partial \mathbf{Q}}{\partial |\bar{\mathbf{E}}|} & \frac{\partial \mathbf{Q}}{\partial \boldsymbol{\theta}} \end{bmatrix}. \quad (3.5)$$

It is worth observing that such a method does not allow to compute the sensitivities against the transformers tap-changers positions. Additionally, as known, the sub-matrix $\frac{\partial \mathbf{Q}}{\partial |\bar{\mathbf{E}}|}$ is usually adopted to express voltage variations as a function of reactive power injections when the ratio of longitudinal line resistance versus reactance is negligible. It is worth noting that such an assumption is no longer applicable to distribution systems that require in addition to take into account active power injections.

A third method is derived from circuit theory. In this method Tellegen's theorem is applied in power networks and the computation of sensitivities relies on the concept of the so-called adjoint networks (e.g., [88, 89, 90, 91, 92]). This approach requires a base-case load flow solution in order to build a specific adjoint network that needs to be solved in order to infer the desired sensitivities.

3.4.2 Analytical Derivation of Sensitivity Coefficients with respect to Nodal Power Injections

This subsection contains the main analytical development related to the derivation of the voltage sensitivity coefficients⁵.

Voltage Sensitivity Coefficients

The analysis starts with the voltage sensitivity coefficients. To this end, we derive mathematical expressions that link bus voltages to bus active and reactive power

⁵As shown later in this subsection the current sensitivities can be straightforwardly derived from the voltage ones.

3.4. Efficient Computation of Sensitivity Coefficients of Node Voltages and Line Currents in Unbalanced Radial Electrical Distribution Networks

injections. For this purpose, a K -bus 3-phase generic electrical network is considered. The following analysis treats each phase of the network separately and, thus, it can be applied to unbalanced networks.

As known, the equations that link the voltage of each phase of the buses to the corresponding injected current are in total $M = 3K$ and they are given by:

$$[\bar{\mathbf{I}}_{\text{abc}}] = [\bar{\mathbf{Y}}_{\text{abc}}] \cdot [\bar{\mathbf{E}}_{\text{abc}}] \quad (3.6)$$

where $[\bar{\mathbf{I}}_{\text{abc}}] = [\bar{I}_a^1, \bar{I}_b^1, \bar{I}_c^1, \dots, \bar{I}_a^K, \bar{I}_b^K, \bar{I}_c^K]^T$, $[\bar{\mathbf{E}}_{\text{abc}}] = [\bar{E}_a^1, \bar{E}_b^1, \bar{E}_c^1, \dots, \bar{E}_a^K, \bar{E}_b^K, \bar{E}_c^K]^T$. We denote by a, b, c the three network phases. The $[\bar{\mathbf{Y}}_{\text{abc}}]$ matrix is formed by using the so-called compound admittance matrix (e.g., [103]) as follows:

$$[\bar{\mathbf{Y}}_{\text{abc}}] = \begin{bmatrix} \bar{Y}_{aa}^{11} & \bar{Y}_{ab}^{11} & \bar{Y}_{ac}^{11} & \dots & \bar{Y}_{aa}^{1K} & \bar{Y}_{ab}^{1K} & \bar{Y}_{ac}^{1K} \\ \bar{Y}_{ba}^{11} & \bar{Y}_{bb}^{11} & \bar{Y}_{bc}^{11} & \dots & \bar{Y}_{ba}^{1K} & \bar{Y}_{bb}^{1K} & \bar{Y}_{bc}^{1K} \\ \bar{Y}_{ca}^{11} & \bar{Y}_{cb}^{11} & \bar{Y}_{cc}^{11} & \dots & \bar{Y}_{ca}^{1K} & \bar{Y}_{cb}^{1K} & \bar{Y}_{cc}^{1K} \\ \vdots & \vdots & \vdots & \vdots & \vdots & \vdots & \vdots \\ \bar{Y}_{aa}^{K1} & \bar{Y}_{ab}^{K1} & \bar{Y}_{ac}^{K1} & \dots & \bar{Y}_{aa}^{KK} & \bar{Y}_{ab}^{KK} & \bar{Y}_{ac}^{KK} \\ \bar{Y}_{ba}^{K1} & \bar{Y}_{bb}^{K1} & \bar{Y}_{bc}^{K1} & \dots & \bar{Y}_{ba}^{KK} & \bar{Y}_{bb}^{KK} & \bar{Y}_{bc}^{KK} \\ \bar{Y}_{ca}^{K1} & \bar{Y}_{cb}^{K1} & \bar{Y}_{cc}^{K1} & \dots & \bar{Y}_{ca}^{KK} & \bar{Y}_{cb}^{KK} & \bar{Y}_{cc}^{KK} \end{bmatrix}.$$

In order to simplify the notation, in what follows we will assume the following correspondences: $[\bar{\mathbf{I}}_{\text{abc}}] = [\bar{I}_1, \dots, \bar{I}_M]^T$, $[\bar{\mathbf{E}}_{\text{abc}}] = [\bar{E}_1, \dots, \bar{E}_M]^T$ and

$$[\bar{\mathbf{Y}}_{\text{abc}}] = \begin{bmatrix} \bar{Y}_{11} & \dots & \bar{Y}_{1M} \\ \vdots & \dots & \vdots \\ \bar{Y}_{1M} & \dots & \bar{Y}_{MM} \end{bmatrix}.$$

For the rest of the analysis we will consider the network as composed by S slack buses and N buses with PQ injections, (i.e., $\{1, 2, \dots, M\} = S \cup N$, with $S \cap N = \emptyset$). The PQ injections are considered constant and independent of the voltage. In this respect, we are assuming that for each separate perturbation of nodal power injections, the other loads/generators do not change their power set-points. Therefore, the computation of the sensitivities inherently accounts for the whole response of the network in terms of variation of both active and reactive power flows. Such a consequence allows to compute the sensitivities in the close vicinity of the network state.

The link between power injections and bus voltages reads:

$$\underline{S}_i = \underline{E}_i \sum_{j \in S \cup N} \bar{Y}_{ij} \bar{E}_j \quad , i \in N. \quad (3.7)$$

The derived system of equations (3.7) holds for all the phases of each bus of the network. Since the objective is to calculate the partial derivatives of the voltage magnitude over the active and reactive power injected in the other buses, we have to consider separately

the slack bus of the system. As known, the assumptions for the slack bus equations are to keep its voltage constant and equal to the network rated value, by also fixing its phase equal to zero. Hence, for the three phases of the slack bus, it holds that:

$$\frac{\partial \bar{E}_i}{\partial P_l} = 0, \forall i \in \mathcal{S}. \quad (3.8)$$

At this point, by using equation (3.7) as a starting point one can derive closed-form mathematical expressions to define and quantify voltage sensitivity coefficients with respect to active and reactive power variations in correspondence of the N buses of the network. To derive voltage sensitivity coefficients, the partial derivatives of the voltages with respect to the active and reactive power P_l and Q_l of a bus $l \in \mathcal{N}$ have to be computed. The partial derivatives with respect to active power satisfy the following system of equations:

$$\mathbb{1}_{\{i=l\}} = \frac{\partial \underline{E}_i}{\partial P_l} \sum_{j \in \mathcal{S} \cup \mathcal{N}} \bar{Y}_{ij} \bar{E}_j + \underline{E}_i \sum_{j \in \mathcal{N}} \bar{Y}_{ij} \frac{\partial \bar{E}_j}{\partial P_l} \quad (3.9)$$

where it has been taken into account that:

$$\frac{\partial \underline{S}_i}{\partial P_l} = \frac{\partial \{P_i - jQ_i\}}{\partial P_l} = \mathbb{1}_{\{i=l\}}. \quad (3.10)$$

The system of equations (3.9) is not linear over complex numbers, but it is linear with respect to $\frac{\partial \bar{E}_i}{\partial P_l}, \frac{\partial \underline{E}_i}{\partial P_l}$, therefore it is linear over real numbers with respect to rectangular coordinates. As we show next, it has a unique solution for radial networks and can therefore be used to compute the partial derivatives in rectangular coordinates to reduce the computational effort.

A similar system of equations holds for the sensitivity coefficients with respect to the injected reactive power Q_l . With the same reasoning, by taking into account that:

$$\frac{\partial \underline{S}_i}{\partial Q_l} = \frac{\partial \{P_i - jQ_i\}}{\partial Q_l} = -j\mathbb{1}_{\{i=l\}} \quad (3.11)$$

we obtain that:

$$-j\mathbb{1}_{\{i=l\}} = \frac{\partial \underline{E}_i}{\partial Q_l} \sum_{j \in \mathcal{S} \cup \mathcal{N}} \bar{Y}_{ij} \bar{E}_j + \underline{E}_i \sum_{j \in \mathcal{N}} \bar{Y}_{ij} \frac{\partial \bar{E}_j}{\partial Q_l}. \quad (3.12)$$

By observing the above linear systems of equations (3.9) and (3.12), we can see that the matrix that needs to be inverted in order to solve the system is fixed independently of the power of the l -th bus with respect to which we want to compute the partial derivatives. The only element that changes is the left hand side of the equations.

Once $\frac{\partial \bar{E}_i}{\partial P_l}, \frac{\partial \underline{E}_i}{\partial P_l}$ are obtained, the partial derivatives of the voltage magnitude can be

3.4. Efficient Computation of Sensitivity Coefficients of Node Voltages and Line Currents in Unbalanced Radial Electrical Distribution Networks

expressed as:

$$\frac{\partial |\bar{E}_i|}{\partial P_l} = \frac{1}{|\bar{E}_i|} \text{Re}(\bar{E}_i \frac{\partial \bar{E}_i}{\partial P_l}) \quad (3.13)$$

and similar equations hold for derivatives with respect to reactive power injections.

Theorem 1. *The system of equations (3.9), where l is fixed and the unknowns are $\frac{\partial \bar{E}_i}{\partial P_l}$, $i \in \mathcal{N}$, has a unique solution for every radial electrical network. The same holds for the system of equations (3.12), where the unknowns are $\frac{\partial \bar{E}_i}{\partial Q_l}$, $i \in \mathcal{N}$.*

Proof. Since the system is linear with respect to rectangular coordinates and there are as many unknowns as equations, the theorem is equivalent to showing that the corresponding homogeneous system of equations has only the trivial solution. The homogeneous system can be written as:

$$0 = \Delta_i \sum_{j \in \mathcal{S} \cup \mathcal{N}} \bar{Y}_{ij} \bar{E}_j + \bar{E}_i \sum_{j \in \mathcal{N}} \bar{Y}_{ij} \bar{\Delta}_j, \quad \forall i \in \mathcal{N} \quad (3.14)$$

where $\bar{\Delta}_i$ are the unknown complex numbers, defined for $i \in \mathcal{N}$. We want to show that $\bar{\Delta}_i = 0$ for all $i \in \mathcal{N}$. Let us consider two electrical networks with the same topology, i.e., same $[\bar{Y}_{abc}]$ matrix, where the voltages are given. In the first network, the voltages are

$$\begin{aligned} \bar{E}'_i &= \bar{E}_i, & \forall i \in \mathcal{S} \\ \bar{E}'_i &= \bar{E}_i + \bar{\Delta}_i, & \forall i \in \mathcal{N} \end{aligned} \quad (3.15)$$

and in the second network they are

$$\begin{aligned} \bar{E}''_i &= \bar{E}_i, & \forall i \in \mathcal{S} \\ \bar{E}''_i &= \bar{E}_i - \bar{\Delta}_i, & \forall i \in \mathcal{N} \end{aligned} \quad (3.16)$$

Let \underline{S}'_i be the conjugate of the absorbed/injected power at the i th bus in the first network, and \underline{S}''_i in the second. Apply equation (3.7) to bus $i \in \mathcal{N}$ in the first network:

$$\begin{aligned} \underline{S}'_i &= \bar{E}'_i \sum_{j \in \mathcal{S} \cup \mathcal{N}} \bar{Y}_{ij} \bar{E}'_j \\ &= (\bar{E}_i + \Delta_i) \left(\sum_{j \in \mathcal{S}} \bar{Y}_{ij} \bar{E}_j + \sum_{j \in \mathcal{N}} \bar{Y}_{ij} (\bar{E}_j + \bar{\Delta}_j) \right) \\ &= \bar{E}_i \sum_{j \in \mathcal{S} \cup \mathcal{N}} \bar{Y}_{ij} \bar{E}_j + \Delta_i \sum_{j \in \mathcal{N}} \bar{Y}_{ij} \bar{\Delta}_j \\ &\quad + \Delta_i \sum_{j \in \mathcal{S} \cup \mathcal{N}} \bar{Y}_{ij} \bar{E}_j + \bar{E}_i \sum_{j \in \mathcal{N}} \bar{Y}_{ij} \bar{\Delta}_j \end{aligned}$$

Similarly, for the second network and for all buses $i \in \mathcal{N}$:

$$\begin{aligned} \underline{S}''_i &= \bar{E}_i \sum_{j \in \mathcal{S} \cup \mathcal{N}} \bar{Y}_{ij} \bar{E}_j + \Delta_i \sum_{j \in \mathcal{N}} \bar{Y}_{ij} \bar{\Delta}_j \\ &\quad - \Delta_i \sum_{j \in \mathcal{S} \cup \mathcal{N}} \bar{Y}_{ij} \bar{E}_j - \bar{E}_i \sum_{j \in \mathcal{N}} \bar{Y}_{ij} \bar{\Delta}_j \end{aligned}$$

Subtract the last two equations and obtain

$$\underline{S}'_i - \underline{S}''_i = 2 \left(\underline{\Delta}_i \sum_{j \in \mathcal{S} \cup \mathcal{N}} \bar{Y}_{ij} \bar{E}_j + \underline{E}_i \sum_{j \in \mathcal{N}} \bar{Y}_{ij} \bar{\Delta}_j \right)$$

By equation (3.14), it follows that $\underline{S}'_i = \underline{S}''_i$ for all $i \in \mathcal{N}$. Thus, the two networks have the same active and reactive powers at all non-slack buses and the same voltages at all slack buses. As discussed in [104] for radial distribution networks such an assumption means that the load flow problem has a unique solution. Therefore, it follows that the voltage profile of these networks must be exactly the same, i.e., $\bar{E}_i - \bar{\Delta}_i = \bar{E}_i + \bar{\Delta}_i$ for all $i \in \mathcal{N}$ and thus $\bar{\Delta}_i = 0$ for all $i \in \mathcal{N}$. \square

Current Sensitivity Coefficients

From the previous analysis, the sensitivity coefficients linking the power injections to the voltage variations are known. Thus, it is straightforward to express the branch current sensitivities with respect to the same power injections. Assuming to represent the lines that compose the network by means of π models, the current flow \bar{I}_{ij} between nodes i and j can be expressed as a function of the phase-to-ground voltages of the relevant i, j nodes as follows⁶:

$$\bar{I}_{ij} = \bar{Y}_{ij}(\bar{E}_i - \bar{E}_j) \quad (3.17)$$

where \bar{Y}_{ij} is the generic element of $[\bar{\mathbf{Y}}_{\text{abc}}]$ matrix between node i and node j .

Since the voltages can be expressed as a function of the power injections into the network buses, the partial derivatives of the current with respect to the active and reactive power injections in the network can be expressed as:

$$\begin{aligned} \frac{\partial \bar{I}_{ij}}{\partial P_l} &= \bar{Y}_{ij} \left(\frac{\partial \bar{E}_i}{\partial P_l} - \frac{\partial \bar{E}_j}{\partial P_l} \right) \\ \frac{\partial \bar{I}_{ij}}{\partial Q_l} &= \bar{Y}_{ij} \left(\frac{\partial \bar{E}_i}{\partial Q_l} - \frac{\partial \bar{E}_j}{\partial Q_l} \right) \end{aligned} \quad (3.18)$$

Applying the same reasoning as earlier, the branch current sensitivity coefficients with respect to an active power P_l can be computed using the following expressions:

$$\frac{\partial |\bar{I}_{ij}|}{\partial P_l} = \frac{1}{|\bar{I}_{ij}|} \text{Re} \left(\bar{I}_{ij} \frac{\partial \bar{I}_{ij}}{\partial P_l} \right). \quad (3.19)$$

Similar expressions can be derived for the current coefficients with respect to the

⁶Note that the current expressed by (3.17) is the current flow across the longitudinal elements of the network lines. The current flow that includes the shunt capacitances of the lines can be expressed as $\bar{I}_{ij} = \bar{Y}_{ij}(\bar{E}_i - \bar{E}_j) + \bar{Y}_{i0} \bar{E}_i$, where \bar{Y}_{i0} is the shunt element on the receiving end of line $i-j$. In this case, the analysis that follows for the computation of the current sensitivities still holds by modifying accordingly equations 3.18.

3.4. Efficient Computation of Sensitivity Coefficients of Node Voltages and Line Currents in Unbalanced Radial Electrical Distribution Networks

reactive power in the buses as:

$$\frac{\partial |\bar{I}_{ij}|}{\partial Q_l} = \frac{1}{|\bar{I}_{ij}|} \text{Re}(\bar{I}_{ij} \frac{\partial \bar{I}_{ij}}{\partial Q_l}). \quad (3.20)$$

3.4.3 Sensitivity Coefficients with respect to Transformers OLTC

This subsection is devoted to the derivation of analytical expressions for the voltage sensitivity coefficients⁷ with respect to tap positions of a transformer. We assume that transformers tap-changers are located in correspondence of the slack buses of the network as for distribution networks these represent the connections to external transmission or sub-transmission networks. As a consequence, the voltage sensitivities as a function of the tap positions are equivalent to the voltage sensitivities as a function of the slack reference voltage. We assume that the transformers voltage variations due to tap position changes are small enough so that the partial derivatives considered in the following analysis are meaningful. Furthermore, we assume that the power injections at the network buses are constant and independent of the voltage.

With the same reasoning as in Section 3.4.2, the analysis starts in equation (3.7). We write $\bar{E}_\ell = |\bar{E}_\ell|e^{j\theta_\ell}$ for all buses ℓ . For a bus $i \in \mathcal{N}$ the partial derivatives with respect to the voltage magnitude $|\bar{E}_k|$ of a slack bus $k \in \mathcal{S}$ are considered:

$$-\bar{E}_i \bar{Y}_{ik} e^{j\theta_k} = \bar{W}_{ik} \sum_{j \in \mathcal{S} \cup \mathcal{N}} \bar{Y}_{ij} \bar{E}_j + \bar{E}_i \sum_{j \in \mathcal{N}} \bar{Y}_{ij} \bar{W}_{jk}, \quad (3.21)$$

where

$$\bar{W}_{ik} := \frac{\partial \bar{E}_i}{\partial |\bar{E}_k|} = \left(\frac{1}{|\bar{E}_i|} \frac{\partial |\bar{E}_i|}{\partial |\bar{E}_k|} + j \frac{\partial \theta_i}{\partial |\bar{E}_k|} \right) \bar{E}_i, \quad i \in \mathcal{N}.$$

We have taken into account that:

$$\frac{\partial}{\partial |\bar{E}_k|} \sum_{j \in \mathcal{S}} \bar{Y}_{ij} \bar{E}_j = \bar{Y}_{ik} e^{j\theta_k} \quad (3.22)$$

and

$$\frac{\partial \bar{S}_i}{\partial |\bar{E}_k|} = 0. \quad (3.23)$$

The derived system of equations (3.21) is linear with respect to \bar{W}_{ik} and \bar{W}_{jk} , and has the same associated matrix as the system in (3.9). Since the resulting homogeneous system of equations is identical to the one in (3.14), by Theorem 1 it has a unique solution.

After resolution of (3.21), we find that the sensitivity coefficients with respect to

⁷Note that as shown earlier once the voltage sensitivities are obtained, the ones of currents can be computed directly.

the tap position of the transformer at bus k are given by

$$\frac{\partial |\bar{E}_i|}{\partial |\bar{E}_k|} = |\bar{E}_i| \operatorname{Re} \left(\frac{\bar{W}_{ik}}{\bar{E}_i} \right). \quad (3.24)$$

3.4.4 Computational Cost Analysis

The aim of this subsection is to show the computational advantage of the proposed method compared to the classic approach with respect to the computation of voltage sensitivities as a function of power injections only⁸. Furthermore, the two methods are applied to the IEEE 13 and 34 node test feeders and compared in terms of CPU time necessary to calculate the voltage sensitivity coefficients.

We are assuming that:

1. there are loads/injections in all three phases of the system and
2. the phasors of phase-to-ground voltages in all the network are known (e.g., coming from a state estimation process [105]).

Algorithm 1 shows the steps required to calculate the voltage sensitivity coefficients using the traditional method and Algorithm 2 shows the corresponding steps using the analytical method proposed here.

For the traditional method an updated Jacobian needs to be built, and its inverse will provide the desired voltage sensitivities. For the analytical method the corresponding steps refer to inverting a square matrix of size $2N$ (as reported in Section 3.4.2, N refers to the number of network buses with PQ injections) and multiplying the inverse matrix with one column vector for each PQ bus in the network.

Algorithm 1 Computation of voltage sensitivity coefficients using the Jacobian method

- 1: build Jacobian matrix associated to the Newton Raphson method
 - 2: invert matrix J of size $2N \times 2N$
 - 3: extract the sub-matrices corresponding to the desired sensitivity coefficients
-

Algorithm 2 Computation of voltage sensitivity coefficients using the analytical method

- 1: build the matrix of the linear system of equations
 - 2: invert matrix of size $2N \times 2N$
 - 3: do N multiplications of the inverse matrix with vectors of size $2N \times 1$
-

In Table 3.1 the mean CPU time necessary to calculate the voltage sensitivity coefficients is presented for the IEEE 13- and 34-nodes test feeders respectively, when

⁸As already pointed out in Section 3.4.1 traditional Jacobian-based sensitivity computations do not account indeed for the variations of tap-changers.

3.4. Efficient Computation of Sensitivity Coefficients of Node Voltages and Line Currents in Unbalanced Radial Electrical Distribution Networks

Table 3.1: CPU time necessary for calculating voltage sensitivity coefficients in the IEEE 13- and the 34-nodes test feeders when all phases of all buses have loads

	Jacobian	Analytical	ratio
13 bus feeder	28.8 ± 0.18 msec	12.5 ± 0.43 msec	2.34
34 bus feeder	209.8 ± 1.30 msec	83.4 ± 0.59 msec	2.52

1000 iterations of the method are executed. It can be observed that the analytical approach exhibits an improvement of performance which is of 2.34 for the IEEE 13-nodes test feeder and 2.52 for the IEEE 34-nodes test feeder. In the same table the relevant 95% confidence intervals are also reported for the computation of the coefficients for the two benchmark feeders. One can observe the advantage of the proposed analytical method as the number of buses in the network increases. It is worth observing that such an improvement depends not only on the number of buses but also on the network topology (i.e., sparsity of the $[\mathbf{Y}]$ admittance matrix).

3.4.5 Numerical Validation

The numerical validation of the proposed method for the computation of voltage/current sensitivities is performed using two different approaches. In particular, as the inverse of the load flow Jacobian matrix provides the voltage sensitivities, the comparison reported below makes reference to such a method for the voltage sensitivities only. On the contrary, as the inverse of the load flow Jacobian matrix does not provide current sensitivity coefficients, their accuracy is evaluated by using a numerical approach where the load flow problem is solved by applying small injection perturbations into a given network (see Section 3.4.1). A similar approach is deployed to validate the sensitivities with respect to OLTC positions of the transformers, i.e., small perturbations of the voltage magnitude of one phase of the slack bus and solution of the load flow problem. Figure 3.2 shows the IEEE 13-nodes test feeder implemented in the EMTP-RV simulation environment ([106, 107, 108]) adopted to perform the multiphase load flow.

For the sake of brevity we limit the validation of the proposed method to a reduced number of buses exhibiting the largest voltage sensitivity against PQ load/injections. In particular, we refer to the variation of voltages at bus 8 with respect to load/injection at bus 9:

$$\frac{\partial |\bar{E}_8^a|}{\partial P_9^b}, \frac{\partial |\bar{E}_8^b|}{\partial P_9^b}, \frac{\partial |\bar{E}_8^a|}{\partial Q_9^b}, \frac{\partial |\bar{E}_8^b|}{\partial Q_9^b}$$

In Figure 3.3(a) the voltage sensitivity of phase b bus 8 is shown with respect to active power absorption and generation at phase b of bus 9. We assume the convention that positive values of P and Q denote power absorption, whereas negative values correspond to power generation. Figure 3.3(b) shows for the same buses as Figure 3.3(a), the same sensitivity but referring to voltage and power belonging to different phases.

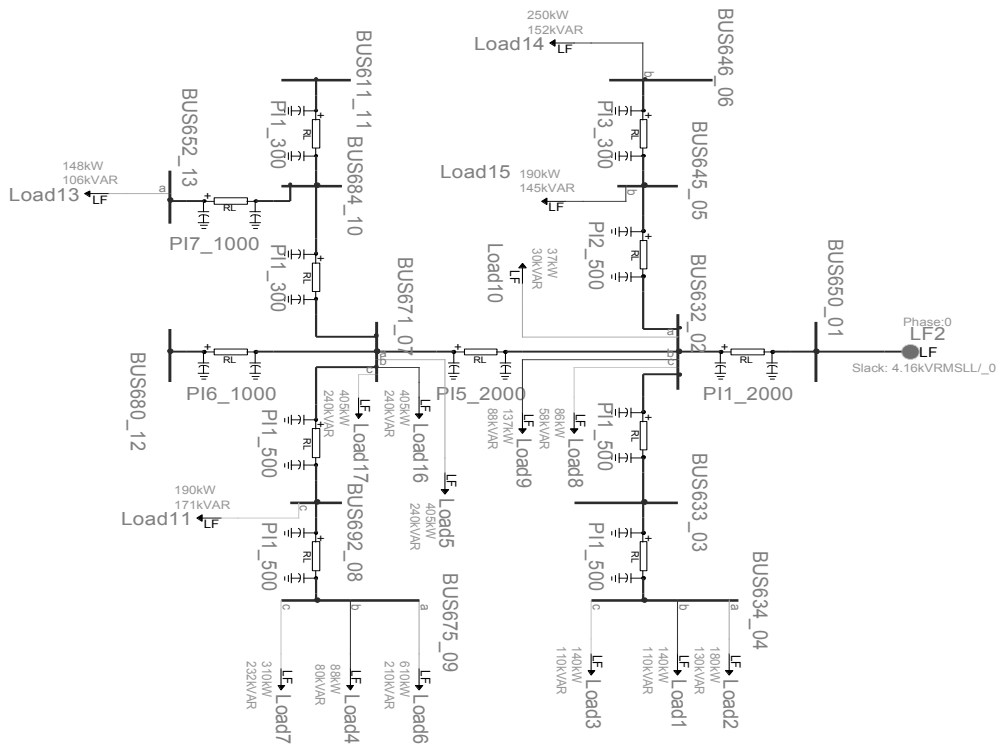


Figure 3.2: IEEE 13-nodes test feeder represented in the EMTP-RV simulation environment.

Additionally, Figure 3.3(c) and 3.3(d) show the voltage sensitivity of bus 8 with respect to reactive power absorption and generation at bus 9. In all these four figures the dashed line represents the relative error between the traditional approach (i.e., based on the inverse of the Jacobian matrix) and the analytical method proposed here. As it can be observed, the overall errors are in the order of magnitude of 10^{-6} .

In Figure 3.4(a) and Figure 3.4(b) the current sensitivity coefficient of phase *a* of branch 10–13 is presented with respect to active and reactive power absorption/generation at phase *a* of bus 13. In the same figures, the dashed lines represent the relative error between the analytical values and the numerical ones. Even for these coefficients extremely low errors are obtained⁹.

Concerning the validation of voltage sensitivities against tap-changer positions, we have made reference to the IEEE 13-nodes test feeder where the slack bus and therefore the primary substation transformer is placed in correspondence of node 1. We assume to vary the slack bus voltage of $\pm 6\%$ over 72 tap positions (where position

⁹Note that the current sensitivities shown in Figures (3.4(a))-(3.4(b)) correspond to the ones expressed in equations (3.18).

3.4. Efficient Computation of Sensitivity Coefficients of Node Voltages and Line Currents in Unbalanced Radial Electrical Distribution Networks

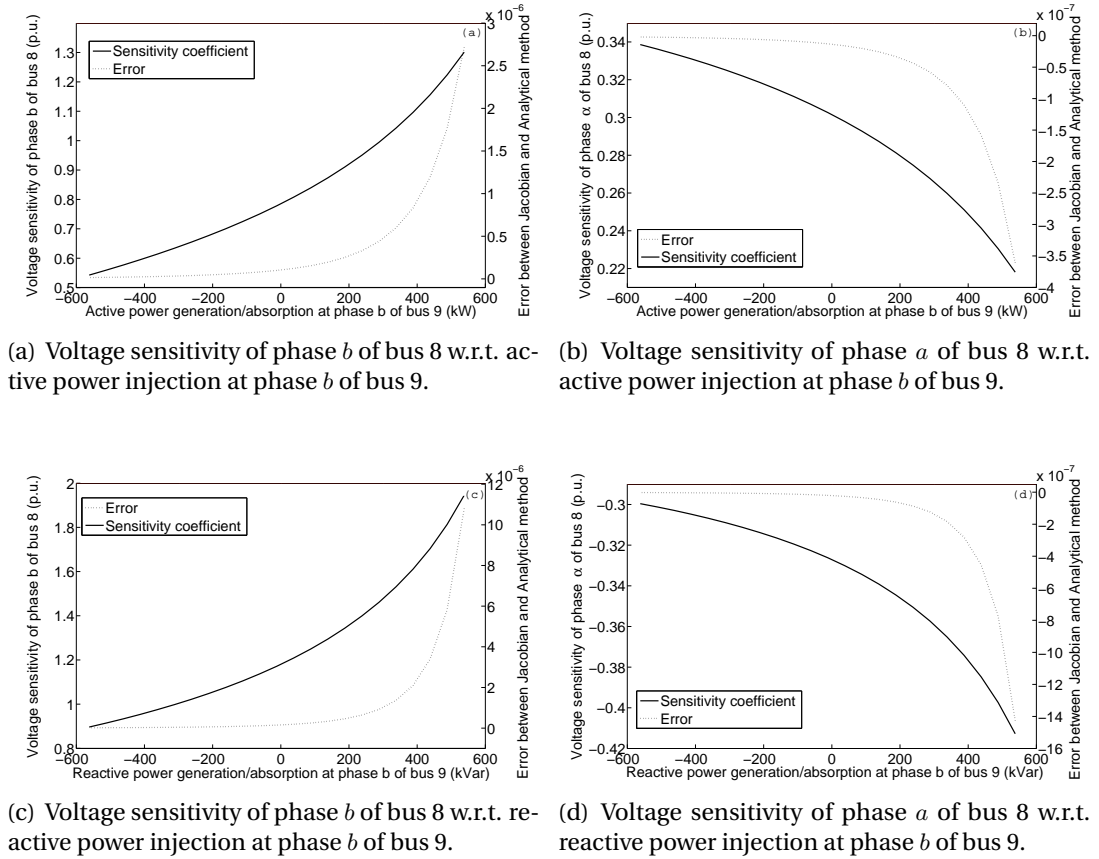


Figure 3.3: Voltage sensitivities of bus 8 as a function of power injections at bus 9.

"0" refers to the network rated voltage). In Figure 3.5 the sensitivity of voltage in phase a of bus 7 is shown w.r.t. the tap positions in phase a , b and c of the slack. Also, in this case the difference between the analytically inferred sensitivities and the numerical computed ones is negligible (i.e., in the order of magnitude of 10^{-4}).

It is worth observing that for the case of the voltage sensitivities, coefficients that refer to the voltage variation as a function of a perturbation (power injection or tap-changer position) of the same phase, show the largest coupling although a non-negligible cross dependency can be observed between different phases.

Finally, Figure 3.6 depicts the variation of voltage sensitivity coefficients in all the network with respect to active and reactive power absorption at phase a of bus 13 as a function of the distance from the slack bus in feet.

This type of representation allows to observe the overall network behavior against specific PQ buses absorptions/injections. In particular, we can see that larger sensitivities are observed when the distance between the considered voltage and the slack bus increases. Furthermore, a lower, but quantified dependency between coefficients re-

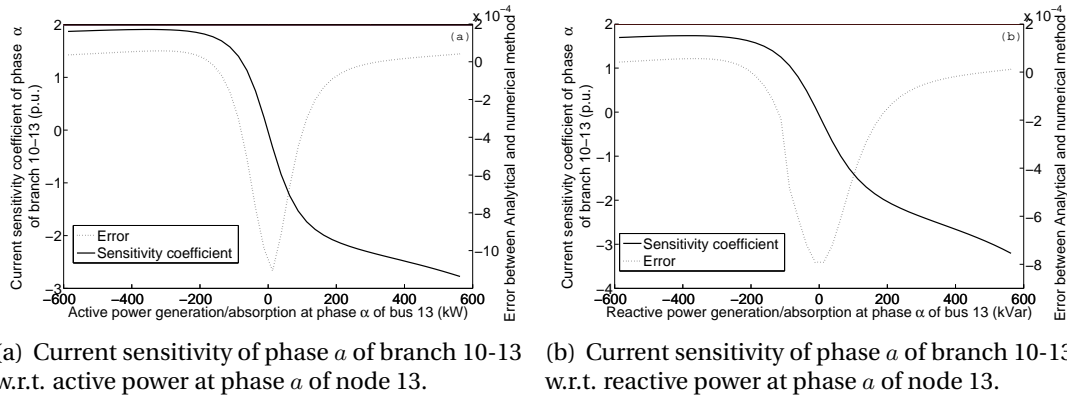


Figure 3.4: Current sensitivity of branch 10-13 as a function of power injections at node 13.

lated to different phases, can be observed. Also, as expected, reactive power has a larger influence on voltage variations although the active power exhibits a non negligible influence.

From the operational point of view it is worth observing that, figures as Figure 3.6, provide to network operators an immediate view of the response of the electrical network against specific loads/injections that could also be used for closed loop control or contingency analysis.

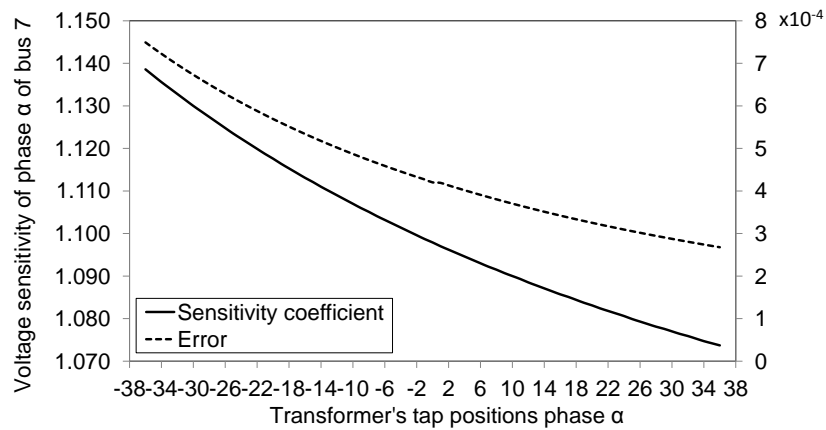
3.5 Application Examples

For the application part, the IEEE 34-nodes test feeder is considered as depicted in Figure 3.7 ([109]). Note that the regulators and shunt-capacitors are excluded to make the network weaker. The network comprises a number of controllable distributed generation units. We consider two different application examples. In the first one, only voltage control is performed by coordinating the DERs' power production with the OLTC positions. In the second one, both voltage control and lines congestion management are included in the optimization problem and the control variables are solely the DERs' active and reactive power production. For both application examples we consider two different test cases, namely one where the DNO can control each phase of the DERs independently of the others and one where the DERs' output is controlled in a balanced way, i.e., all three phases can inject the same amount of power.

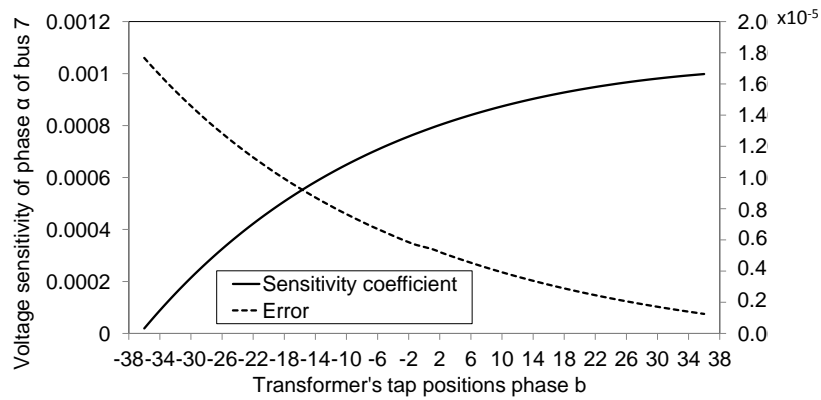
Example 1: In buses 18, 23, 24 and 33 of the IEEE 34-nodes test feeder we assume to have distributed energy resources that the DNO can control in terms of active and reactive power. Their initial operating values, as well as their rated power outputs, are shown in Table 3.2. Furthermore, the DNO has control on the transformer's OLTC positions.

The optimal control problem is formulated as a linearized one taking advantage of

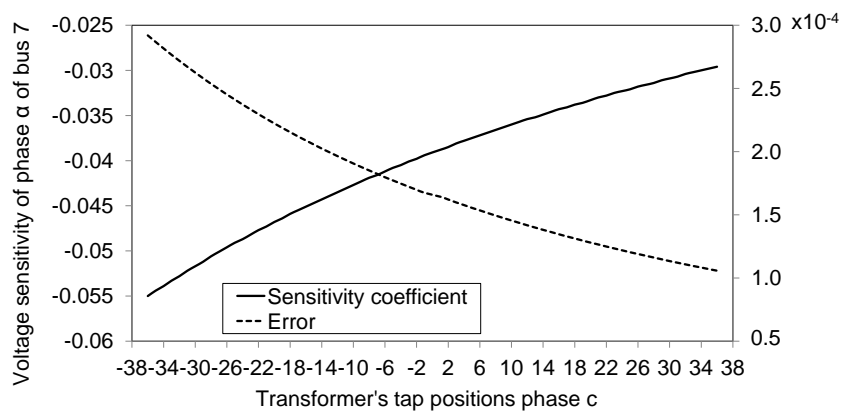
3.5. Application Examples



(a) Voltage sensitivity of phase a of bus 7 w.r.t. OLTC position at phase a of the slack bus.



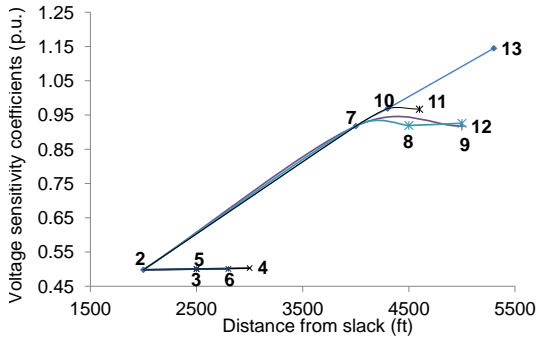
(b) Voltage sensitivity of phase a of bus 7 w.r.t. OLTC position at phase b of the slack bus.



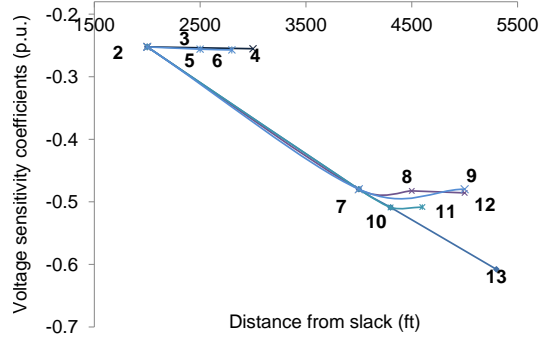
(c) Voltage sensitivity of phase a of bus 7 w.r.t. OLTC position at phase c of the slack bus.

Figure 3.5: Voltage sensitivity of bus 7 as a function of transformer's OLTC positions.

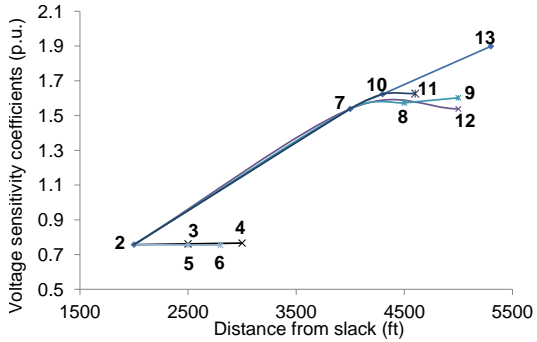
Chapter 3. Centralized and Linearized Control Strategies in ADNs



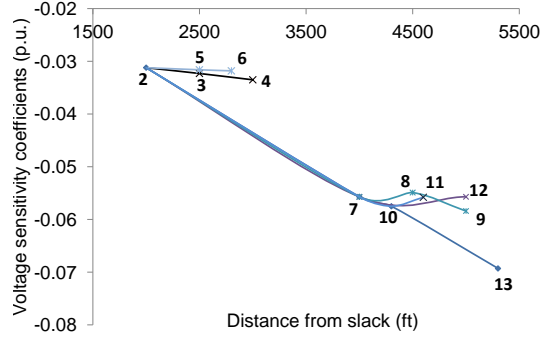
(a) Voltage sensitivities $\frac{\partial |\bar{E}_i^a|}{\partial P_{13}^a}$ w.r.t. active power at phase a of node 13 as a function of the distance from the slack bus.



(b) Voltage sensitivities $\frac{\partial |\bar{E}_i^b|}{\partial P_{13}^a}$ w.r.t. active power at phase a of node 13 as a function of the distance from the slack bus.



(c) Voltage sensitivities $\frac{\partial |\bar{E}_i^a|}{\partial Q_{13}^a}$ w.r.t. reactive power absorption at phase a of node 13 as a function of the distance from the slack bus.



(d) Voltage sensitivities $\frac{\partial |\bar{E}_i^b|}{\partial Q_{13}^a}$ w.r.t. reactive power at phase a of node 13 as a function of the distance from the slack bus.

Figure 3.6: Voltage sensitivities with respect to power absorption at bus 13 as a function of the distance from the slack bus.

the voltage sensitivity coefficients. The controlled variables are the bus node voltages and the control variables are the DER's active and reactive power injections and the OLTC positions under the control of the DNO, $\Delta \mathbf{x} = [\Delta \mathbf{P}_{DER}, \Delta \mathbf{Q}_{DER}, \Delta \mathbf{n}]$. It is important to state that, formally, this problem is a mixed integer optimization problem due to the inclusion of OLTC. However, for reasons of simplicity, in this example, the tap positions are considered pseudo-continuous variables which are rounded to the nearest integer once the optimal solution is reached. The objective of the linear optimization problem considered in this example is essentially the first term of the function in 3.1 with $\delta=0$:

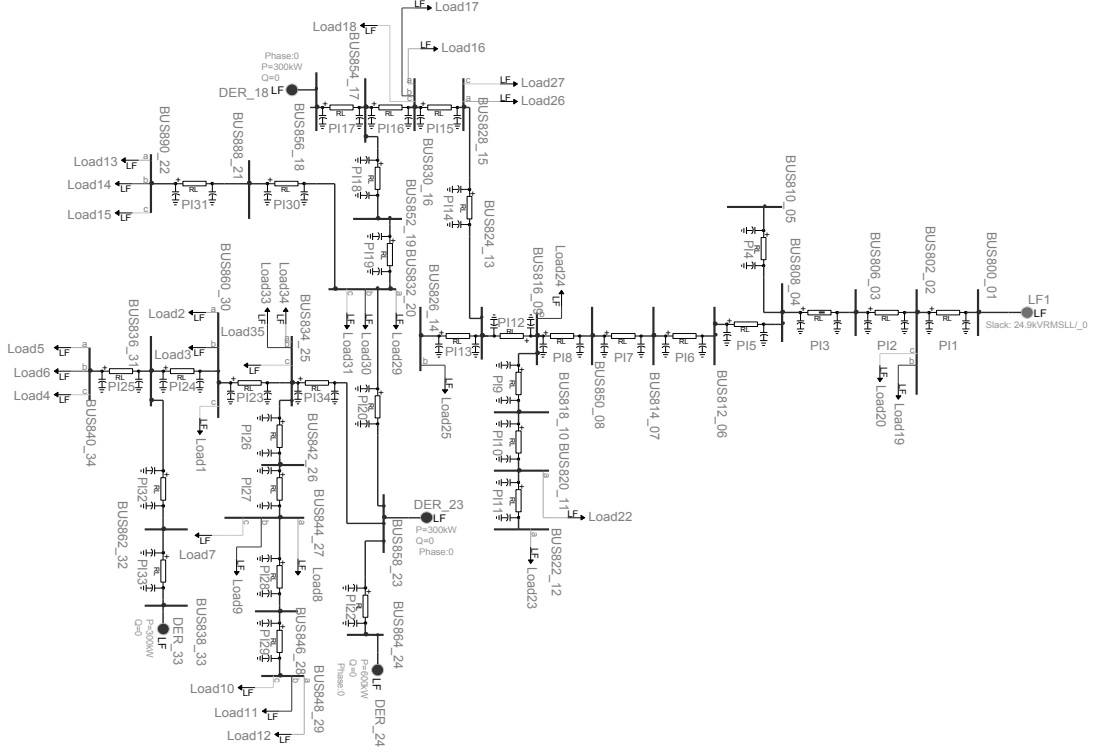


Figure 3.7: IEEE 34 node test feeder represented in the EMTP-RV simulation environment.

$$\min_{\Delta(\mathbf{P}, \mathbf{Q}, \mathbf{n})} \sum_i [(|\bar{E}_i(t)| + (\mathbf{K}_{\mathbf{P}, \mathbf{Q}, \mathbf{n}}(t) \Delta(\mathbf{P}, \mathbf{Q}, \mathbf{n}))_i - |E_o|)^2] \quad (3.25)$$

The imposed constraints on the operational points of the DERs and the OLTC positions are the following:

$$\begin{aligned} 0 &\leq P_{DER_i} \leq P_{DER_{i,max}} \\ Q_{DER_{i,min}} &\leq Q_{DER_i} \leq Q_{DER_{i,max}} \\ n_{min} &\leq n \leq n_{max} \end{aligned} \quad (3.26)$$

In order to simplify the analysis, we have assumed that the DER capability curves are rectangular ones in the PQ plane.

The formulated linearized problem is solved by using the linear least squares method. The method used to calculate analytically the sensitivity coefficients allows us to consider two different optimization scenarios. In the first (opt_1), the operator

Table 3.2: Initial and maximum operational set-points of the DERs and the OLTC in the 34-nodes test feeder

	P_{init} (kW)	P_{max} (kW)	n_{init}	n_{min}	n_{max}
DER ₁₈	210	300	0	-36	+36
DER ₂₃	100	600			
DER ₂₄	250	600			
DER ₃₃	150	300			

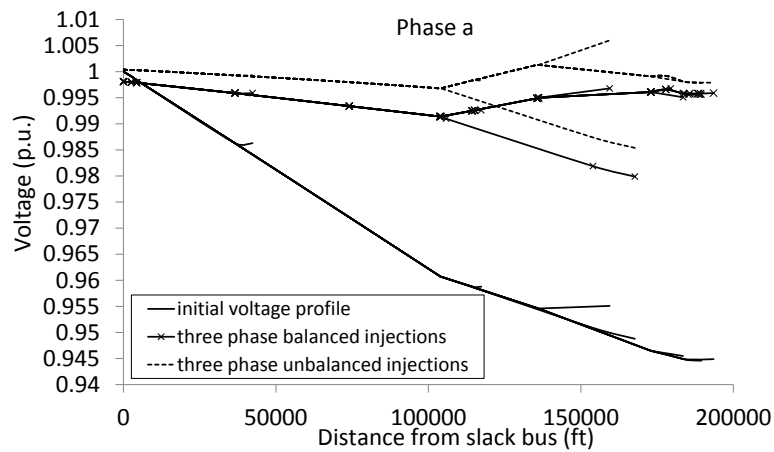
Table 3.3: Optimal operational set-points of the DERs and the tap-changers in the 34-nodes test feeder when the system operator has control on their 3-phase output

	P_{opt_1} (kW)	Q_{opt_1} (kvar)	n_{opt_1}
DER ₁₈	300	300	-2
DER ₂₃	600	600	
DER ₂₄	600	264.06	
DER ₃₃	300	-14.46	

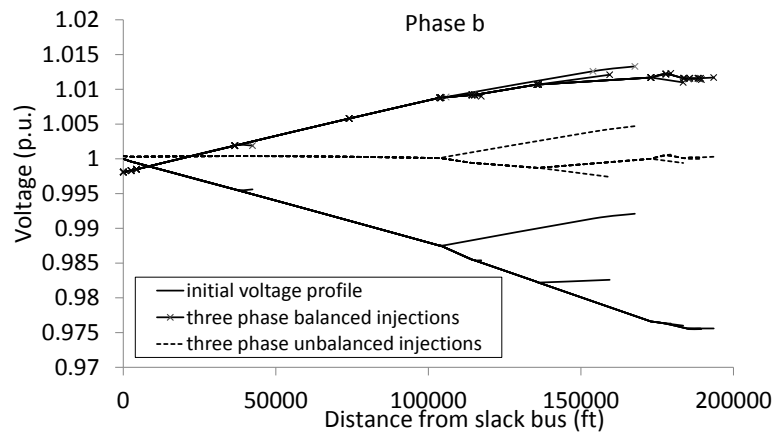
of the system is assumed to control the set-points of the DERs considering that they are injecting equal power into the three phases, whereas in the second case (opt_2) it is assumed to have a more sophisticated control on each of the phases independently except for the tap-changers positions. It is worth noting that this second option, although still far from a realistic implementation, allows us to show the capability of the proposed method to deal with the inherent unbalanced nature of distribution networks. Table 3.3 and Table 3.4 show the optimal operational set-points corresponding to these cases.

Additionally, in Figure 3.8 the voltage profile of the buses of the system is presented in the initial and the optimal cases. The solid line in the figures shows the initial voltage profile, the solid line with the markers shows the first case optimal scenario (opt_1) and the dashed line represents the second case where the DNO has full control in each of the phases of the DERS (opt_2). The offset in the graphs, observed in the slack bus, depicts the optimal OLTC position in each case. What can be observed is that, when there is a possibility to control each of the three phases of the DERs output, the optimal voltage profile is better than the one corresponding to control of the balanced 3-phase output of the set-points of the DERs.

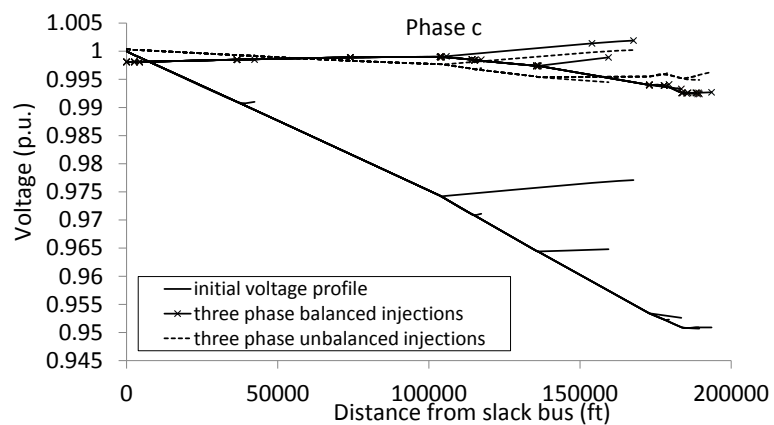
Example 2: We consider once again the IEEE 34-nodes test feeder equipped with 6 generators, with a maximum three-phase power of 900 kW, located in buses 4, 9, 14, 18, 24, and 34. In this example we assume that the OLTCs are not controllable and are set to position “0”. Both voltage control and lines congestion management are



(a) IEEE 34-nodes test feeder - Voltage profile of phase *a* of the buses.



(b) IEEE 34-nodes test feeder - Voltage profile of phase *b* of the buses.



(c) IEEE 34-nodes test feeder - Voltage profile of phase *c* of the buses.

Figure 3.8: Initial and optimized voltage profile of the IEEE 34-nodes test feeder. 41

Table 3.4: Optimal operational set-points of the DERs and the tap-changers in the 34-nodes test feeder when the system operator has control on each of the three phases independently

	P_{opt_2} (kW)	Q_{opt_2} (kvar)	n_{opt_2}
DER ₁₈ ^a	100	100	+1
DER ₁₈ ^b	100	-88.56	
DER ₁₈ ^c	0	83	
DER ₂₃ ^a	200	200	
DER ₂₃ ^b	200	200	
DER ₂₃ ^c	0	200	
DER ₂₄ ^a	200	102.81	
DER ₂₄ ^b	196.51	200	
DER ₂₄ ^c	111.40	200	
DER ₃₃ ^a	100	-27.88	
DER ₃₃ ^b	100	100	
DER ₃₃ ^c	98.40	100	

taken into account. Consequently, the following objective function is considered:

$$\min_{\Delta(\mathbf{P}, \mathbf{Q})} \sum_i \lambda_i [(|\bar{E}_i(t)| + (\mathbf{K}_{\mathbf{P}, \mathbf{Q}}(t) \Delta(\mathbf{P}, \mathbf{Q}))_i - |E_o|)^2 - \delta^2]^+ \quad (3.27)$$

$$+ \sum_k \mu_k [(|\bar{I}_k + (\mathbf{H}_{\mathbf{P}, \mathbf{Q}}(t) \Delta(\mathbf{P}, \mathbf{Q}))_k|^2 - \epsilon^2]^+$$

$$\text{subject to: } (P_j, Q_j) \in \mathcal{H}_j, j = 1, \dots, N_{DER} \quad (3.28)$$

$$(3.29)$$

The ampacity of the network lines is fixed to 100A, which is a typical value for lines in distribution networks. The constants δ and ϵ represent the voltage and current thresholds respectively, which define the bounds above which the controller optimizes the voltage and the current flows. In this case $\delta=0.03$ p.u. and $\epsilon=0.8$ p.u. of line ampacities, i.e., only the buses with a voltage below 0.97 p.u. or above 1.03 p.u., and only the lines with a current above 80% of their ampacity value, will be taken into account in the optimization problem. This avoids the minimization of the voltage deviations and the current flows when they are within acceptable limits imposed by DNOs.

The loads are unbalanced, and the total load profile of the network is depicted in Figure 3.9 in terms of 24hr active and reactive power injections for each phase. As it can be observed from Figure 3.9, the three phases are loaded in an unbalanced way. Figure 3.10 shows the generators' scheduling when no voltage and lines congestion control action is applied. In this case we have considered that the generators inject the same amount of power per-phase (balanced injection). Therefore, for the sake of brevity, Figure 3.10 shows only the injected power of phase *a*.

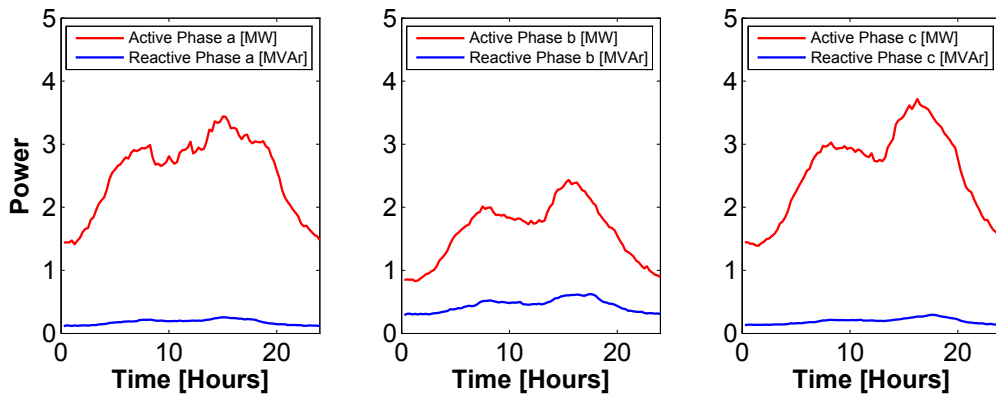


Figure 3.9: Total daily load profile in the network.

We have considered two different test cases for the settings of each of the six generators that are present in the network. In the first case (Case A) each generator is equipped with a traditional transformer that can control the 3-phase output of the DG (balanced control). Their overall output is assumed to have a rectangular capability curve with 0.95 lag-to-lead range. For the second case (Case B) a smart transformer interfaces each generator with the network which allows the per-phase control of the output power of the DG units. Additionally, the smart transformer output is assumed to have a triangular capability curve as depicted in Figure 3.11. The maximum range varies between 0.95p.u. lag and 0.925p.u. lead, as suggested in [110] for photovoltaic and wind power plants in MV installations in Germany. In both test

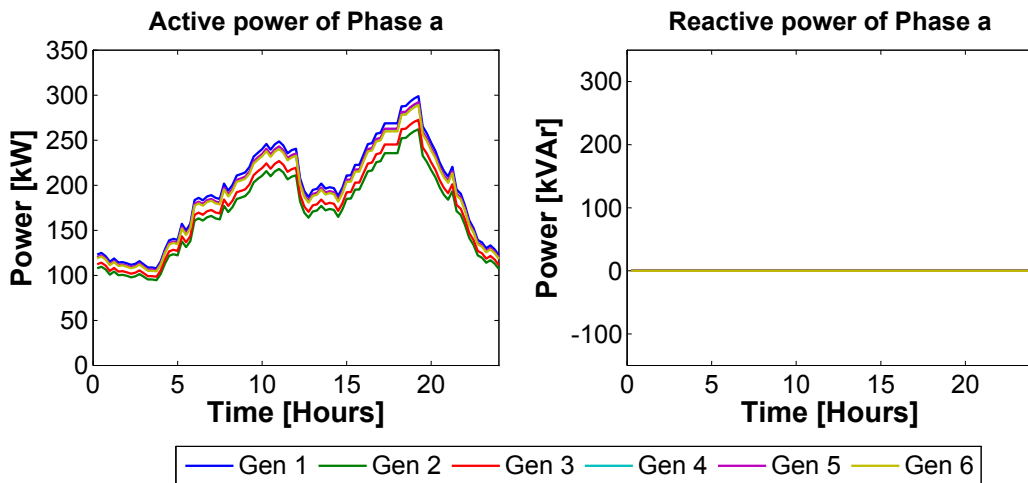


Figure 3.10: Total daily generators scheduling.

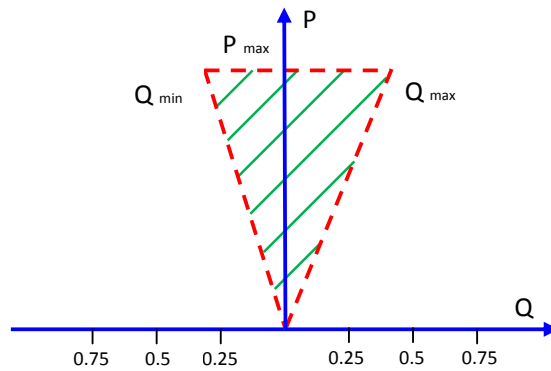


Figure 3.11: Test Case B capability curve of the generators adopted from [110].

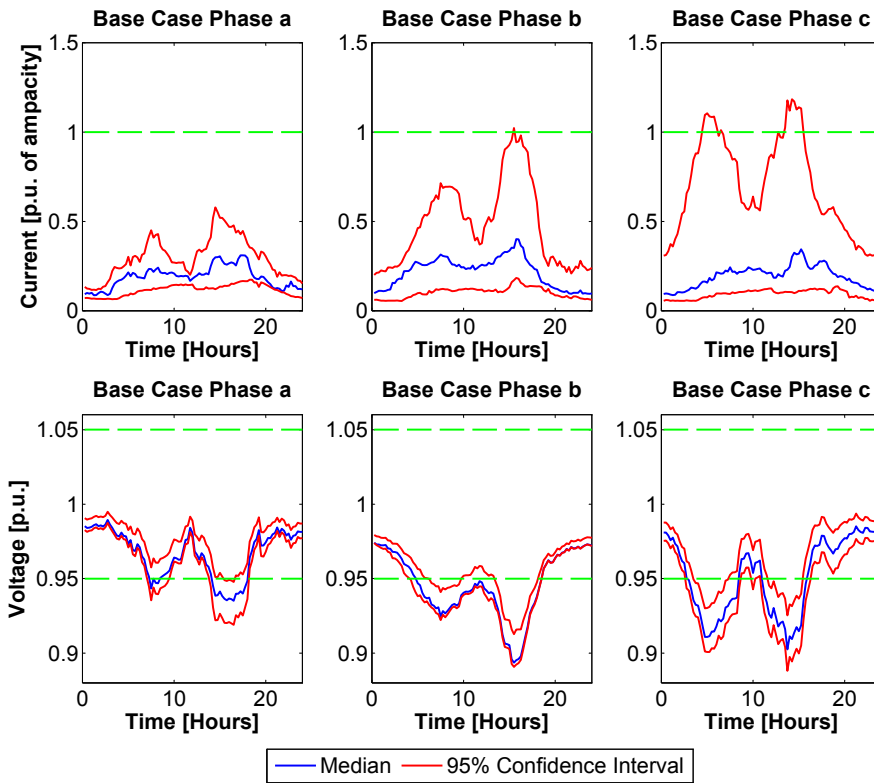


Figure 3.12: Base case 24hr per-phase current and voltage profiles (median and 95% confidence intervals).

cases the transformers' size is 1.5MVA.

The DNO performs voltage and lines congestion management by scheduling the DG units available in the network. We show in Figure 3.12 the per-phase network current and voltage profiles, for the base-case load and generators' profiles shown in Figure 3.9 and Figure 3.10.

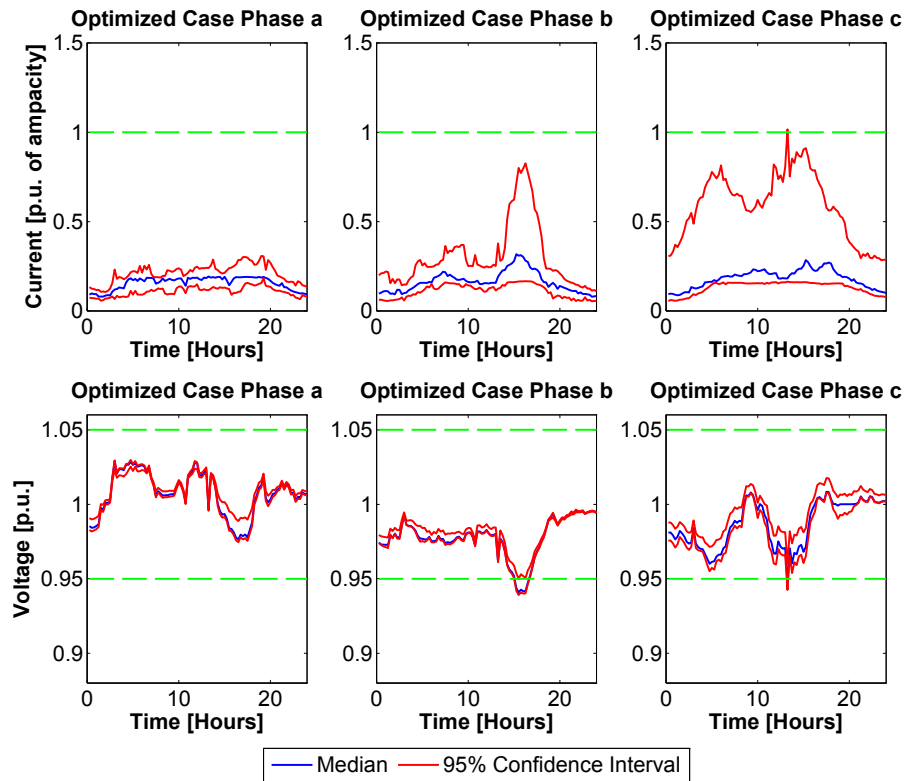


Figure 3.13: Test Case A 24hr per-phase current and voltage profiles (median and 95% confidence intervals).

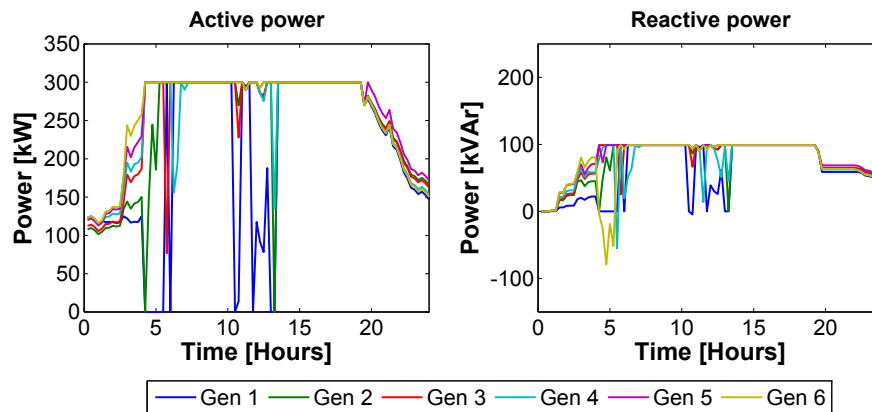


Figure 3.14: Test Case A 24hr generators' active and reactive power scheduling.

For the sake of brevity we show in blue the median of the voltage and current values of the network nodes and lines respectively, and in red lines the corresponding 95% confidence intervals. The light green dashed lines represent the voltage, as well as the current limits. For the voltage, these limits are ± 0.05 p.u. of the network voltage

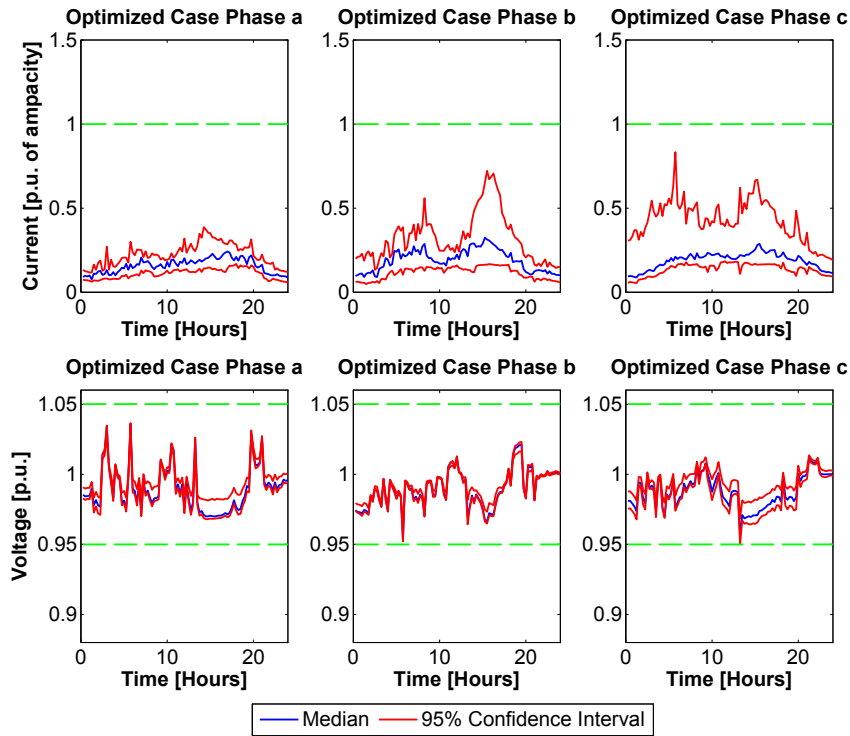


Figure 3.15: Test Case B 24hr per-phase current and voltage profiles (median and 95% confidence intervals).

rated value and for the current, 1p.u. of the line ampacity. Due to the heavy loading of the network there are periods during the day when both the voltage and the current profiles exceed the allowed limits.

In order to avoid a possible curtailment of the load the DNO is forced to re-dispatch the generators. In Case A the DNO uses a traditional transformer interfaced with the generators, and thus the generators inject the same amount of power per phase. For this case, Figure 3.13 shows the resulting network current and voltage profiles.

As it can be observed, the proposed algorithm improves the voltage and current profiles in the network, particularly in phase *a*, but the control action is not sufficient to manage efficiently the voltage control and current congestion management in phases *b* and *c*, due to the balanced control of the generators' output. The corresponding scheduling of the generators' active and reactive power injections for the same test case is shown in Figure 3.14.

Figure 3.14 shows that the active and reactive powers are almost saturated for all six generators almost throughout the 24hr period. This is explained by the fact that even though not all phases are equally loaded, the algorithm is forced to adapt the set-points of the generators to phases *b* and *c*.

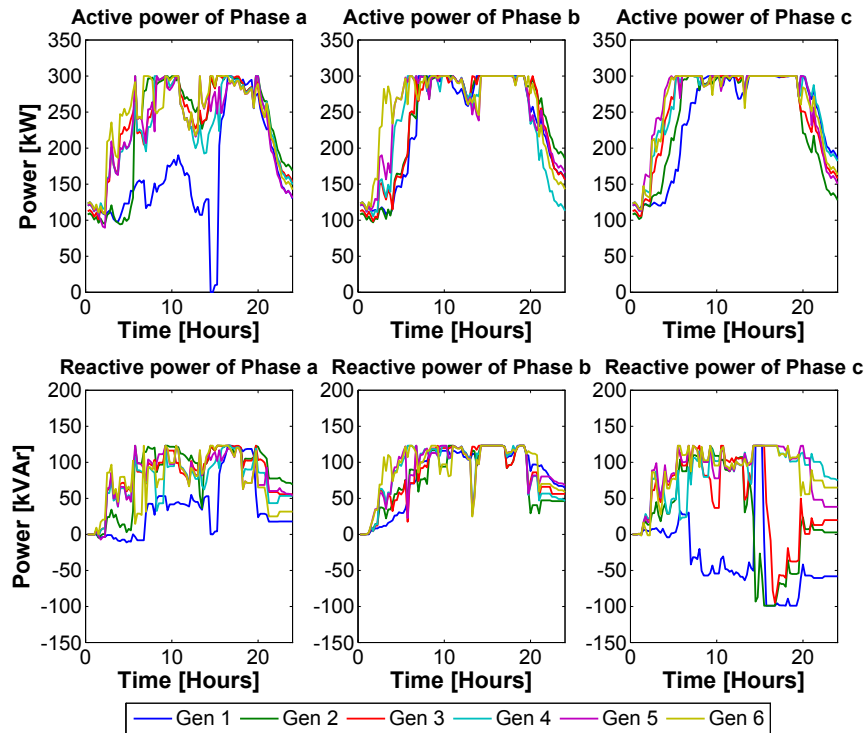


Figure 3.16: Test Case B 24hr generators' active and reactive power scheduling.

In Case B, the DNO deploys a smart transformer to interface the generators with the distribution network. The smart transformer can perform a phase-per-phase control. In this way, the power injection of each phase is scheduled separately throughout the day, independently from the other two phases. Applying the proposed algorithm to this test case, results in the profiles of the network currents and voltages as shown in Figure 3.15. The smart transformer is able to bring the voltage and current profiles of all three phases within the acceptable limits for safe operation.

For the same test case, Figure 3.16 shows the 24hr scheduling of the active and reactive power injections for all six generators. The phase-per-phase control results in different profiles with respect to Case A. As it can be observed, only the active power profiles of phase *b* and *c* are saturated throughout the day. On the contrary, phase *a* requires less power during the day with respect to the traditional transformer case.

Concerning the reactive power profiles, we obtain a significantly different distribution along the three phases. The three phases are less overloaded than in Case A, and the reactive power profiles are not saturated during the day.

3.6 A Robust Optimization Approach to ADNs Control with Uncertain Feeder Parameters

In this section we assume that the network admittance matrix is known with some level of uncertainty and in particular that the feeder parameters vary in a range around their nominal values. We show the effect of an erroneous admittance matrix on the voltage control solution and we formulate the control problem as a robust optimization problem using the framework presented in [111].

3.6.1 The Nominal Control Problem and the Sources of Data Uncertainty

As before, the DNO wishes to schedule the active and reactive power injections of a number, N_{DER} , of controllable DERs present in the network in coordination with the transformers' OLTC. The DNO is assumed to have available nominal values of the feeder parameters that allow the computation of the nominal value of the network admittance matrix, denoted hereafter as \tilde{Y} . Using this information, the DNO can compute, subsequently, the nominal values of the voltage sensitivity coefficients with respect to absorbed/injected power of a bus ℓ where a controllable resource is connected, as well as with respect to the transformer's tap-changers positions $\tilde{K}_{P,il}, \tilde{K}_{Q,il}, \tilde{K}_{n,i}$ for example by solving the linear systems of equations presented in Section 3.4.

At this stage, using the sensitivity coefficients $\tilde{K}_{P,Q,n}$ the DNO can compute the optimal required power adjustments in the buses and the optimal OLTC positions $\{\Delta(P, Q, n)^*\}$ which lead to the desired operation set-point for optimal grid control. In particular, in this section, we formulate the control problem as a linear one as follows:

$$\min_{\Delta(P,Q,n)} \sum_{i,i \neq 1} ||\bar{E}_i| + (\tilde{K}_{P,Q,n} \Delta(P, Q, n))_i - E_0| \quad (3.30)$$

$$\text{subject to: } P_{min_j} \leq P_j \leq P_{max_j}, j = 1, \dots, N_{DER} \quad (3.31)$$

$$- P_j \gamma_j \leq Q_j, j = 1, \dots, N_{DER} \quad (3.32)$$

$$Q_j \leq P_j \gamma_j, j = 1, \dots, N_{DER} \quad (3.33)$$

$$n_{min} \leq n \leq n_{max}, \quad n \in \mathcal{Z} \quad (3.34)$$

where the slack bus (bus 1) is not taken into account in the minimization problem as it is assumed that its voltage is constant, equal to 1 p.u. and is not affected by changes in the loads/injections in the network. Constraints (3.31)-(3.33) represent the capability curves of the controllable resources. In particular, $\gamma_j = \tan(\cos^{-1}(\phi_{min_j}))$. Therefore, for the active power, the limits are represented as upper and lower bounds whereas the reactive power limits are imposed indirectly by assuming a minimum power factor value. The last constraint (3.34) represents the minimum and maximum OLTC positions allowed.

It is worth noting that the problem in (3.30)-(3.34) is a mixed-integer linear pro-

3.6. A Robust Optimization Approach to ADNs Control with Uncertain Feeder Parameters

gramming problem. To eliminate the absolute value in the objective function, we consider slack variables \mathbf{u} such that each $u_i = ||\bar{E}_i| + (\tilde{\mathbf{K}}_{\mathbf{P},\mathbf{Q},\mathbf{n}}(t)\Delta(\mathbf{P}, \mathbf{Q}, \mathbf{n}))_i - E_0|$. Then the problem in (3.30)-(3.34) is equivalent to the following problem:

$$\min_{\Delta(\mathbf{P},\mathbf{Q},\mathbf{n}),\mathbf{u}} \sum_{i,i \neq 1} u_i \quad (3.35)$$

$$\text{subject to: } P_{\min_j} \leq P_j \leq P_{\max_j}, j = 1, \dots, N_{DER} \quad (3.36)$$

$$-P_j \gamma_j \leq Q_j, j = 1, \dots, N_{DER} \quad (3.37)$$

$$Q_j \leq P_j \gamma_j, j = 1, \dots, N_{DER} \quad (3.38)$$

$$n_{\min} \leq n \leq n_{\max}, \quad n \in \mathcal{Z} \quad (3.39)$$

$$u_i \geq |\bar{E}_i| + (\tilde{\mathbf{K}}_{\mathbf{P},\mathbf{Q},\mathbf{n}}\Delta(\mathbf{P}, \mathbf{Q}, \mathbf{n}))_i - E_0, \forall i, i \neq 1 \quad (3.40)$$

$$u_i \geq E_0 - (\tilde{\mathbf{K}}_{\mathbf{P},\mathbf{Q},\mathbf{n}}\Delta(\mathbf{P}, \mathbf{Q}, \mathbf{n}))_i - |\bar{E}_i|, \forall i, i \neq 1 \quad (3.41)$$

When the nominal value of the network admittance matrix $\tilde{\mathbf{Y}}$ coincides with the true one, corresponding to the observed network state \bar{E}_i , then the solution of the problem (3.35)-(3.41) is the accurate optimal active and reactive power set-points, as well as the OLTC adjustments required to minimize the voltage deviations in the network buses. However, there are several cases where the DNO might have erroneous information concerning the data of the feeder parameters, therefore an inaccurate network admittance matrix (e.g., [80, 81]). Additionally, there are factors, such as the temperature that can cause variations on the values of the resistances of the network branches during the day and are not taken into account in the computation of the admittance matrix (e.g., [82]). Such uncertainties in the feeder parameters result eventually in uncertainties in the sensitivity coefficients, as the latter are, essentially, a function of the network admittance matrix and the network state. Such uncertainties, when not taken into account, can lead to wrong computation of the voltage sensitivities and consequently to control decisions that are meaningless for the grid operation.

In this section, the values of the resistances of the network branches are assumed to vary in a range around their nominal values. In particular, the resistance \tilde{R}_k of the k -th branch is considered unknown but bounded, taking values in the interval $[\hat{R}_k - \tilde{R}_k; \tilde{R}_k + \hat{R}_k]$.

This uncertainty in the network branch resistances is reflected to an uncertainty in the values of the sensitivity coefficient matrices, and consequently affects the inequalities (3.40)-(3.41) of the optimal control problem. To be able to obtain uncertainty bounds for the coefficients and validate the performances of the RO formulation, a Monte Carlo simulation is used. Two different loading scenarios are considered in the network, namely heavy loading/low generation and light load/increased generation. For each of the two scenarios the DNO is assumed to know the state of the grid, i.e., the voltage phasors of the network buses. For each network branch, a large number M of variables is drawn for the resistance uniformly from the range $[\hat{R}_k - \tilde{R}_k; \tilde{R}_k + \hat{R}_k]$. Uniform distributions are assumed for the network uncertain parameters since the

operator does not have the means to infer their actual distribution. For each combination of values for the branch parameters, a new admittance matrix is constructed and new values for the sensitivity coefficients can be obtained by solving the linear system in Section 3.4. In the end of the MC simulation, the DNO has available bounds for each of the elements of the sensitivity coefficients matrices, $\tilde{\mathbf{K}}_{\mathbf{P},\mathbf{Q},n}$.

Once these bounds are computed, the goal of the DNO is to obtain a solution to the problem in (3.35)-(3.41) that is guaranteed to satisfy the constraints (3.36)-(3.41) for all possible values of the sensitivity coefficients in the obtained range. The resulting problem is essentially a semi-infinite program. In what follows, we briefly recall the robust counterpart of a generic linear programming problem as described in [84]. In this case, the resulting RO problem is tractable and, in fact, remains linear, and thus extends readily to the case of discrete optimization.

3.6.2 Robust Formulation of Uncertain Linear Programming Problems

One of the important aspects when dealing with RO counterparts of optimization problems is the tractability of the resulting RO problem ([112]). Robust counterparts of linear programs with data exhibiting interval uncertainty are well known since the early seventies (e.g., [113]). While in these early efforts the proposed robust solution remains a linear program, the produced solutions are too conservative, namely the worst-case scenario is always taken into account in the optimization. Later efforts addressed this problem of over-conservatism, by considering ellipsoidal uncertainty for the problem data (e.g., [114]). However, in this case the resulting robust counterparts of the nominal problem are conic quadratic problems. Therefore, the complexity of the problem increases significantly.

In this section, the robust formulation presented in [84, 111] is adopted because the resulting robust problem remains linear and is able to cope with parameter uncertainty without significantly affecting the objective function. Let us consider a generic linear program (LP) with uncertain data:

$$\max_{\mathbf{x}} \mathbf{c}^T \mathbf{x} \tag{3.42}$$

$$\text{subject to: } \mathbf{A} \mathbf{x} \leq \mathbf{b} \tag{3.43}$$

$$\mathbf{lb} \leq \mathbf{x} \leq \mathbf{ub} \tag{3.44}$$

where only the matrix \mathbf{A} exhibits uncertainty. According to [84] in the i -th row of the matrix \mathbf{A} , J_i denotes the set of coefficients that are subject to interval uncertainty. In particular, each entry a_{ij} , $j \in J_i$ is assumed to be a symmetric and bounded variable with values ranging in $[a_{ij} - \hat{a}_{ij}; a_{ij} + \hat{a}_{ij}]$. For every row i , a parameter Γ_i is introduced, not necessarily integer, with $\Gamma \in [0; |J_i|]$. The role of this parameter is to allow a trade-off between the robustness of the proposed method and the conservatism of the solution. Namely, the solution of the RO problem is immunized against all cases that up to Γ_i of the row elements are allowed to change, and one element is allowed to

3.6. A Robust Optimization Approach to ADNs Control with Uncertain Feeder Parameters

change by $\Gamma_i - \lfloor \Gamma_i \rfloor$. This choice is motivated by the fact that not all the coefficients are expected to change and take their worst value, thus, significantly affect the solution. The goal in [84] is to obtain a robust solution that will be feasible deterministically, and moreover, even in cases when more than $\lfloor \Gamma_i \rfloor$ elements change, then the robust solution will be feasible with very high probability. The robust counterpart of this uncertain LP problem turns out to be also a LP problem as follows ([84, 111]):

$$\max_{\mathbf{x}, \mathbf{y}, \mathbf{z}, \mathbf{p}} \mathbf{c}^T \mathbf{x} \quad (3.45)$$

$$\text{subject to: } \sum_j a_{ij} x_j + z_i \Gamma_i + \sum_{j \in J_i} p_{ij} \leq b_i, \forall i \quad (3.46)$$

$$z_i + p_{ij} \geq \hat{a}_{ij} y_j, \forall i, j \in J_i \quad (3.47)$$

$$-y_j \leq x_j \leq y_j, \forall j \quad (3.48)$$

$$-lb_j \leq x_j \leq ub_j, \forall j \quad (3.49)$$

$$p_{ij} \geq 0 \quad (3.50)$$

$$y_j \geq 0 \quad (3.51)$$

$$z_i \geq 0 \quad (3.52)$$

It is worth noting that the targeted RO problem is tractable as it remains a LP problem. However, the size of the robust counterpart is larger due to the introduction of the slack variables $\mathbf{y}, \mathbf{z}, \mathbf{p}$. Furthermore, the formulation extends in a straightforward manner to discrete optimization problems [111].

3.6.3 Robust Counterpart of the Optimal Control Problem

The problem in (3.35)-(3.41) can be readily transformed into the generic form of (3.42)-(3.44). In fact, in our case, the control variables are $\mathbf{x} = [\Delta \mathbf{P}, \Delta \mathbf{Q}, \Delta \mathbf{n}, \mathbf{u}]$. The matrix \mathbf{A} is constructed as follows:

$$\mathbf{A} = \begin{pmatrix} -\gamma \mathbf{1}_{\{N_{DER} \times N_{DER}\}} & -\mathbf{1}_{\{N_{DER} \times N_{DER}\}} & \mathbf{0}_{\{N_{DER} \times N\}} \\ -\gamma \mathbf{1}_{\{N_{DER} \times N_{DER}\}} & \mathbf{1}_{\{N_{DER} \times N_{DER}\}} & \mathbf{0}_{\{N_{DER} \times N\}} \\ \tilde{\mathbf{K}}_{\mathbf{P}, \mathbf{Q}} & \tilde{\mathbf{K}}_{\mathbf{n}} & -\mathbf{1}_{\{N \times N\}} \\ -\tilde{\mathbf{K}}_{\mathbf{P}, \mathbf{Q}} & -\tilde{\mathbf{K}}_{\mathbf{n}} & -\mathbf{1}_{\{N \times N\}} \end{pmatrix}$$

Then, the RHS \mathbf{b} of the inequality constraint in (3.43) is in our case:

$$\mathbf{b} = \begin{pmatrix} \mathbf{Q} + \mathbf{P}\gamma \\ -\mathbf{Q} + \mathbf{P}\gamma \\ \mathbf{E}_0 - |\bar{\mathbf{E}}| \\ |\bar{\mathbf{E}}| - \mathbf{E}_0 \end{pmatrix}$$

Finally, the limits in (3.36) are translated in the upper and lower bounds in (3.44).

It is worth noting that in the control problem of interest only the submatrices $\tilde{\mathbf{K}}_{\mathbf{P}, \mathbf{Q}, \mathbf{n}}$ of matrix \mathbf{A} are subject to uncertainty. Moreover, constraints (3.40)-(3.41) are

affected in the same way by the uncertainty in the sensitivity coefficients.

Once the bounds on the sensitivity coefficients are computed, we can formulate the RO counterpart of the problem in (3.35)-(3.41) using the aforementioned approach. In particular, let us consider that the elements of the matrix $\tilde{\mathbf{K}}_{\mathbf{P},\mathbf{Q},\mathbf{n}}$ are random variables varying in a range $[\tilde{\mathbf{K}}_{\mathbf{P},\mathbf{Q},\mathbf{n}} - \hat{\mathbf{K}}_{\mathbf{P},\mathbf{Q},\mathbf{n}}, \tilde{\mathbf{K}}_{\mathbf{P},\mathbf{Q},\mathbf{n}} + \hat{\mathbf{K}}_{\mathbf{P},\mathbf{Q},\mathbf{n}}]$. Note that the range in which the sensitivities are varying is considered element-wise. Then the RO counterpart of the problem is as follows:

$$\min_{\Delta(\mathbf{P},\mathbf{Q},\mathbf{n}),\mathbf{u},\mathbf{y},\mathbf{z},\mathbf{p}} \sum_{i,i \neq 0} u_i \quad (3.53)$$

$$\text{subject to: } P_{min_j} \leq P_j \leq P_{max_j}, j = 1, \dots, N_{DER} \quad (3.54)$$

$$- P_j \gamma_j \leq Q_j, j = 1, \dots, N_{DER} \quad (3.55)$$

$$Q_j \leq P_j \gamma_j, j = 1, \dots, N_{DER} \quad (3.56)$$

$$n_{min} \leq n \leq n_{max}, \quad n \in \mathcal{Z} \quad (3.57)$$

$$(\tilde{\mathbf{K}}_{\mathbf{P},\mathbf{Q},\mathbf{n}} \Delta(\mathbf{P}, \mathbf{Q}, \mathbf{n}))_i + z_i \Gamma_i + \sum_{j \in J_i} p_{ij} - u_i \leq E_o - E_i, \forall i \quad (3.58)$$

$$- (\tilde{\mathbf{K}}_{\mathbf{P},\mathbf{Q},\mathbf{n}} \Delta(\mathbf{P}, \mathbf{Q}, \mathbf{n}))_i + z_i \Gamma_i + \sum_{j \in J_i} p_{ij} - u_i \leq E_i - E_o, \forall i \quad (3.59)$$

$$- \mathbf{y} \leq \Delta(\mathbf{P}, \mathbf{Q}, \mathbf{n}) \leq \mathbf{y} \quad (3.60)$$

$$z_i + p_{ij} \geq \hat{\mathbf{K}}_{\mathbf{P},\mathbf{Q},\mathbf{n}}(i, j) y_j, \forall i \text{ and } j \in J_i \quad (3.61)$$

$$\mathbf{y}, \mathbf{z}, \mathbf{p} \geq 0 \quad (3.62)$$

In the following section we first show how the data uncertainty affects the optimal solution of the nominal problem and we evaluate the performances of the proposed algorithm using a benchmark network.

3.6.4 Evaluation

Case Study

For the evaluation of the proposed algorithm we have considered a modified IEEE 13-nodes test feeder ([109]). The modifications are: (i) balanced lines, and (iii) lines five times longer to render the network weaker.

In buses 4, 6, and 9 we assume to have distributed energy resources that the DNO can control in terms of active and reactive power. We assume two different test cases. Case I corresponds to a period of the day where the network is overloaded, hence under-voltages occur in the system without any control action and Case II corresponds to a scenario where the generation units produce more than the loads consume, therefore over-voltages occur in the network buses. The DERs' initial operating values, as well as their rated power outputs for both test cases, are shown in Table 3.5. In the same table we report the minimum and maximum allowed OLTC positions. The minimum power factor for all the DERs in both test cases is 0.85. As far as the OLTCs are considered, we

3.6. A Robust Optimization Approach to ADNs Control with Uncertain Feeder Parameters

assume to vary the slack bus voltage of 6% over 72 tap positions (where position "0" refers to the network rated value).

A specific Matlab code has been developed to represent the network model and to formulate and solve the proposed voltage control problem, as well as its robust counterpart. For the solution of the MILP we have used the Matlab solver *intlinprog*.

Table 3.5: Initial and maximum operational set-points of the DERs and OLTC constraints

	$P_{\text{init}}(\text{MW})(\text{I/II})$	$P_{\text{max}}(\text{MW})$	n_{min}	n_{max}
DER ₄	0.5/4.3	5.5	-36	36
DER ₆	0.45/4.5	6		
DER ₈	0.48/3.8	4.5		

Effect of Data Uncertainty on the Optimal Voltage Control Problem

In this paragraph we show how the uncertainties in the feeder parameters can affect the optimal solution of the voltage control problem. To this end we perform the following experiment. We assume a nominal value for the network admittance matrix, \tilde{Y} . We consider specific values of the network loads and generation values as in Table 3.5 for both test cases. Finally, we consider two sets of monitored voltage magnitudes, \tilde{E} , corresponding to \tilde{Y} and the two considered test cases¹⁰.

Using this information we solve the non-robust problem described in (3.35)-(3.41). This provides us with the nominal solution, namely the result of the voltage control problem if no uncertainties are present in the network and the DNO has an accurate knowledge of the feeder parameters. The network voltage profile as a function of the distance from the primary substation for both test cases is shown in Figure 3.17 before (solid line) and after the scheduling of the generation units (solid line with markers). One can observe that the control mechanism is able to decrease the voltage deviations, resulting in an almost flat voltage profile for the network buses. Next, we assume that the DNO continues to observe the same set of monitored voltage magnitudes (solid lines), but this time has an erroneous admittance matrix Y , which is used for the computation of the sensitivity coefficients and the solution of the optimization problem. This erroneous admittance matrix is obtained by assuming that the resistances of only the branches 1–2, 2–7 and 10–13 are different than the nominal ones. The nominal values of the branch resistances, as well as the ones the DNO uses are shown in Table 3.6. The resulting solution of the optimal voltage control problem is shown in Figure 3.17 with the dashed line. It is worth observing that the voltage profile is significantly different than the optimal solution, and also that there are buses that exhibit voltage deviations from the network nominal value that are close

¹⁰To obtain these sets of nominal voltage magnitudes we solve the load flow problem using \tilde{Y} and the given values for the loads and generation.

Table 3.6: Initial and Erroneous Values of the Branch Impedances (p.u.)

	Nominal Resistance	Erroneous Resistance
Branch ₁₋₂	0.0380	0.0053
Branch ₂₋₇	0.0442	0.0061
Branch ₁₀₋₁₃	0.0152	0.0021

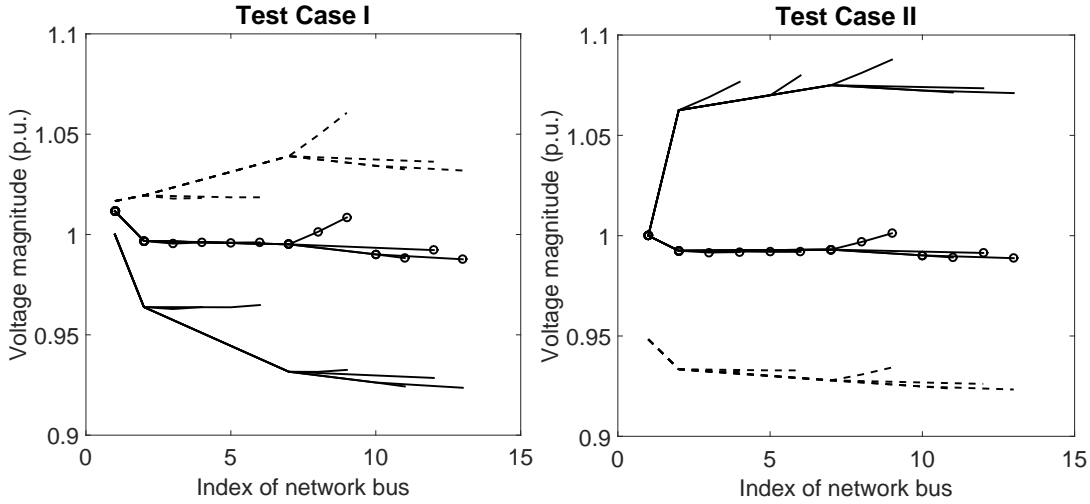


Figure 3.17: Base case network voltage profile (solid line), optimal voltage profile when there is no uncertainty (line with markers) and resulting voltage profile when the DNO has an erroneous admittance matrix (dashed line).

or even violating the allowed limits for safe operation.

The corresponding active and reactive optimal scheduling of the distributed resources, as well as the OLTC positions are shown in Tables 3.7 and 3.8. It is worth noting that, similar to the network voltage profiles, the resulting active and reactive power profiles when the DNO is using the erroneous admittance matrix, are significantly different from the nominal ones, obtained with perfect knowledge of the system model.

From the aforementioned results, it is evident that, in cases where the system model is not accurate, the solution of the voltage control problem can be far away from the optimal, resulting in a non-optimal operation of the grid. Therefore, it is important to immunize the solutions of the optimization problem against uncertainties in the data. In what follows we run a MC simulation to obtain uncertainty bounds on the voltage sensitivities.

Uncertainty Bounds on Voltage Sensitivity Coefficients

In this section, it is assumed that the DNO has available a nominal value of the network admittance matrix. Furthermore, it is assumed that the resistances of the network

3.6. A Robust Optimization Approach to ADNs Control with Uncertain Feeder Parameters

Table 3.7: Operational DERs and OLTC set-points under Correct and Erroneous Y - Case I

	Correct Y			Erroneous Y		
	P(MW)	Q(Mvar)	n	P(MW)	Q(Mvar)	n
DER ₄	0.503	-0.312	7	0.108	0.067	10
DER ₆	0.040	0.025		0	0	
DER ₉	4.500	-1.033		4.500	2.789	

Table 3.8: Operational DERs and OLTC set-points under Correct and Erroneous Y - Case II

	Correct Y			Erroneous Y		
	P(MW)	Q(Mvar)	n	P(MW)	Q(Mvar)	n
DER ₄	0.081	0.050	0	0.016	-0.001	-31
DER ₆	0	0		0	0	
DER ₉	1.637	1.015		2.915	- 1.807	

branches are uncertain and vary in a range around their nominal values. In particular, we consider that the branches 1–2, 2–7 and 10–13 are characterized by an interval uncertainty in the order of 70%, whereas the rest of the network branch impedances exhibit interval uncertainty in the order of 20% around their nominal values. The DNO also observes the network voltage profile (\mathbf{E}^{True}) that corresponds to the true admittance matrix, which is different than the nominal, but contains values in the aforementioned range.

We perform the following MC simulation. For a large number of iterations (10000 in our case), the DNO draws uniformly and independently values for the resistances of the network branches in the ranges mentioned above. For each of these combinations of values a new admittance matrix \mathbf{Y}^{MC} is obtained. Using this matrix, in combination with (\mathbf{E}^{True}), a new matrix of sensitivity coefficients can be obtained for each MC iteration, $\mathbf{K}_{P,Q,n}^{\text{MC}}$. Using these sensitivities, new set-points can be computed as a solution to the problem in (3.35)-(3.41) and a new voltage profile can be obtained after scheduling the DERs' set-points (\mathbf{E}^{MC}). Clearly the obtained voltage profile is not the optimal one for the grid operation as the admittance matrix used in the solution of the optimization problem does not correspond to the true admittance matrix of the network. In the end of the MC simulation, the DNO has available bounds on each entry of the sensitivity coefficients matrix that can be used in the formulation of the RO problem in (3.53)-(3.62). In Figures 3.18 and 3.19 the obtained distributions of the voltage sensitivities are shown for Case I and II respectively. For the sake of brevity we show only the results for the voltage sensitivities with respect to the active power injection of the DER located at bus 9, the reactive power injection of the DER at bus 4 and the OLTC positions. It is worth observing that the obtained bounds for the

sensitivity coefficients with respect to active power injections are significantly larger than the ones with respect to reactive power and OLTC positions.

Additionally, we can perform an assessment of the error that occurs in the network voltage profile when solving the optimization problem using an erroneous admittance matrix. Figure 3.20 shows for Case I the obtained minimum and maximum values of the bus voltages, as well as the uncontrolled true voltage (E^{True}) and the optimal voltage profile when the true admittance matrix is known. Figure 3.21 show the same results for Case II.

At each MC iteration, in addition to the aforementioned quantities, we also use the Y^{MC} matrix to run a load flow and obtain the network state corresponding to this matrix. This allows us to solve the optimization problem and obtain the optimal voltage profile that the DNO would compute if the true admittance matrix was known. In this way we obtain bounds on the actual optimal voltages for this range of branch parameters. Figure 3.22 (3.23) shows for Case I (Case II) the bounds on the voltages of each network bus before any control, as well as after the optimal control when the admittance matrix is known with certainty.

Once the bounds for the sensitivity coefficients are obtained, the robust counterpart of the voltage control problem can be formulated and solved.

Robust Voltage Control Problem

We consider that the DNO has available a nominal admittance matrix, that is not the true one and observes the same voltage profiles E^{True} for the two test cases as before.

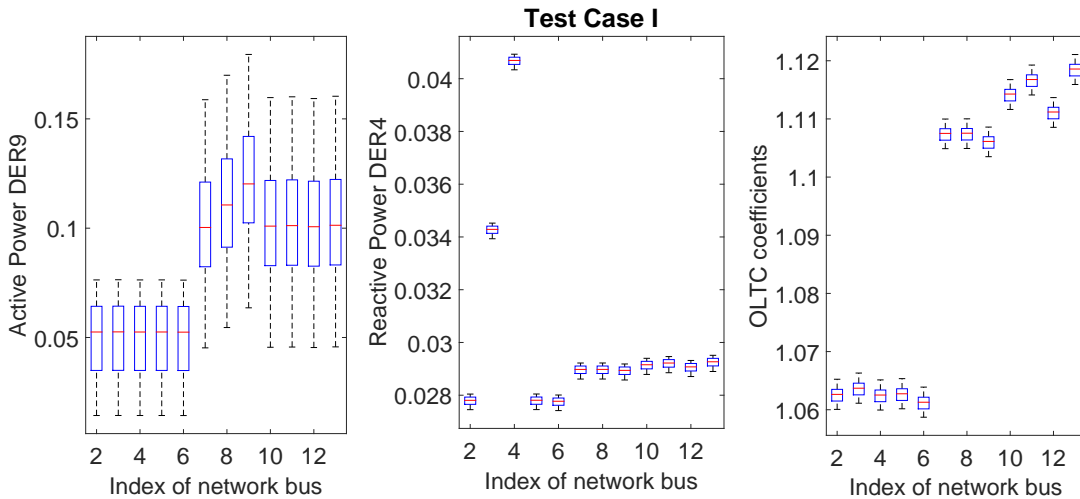


Figure 3.18: Distribution of voltage sensitivity coefficients w.r.t. active power at bus 9, reactive power at bus 4 and OLTC positions when the feeder parameters exhibit interval uncertainty (Case I).

3.6. A Robust Optimization Approach to ADNs Control with Uncertain Feeder Parameters

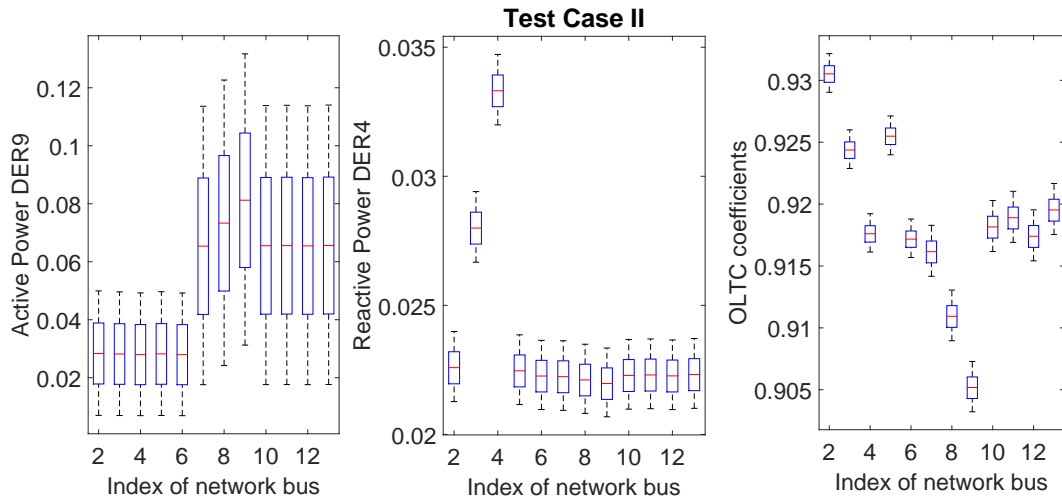


Figure 3.19: Distribution of voltage sensitivity coefficients w.r.t. active power at bus 9, reactive power at bus 4 and OLTC positions when the feeder parameters exhibit interval uncertainty (Case II).

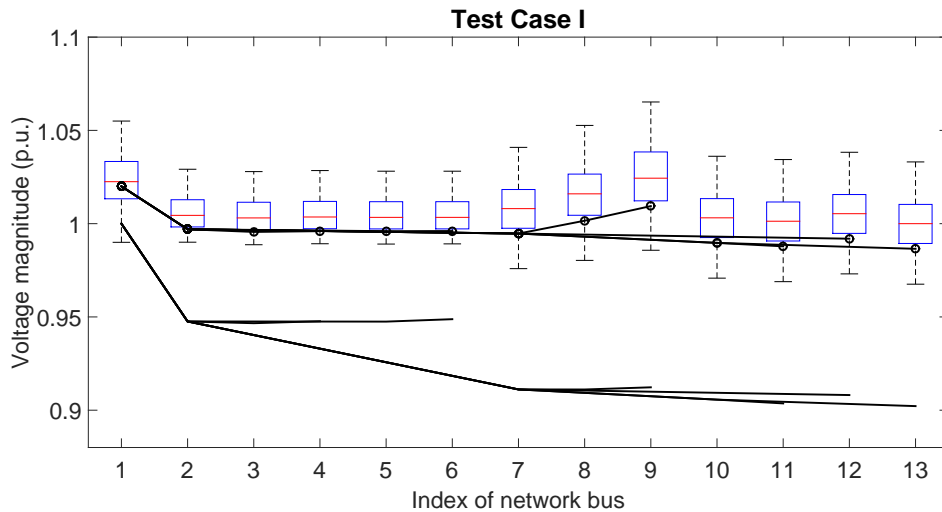


Figure 3.20: Distribution of network voltages when using a wrong admittance matrix (boxplot), uncontrolled observed voltage profile (solid line) and optimal voltage profile when the true admittance matrix is known (line with markers) for Case I.

However, bounds are available for the sensitivity coefficients and the RO problem described in (3.53)-(3.62) is solved instead of the nominal one.

Figures 3.24 and 3.25 show in black solid line the voltage profiles for both test cases obtained as a solution to the RO problem. Also, the optimal solution when the true admittance matrix is known without errors is shown in gray.

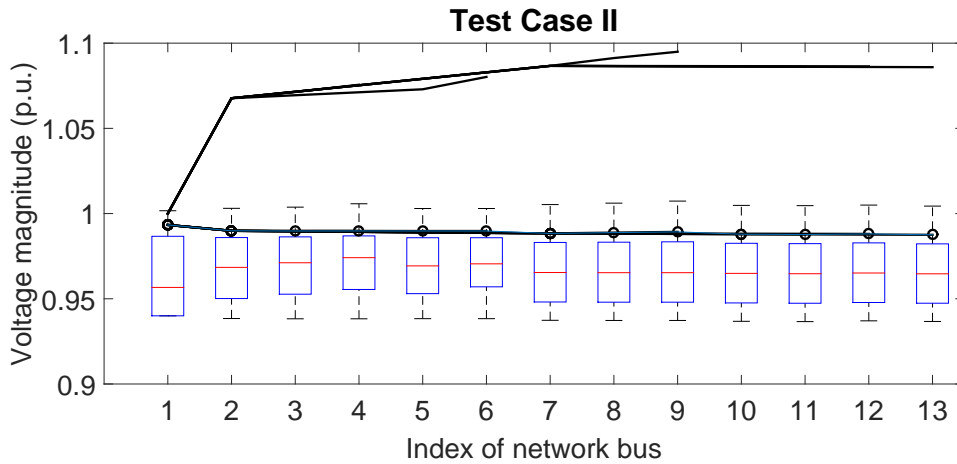


Figure 3.21: Distribution of network voltages when using a wrong admittance matrix (boxplot), uncontrolled observed voltage profile (solid line) and optimal voltage profile when the true admittance matrix is known (line with markers) for Case II.

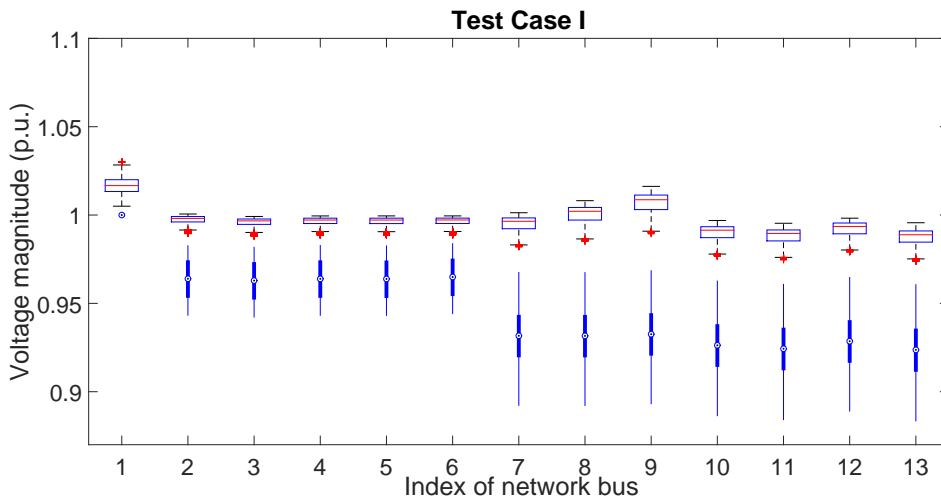


Figure 3.22: Distribution of uncontrolled (boxplot in blue) and optimal network voltages when using the correct admittance matrix (Case I).

For ease of comparison, the results are superposed to the bounds on the uncontrolled and actual optimal voltage profiles for this range of feeder parameters. It is worth observing that the solution of the RO problem is such that the voltage profiles are essentially controlled via scheduling of the OLTCs. This is evident in Figures 3.24 and 3.25 where the voltage of bus 1 (slack bus) after the RO control action takes its minimum (0.94) and maximum (1.06) allowed value. The offset in the voltage of bus 1 is in fact the optimal OLTC position which takes its minimum (-36) and maximum (36)

3.6. A Robust Optimization Approach to ADNs Control with Uncertain Feeder Parameters

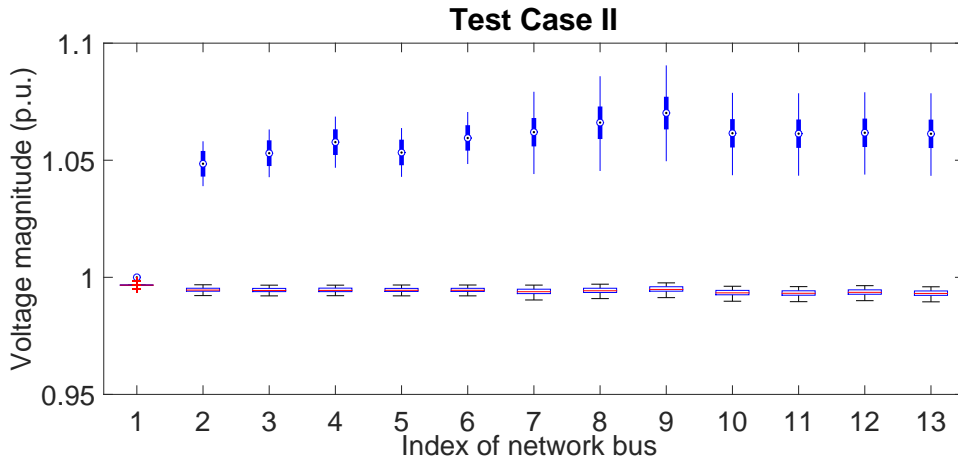


Figure 3.23: Distribution of uncontrolled (boxplot in blue) and optimal network voltages when using the correct admittance matrix (Case II).

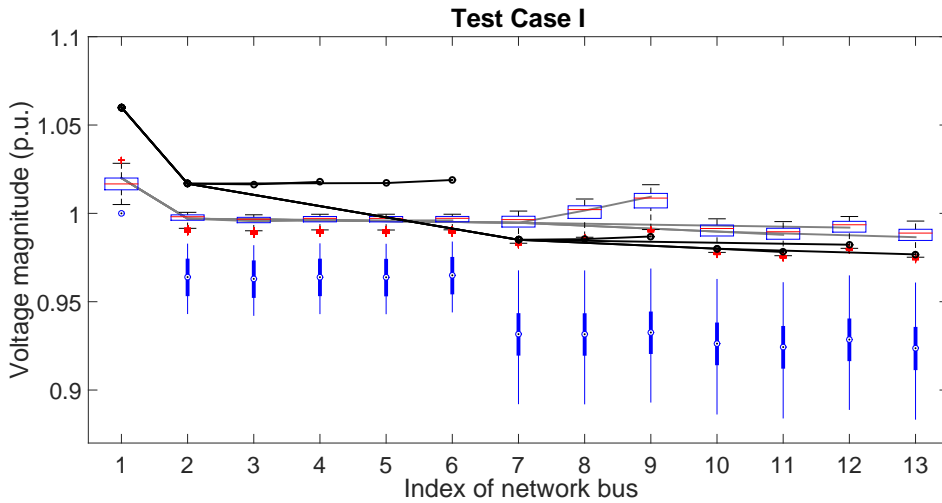


Figure 3.24: Uncontrolled voltage profiles (boxplot in blue) for both test cases, optimal set of voltage profiles when the true admittance matrix is known (boxplot), RO solution (solid line with markers) and optimal solution when the true admittance matrix is known without errors (gray solid line) for Case I.

value respectively. This is a consequence of the fact that the obtained bounds for the sensitivities with respect to OLTCs exhibit small variability. It is worth observing that for both test cases, the result of the RO problem is within acceptable limits for safe grid operation and also much closer to the optimal voltage profile than the solution of the nominal problem with the erroneous admittance matrix.

The DERs set-points and OLTCs positions corresponding to the solution of the RO

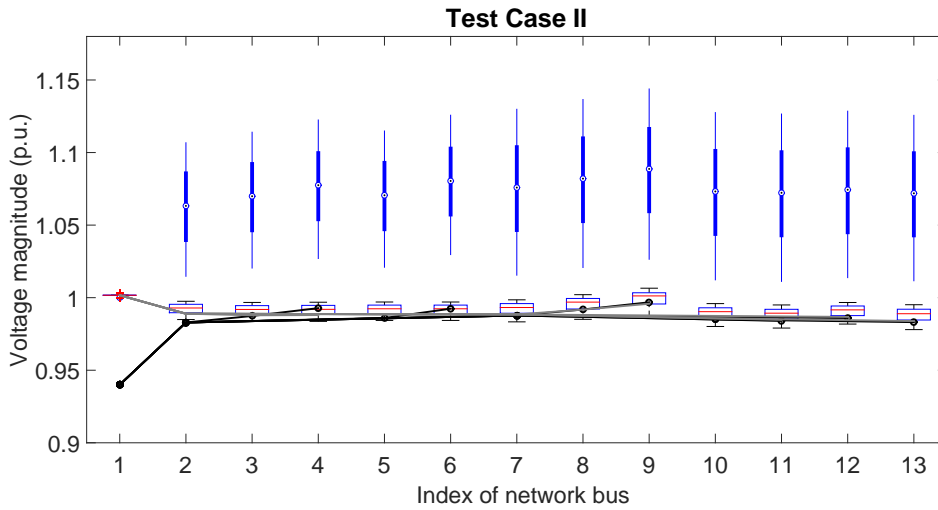


Figure 3.25: Uncontrolled voltage profiles (boxplot in blue) for both test cases, optimal ones when the true admittance matrix is known (boxplot), RO solution (solid line with markers) and optimal solution when the true admittance matrix is known without errors (gray solid line) for Case II.

as well as the solution of the nominal problem using an erroneous admittance matrix are shown in Tables 3.9 and 3.10 respectively. It can be observed that the solutions of the two problems are significantly different.

3.7 Measurement-based Computation of Voltage Sensitivities in Unbalanced Electrical Distribution Networks

In this section we go one step further and we assume that both the grid model and the system state are not known and we propose a method to compute voltage sensitivity coefficients, as they are defined in Section 3.4.2, using measurements only. The method described below is generic and can be applied to the case of unbalanced networks as it treats each phase of the network separately.

Table 3.9: Operational DERs and OLTC set-points for the RO problem and the Nominal Problem with Erroneous Y - Case I

	RO solution			Erroneous Y		
	P(MW)	Q(Mvar)	n	P(MW)	Q(Mvar)	n
DER ₄	0.529	0.328	36	0.170	0.105	15
DER ₆	0.478	0.296		0	0	
DER ₉	0.494	0.306		2.891	1.791	

3.7. Measurement-based Computation of Voltage Sensitivities in Unbalanced Electrical Distribution Networks

Table 3.10: Operational DERs and OLTC set-points for the RO problem and the Nominal Problem with Erroneous Y - Case II

	RO solution			Erroneous Y		
	P(MW)	Q(Mvar)	n	P(MW)	Q(Mvar)	n
DER ₄	4.013	-2.487	-36	0	0	-15
DER ₆	4.231	-2.622		0	0	
DER ₉	3.669	-2.274		0.957	0.593	

3.7.1 Problem Statement

In what follows we rely on the following main hypotheses.

- H1. The DNO wishes to compute voltage sensitivity coefficients with respect to nodal power injections, i.e., ($K_{P,il}(t) := \frac{\partial |\bar{E}_i|}{\partial P_\ell}$ and $K_{Q,il}(t) := \frac{\partial |\bar{E}_i|}{\partial Q_\ell}$) while not having knowledge of the network admittance matrix [\mathbf{Y}] and system state, i.e., voltage phasors of network buses.
- H2. A monitoring infrastructure is available that provides the DNO with measurements at frequent time-intervals of the voltage magnitude of each network bus i , ($|\bar{E}_i(t)|$) and of the nodal power injections ($P_i(t)$, $Q_i(t)$). Note that we do not require the measurements to be highly synchronized as availability of PMUs is still limited in distribution grids and we rely on conventional metering devices. A reasonable assumption is that metering devices are aligned with the network time protocol (NTP) ([115]).
- H3. The desired sensitivities do not vary significantly over a time window of duration τ during which an adequate number of measurements can be obtained for their computation.

Recall that the relation between variation in the voltage magnitude of bus i and variations of nodal active/reactive powers $\Delta \mathbf{P}$, $\Delta \mathbf{Q}$ (see Section 3.3.2) can be linearized:

$$\Delta |\bar{E}|_i \approx \mathbf{K}_{P_i} \Delta \mathbf{P} + \mathbf{K}_{Q_i} \Delta \mathbf{Q} \triangleq (\mathbf{K}_{P,Q} \Delta(\mathbf{P}, \mathbf{Q}))_i \quad (3.63)$$

where $\mathbf{K}_{P_i} = [K_{P_{i1}}, \dots, K_{P_{iN}}]$, $\mathbf{K}_{Q_i} = [K_{Q_{i1}}, \dots, K_{Q_{iN}}]$, are the vectors of voltage sensitivity of bus i with respect to nodal active and reactive powers respectively that we wish to estimate¹¹.

The key idea behind the method is to use the available measurements in order to compute variations of the voltage magnitudes and corresponding variations of the nodal power injections. Then using the computed variations, a system of linear

¹¹As reported in Section 3.4.2, N refers to the number of network buses with PQ injections, therefore the buses with respect to which the DNO wishes to compute the voltage sensitivities.

equations can be obtained starting from Eq. 3.63 that we can solve to obtain the desired coefficients. In particular, between two consecutive sets of measurements available at time t and $t + \Delta t$ (for a small $\Delta t > 0$), we define $\Delta P_i(t + \Delta t) = P_i(t + \Delta t) - P_i(t)$ and $\Delta Q_i(t + \Delta t) = Q_i(t + \Delta t) - Q_i(t)$. Similarly for the voltages, the desired variation is computed as $\Delta|\bar{E}_i(t + \Delta t)| = |\bar{E}_i(t + \Delta t)| - |\bar{E}_i(t)|$. If we have a large number of available measurements over a given time window $\tau = [t_1, t_m]$ and we make the assumption that the desired sensitivities do not vary significantly during this time period then we can construct the following system of linear equations for each network bus i :

$$\begin{pmatrix} \Delta|\bar{E}_i(t_1)| \\ \vdots \\ \Delta|\bar{E}_i(t_m)| \end{pmatrix} = \begin{pmatrix} \Delta P_1(t_1) & \cdots & \Delta P_N(t_1) & \Delta Q_1(t_1) & \cdots & \Delta Q_N(t_1) \\ \vdots & \ddots & \vdots & \vdots & \ddots & \vdots \\ \Delta P_1(t_m) & \cdots & \Delta P_N(t_m) & \Delta Q_1(t_m) & \cdots & \Delta Q_N(t_m) \end{pmatrix} \cdot \begin{pmatrix} K_{P_{i1}} \\ \vdots \\ K_{P_{iN}} \\ K_{Q_{i1}} \\ \vdots \\ K_{Q_{iN}} \end{pmatrix}$$

$$\Rightarrow \Delta|\bar{E}|_{i,\tau} = \Delta(\mathbf{P}, \mathbf{Q})_{\tau} \mathbf{K}_{\mathbf{P}\mathbf{Q}_i} + \boldsymbol{\omega}$$

The additional vector $\boldsymbol{\omega}$ contains the errors from the measurements. These errors are a combination of the measurement errors for both voltages and powers. Among these two, we assume that the effect of the errors linked to the power measurements is negligible compared to the one of the errors in voltage measurements. In order to take into account the voltage measurement noise, we first use a pre-filtering of the acquired measurements. In particular, for each time-step t , at least one value of the $\Delta|\bar{E}_i(t)|$ among all the network buses should be higher than a pre-specified threshold. The value of this threshold is determined based on the uncertainty of the voltage sensors. To fix ideas, this threshold can be $3\sigma_E$, where σ_E is the variance of a type II uncertainty of a voltage meter. After the filtering, in order to maintain an acceptable number of values that will allow the solution of the problem, the filtered values are replaced by older measurements that satisfy the criterion.

Furthermore, in order to properly model the noise in the problem formulation we take into account the correlation of the errors on the voltage measurements between consecutive time steps. The errors of the voltage measurements are considered gaussian and independent and identically distributed (i.i.d.) with a standard deviation that reflects the accuracy of the metering equipment¹². However, we formulate the problem using voltage differences and therefore the noise term $\boldsymbol{\omega}$ exhibits correlation between two consecutive time steps that cannot be neglected. In particular, the voltage measurement of bus i at time-step t , $|\bar{E}_i(t)|$ is characterized by an error $\epsilon_i(t) \sim \mathcal{N}(0, \sigma_E)$ ¹³. Under this assumption, the voltage difference $\Delta|\bar{E}_i(t + \Delta t)| = |\bar{E}_i(t + \Delta t)| - |\bar{E}_i(t)|$,

¹²Note that by metering equipment in this section we refer to industrial-grade metering infrastructure.

¹³The errors associated with the voltage measurements are assumed i.i.d between different time steps and different buses.

3.7. Measurement-based Computation of Voltage Sensitivities in Unbalanced Electrical Distribution Networks

is characterized by an error $\omega_i(t + \Delta t) \triangleq \epsilon_i(t + \Delta t) - \epsilon_i(t) \sim \mathcal{N}(0, \sqrt{2}\sigma)$, which is still gaussian as the difference of two gaussian variables but exhibits correlation.

The correlation coefficient between two consecutive time-steps is:

$$\rho(\omega_i(t), \omega_i(t + \Delta t)) = \frac{\text{cov}(\omega_i(t), \omega_i(t + \Delta t))}{\sigma_{\omega_i(t)}\sigma_{\omega_i(t+\Delta t)}} = -\frac{1}{2} \quad (3.64)$$

where

$$\begin{aligned} \text{cov}(\omega_i(t), \omega_i(t + \Delta t)) &= \mathbb{E}[(\omega_i(t) - \mathbb{E}[\omega_i(t)])(\omega_i(t + \Delta t) - \mathbb{E}[\omega_i(t + \Delta t)])] \\ &= \mathbb{E}[(\epsilon_i(t) - \epsilon_i(t - \Delta t))(\epsilon_i(t + \Delta t) - \epsilon_i(t))] = -\sigma^2 \end{aligned} \quad (3.65)$$

Note that, due to the i.i.d and zero-mean assumptions on the errors ϵ_i , it holds that $\mathbb{E}[(\epsilon_i(t + k\Delta t)\epsilon_i(t + \mu\Delta t))] = 0, \forall k \neq \mu$. Therefore, the correlation coefficient of the errors ω_i between two non-consecutive time-steps is equal to 0 and the resulting correlation matrix has the following structure¹⁴:

$$\Sigma = \begin{pmatrix} 1 & -0.5 & & & & \\ -0.5 & \ddots & \ddots & 0 & & \\ & \ddots & \ddots & \ddots & & \\ & & 0 & \ddots & \ddots & -0.5 \\ & & & & -0.5 & 1 \end{pmatrix}$$

Provided that $t_m > 2N$, we have formulated the problem as an over-determined system of linear equations which can be solved, for instance, using a least squares method. In such a case, the sensitivity coefficients are obtained analytically through solution of the following equations:

$$\mathbf{K}_{\mathbf{P}\mathbf{Q}_i} = (\Delta(\mathbf{P}, \mathbf{Q})_{\tau}^T \Sigma^{-1} \Delta(\mathbf{P}, \mathbf{Q})_{\tau})^{-1} \Delta(\mathbf{P}, \mathbf{Q})_{\tau}^T \Sigma^{-1} \Delta|\bar{\mathbf{E}}|_{i,\tau} \quad (3.66)$$

In the following section, we evaluate the proposed algorithm using real measurements coming from a real distribution feeder in Switzerland.

3.7.2 Numerical Validation

The numerical validation of the proposed methodology is carried out using real measurements coming from a real three-phase LV feeder in Switzerland that is equipped with an appropriate monitoring infrastructure. The network topology graph is shown in Figure 3.26.

In order to be able to compare the performances of the proposed method with the

¹⁴Note that Σ is correct for the ideal case where the errors in the power measurements are less dominant than those of the voltages. If both errors need to be accounted for, Σ is not known a priori and its assessment might require a more sophisticated analysis.

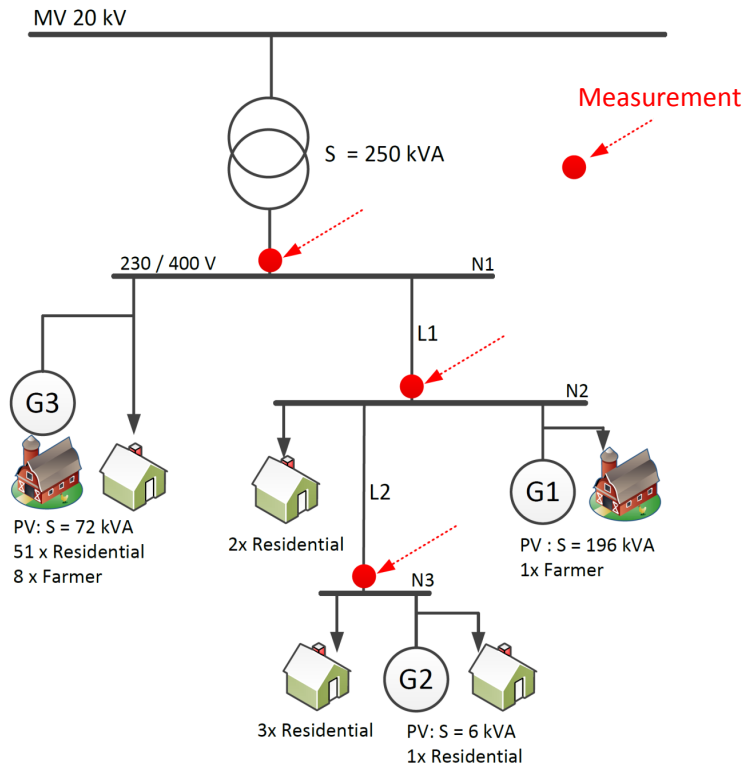


Figure 3.26: Network used in the evaluation of the measurement-based computation of the voltage sensitivity coefficients.

formal analytic method presented in [17] we need to have access to the true grid state and the true topological information that correspond to the obtained measurements. To this end, we adopt the following procedure. We consider the nodal power profiles given by a set of real measurements¹⁵. Figure 3.27 shows the active and reactive power measurements of phases α , b and c of bus 2 during a time window of 9.22hrs. Moreover, we use the nominal values of the network admittance matrix that, for the sake of validation, is available. Using this data, we perform a three-phase load flow calculation to obtain the voltage phasors that correspond to the nominal admittance matrix and the measured power profiles. This provides us with the ground truth and allows the computation of the exact sensitivity coefficients. Next, we use the load-flow voltage magnitude profiles and we create a set of pseudo-measurements by adding white Gaussian noise with a standard deviation of $2.17E-4$ that represents the accuracy of the metering equipment. This set of pseudo-measurements, along with the true measurements of the nodal power injections, are used as input for the measurement-based computation of the sensitivity coefficients.

Figures 3.28-3.30 show a set of results of the validation process. In what follows

¹⁵In this study we use measurement-traces acquired during February and July to capture the different loading conditions of the grid during different seasons.

3.7. Measurement-based Computation of Voltage Sensitivities in Unbalanced Electrical Distribution Networks

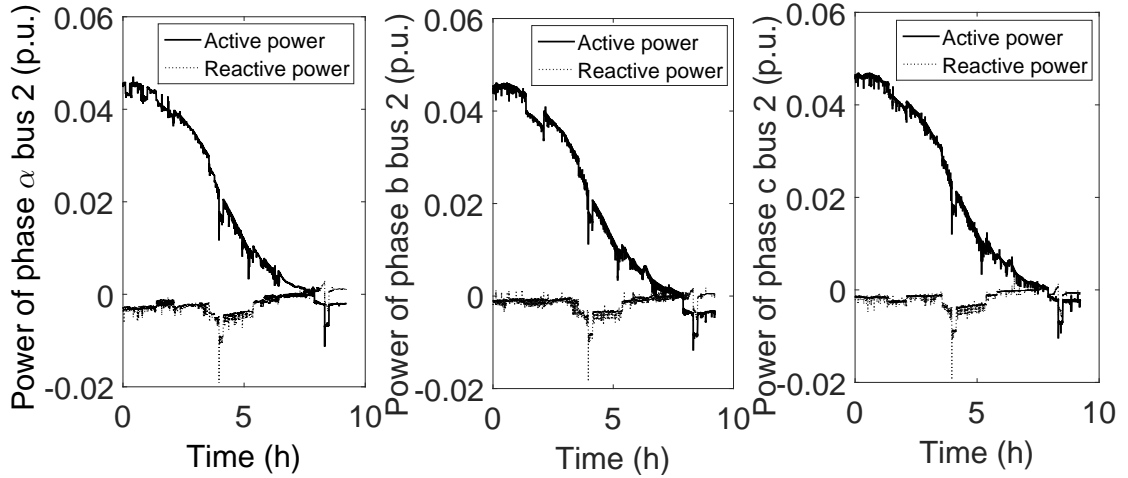


Figure 3.27: Nodal-power measurements (p.u.) of phases α , b and c of bus 2.

we choose to estimate the desired coefficients using a measurement time-window of 2000sec¹⁶. Figures 3.28-3.30 show the exact voltage sensitivities in red line and the measurement-based sensitivities in blue. In particular, Figure 3.28 shows the sensitivity of phase c of bus 2 w.r.t. active power of phase c of bus 2, Figure 3.29 shows the sensitivity of phase α of bus 3 w.r.t. active power of phase α of bus 3 and Figure 3.30 shows the sensitivity of phase b of bus 3 w.r.t. reactive power of phase b of bus 3. Note that cross-phase coefficients are not shown, because they are zero in this case as the grid topology is balanced despite the imbalances in the network

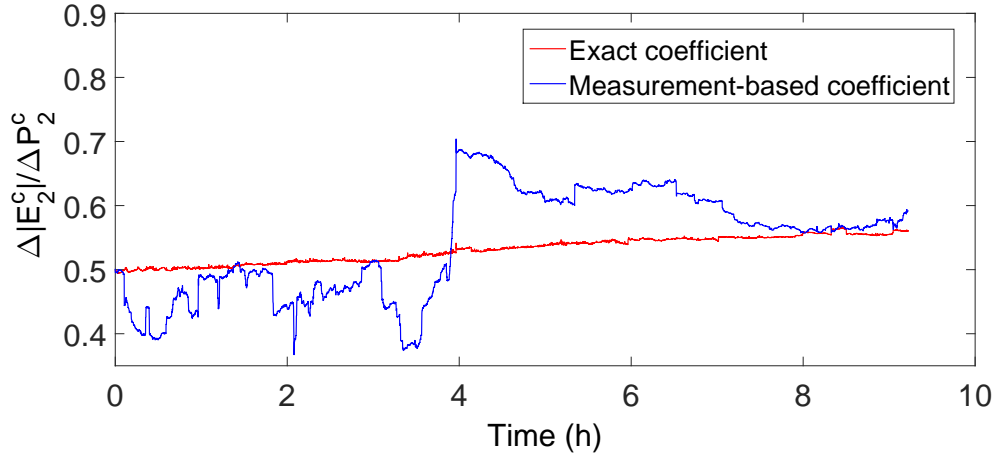


Figure 3.28: Exact and measurement-based voltage sensitivity coefficients of bus 2 phase c with respect to the active power of bus 2 phase c .

¹⁶The final size of the time-window was decided by performing a series of simulation experiments with different time-windows varying from 200sec to 5000sec and keeping the smallest value which did not result in large condition numbers of the least squares matrix.

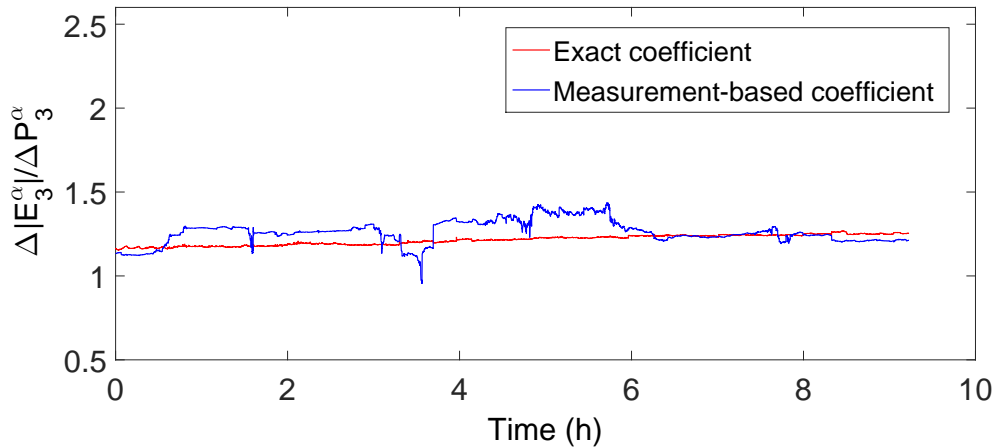


Figure 3.29: Exact and measurement-based voltage sensitivity coefficients of bus 3 phase *a* with respect to the active power of bus 3 phase *a*.

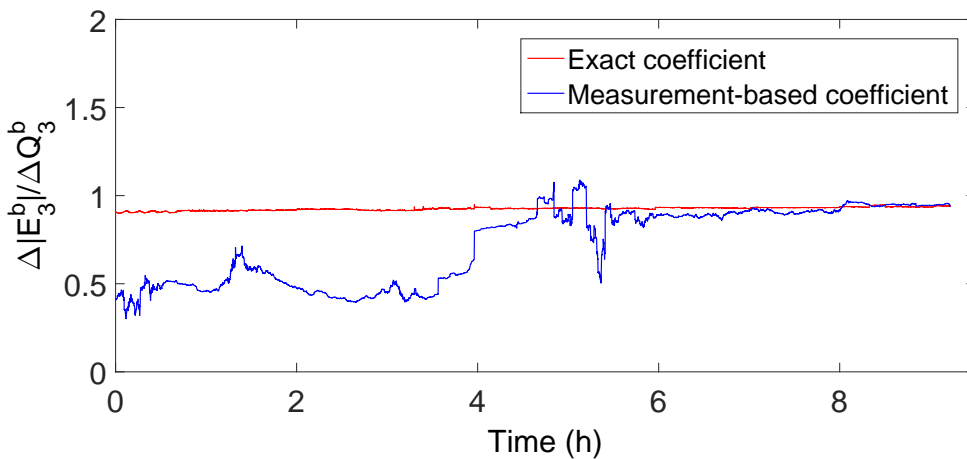


Figure 3.30: Exact and measurement-based voltage sensitivity coefficients of bus 3 phase *b* with respect to the reactive power of bus 3 phase *b*.

load. It can be observed that for all the cases, the measurement-based coefficients, although not identical as expected, are quite close to the exact ones. These preliminary results indicate that the DNO can use the measurement-based obtained coefficients to perform voltage control even in cases when the admittance matrix is not known at all.

3.8 Conclusions

In this chapter we consider a centralized real-time control architecture for voltage regulation and lines congestion management in ADNs that is based on a linearized

approach that links control variables (e.g., voltages, current flows) and controlled quantities (e.g., power injections, transformers tap positions) by means of sensitivity coefficients.

We validate the proposed analytical method by making reference to typical IEEE 13- and 34-nodes distribution test feeders. The numerical validation of the computation of the coefficients is performed using the IEEE 13-nodes test feeder and it shows that the errors between the traditional approaches (i.e., based on the inverse of the Jacobian matrix) and the analytical method are extremely low (in the order of magnitude of 10^{-4} – 10^{-6}). The IEEE 34-nodes test feeder is used to show application examples related to a possible integration of the proposed method for the problem of optimal voltage control and lines congestion management in unbalanced distribution systems. The simulation results show that the proposed algorithm is able to improve the voltage and current profiles in the network, and also that when each of the three phases of the DERs can be controlled independently of the others the resulting optimal voltage and current profiles are better than the ones corresponding to the balanced control of the 3-phase output of the set-points of the DERs. Finally, it is worth observing that the proposed analytical computation of voltages and currents sensitivities exhibits an improvement of performance, compared to traditional Jacobian-based methods, which is in the order of 2.34 for the IEEE 13-nodes test feeder and 2.52 for the IEEE 34-nodes test feeder. This improvement enables the reduction of the computational time of several traditional power systems problems involving non-negligible computational efforts, such as contingency analysis or optimal planning in addition to real-time centralized controls.

As a further step, we relax the assumption that the DNO has an accurate knowledge of the system model, i.e., a correct network admittance matrix $[Y]$ and we adapt the proposed centralized control architecture to such a scenario. We show that it is still possible to perform control and improve the voltage profile in cases where the system model is not accurate or it is known with some level of uncertainty. We first show that the effect of using an erroneous admittance matrix in the solution of the voltage control problem can result in voltage deviations from the network nominal value that are close or even violating the allowed limits for safe operation. As a solution to this problem we adopt a robust optimization framework that is shown to immunize the solution of the voltage control problem against uncertainties in the system model. Finally, in the case where the network admittance matrix is not available at all we show using a real distribution feeder that it is possible to obtain an accurate estimate of voltage sensitivity coefficients, and consequently perform voltage control, using solely measured quantities.

As far as future work is concerned on the topics presented in this chapter, first, it is interesting to derive analytical procedures in order to obtain voltage sensitivity coefficients taking into account voltage-dependent injections, which are non-negligible especially when nodal powers are driven by loads. Indeed, for DG and storage, it

is reasonable to assume that they are interfaced via power electronic converters capable to realize voltage-independent power injections. Then, in the context of the measurement-based computation of the sensitivities it is interesting to improve the method so that measurements are weighted relatively to the accuracy of the metering equipment used. Also, possible outliers or bad data in the incoming measurements in addition to the measurement noise should be taken into account. In particular, we refer to bad data processes relying on pre-filtering by approaches that do not rely on the knowledge of $[\mathbf{Y}]$. After the validation of the method, the next step will be to perform a dedicated real-field experimental testing. Finally, regarding the RO formulation of the control problem, we make the strong assumption that monitoring of the voltage profile is available. In a more realistic setting it is reasonable to assume a SE process that uses the uncertain admittance matrix and provides uncertainty bounds for the observed voltages as well. Also, in the same direction, it is worth investigating analytical methods for obtaining bounds on the sensitivity coefficients, such as interval arithmetics.

4 A Unified Broadcast-based Control Strategy for ADNs

4.1 Introduction

With the increasing availability of communication technologies, we can envision that, in distribution networks, ancillary services, typically employed in the HV transmission networks, can be provided by distributed controllable energy resources already present in these systems, such as elastic loads, and energy storage systems. Clearly, directly controlling each single resource is not a viable solution when resources are numerous and diverse. In fact, control schemes that rely on two-way communication between the controllable entity and the DNO (e.g., [116, 117]) can quickly result in algorithms that cannot scale in the number of network buses and controllable resources. Additionally, the adoption of completely different architectures for the control of different energy resources, renders the problem difficult when heterogeneous energy resources need to be coordinated to achieve a common goal. In such cases, the distributed and heterogeneous nature of the available controllable resources, as well as their large number and small individual impact motivates the need for unified, scalable control mechanisms.

In this direction, the centralized control architecture for ADNs proposed in Chapter 3 exhibits some limitations, as it relies on a point-to-point communication from the DNO's controller to each controllable DER and, thus, is suitable for the real-time control of a relatively small number of distributed energy resources. A possible solution to the aforementioned issues is to keep the system tractable by using broadcast-based control schemes that rely on state estimation for the feedback channel (e.g., [118, 119]).

In this respect, in this chapter, we propose a low-overhead broadcast-based control mechanism, henceforth called Grid Explicit Congestion Notification (GECN), intended for deployment by DNOs to provide grid ancillary services by a seamless control of large populations of distributed, heterogeneous energy resources [120, 16]. GECN is a decentralized control scheme inspired by the congestion control mechanism used in the transmission control protocol (TCP) [121]. Specifically, the proposed mechanism was conceived to provide primary voltage control in a scalable way by broadcasting low bit-rate control signals to large populations of distributed energy resources in order to

manage the variations of the nodal power injections in the network buses.

The proposed control architecture is essentially composed of two parts. The first part is a centralized network controller that, similarly to the online scheduler presented in Section 3.3.2, observes at each time-step the system state and solves an optimization problem to obtain the optimal active and reactive nodal power set-points that lead to the desired operating point for voltage control. Once the optimal set-points are computed, they are translated to broadcast signals, henceforth called GECN signals, and they are communicated to those network buses where controllable DERs are connected. The second component of the GECN architecture is the design of appropriate local controllers tailored to the characteristics of the various controllable resources that receive, interpret the broadcast signals and respond according to each device's capabilities and internal-state constraints.

It is worth noting that one of the advantages in the design of GECN is that it is characterized by a "separation of concerns". The GECN network controller only requires the knowledge of the network state and does not need to know the particular nature or actual state of the various DERs. In contrast, local resource controllers are specific, but their functionalities are simpler, as they are called to modify their state as a function of the received GECN signal and their individual capabilities. In other words, the local controllers that need to know details of diverse DERs are simple, whereas the central controller that needs to take control decisions has a simple view of the grid with no details of the controllable resources. Such a design allows completely heterogeneous energy resources to participate to the control actions towards a common goal.

Two very promising candidates in terms of controllable resources, expected to be deployed for ADN ancillary services in the near future, are energy storage systems (ESSs) and elastic demand. In this chapter we investigate the potential of a large aggregation of small electrical loads, as well as of distributed energy storage systems for providing primary voltage control. The elastic appliances, in our case, consist of thermostatic loads (e.g., space/water heating, refrigeration). These kinds of loads are a promising category for engaging in short-term ancillary services as they are typically characterized by slow-evolving states (e.g., temperature with hourly time dynamics) that allow for control flexibility (e.g., [122, 123, 124]). The targeted ESSs are electrochemical-based storage systems and they are selected as the targeted energy resources because they are expected to cover a wide spectrum of applications in distribution networks. They are characterized by charge/discharge cycles that could range from seconds (typically in high-power applications) to hours or even days (in high-energy applications) [125, 126, 127]. As a consequence, ESSs, according to their type, are able to compensate instantaneous imbalances (e.g., fluctuations of renewable generation), to time-shift the energy production or consumption (e.g., slow variations in renewable generation), and to contribute to voltage support (e.g., [128, 129]). In this chapter, we design smart local controllers to allow both of the aforementioned categories of resources to participate to primary voltage control.

The main contributions of this chapter can be summarized as follows. We describe in detail the principles and operation of the GECN control mechanism. We provide the architecture of the GECN network controller and the design of two different local GECN controllers tailored to the characteristics of thermostatically controlled loads (TCLs) and electrochemical-based energy storage systems respectively. Furthermore, we investigate the potential of real-time demand response (DR) for providing grid ancillary services and we indirectly reveal storage capabilities of end-customers. Contrary to classic DR approaches, we design GECN to act on a fast time scale (in the order of few seconds) without significantly impacting the end-customers. In particular, we take into account in the design of the load controllers the issue of limiting the frequency of cycles of the elastic appliances and avoid possible synchronization (i.e., cold load pick-up [130]) after the DR actions. As a second step we evaluate the potential of distributed energy storage systems (ESSs) for providing primary voltage control via broadcast signals. In the case of ESSs control, we propose a method for estimating the energy reserve required for successfully performing voltage control depending on the characteristics of the network lines. Additionally, we evaluate the effect of reactive versus active power controlled injections on the voltage control actions, depending on the network line characteristics. We show that without altering the demand-response signal, a suitably designed controller implemented in the storage devices enables them to successfully contribute to primary voltage control and allows the successful use of the same broadcast signal for the control of heterogeneous energy resources. Finally, we assess the performances of the proposed control mechanism in real-time using a hardware-in-the-loop (HIL) set-up where all the chain including the models of the network and measurement devices, the real-time SE and the control mechanism is presented. This allows us to assess the performances, in terms of accuracy and latencies, of the whole control process.

4.2 Related Work

As a potential solution for the design of control algorithms specifically applied to ADNs, several efforts in the literature have proposed to take advantage of the increasing availability of communication technologies, and engage distributed energy resources, such as DG, elastic demand and energy storage systems for providing grid ancillary services (e.g., [9, 131, 132, 128, 129]).

In the case of demand response (DR), all intentional modifications to the consumption patterns of end-use electrical grid customers are included, which result in altering the time, the level of instantaneous demand, or the total electricity consumption. The majority of existing DR schemes target peak-shaving and, in general, alter the total electricity consumption on a time scale of minutes up to several hours (e.g., [133]). However, with the increasing availability of advanced monitoring and communication technologies, it is also possible to envision using real-time DR mechanisms in order to engage large populations of small electrical loads to provide grid

ancillary services (e.g., [134]). In this direction, in [135] DR is deployed to mitigate forecast errors due to the integration of renewable resources, whereas in [136] DR is considered in the context of islanded microgrids where it aims at providing a form of reserve. Furthermore, inspired by traditional frequency droop controls, there has already been an effort to investigate DR schemes as a way to provide primary and secondary frequency-control to the grid. In particular, in [137] electric vehicles are considered for providing frequency-control, whereas in [138] domestic loads are investigated for primary frequency-control. In this respect, it is worth noting that this type of DR contribution to frequency-control appears interesting in the case of islanded grids but, as it was recently requested by the European Network of Transmission System Operators for Electricity (ENTSO-E), it might be extended to distribution networks that will be requested to provide grid ancillary services (e.g., [2]).

Compared to the existing literature, the purpose of our work is to develop a new DR control mechanism in order to investigate the potential of a large aggregation of small electrical loads for providing a different ancillary service, specifically the primary voltage control of active distribution networks. Contrary to classic DR approaches, GECN acts on a fast time-scale (in the order of few seconds) without significantly impacting the end-customers. Under normal grid operation, the proposed scheme can be used similarly to classic demand response schemes for peak shaving or for maintaining the balance between generation and consumption in the network (when there is not enough capacity or when there are renewable resources whose generation cannot be fully predicted).

The second most likely candidate to be used for ADNs ancillary services is ESSs. ESSs are expected to cover a wide spectrum of applications in distribution networks. They are characterized by charge/discharge cycles that could range from seconds (typically in high-power applications) to hours or even days (in high-energy applications) [125, 126, 127]. Due to their wide range of applications, the use of electrochemical storage systems within the context of ancillary services provided to power distribution networks has been addressed by several contributions to the literature (e.g. [129, 139]). A typical application of ESSs is the compensation of the short-term volatility in the production of renewable resources (e.g., [131]). Within the context of ADN ancillary services provided by distributed storage systems, in [129, 128] the capability of these systems to provide voltage support to distribution networks is illustrated.

In general, the concerned storage technologies for grid ancillary services are represented by battery storage systems. Within the context of ADNs primary voltage control, we propose the use of supercapacitors as the targeted ESS. Due to their high power density, short charge time and long life duration, these devices are particularly interesting in the ESS applications that require rapid cycles (e.g., primary voltage control via fast compensation of renewable DG, fast charging of electric vehicles) [140]. Furthermore, compared to the existing literature, we specifically model the SCs via an

4.3. The Grid Explicit Congestion Notification Mechanism: Hypotheses and Architecture

equivalent circuit model that enables us to correctly represent both the quasi-static and dynamic behavior of a SC, accounting for the so-called “charge redistribution-effect” that plays a major role in its dynamic behavior. Also, we specifically provide a method for estimating the energy reserve required for successfully performing voltage control using GECN.

Despite their differences, most DR and ESSs control schemes found in the literature rely on two-way communication between the controllable entity and the distribution network operator (DNO) (e.g., [116, 117]). However, the distributed nature of the controllable resources, as well as their large number and small individual impact motivates the use of a control mechanism based on one-way communication. In this direction, in [118], the charging rate of electric vehicles is controlled via broadcast signals so as to avoid overloading the distribution feeders. Furthermore, the authors in [119] propose the use of a universal broadcast signal to control the charge rate of a fleet of electric vehicles for the local compensation of renewable production volatility. Additionally, a decentralised control scheme of micro-storage systems via broadcast pricing signals is presented in [141].

Compared to the existing literature on broadcast-based control schemes, we go one step further and we show that heterogeneous controllable resources in the network can contribute to primary voltage control, by responding to the same broadcast signal. We show that with GECN this is indeed possible, without any change to the control architecture. The same GECN signals are broadcasted to the different buses of the network and it is the local controller of each elastic appliance or storage system that decides the system’s response to the received signal. Furthermore, we design GECN in such a way that, in case the DNO seeks to use traditional solutions, the proposed mechanism can be used to provide further support to the network, in addition to the DNO’s own resources. It is for this reason that the proposed GECN algorithm was initially conceived and designed to coexist with traditional solutions such as OLTCs and reactive power compensators.

4.3 The Grid Explicit Congestion Notification Mechanism: Hypotheses and Architecture

We wish to design a scalable control scheme for providing ancillary services to ADNs by managing centralized resources such as transformers’ on-load tap changers (OLTC) and, at the same time, nodal power injections of the network buses where a large population of distributed, heterogeneous energy resources is connected. The Grid Explicit Congestion Notification Mechanism [120, 16] is conceived for these purposes. GECN is a unified control mechanism that uses low bit-rate broadcast control signals and relies on five main hypotheses:

H1. Knowledge of the network admittance matrix $[Y]$.

- H2. Availability of a monitoring infrastructure and a state estimation process (e.g., [100]) that allows the DNO to observe the network state in each bus i , i.e., voltage phasors $\bar{E}_i(t)$ ¹. As known this hypothesis together with H1 allows the computation of the nodal power injections, $P_i(t)$, $Q_i(t)$, as well as the flows of each line k , \bar{I}_k .
- H3. Formulation and solution of an optimization problem to obtain desired power adjustments $(\Delta P_i(t), \Delta Q_i(t))$ in each bus i equipped with controllable resources. The formulation of the optimization problem relies on the linearization of the power flow equations by means of sensitivity coefficients.
- H4. One-way communication infrastructure and use of broadcast signals for the control of active and/or reactive nodal power injections.
- H5. Development of appropriate local controllers tailored to the characteristics of the various controllable resources that receive, interpret the broadcast signals and respond according to each device's capabilities and internal state constraints.

In the rest of the chapter, we consider a distribution network comprising M 3-phase buses. The GECN control architecture is shown in Figure 4.1. At each time-step, first, the DNO uses a SE process to obtain the network state and estimates of the aggregate power at all the network buses. At each bus both elastic and non-elastic loads are present, as well as non-dispatchable active power injections provided by distributed generators. The DNO uses the estimated state to compute voltage sensitivity coefficients and to formulate and solve a constrained optimization problem. The optimal solution is the desired active and reactive nodal power set-points for the network buses that are equipped with controllable resources. The DNO does not aim to individually control each appliance. Instead, the DNO computes and broadcasts on each bus a unique control signal that is transparent to the non-elastic appliances. Therefore, this signal impacts solely the behavior of the elastic loads. Note that we cannot use frequency deviation as alternative to an explicit broadcast control signal, since we are targeting voltage control and voltage deviations in a local bus may appear independently of frequency deviations. The actual computation of the GECN broadcast signal is shown in Figure 4.1. In this figure we detail the feedback loop for the active power broadcast signal g_P . A similar closed-loop controller is adopted for the reactive power. In this way broadcast signals can be computed for both power set-points. The GECN signal at time t is computed as a function of (i) the optimal set-points at the current time-step and (ii) the mismatch between the optimal and the actual set-points that the DNO observed at the previous time-step $t-1$. Once computed, the GECN signal is communicated to the network buses. The bit rate of the signal is very low (a few bits per second), therefore it can be transmitted using existing power-line communication for advanced metering². Each elastic appliance is assumed to be equipped with a

¹The rated value of the voltage in the network is denoted by E_o .

²It is worth mentioning that details of the telecommunication infrastructure are outside the scope of this thesis.

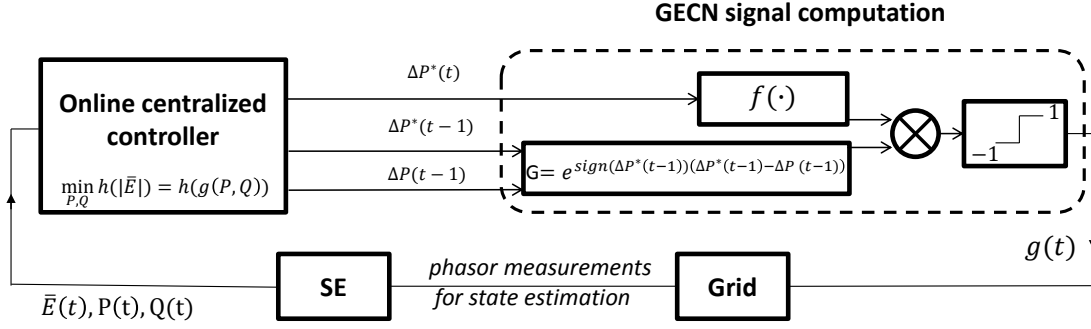


Figure 4.1: GECN control architecture.

simple programmable controller that decides its power consumption based on the internal state and the received signal. The resulting variation of the aggregate power at the bus provides the DNO with an implicit feedback to the control signal, which is used to estimate the responsiveness of the bus resources and to decide the subsequent control signal.

In the following sections we describe in detail the operations of the GECN central network controller, as well as the design of local resources' controllers.

4.4 GECN Central Network Controller

As anticipated, the DNO wishes to use GECN signals to perform primary voltage control. The DNO is assumed to have imperfect 24hr forecasts for load and renewable profiles $(\mathbf{P}, \mathbf{Q})_f$, from which deviation is penalized in order to reduce costs of operation. Finally, the operator is assumed to be able to control the primary substation OLTC located in correspondence to the slack bus of the network³. The tap-changers positions are a means to provide a further leverage for the operator in coordination with the proposed control mechanism.

At each time-step t , the DNO observes the state of the network on every bus i , i.e., the per-bus aggregate power injections $P_i(t)$ and $Q_i(t)$, along with the phasors of the phase to ground voltage $\bar{E}_i(t)$. Subsequently, the DNO computes the voltage sensitivity coefficients with respect to absorbed/injected power of a bus ℓ , as well as transformer's tap-changers positions

$$K_{P,il}(t) := \frac{\partial |\bar{E}_i|}{\partial P_\ell}(t), K_{Q,il}(t) := \frac{\partial |\bar{E}_i|}{\partial Q_\ell}(t)$$

$$K_{n,i}(t) := \frac{\partial |\bar{E}_i|}{\partial E_{slack}}(t)$$

³We disregard the presence of static var compensators. Note that they can be taken into account in the sensitivity matrix \mathbf{K}_Q .

e.g., by solving the linear systems of equations presented in Section 3.4.2. Therefore, the following linear relation between variation in bus voltages and variations of active/reactive power $\Delta P_i, \Delta Q_i$ and tap-changers positions Δn can be derived (e.g., [9]):

$$\begin{aligned}\Delta|\bar{E}|_i &\approx \mathbf{K}_{P_i}\Delta\mathbf{P} + \mathbf{K}_{Q_i}\Delta\mathbf{Q} + \mathbf{K}_n\Delta\mathbf{n} \\ &\triangleq (\mathbf{K}_{P,Q,n}(t)\Delta(\mathbf{P}, \mathbf{Q}, \mathbf{n}))_i.\end{aligned}$$

where $\mathbf{K}_{P_i} = [K_{P_{i1}}, \dots, K_{P_{iM}}]$, $\mathbf{K}_{Q_i} = [K_{Q_{i1}}, \dots, K_{Q_{iM}}]$ and $\mathbf{K}_n = [K_{n_1}, \dots, K_{n_M}]$.

At this stage the DNO can detect which areas of the network are congested or exhibiting voltage variations close to the limits allowed for safe operation (typically $\pm 5\%$ of the rated value). Using the sensitivity coefficients $\mathbf{K}_{P,Q,n}$ the DNO can compute the optimal required power adjustments $\{\Delta(\mathbf{P}, \mathbf{Q})^*(t)\}$ in the buses and, at the same time, the optimal variations in the tap-changers positions $\{\Delta\mathbf{n}^*(t)\}$ which lead to the desired operation set-point for voltage control via the following constrained optimization problem:

$$\begin{aligned}&\min_{\Delta(\mathbf{P}, \mathbf{Q}, \mathbf{n})} \sum_i \mu_i \left(\Delta(\mathbf{P}, \mathbf{Q})_i - \Delta(\mathbf{P}, \mathbf{Q})_{f_i} \right)^2 + & (4.1) \\ &\sum_i \lambda_i \left[(|\bar{E}_i| + (\mathbf{K}_{P,Q,n}(t)\Delta(\mathbf{P}, \mathbf{Q}, \mathbf{n}))_i - E_o)^2 - \alpha^2 \right]^+ + \\ &\psi_1 \left(\sum_i \hat{g}_i \right) \psi_2 \left(\sum_t |\Delta n(t)| \right) \Delta\mathbf{n}^2 \\ \text{subject to: } &\gamma_i \leq \cos \varphi_i \leq 1 \\ &n_{min} \leq n(t) \leq n_{max} \\ \text{where } &\hat{g}_i(t) = \sum_{s=0}^{W-1} k_s g_i(t-s) \\ \text{and } &n(t) = n(t_0) + \sum_{\tau=t_0}^t \Delta n(\tau)\end{aligned}$$

γ_i is the constraint on the power factor, $\cos \varphi_i$, on a specific bus i , n_{min} and n_{max} are the minimum and maximum OLTC positions allowed, the parameter α denotes the value of the voltage deviation from the rated value tolerated by the DNO, \hat{g}_i is the moving average of the control signal g over a time window of W time-steps, and ψ_1 and ψ_2 are penalty functions for altering the OLTC position⁴. The first two terms in the objective function are weighted by parameters λ_i and μ_i ⁵. The first term of Eq. 4.1 represents the compensation of errors in the forecasted aggregated loads. The second and third terms describe the voltage control part. The operator can perform this type of control

⁴As we deal with primary voltage control, Eq. 4.1 has to penalize the changes of OLTC as these devices are typically used by the DNO rarely. This will be explained next with more details.

⁵The choice of the weights in the objective function is related to the topology of the network and the parameters of the lines (i.e., the network admittance matrix).

by deploying solely demand response or by coordinating control of the DERs and the OLTC positions. In the case where the tap-changers are included, the DNO seeks to utilize them only in periods when demand response cannot provide the desirable operating set-points. This is represented by the term ψ_1 of Eq. 4.1 which is a function that assumes large values in normal operation (i.e., $|\hat{g}| \simeq 0$) and low values when the GECN signal saturates (i.e., $|\hat{g}| \simeq 1$). More specifically, we have chosen:

$$\psi_1\left(\sum_i \hat{g}_i\right) := a_1 e^{-a_2 |\sum_i \hat{g}_i|} \quad (4.2)$$

In order to account for the limited number of operations that an OLTC can perform, a further penalty function, ψ_2 , has been included in Eq. 4.1. This function multiplies the OLTC set-points variation and increases with the number of OLTC operations in a given time window⁶. Specifically, we have chosen:

$$\psi_2\left(\sum_t |\Delta n(t)|\right) := e^{a_3 \sum_{t_i < t < t_i + \tau_o} a_4(n(t_i)\Delta n(t_i))|\Delta n(t_i)|} \quad (4.3)$$

where a_3 is a constant and a_4 is 1 if $n(t)\Delta n(t) \geq 0$ and 0 otherwise. Such an expression of ψ_2 allows to weight in an exponential way the accumulated number of OLTC changes within a given time window τ_o . Furthermore, it is able to account for the direction of the OLTC changes together with their distance from the central OLTC position $n = 0$. In view of the expression used to weight the penalty on Δn , the DNO can decide the leverage on the OLTC compared to the use of other resources (i.e., storage and/or loads).

After having determined the optimal operation set-points of the network at time t , the goal is to adaptively compute GECN signals which drive the system towards these desired set-points. This is implemented using the control loop depicted in Figure 4.1. The current optimal set-points are the input to a saturation function f that maps $\Delta P_i^*(t)$ every time-step to a value in $[-1, 1]$:

$$f(\Delta P_i^*(t)) = \text{sign}(\Delta P_i^*(t))(1 - e^{-|\Delta P_i^*(t)|/b_i}) \quad (4.4)$$

where $\Delta P_i^*(t)$ are the optimal set-points that the DNO targets at time t , and b_i is a parameter affecting the slope of the saturation function (i.e., the smallest the value of b , the steepest the slope of the saturation function). The outcome of this operation is weighted by a factor G , which is an exponential function of the mismatch between the optimal set-points and the actual set-points the DNO observes at the previous time-step $t-1$:

$$G = e^{\text{sign}(\Delta P_i^*(t-1))(\Delta P_i^*(t-1) - \Delta P_i(t-1))} \quad (4.5)$$

⁶By including this function, even in cases where the saturation of the signal occurs for a long period of time, the DNO has the option to upper-bound the total number of OLTC operations, thus respecting the nature and cost of these devices.

Thus, the proposed control loop continuously adapts the GECN signal to adjust the aggregate power at each bus to the variations of the optimal set-points. Replacing ΔP_i^* with ΔQ_i^* in 4.4 and 4.5 allows the computation of GECN signals for the control of the reactive power, in cases where the controllable resources have also reactive power capabilities, e.g. ESSs.

In order to evaluate the performances of the proposed mechanism for primary voltage control in ADNs, we need GECN-enabled resources. In this direction, in the following section we choose to design local controllers for TCLs, and in particular refrigerators and ESSs, in our case represented by SC arrays.

4.5 GECN Local Resources Controllers

4.5.1 The Case of Thermostatically Controlled Loads

Load response representation

In this section, we give the main assumptions on both elastic and non-elastic demand. Let us consider thermostatic loads for which their state is given by their temperature (e.g., air conditioners or refrigerators). We consider L types of elastic appliances. We assume that each type ℓ has a set of operating modes that we denote by $\mathcal{X}_\ell \subseteq [0, 1]$, a maximum rated power P_ℓ^r , and a constant power factor $\cos \varphi_\ell$. When an appliance of type ℓ is in a specific operating mode $x \in \mathcal{X}_\ell$, it consumes a fraction x of the rated power, i.e., xP_ℓ^r and the corresponding proportional reactive power, obtained via the power factor.

In what follows, we consider discrete time-steps $\{0, 1, \dots, t, \dots\}$. Let us consider a single appliance of type ℓ . We denote the process describing its operating mode by $(X(t) \in \mathcal{X}_\ell)_t$. The internal state process of the appliance is influenced by the operating mode and by external factors; we denote it by $(\theta(t) \in \mathbb{R})_t$. At all times $t \geq 0$, the controller of the appliance chooses an operating mode $X(t)$ such that the internal state constraints $\Theta_\ell \subset \mathbb{R}$ are satisfied, i.e., $\theta(t) \in \Theta_\ell$.

The duty-cycle function $h_\ell : \mathcal{X}_\ell \times \mathbb{R} \rightarrow \mathcal{X}_\ell$ for an appliance of type ℓ determines the default operating mode of the appliance $X(t+1)$, taking into account the previous operating mode $X(t)$ and the internal state of the appliance $\theta(t)$:

$$X(t+1) = h_\ell(X(t), \theta(t)), t > 0. \quad (4.6)$$

For presentation ease, we describe the behavior of a cooling thermostatic device. Such an appliance is assumed to operate in a binary mode $\mathcal{X} = \{0, 1\}$, and its internal state is given by the cooling compartment temperature, constrained in the form of a deadband $\Theta = [\theta_{\min}, \theta_{\max}]$ (e.g., [142]). The internal temperature of these kinds of loads can be modeled, for instance, as proposed in [143]:

$$\theta(t+1) = \epsilon\theta(t) + (1-\epsilon)\left(\theta_0 - \eta \frac{X(t)P_r}{A}\right) + \omega(t) \quad (4.7)$$

where θ_0 is the ambient temperature, $\epsilon = e^{-\tau A/m_c}$ is the factor of inertia of the appliance, τ is the time-step and m_c is the thermal mass, η is its coefficient of performance, and A is the thermal conductivity. The process $\omega(t)$ is a noise process-modeling of the random external heat injections in thermostatically controlled loads having a distribution that follows hourly data presented in [135]. A typical duty-cycle function (Figure 4.2) is:

$$\begin{aligned} h(X = 0, \theta) &= \mathbb{1}_{\{\theta \geq \theta_{\max}\}} \\ h(X = 1, \theta) &= \mathbb{1}_{\{\theta \geq \theta_{\min}\}} \end{aligned} \quad (4.8)$$

In what follows, we assume that at each network bus i a population of the aforementioned elastic appliances is connected, each one having a state that evolves like Eq. 4.7 and a duty cycle function given by Eq. 4.8. In addition to the controllable loads, in each network bus, non-elastic demand, non-controllable by the DNO is assumed, represented by typical 24-hr load profiles. The aggregate power at a bus level consists of the combination of the above types of loads.

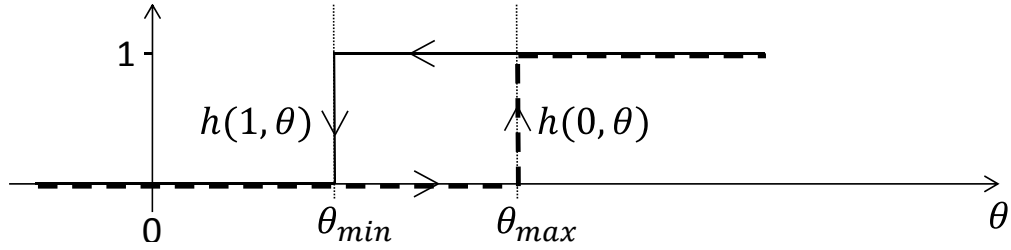


Figure 4.2: Duty-cycle for appliances with deadband-constrained state.

Load Controller

All the elastic appliances connected to a network bus i receive at each time-step t the GECN control signal $g_i(t)$ broadcasted by the DNO. The signal represents a real number $g_i(t) \in [-1, 1]$ coded, for example, on 16 bits. The control signal $g_i(t)$ is proportional to the DNO's desire to inhibit consumption. Hence, a negative g_i encourages consumption, a positive g_i inhibits consumption, whereas $g_i = 0$ does not impact the behavior of the appliance⁷.

In what follows, we propose a controller that takes into account the GECN signal. In the absence of the GECN control signal (i.e., $g_i(t) = 0$), the duty-cycle function in Eq. 4.8 provides the controller with the next operating mode $X(t + 1)$. In response to a non-zero GECN signal, the controller can decide to switch to a different operating mode than the one dictated by the duty-cycle. When such a decision is made, the controller

⁷The proposed algorithm aims at maximizing the usage of network resources (i.e., loads/storage) to locally provide ancillary services to the grid. In this respect, an imbalance of the production/consumption towards the production encourages consumption, whereas an imbalance towards the consumption inhibits consumption in order to keep the voltage levels within the allowed limits.

sets a counter $T(t)$ to a predefined value $T_{\ell,0}$ (which depends on the appliance type); the value $T(t)$ then decreases over time, until it reaches 0. When the value of $T(t)$ is strictly positive, the appliance does not react to any received GECN signals. This ensures a smooth operation of the appliance by limiting the number of imposed operating mode switches.

For presentation ease, in what follows we define the operation of the controller for a cooling thermostatic device as described in Section 4.5.1. For such an appliance, at each time-step, the controller decides the next value $X(t+1)$ as a function of $X(t)$, its current state $\theta(t)$ (temperature), and the GECN signal $g_i(t)$ as follows:

1. If the value of the counter $T(t)$ is not equal to zero, then the appliance disregards the GECN signal and continues its normal operation, as previously explained.
2. If $T(t) = 0$, the intensity of the signal is taken into account: upon receiving $g_i(t)$ the controller draws a Bernoulli random variable Y with parameter $p = |g_i(t)|$ (i.e., $Y = 1$ with probability p and $Y = 0$ with probability $1 - p$) that reflects the desired response by the DNO. If Y is set to 1, then the appliance proceeds to the next step, otherwise it continues with normal operation.
3. Finally, if $Y = 1$, the actual response of the appliance depends on its current operating mode $X(t)$ and internal state $\theta(t)$. Specifically, the controller draws a second, independent Bernoulli random variable Z with parameter $q(X(t), \theta(t), g_i(t))$, where $q(x, \vartheta, g)$ characterizes the appliance's propensity to switch operating mode given that $X(t) = x$, $\theta(t) = \vartheta$, and $g_i(t) = g$. The appliance then switches state if $Z = 1$, else it does not.

For example, when the cooling appliance is on, the closer the temperature is to the maximum θ_{\max} , the less likely it is that the appliance responds to a signal requiring it to switch off. Thus, when the DNO wants to inhibit consumption ($g > 0$) and the appliance is on, the probability q should be chosen so that $q = 1$ whenever $\vartheta < \theta_{\min}$, $q = 0$ whenever $\vartheta > \theta_{\max}$, and decreasing with ϑ in $\vartheta \in [\theta_{\min}, \theta_{\max}]$.

We use $q(x, \vartheta, g) = \min\{\tilde{q}(x, \vartheta, g)^+, 1\}$ where

$$\tilde{q}(x, \vartheta, g) = \begin{cases} Cx[1 - e^{-(\theta_{\max} - \vartheta)/\xi}]^+ & \text{if } g \geq 0 \\ C(1 - x)[1 - e^{-(\vartheta - \theta_{\min})/\xi}]^+ & \text{if } g < 0 \end{cases}$$

and $C = [1 - e^{-(\theta_{\max} - \theta_{\min})/\xi}]^{-1}$ is a normalization constant ⁸.

⁸We used the notation $[a]^+ := \max(a, 0)$. The denominator of the exponent, ξ , has been selected empirically to modulate the appliances' response to the GECN signal. However, such a coefficient does not influence the behavior of the proposed control mechanism.

We can summarize the proposed controller's response to the GECN signal as

$$X(t+1) = \begin{cases} 1 - X(t), & \text{if } Y = Z = 1, \\ h(X(t), \theta(t)), & \text{otherwise.} \end{cases} \quad (4.9)$$

Thus an appliance can disregard a GECN $g_i(t)$ signal for three reasons: (i) a too recent reaction to the GECN signal, in other words, the counter $T(t)$ is not equal to 0 – this avoids the appliance operation in “mini-cycles”, (ii) a small magnitude of $g_i(t)$, implying low requirement from the DNO side, or (iii) an inopportune internal state of the appliance.

4.5.2 The Case of Distributed Energy Storage Systems

In this section, the general representation of electrochemical energy storage systems is presented and a controller, tailored to the characteristics of storage devices, is proposed.

Storage System Representation

1. General Formulation of the State-of-Charge of Electrochemical-Based Storage Systems

The estimation of the so-called state of charge (SoC) of an electrochemical-based storage system is of great importance in the majority of applications dealing with operation and control of electrochemical ESSs [144].

Several methods, that use different criteria in order to estimate the SoC, are proposed in the literature. As discussed in [145] the five most important criteria, with particular reference to batteries, are (i) measurement of electrolyte specific gravity (ii) battery current time-integration (iii) battery impedance/resistance estimation (iv) measurement of the battery open circuit voltage and (v) inclusion of electrolyte temperature, discharge, rate and other battery parameters. A general equation, that defines the SoC at a specific time instant and is a combination of the above criteria, is (e.g., [144, 146, 147, 148]):

$$SoC(t) = \frac{C(t_0) - \alpha(I, \theta) \int i(t) dt}{C(I, \theta)} \quad (4.10)$$

where $C(I, \theta)$ is the ESS capacity for a constant current discharge rate I at electrolyte temperature θ , $C(t_0)$ is the ESS capacity at time t_0 , $i(t)$ is the instantaneous value of the current and α is the charge-efficiency coefficient associated to charge and discharge phases⁹.

The SoC, computed as in (4.10), will be incorporated by the storage controller as better discussed below.

⁹As a first approximation $\alpha(I, \theta)$ can be assumed equal to 1. Specific tests on the targeted storage systems can infer this function.

2. Circuit-Based Model of Electrochemical ESS Applied to the Case of Supercapacitors

A general approach in modeling electrochemical ESSs is to represent a single cell with an equivalent circuit-based model that simulates their behavior (e.g., [149, 150, 151]). Such models provide simple structures that can represent sufficiently the dynamic behavior of these ESSs as they are directly related to the physics/chemistry of the cell configuration. The major advantage of this approach is that the relationship between the cell voltage and the current drawn or supplied to the cell can often be expressed analytically by solving a system of ordinary differential equations [152].

In this chapter, supercapacitors (SC) have been selected as the targeted ESS. Due to their high power density, short charge time and long life duration, these devices are particularly interesting in the ESS applications that require rapid cycles (e.g., primary voltage control via fast compensation of renewable DG, fast charging of electric vehicles) [140]. Several circuit-based models, which can represent the SC behavior in both steady-state and dynamic conditions, are proposed in the literature (e.g., [153, 154]). In this section, the model developed in [154] is considered, for which the equivalent circuit model is depicted in Figure 4.3. This model enables us to correctly represent both the quasi-static and dynamic behavior of a SC accounting for the so-called “redistribution-effect” that plays a major role in its dynamic behavior.

For this specific model, the SC terminal voltage, V^{DC} , is linked to the input current, I^{DC} , via the following system of ordinary differential equations:

$$\begin{aligned} \frac{dV_1}{dt} &= \left(-(I^{DC} + I_{ch}) + \frac{V_1 - V_2}{R_2} + V_1 \frac{dC_v}{dt} - I_{red} \right) \frac{-1}{C_v} \\ \frac{dV_2}{dt} &= \left(\frac{V_2 - V_3}{R_3} - \frac{V_1 - V_2}{R_2} + V_2 \frac{dC_2}{dt} \right) \frac{-1}{C_2} \\ \frac{dV_3}{dt} &= \left(-\frac{V_2 - V_3}{R_3} + V_3 \frac{dC_3}{dt} \right) \frac{-1}{C_3} \\ V^{DC} &= V_1 + (I^{DC} + I_{ch})(R_1 + R_L) \end{aligned} \quad (4.11)$$

where R_1 is the input electrode resistance; R_L and C_v are the resistance and the capacitance of the so-called “SC network system model” and; R_2 , C_2 and R_3 , C_3 are the resistances and the capacitances of the second and third branch respectively. All the capacitances exhibit a non-linear dependence on the voltage. This dependence is taken into account by curve-fitting measurements obtained via experimental tests. As proposed in [154], the two current sources, I_{ch} and I_{red} , allow for improving the dynamics of the SC by taking into account the diffusion of the residual charge during the charge/discharge phases (short-term phenomenon), as well as during the redistribution phase (long-term phenomenon).

In the rest of the chapter, we assume that SC cells are arranged in parallel and series connections suitable to form an array of a given total energy and power capacities. A bidirectional DC/AC converter is used to interface the SC with the network. The state of each cell is assumed to be its terminal voltage and the evolution of this state is

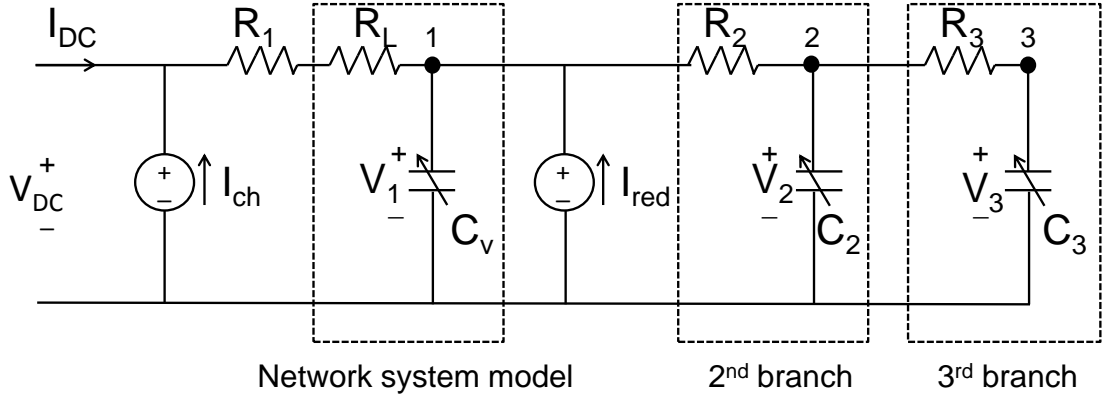


Figure 4.3: Proposed SC model (adapted from [154]).

described by (4.11). In order to model the power converter, the constraints on the AC active and reactive power should be taken into account. The PQ capability curve of the converter is described by the following inequality constraint:

$$\sqrt{(P^{AC})^2 + (Q^{AC})^2} \leq S_r \quad (4.12)$$

where, S_r is the rated power of the converter and P^{AC}, Q^{AC} the active/reactive power flows on the AC-side of the power converter interfacing the SC towards the grid.

It is assumed, as a first approximation, that the DC/AC converter is characterized by an efficiency (η) independent of its power flow. It is also assumed that this power converter can operate in four quadrants.

Storage Controller

In comparison with the TCL controller presented earlier, where active power signals were used, the storage devices connected to a network bus i receive at each time-step t two broadcast control signals, $g_{P_i}(t)$ for the active power and $g_{Q_i}(t)$ for the reactive power. Each signal represents a real number $g_{P_i}(t), g_{Q_i}(t) \in [-1, 1]$. The control signals $g_{P_i}(t), g_{Q_i}(t)$ reflect, as before, the DNO's desire to inhibit (or encourage) consumption. Hence, a negative g_{P_i} encourages charging, a positive g_{P_i} encourages discharging, and $g_{P_i} = 0$ does not have an effect on the storage devices. Similarly, a negative g_{Q_i} calls for reactive power absorption, a positive g_{Q_i} requests for more reactive power support, and $g_{Q_i} = 0$ means that the DNO is satisfied with the current state of the ESS.

In the following, we propose a controller that takes into account these signals. As described, in response to non-zero $g_{P_i}(t), g_{Q_i}(t)$ signals, the SC decides to charge or discharge an amount of energy. This decision is a function of the signals, the SoC, the DC voltage, as well as the previous state of the device. When this decision is made, the controller chooses the next state of the device as follows:

1. Upon receiving $g_{P_i}(t)$ and $g_{Q_i}(t)$, the controller considers the signals as requested adjustments in its AC-side active and reactive power set-points expressed as fractions of the rated power:

$$\begin{aligned}\Delta P_i^{AC}(t) &= -S_{ir}g_{P_i}(t) \\ \Delta Q_i^{AC}(t) &= -S_{ir}g_{Q_i}(t)\end{aligned}\quad (4.13)$$

In other words, the two signals are viewed as proportional to the desired response of the resources requested by the DNO.

2. Once the required adjustments to the power set-points are computed, the controller verifies that the constraints on the PQ capability curve of the converter are respected. If this is not the case, $\Delta P_i^{AC}(t)$ and $\Delta Q_i^{AC}(t)$ are adjusted in such a way that the total power set-point is the closest to the feasible region represented by (4.12). Figure 4.4 shows an example where the requested set-points lead the system to a state where the constraints of the converter are violated (point 2 in Figure 4.4) and where an adjustment is required to a new state (point 3 in Figure 4.4). If the size of the SC arrays or the capabilities of the converter are limited, then the requested power set-points are expected to be quite frequently in the limits of the capability curve. The proposed adjustment is chosen in order to avoid staying on the same point in the boundary of the PQ capability curve once this limit is reached.¹⁰
3. The actual response of the storage device depends on the current operating point $(P_i^{AC}(t), Q_i^{AC}(t))$, on the SC internal state $(V_i^{DC}(t))$ and on its state of charge $(SoC_i(t))$. The new AC set-points are computed as a moving average of the previous operating point and the requested operating set-point filtered by a function of the SoC :

$$\begin{aligned}P_i^{AC}(t+1) &= \omega\beta_P(P_i^{AC}(t) + \Delta P_i^{AC}(t)) + (1-\omega)P_i^{AC}(t) \\ Q_i^{AC}(t+1) &= \omega\beta_Q(Q_i^{AC}(t) + \Delta Q_i^{AC}(t)) + (1-\omega)Q_i^{AC}(t)\end{aligned}\quad (4.14)$$

where ω is a fixed gain and β_P and β_Q are variable gains that depend on the current SoC of the SC. Specifically, for the active power $\beta_P = (1 - SoC_i)^2$, when the device is charging ($P_i^{AC}(t) > 0$), and $\beta_P = (SoC_i)^2$ when the device is discharging ($P_i^{AC}(t) < 0$). For the reactive power, $\beta_Q = (SoC_i)^2$ regardless of the sign of the requested reactive power flow¹¹. This coefficient is used to filter the total power provided by the storage devices in order to smooth their response by accounting

¹⁰It is worth observing that if the intercept on the line between points 1 and 2 on Figure 4.4 is chosen as the adjusted point (instead of point 3), then once the limit of the converter is reached and the subsequent set-points are also outside of the capability curve then the controller will stay in the same set-point for several time-steps.

¹¹Note that the request of the reactive power always drains energy from the SC through the losses in the converter regardless of the sign of the reactive power flow.

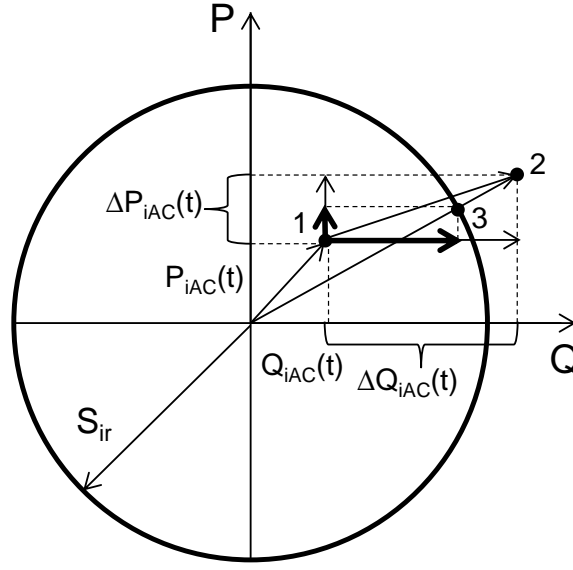


Figure 4.4: Adjustment of the requested power set-points in case of violation of the constraints of the PQ capability curve of the converter.

for their internal state.

4. The internal-state constraints of the storage device are finally taken into account. In particular, if the DC voltage has reached a specific minimum (V_{\min}^{DC}) or maximum (V_{\max}^{DC}) value, then the controller refuses to participate in the action to avoid the intervention of the maximum/minimum voltage relays always used in these types of systems to preserve the power electronics [145]. If the limits are not yet reached, the AC set-points are transformed into DC power requirements and subsequently, in charging/discharging current references as follows:

$$\begin{aligned}
 P_i^{loss}(t+1) &= (1-\eta_i)\sqrt{(P_i^{AC}(t+1))^2 + (Q_i^{AC}(t+1))^2} & (4.15) \\
 P_i^{DC}(t+1) &= P_i^{AC}(t+1) + P_i^{loss}(t+1) \\
 I_i^{DC}(t+1) &= \frac{P_i^{DC}(t+1)}{V_i^{DC}(t)}
 \end{aligned}$$

where P_i^{loss} represents the losses in the i -th power converter. At this point the V_i^{DC} is continuously changing as a function of the charging/discharging current I_i^{DC} based on the model of the i -th ESS. For instance, in the case of supercapacitors, V_i^{DC} is updated based on (4.11). Then the current is updated so as to maintain the P_i^{DC} set-point constant, until the controller receives the next GECN signals.

On the Sizing of the ESSs

The sizing of an ESS is intimately coupled with its control algorithm. In this respect, in this subsection we illustrate a possible procedure for sizing the distributed storage systems to fit the requests of the proposed control algorithm.

It is important to note that the sizing is done in terms of energy capacity. We describe below a method that, based on the observed forecast errors for a given day in the past, determines the required power adjustments from the storage system at each time-step. The minimum energy capacity is deduced from these adjustments.

For the sizing procedure the DNO determines “the worst day” in terms of forecasting errors from historical data. For this day, the DNO has the imperfect 24hr per-bus forecasts for load and renewable profiles by $(\mathbf{P}^f(t), \mathbf{Q}^f(t))$ and the actual per-bus measured power $(\mathbf{P}(t), \mathbf{Q}(t))$ and phase-to-ground voltage $\bar{E}_i(t)$. The DNO solves at each time-step the optimization problem (4.1) and gets the process of optimal required power adjustments $(\Delta\mathbf{P}^*(t), \Delta\mathbf{Q}^*(t))_i$ in the buses. These lead to the desired operation set-points for voltage control for the whole 24hr period.

The solution of (4.1) provides profiles of PQ setpoints for a given scenario of loads and distributed generation. Once the required power adjustments are computed for each bus, the DNO has a rough knowledge of the instantaneous amount of excess or deficit in the active and reactive power throughout the whole 24hr period. Thus, the DNO can compute the energy and, consequently, the size of storage devices that will be needed. The integral of the active power flow in each bus quantifies the required size for a given storage system. Nevertheless, the outcome of such a sizing remains related to the considered scenarios, and for this reason the presented method provides only an approximate sizing.

In our case, the targeted ESSs are SCs. Therefore, as they are characterized by high power density and low energy density, we take into account the nature of these devices and we do not utilize them for performing energy balance. To this end, we assumed as a worst-case condition the one that involves large instantaneous errors in the forecasted PV power production. In particular, Figure 4.5 shows the actual and forecasted daily aggregated profiles of active and reactive power of all the network buses used for the sizing of these devices, as well as the forecasting errors.

4.6 GECN Performance Evaluation and Application Examples: Primary Voltage Control via Demand Response and Distributed Storage Management

In this section, we first evaluate the performances of GECN when primary voltage control is performed via real-time control of TCLs and OLTCs and we investigate the potential of SCs to provide primary voltage control via GECN. Next, we present an application example where both TCLs and SCs are controlled by the same broadcast signal. Subsequently, we investigate the importance of active versus reactive power

4.6. GECN Performance Evaluation and Application Examples: Primary Voltage Control via Demand Response and Distributed Storage Management

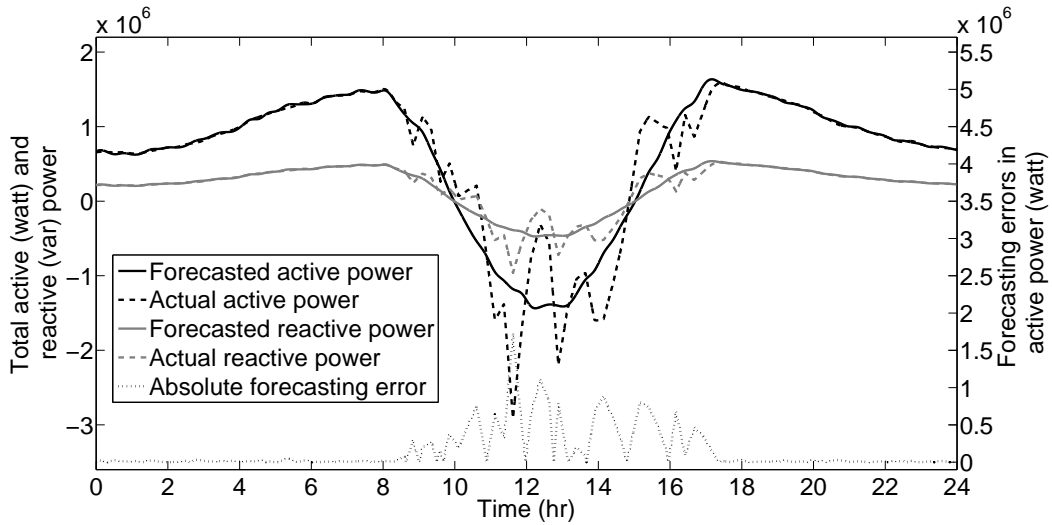


Figure 4.5: Actual/forecasted values of aggregated active and reactive power injections of all network buses used for the sizing of the SC arrays.

support for voltage control in ADNs. Furthermore, we show the capability of the proposed control scheme to cope with fast voltage variations originating from a large load inrush. Finally, we assess the time required by the GECN network controller to solve the optimal voltage control problem.

4.6.1 Primary Voltage Control via Real-time Demand Response

For the evaluation of GECN in the case of TCLs we have considered a modified IEEE 13-nodes test feeder as depicted in Figure 4.6. The modifications are: (i) balanced lines, (ii) inclusion of secondary substations (henceforth called “aggregators”) where voltage-independent PQ equivalents are placed and, (iii) lines ten times longer. As a consequence, using the approach described in Section 3.4.2, we can compute the network voltage sensitivity coefficients. A specific Matlab code has been developed to solve the network load flow problem and to implement the GECN control mechanism.

Each aggregator in the network comprises a large population of heterogeneous household controllable loads along with non-elastic demand and non-dispatchable power injections. The technical characteristics of the elastic loads and the load controller parameters are given in Table 4.6 ([155, 135, 143]). Concerning the non-dispatchable power generation, we assumed to have a typical PV-type profile with peak power that changes for all aggregators within the range of 90% – 180% of each secondary substation’s peak load. Additionally, Figure 4.7 illustrates the total daily load and power injections profile in the network, where the convention used is that negative values represent power injection and positive power consumption.

We assumed three different test cases for the available elastic demand in the net-

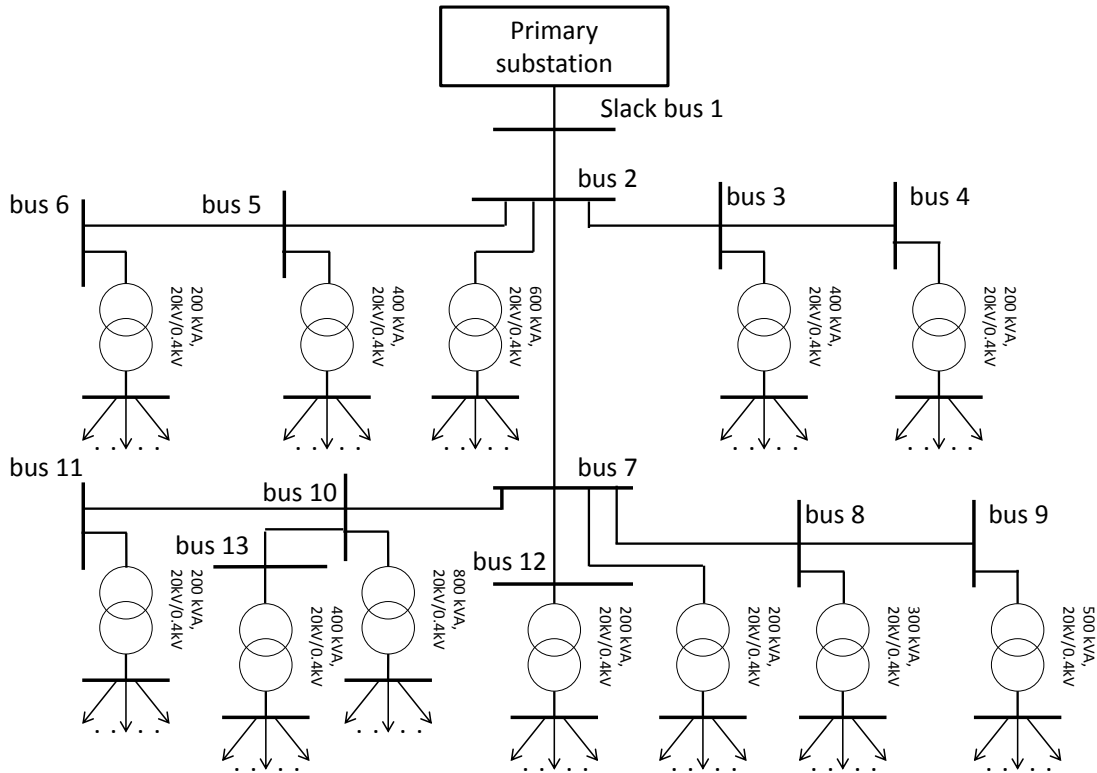


Figure 4.6: Modified IEEE 13 node test feeder used for the evaluation of the proposed DR mechanism.

Table 4.1: Parameters of the elastic appliances and the load controller

Parameter	Value
Temperature deadband, $\Theta(^{\circ}C)$	[3,8]
Ambient temperature, $\theta_0(^{\circ}C)$	$\sim U(10, 15)$
Thermal conductivity, $A(kW/^{\circ}C)$	10.563
Coefficient of performance, (η)	1.5
Rated power, P_r (Watt)	150
Time-step, τ (sec)	1
Time constant, $T_c = m_c/A$ (hrs)	$\sim U(1.326, 2.778)$
Controller time counter, T_0 (sec)	480
Internal state parameter, ξ	0.4
Appliance power factor, $\cos \varphi$	0.85
Parameters of the penalty function ψ_1, a_1, a_2	1000, 2
Parameters of the penalty function ψ_2, a_3, τ_o (hrs)	5,3
Window of \hat{g}, W (time-steps)	3

4.6. GECN Performance Evaluation and Application Examples: Primary Voltage Control via Demand Response and Distributed Storage Management

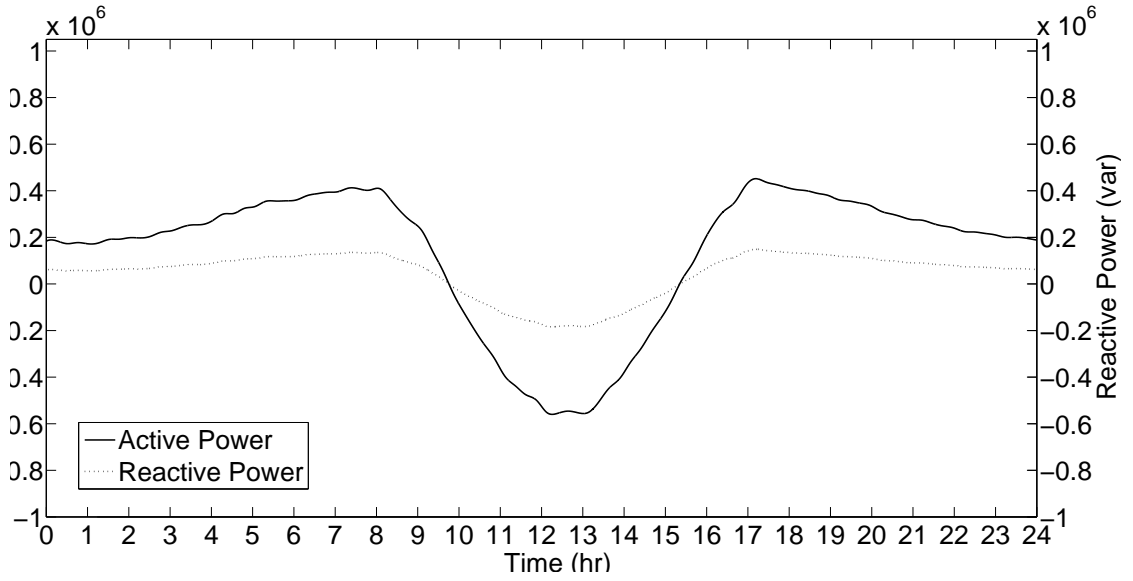


Figure 4.7: Total daily load and power injections profile in the network.

Table 4.2: Number of elastic appliances per network bus

Bus	10% elastic demand	20% elastic demand	30% elastic demand
1	-	-	-
2	93	182	310
3	113	204	328
4	112	192	309
5	114	216	324
6	100	210	304
7	105	197	336
8	118	219	320
9	98	210	325
10	82	217	327
11	115	212	311
12	105	209	314
13	94	211	305

work, 10%, 20% and 30% of the total peak load. In Table 4.2, the number of appliances per bus of the network is shown for these three cases. For each test case two scenarios have been considered. Scenario I relies on the assessment of the voltage controllability by using only the DR control mechanism (by setting the coefficients $K_{n,i}(t)$, and the third term of the objective function in Eq. 4.1 to zero), whereas Scenario II assumes that the DNO uses the DR control mechanism together with the control of the primary substation OLTC (i.e., with the objective function as described in Eq. 4.1).

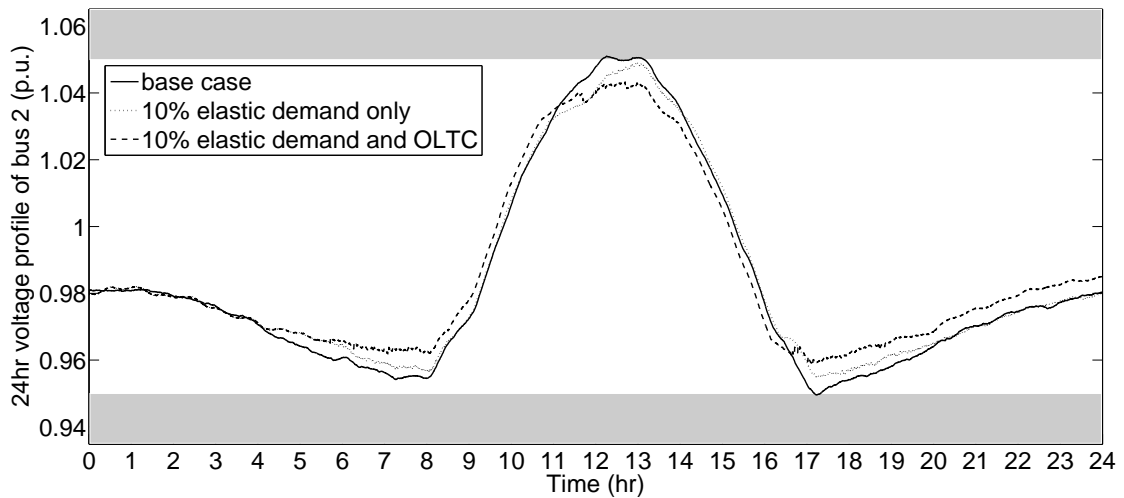
The DNO deploys GECN to continuously penalize the deviation of the voltage in the network buses from the rated value, in order to guarantee a voltage profile for safe operation. To this end, the operator solves at each time-step the optimization problem defined in Eq. 4.1 with $\lambda_i = 0.15$ and $\mu_i = 1$ for both scenarios I and II. Specifically, for scenario II, the moving average of the control signal is computed as $\hat{g}_i(t) = 0.8g_i(t) + 0.1g_i(t-1) + 0.1g_i(t-2)$.

The DNO wishes that the voltage deviations in the network buses are in the range of $\pm 5\%$. In order not to saturate the available DR resources of the network, we assume that there is a tolerance in the voltage deviations from the network-rated value, which is represented by the parameter α in Eq. 4.1. The role of this parameter is to create a deadband within which the DNO is not interested in minimizing the voltage, thus sacrificing the scarce resources. In this section this parameter is set to $\alpha = 0.04$ and the resulting deadband for the voltage profile is $[0.96, 1.04]p.u.$ Additionally, it is assumed that the constraint γ_i on the power factor of the aggregate load in all buses is 0.9. Finally, we assume to have an OLTC that can vary the rated value of the network voltage in the range of $\pm 6\%$, operating in 72 tap positions.

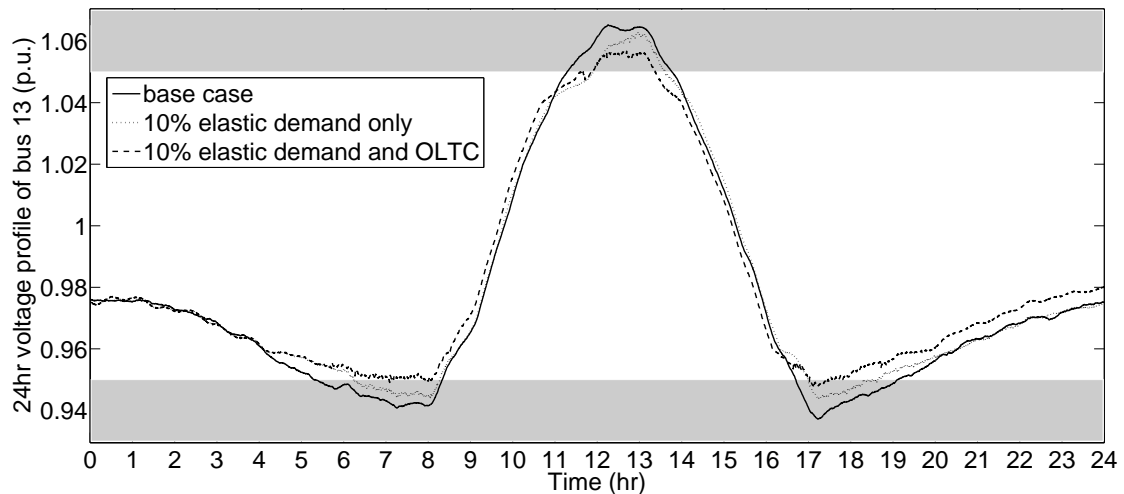
In order to infer the benefits of the proposed mechanism, we assume a base case where the total demand in the network is non-elastic and obtain the daily voltage profile of the network buses. For the sake of brevity, we limit the validation of the proposed method to a reduced number of buses. In particular, we refer mainly to two buses of interest: bus 2, which is the closest one to the slack bus; and bus 13, which is the furthest one from the slack bus of the network. In Figure 4.8 one can observe the voltage profile of these buses for the base case, as well as the improvement in the voltage profile for both considered scenarios when there is 10% of elastic demand in the network. The gray bands indicate the range $[0.95, 1.05]$. Figures 4.9 and 4.10 show the same voltage profiles for the case of 20% and 30% elastic demand respectively. Figure 4.8 shows an improvement of voltage profiles that can be quantified in the range of 1% in correspondence of the maximum aggregated power absorption and power production, whereas, Figures 4.9 and 4.10 show an even larger improvement (in the order of 2%) due to the increased availability of controllable loads. In fact, for the case of 30% elastic demand the improvement is only due to the controllable loads as the number of OLTC operations is zero. This is due to the fact that the increased availability of controllable appliances is already enough to guarantee a voltage profile at all buses in the range of $[0.95, 1.05]p.u.$, thus eliminating the need to leverage on the OLTC. This result reveals the capabilities of the proposed method to enable a non-negligible contribution of controllable loads to voltage control of distribution networks eliminating the need to use other traditional systems like OLTC.

For the same cases as in Figures 4.8, 4.9 and 4.10, Figures 4.11, 4.12 and 4.13 show the GECN signals that were sent by the DNO to achieve the desired behavior of the elastic loads for scenarios I and II. It can be observed that the variation of the GECN signals is smoothed by the control leverage of the OLTC. This aspect appears important

4.6. GECN Performance Evaluation and Application Examples: Primary Voltage Control via Demand Response and Distributed Storage Management



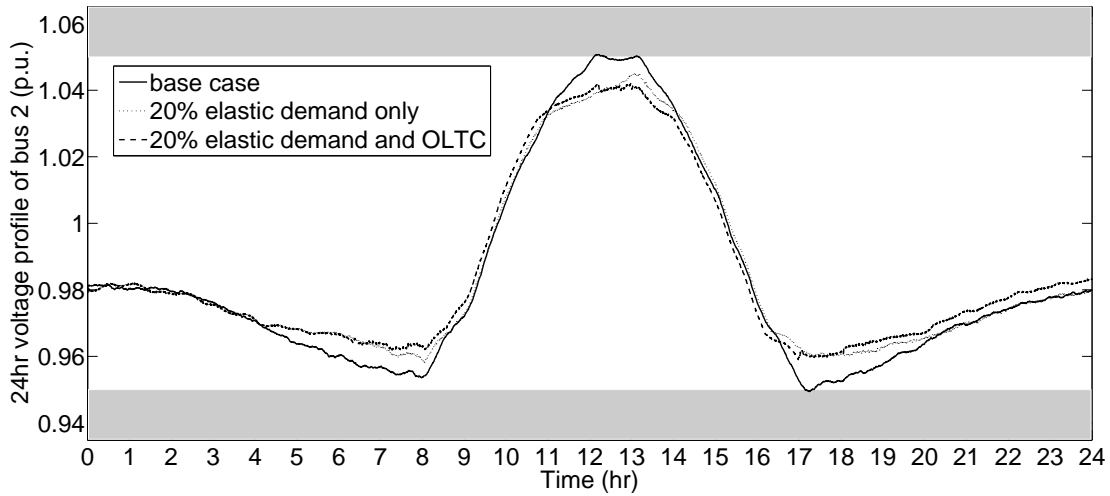
(a) 24hr voltage profile of bus 2



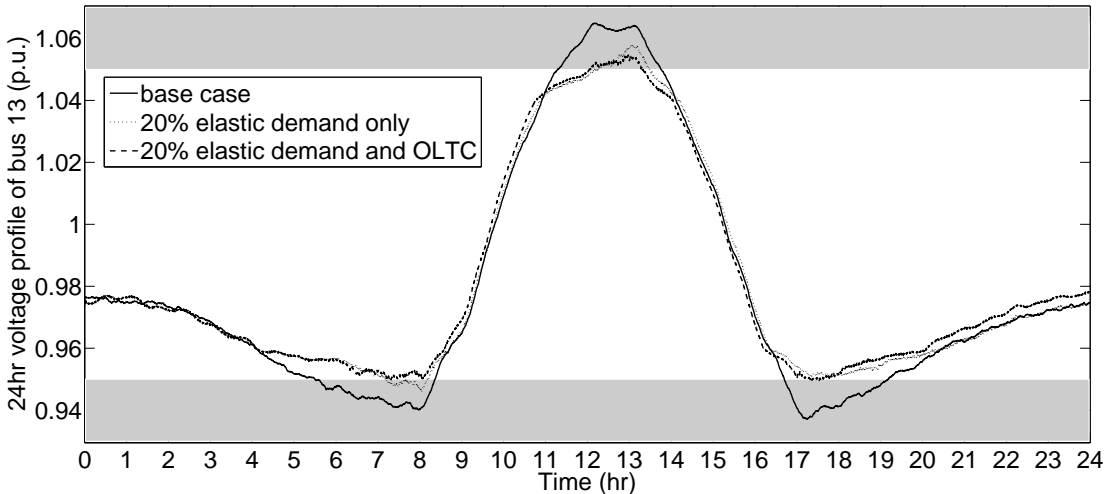
(b) 24hr voltage profile of bus 13

Figure 4.8: 24hr voltage profiles of bus 2 and 13 for 0% of elastic demand (base case) and 10% of elastic demand with (scenario II) and without (scenario I) control of the tap-changers positions.

as it could allow the DNO to choose the better control strategy, namely leveraging more on the load elasticity or on its own resources (i.e., OLTC). These figures also show a large saturation of the GECN signal without the help of the OLTC in the case of 10% and 20% of elastic demand. It is also interesting to observe that the increase of elastic loads from 10% to 20% directly results in a decrease of the GECN saturation. This allows for an indirect quantification of the DR elasticity and, as a consequence, an estimation of the optimal number of OLTC changes allowed per day.



(a) 24hr voltage profile of bus 2



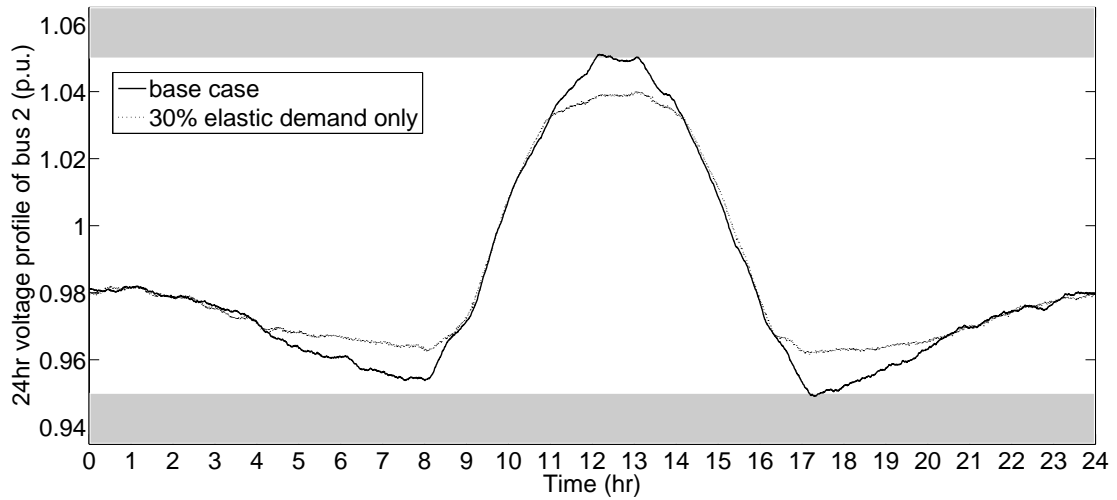
(b) 24hr voltage profile of bus 13

Figure 4.9: 24hr voltage profiles of bus 2 and 13 for 0% of elastic demand (base case) and 20% of elastic demand with (scenario II) and without (scenario I) control of the tap-changers positions.

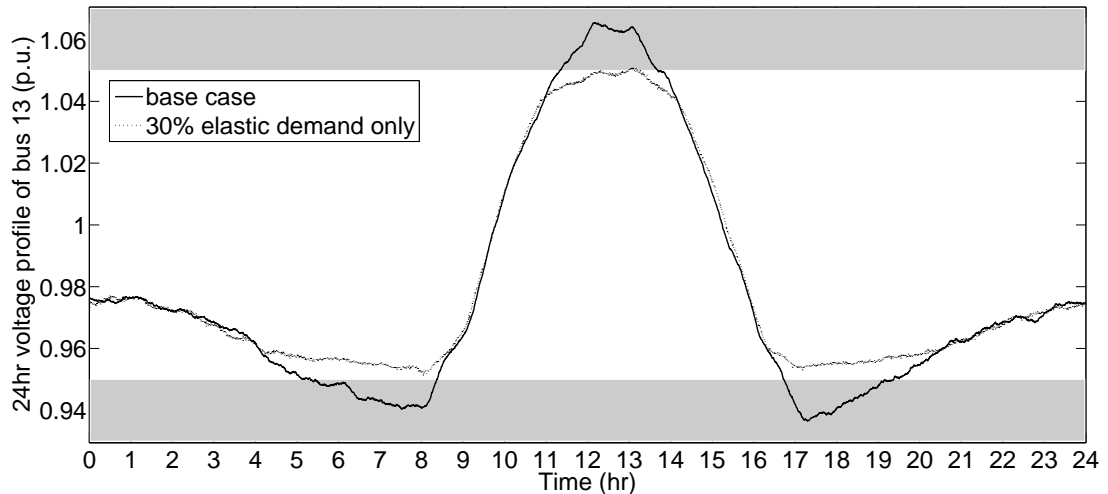
Figure 4.14 shows the daily profile of the OLTC changes provided by scenario II for 10% and 20% of elastic demand. For the case of 30% of elastic demand no OLTC change occurs. As expected in the case of 20% elastic demand the total number of OLTC operations is less than in the case of 10% elastic demand (12 vs 17). Overall, it can be observed that the obtained number of OLTC changes is compatible with a typical operation of such a device.

For the same buses (2 and 13), Figure 4.15 shows the aggregate power of only the

4.6. GECN Performance Evaluation and Application Examples: Primary Voltage Control via Demand Response and Distributed Storage Management



(a) 24hr voltage profile of bus 2

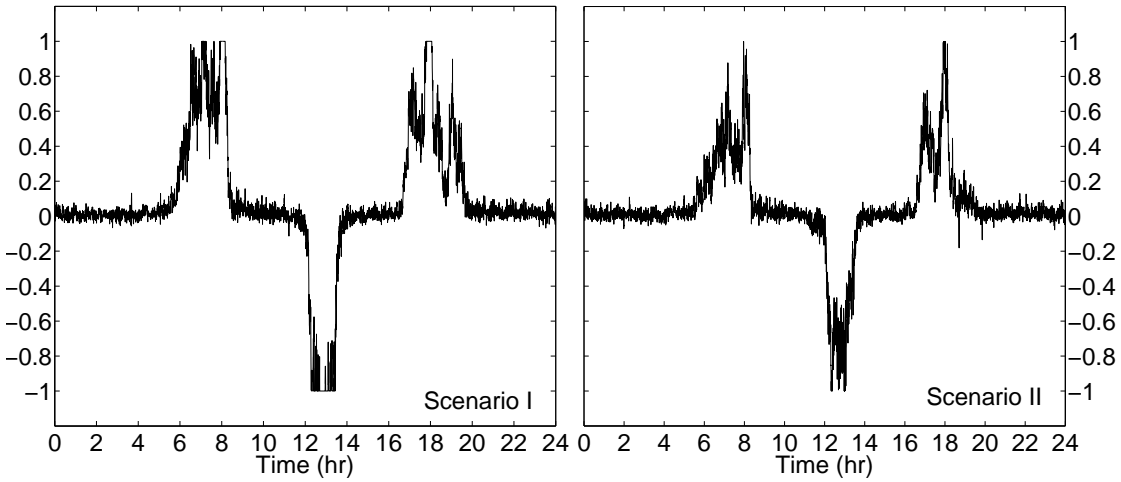


(b) 24hr voltage profile of bus 13

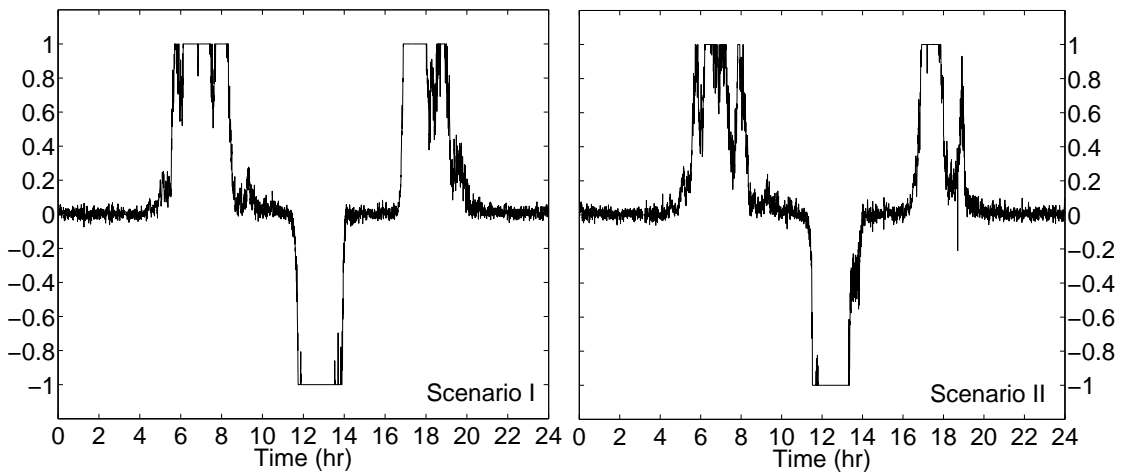
Figure 4.10: 24hr voltage profiles of bus 2 and 13 for 0% of elastic demand (base case) and 30% of elastic demand without (scenario I) control of the tap-changers positions.

elastic appliances in correspondence of the signals presented in Figures 4.11, 4.12 and 4.13 for Scenario I. This figure demonstrates that the proposed DR mechanism allows aggregated loads to follow properly the GECN signal. Also, these figures reveal that for short periods of time (in the order of 15 – 30 minutes) the DNO can drive the aggregate power of even a small number of elastic appliances up to twice or down to one third of their average power consumption by sending the appropriate signal.

Concerning the impact on the appliance internal states (i.e., temperature), Figure 4.16 shows a histogram of the appliances' temperatures at buses 2 and 13 during



(a) 24hr GECN signals sent to bus 2

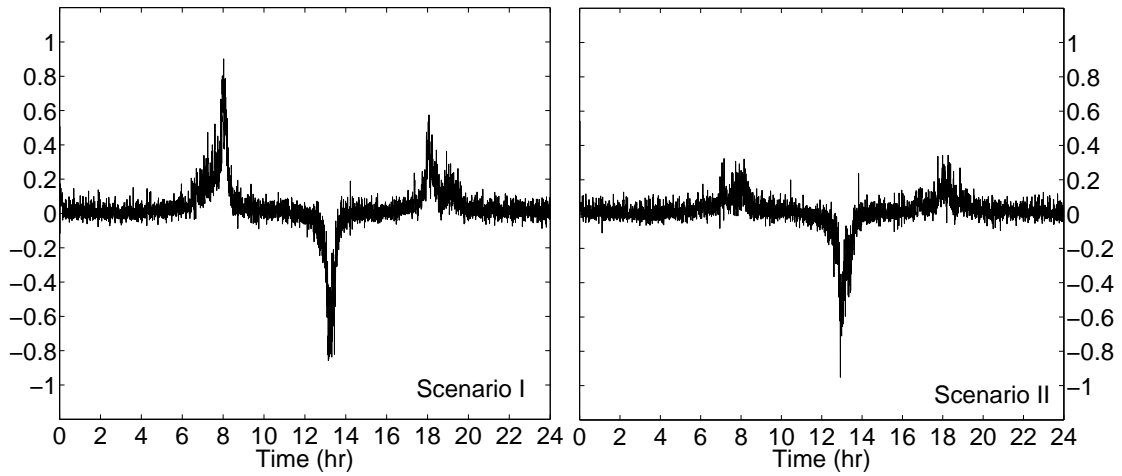


(b) 24hr GECN signals sent to bus 13

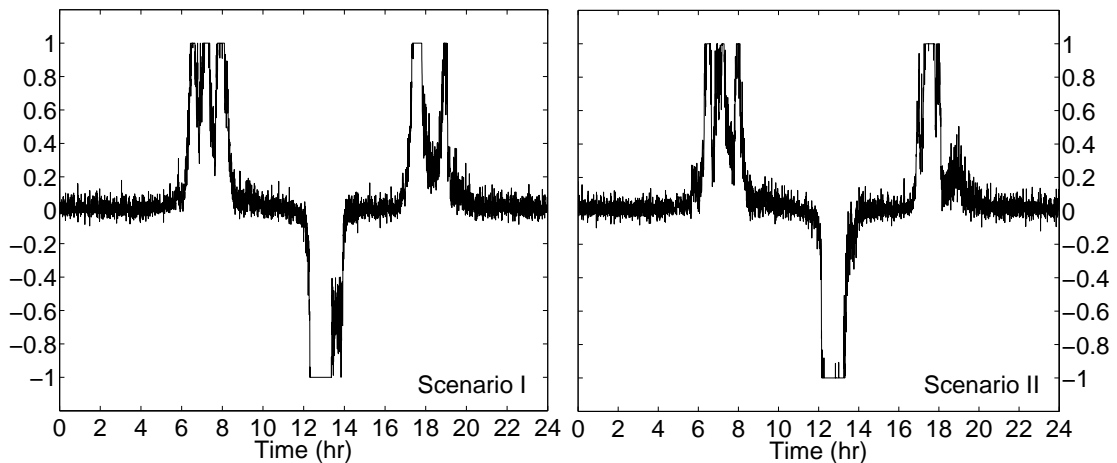
Figure 4.11: GECN signal sent to buses 2 and 13 in the case of 10% of elastic demand with (scenario II) and without (scenario I) control of the tap-changers positions.

different periods of the day for scenario I and 10% of elastic demand. The latter reveals that the operation of the GECN mechanism does not have an impact on the end-users quality of service, as it does not cause any deviation of the appliances temperatures outside of the allowed deadband (i.e., $3^{\circ}-8^{\circ}C$). The temperatures of the elastic loads during hours 1–4 are in compliance with the GECN signal sent that is not saturated. In the same figure, one can observe a large concentration of temperatures in the lower part of the temperature deadband during hours 11–14; this is compatible with the signal sent during these hours to encourage consumption. The opposite effect is ob-

4.6. GECN Performance Evaluation and Application Examples: Primary Voltage Control via Demand Response and Distributed Storage Management



(a) 24hr GECN signals sent to bus 2



(b) 24hr GECN signals sent to bus 13

Figure 4.12: GECN signal sent to buses 2 and 13 in the case of 20% of elastic demand with (scenario II) and without (scenario I) control of the tap-changers positions.

served during hours 17–22 where the peak load results in large, positive signals that dictate the reduction in consumption.

Finally, the slope of the saturation function is a significant parameter in the control law used by the DNO. In order to investigate the impact of the saturation function in the performance of the proposed DR mechanism the parameter b of the saturation function is decreased to half its initial value ($b = 1.4E^{-3}$). The signal sent to bus 3 for the two values of the parameter b is presented in Figure 4.17, where it is assumed that the DNO also controls the tap changers and the elastic demand in the network is 10%.

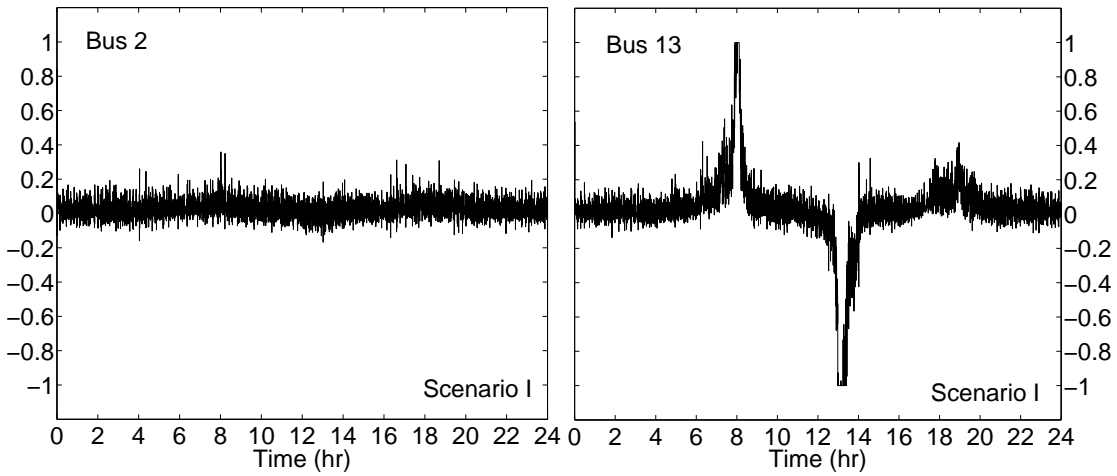


Figure 4.13: GECN signal sent to buses 2 and 13 in the case of 30% of elastic demand without (scenario I) control of the tap-changers positions.

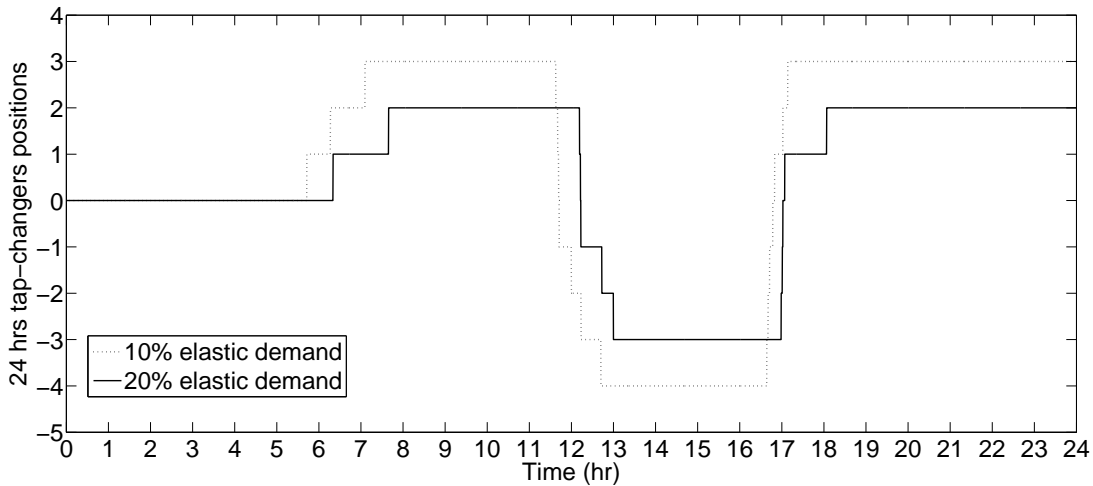
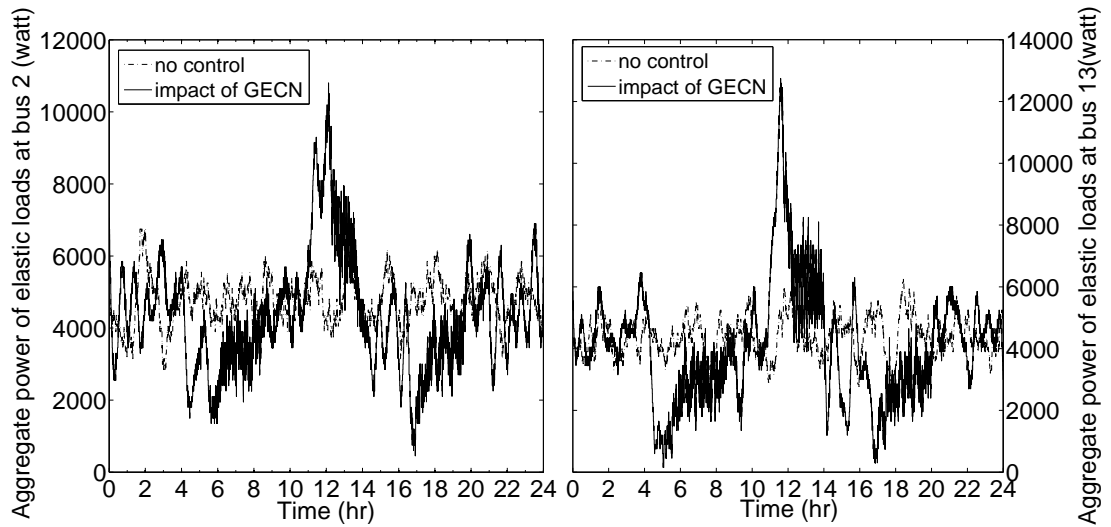


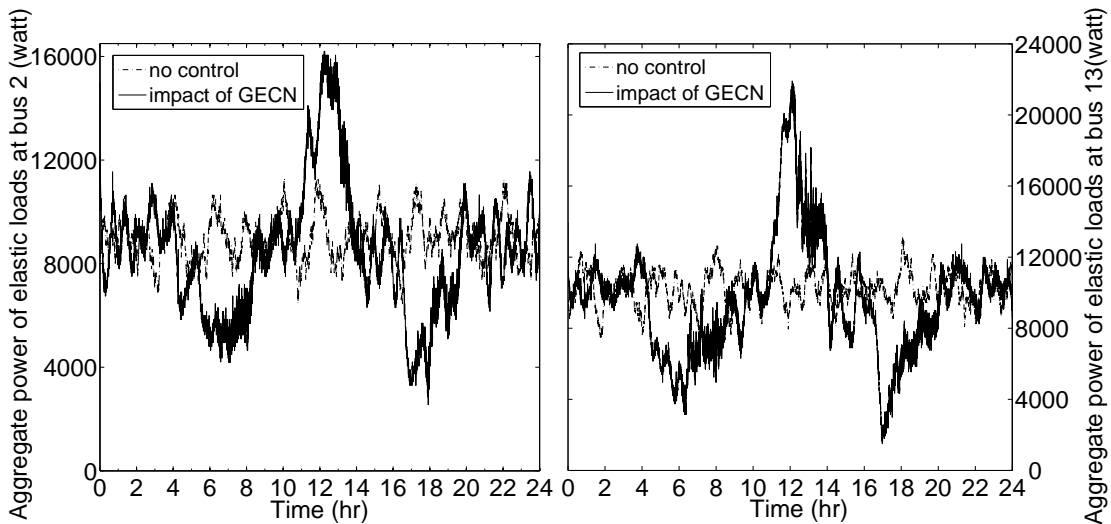
Figure 4.14: 24hrs tap-changers positions for scenario II, 10% and 20% of elastic demand with control of the tap-changers.

One can observe that, the signal does not exhibit peak values variation for the two considered cases. The significant impact of parameter b is related to the generation of larger/smaller errors into the control loop of Figure 4.1. The consequence of this is that higher/lower values of b produce steeper saturation functions that result in lower/larger modifications of the GECN signal amplitude. In Figure 4.18 the daily voltage profile of bus 3 is shown as well as the difference in the voltage profiles for both cases of the parameter b . By observing Figure 4.18, it is possible to conclude that the

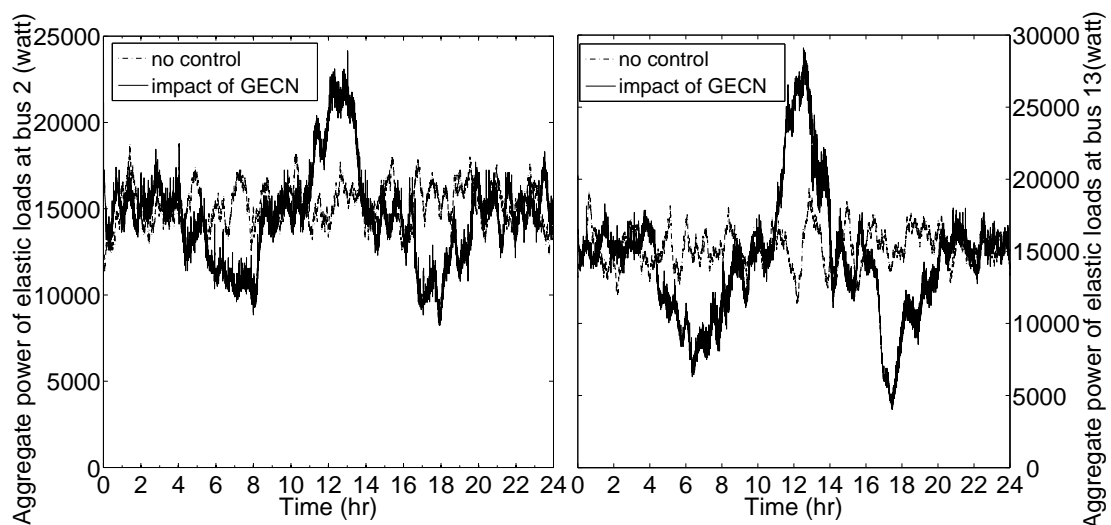
4.6. GECN Performance Evaluation and Application Examples: Primary Voltage Control via Demand Response and Distributed Storage Management



(a) Aggregate power of elastic appliances at bus 2 and 13, 10% elastic demand



(b) Aggregate power of elastic appliances at bus 2 and 13, 20% elastic demand



(c) Aggregate power of elastic appliances at bus 2 and 13, 30% elastic demand

Figure 4.15: Aggregate power of the elastic appliances at buses 2 and 13 for scenario I, 10%,20% and 30% of elastic demand and no control of the tap-changers.

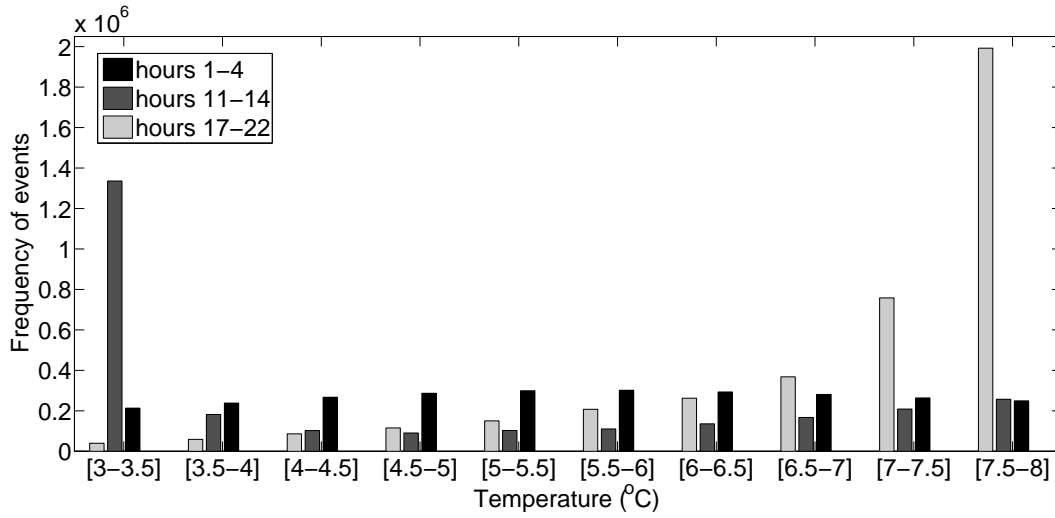


Figure 4.16: Histogram of temperatures of elastic appliances (refrigerators) in buses 2 and 13 during different hours of operation for scenario I, 10% of elastic demand and no control of the tap-changers.

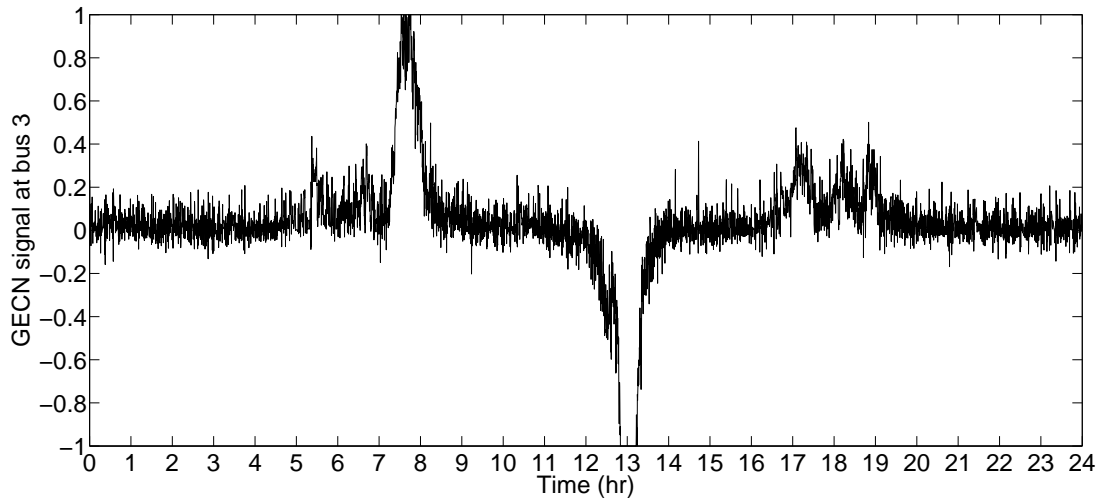
parameter b does not influence the voltage quality.

4.6.2 Primary Voltage Control via Distributed ESSs Management

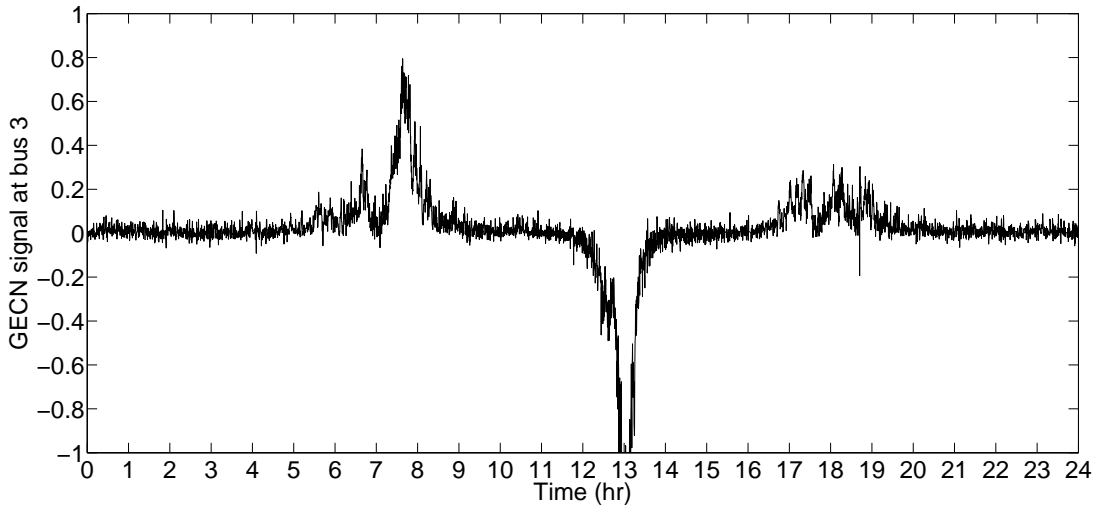
For the evaluation of GECN when the controllable DERs are composed of ESSs, we have considered a modified IEEE 34-nodes test feeder as depicted in Figure 4.19. The modifications are (i) balanced lines and (ii) the elimination of the regulators in line segments 814 – 850, 852 – 832 and of the shunt capacitors in buses 844, 848. The primary substation transformer is taken into account by considering its short-circuit internal impedance. The network load flow problem, the SC model (4.11), as well as the storage control mechanism are simulated in Matlab.

It is assumed that each network bus comprises a SC array, a large population of heterogeneous household controllable loads along with non-elastic demand, as well as non-dispatchable power injections. The elastic appliances consist of refrigerators modeled as in Section 4.5.1, whereas the non-elastic loads are represented by typical 24hr curves. The main technical characteristics of the controllable appliances are the same as in the previous section (Table 4.6). Concerning the non-dispatchable power generation, we assume a PV-type profile with peak power that changes for all buses within the range of 60% – 120% of each secondary substation peak load. As far as the forecasting errors are concerned, two different scenarios are considered. In the first scenario we assume a good 24hr-ahead forecast, whereas in the second scenario we assume large forecasting errors. Figure 4.20 shows the aggregate load profile of all 34 buses in the network for both test cases, where the convention used is that negative values represent power injection and positive power consumption. For

4.6. GECN Performance Evaluation and Application Examples: Primary Voltage Control via Demand Response and Distributed Storage Management



(a) 24hr signal sent to bus 3 with $b = 7E^{-4}$



(b) 24hr signal sent to bus 3 with $b = 1.4E^{-3}$

Figure 4.17: GECN signal sent to bus 3 for different values of the parameter b for scenario I, 10% of elastic demand and no control of the tap-changers.

the first scenario the peak values for the active and reactive power consumption shown in Figure 4.20 is 1.64MW and 538Kvar respectively. The corresponding peak value for the active power production of the distributed generation is 2.95MW. For the second scenario the same load profiles are used, whereas the peak value for the active power production of the distributed generation is 4.24MW.

The SC arrays are sized approximately using the procedure described in Section 4.5.2. To this end, in (4.1) the limit value of the power factor γ_i in bus i is set to 0.9 for all network buses, and the maximum voltage magnitude deviation δ is set to

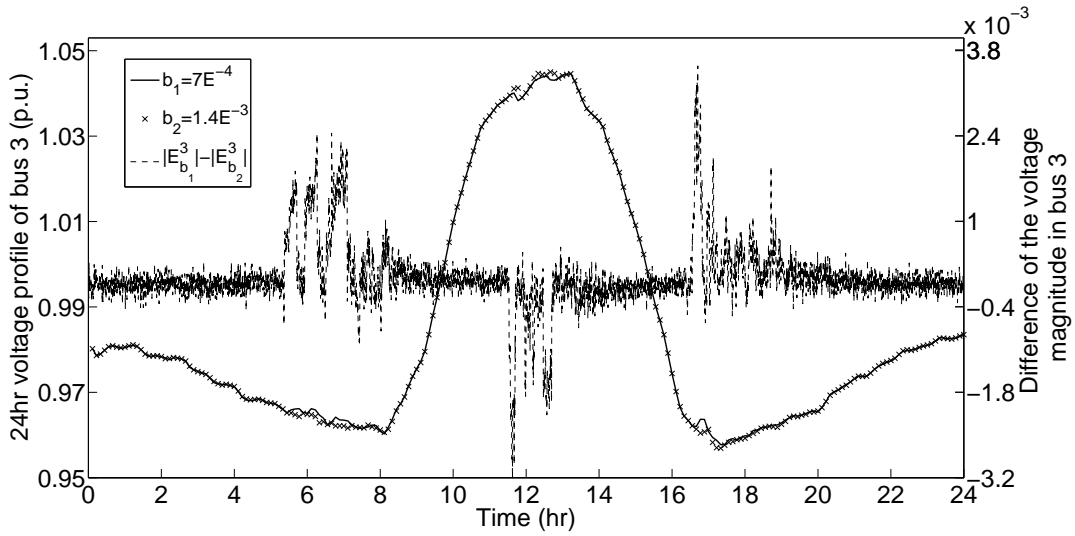


Figure 4.18: Voltage profile of bus 3 for different values of the parameter b for scenario I, 10% of elastic demand and no control of the tap-changers.

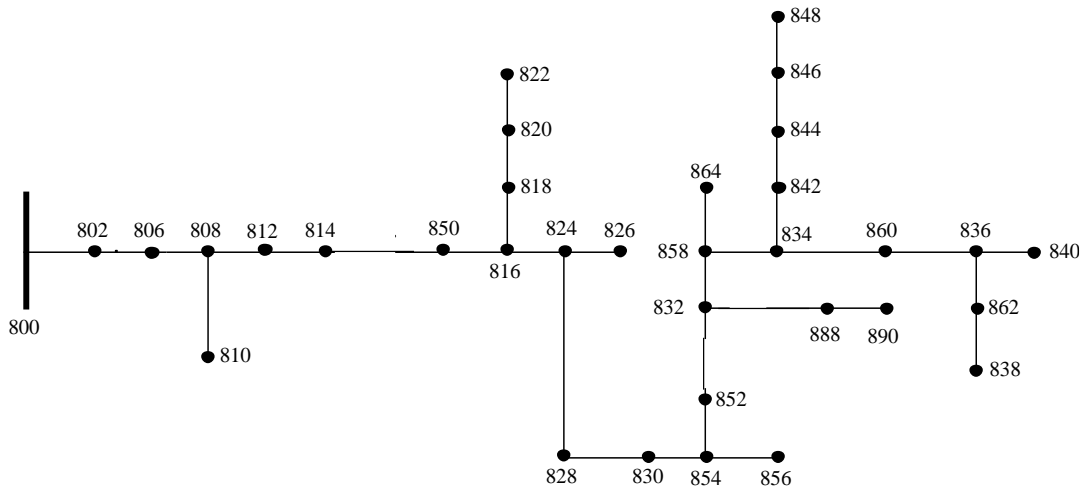


Figure 4.19: Modified IEEE-34 node test feeder used for the evaluation of the proposed control mechanism [109].

0.04 (see [120] for further details). The number of cells in parallel connection, N_p , for each bus of the network is given in Table 4.3. The number of cells in series, N_s , are equal to 149 for all buses¹². In the same table, we also provide the available energy of each array, as well as the rated power that limits the capabilities of the converter

¹²The number of cells in series is determined by dividing the maximum DC voltage required, assumed here 400 Volts, by the SC nominal cell voltage (i.e., 2.7V).

4.6. GECN Performance Evaluation and Application Examples: Primary Voltage Control via Demand Response and Distributed Storage Management

(4.12). The values of the energy reported in Table 4.3 are computed as the integral of the active power flows that resulted from the 24hr offline optimization described in Section 4.5.2. It is worth observing that the amount of energy per bus required by ESS to perform primary voltage control is in the order of few tens of kWh. Such a limited reservoir appears compatible with a specific economic analysis of the use of SC [16]. The parameters of the storage controller, used hereafter, are given in Table 4.4.

In this subsection, we evaluate the performance of the designed SC controller. To this end, the DNO employs the broadcast signals, g_{P_i} and g_{Q_i} , described in Section 4.5.2. The GECN signals are computed and sent to the network buses each 16 seconds.

In order to infer the benefits of using distributed storage for primary voltage control, we show in Figure 4.21 the initial voltage profile in the network, as well as the improvement due to the SC response for both test cases presented above. For the sake of brevity, we show the median value of the network voltages at every time-step (solid line), along with the relevant 99% confidence intervals (dashed lines). In Scenario I the improvement in the voltage profile is in the order of 2%. The largest advantage of the proposed control mechanism emerges in the case of large forecasting errors where the maximum improvement in the daily voltage profile is in the order of 6%. In Figure 4.22 the median value of the SoC of the SC arrays is shown, as well as the relevant 99% confidence intervals.

Finally, we show in Figure 4.23, the GECN signals for the active and reactive power sent to a single network bus. One can observe that when the forecasting errors are small, the request for reactive power is larger than the one for active power. As explained later, this is due to the ratio of R/X of the network lines. Under large errors in the day-ahead PV production, however, the GECN signal adapts itself and becomes significantly larger

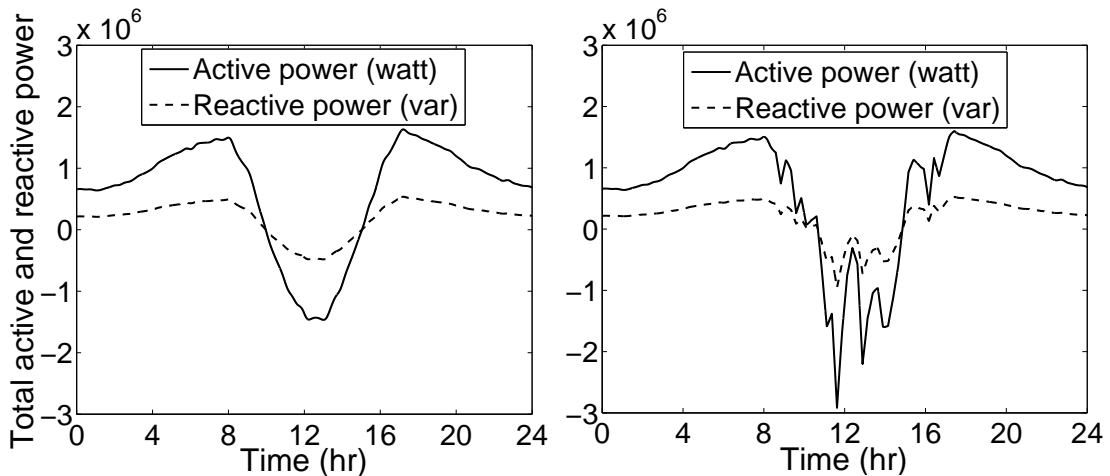


Figure 4.20: Aggregate network active and reactive power profiles for two different scenarios of forecasting errors in the day-ahead PV production.

Table 4.3: Number of parallel SC cells, rated energy of ESS and rated power of the AC/DC converter per network bus

Bus N_o	N_p	Energy(kWh)/ Power(MVA)	Bus N_o	N_p	Energy(kWh)/ Power(MVA)
800	-	-	856	79	43.94 / 1.413
802	49	27.48 / 0.876	852	82	45.61 / 1.466
806	53	29.16 / 0.948	832	82	45.52 / 1.466
808	55	30.38 / 0.983	888	84	46.98 / 1.502
810	55	30.54 / 0.983	890	92	51.00 / 1.645
812	66	36.07 / 1.180	858	82	45.60 / 1.466
814	68	37.03 / 1.216	864	81	44.70 / 1.448
850	68	37.07 / 1.216	834	92	50.31 / 1.645
816	68	37.99 / 1.216	842	86	47.90 / 1.538
818	66	36.18 / 1.180	844	90	49.45 / 1.609
820	66	36.82 / 1.180	846	88	48.02 / 1.573
822	64	35.92 / 1.144	848	88	48.18 / 1.573
824	75	41.99 / 1.341	860	92	50.62 / 1.645
826	71	39.58 / 1.270	836	90	49.54 / 1.609
828	75	41.17 / 1.341	862	84	46.44 / 1.502
830	75	41.31 / 1.341	838	86	47.41 / 1.538
854	75	41.51 / 1.341	840	82	45.54 / 1.466

Table 4.4: Parameters of the storage controller

Parameter	value
Voltage deadband of single cell, V_{DC} (Volts)	[0.8,2.7]
Capacity of single cell, C_{cell} (F)	3600
Gain, ω	0.2
Converter efficiency, η	0.95

for the active than for the reactive power.

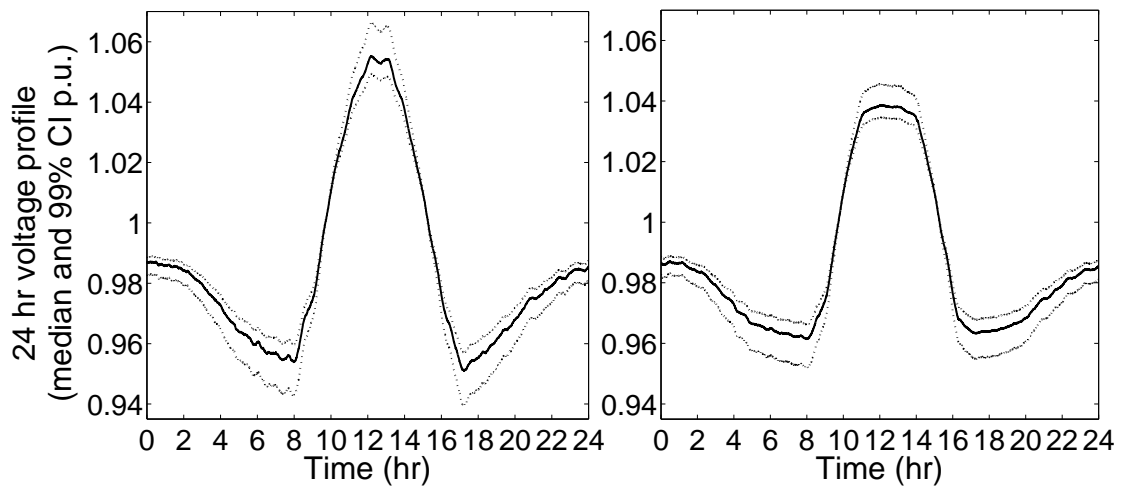
4.6.3 Coordination of Heterogeneous Populations for Primary Voltage Control

This subsection reveals that heterogeneous controllable resources in the network can contribute to primary voltage control, by responding to the same GECN signal. We consider only Scenario II and a large population of elastic thermostatically controlled loads (TCLs) in each network bus as in the previous sections, in addition to the SC arrays. Specifically, the elastic loads are modeled as TCLs and represent 20% of the total peak load in each network bus. The DNO coordinates with the same signal the loads and the SCs.

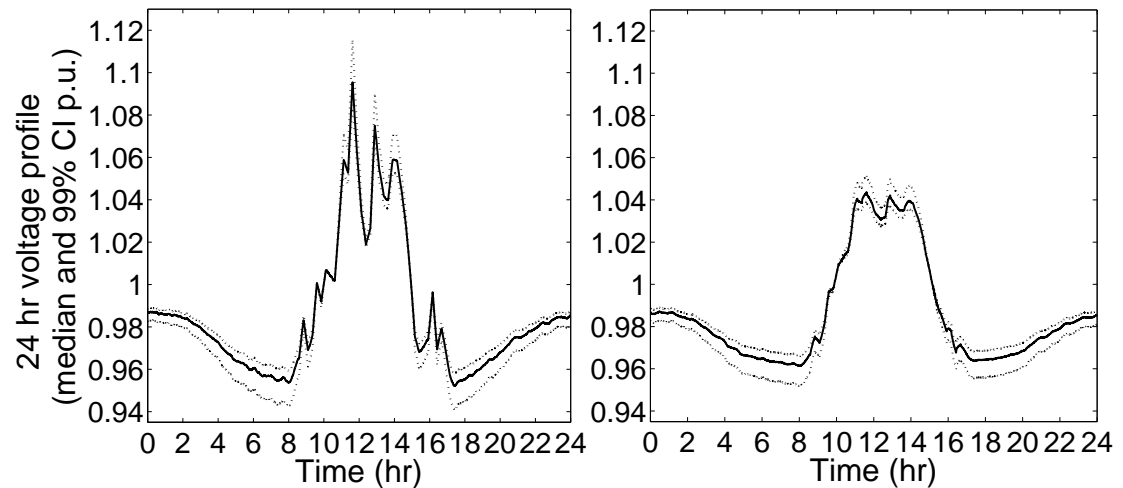
4.6. GECN Performance Evaluation and Application Examples: Primary Voltage Control via Demand Response and Distributed Storage Management

In order to quantify the improvement in the network voltage profile due to the coordinated response of the different kinds of resources, we show in Figure 4.24 the base case voltage profile and the improved voltage profile obtained when both populations react to the same signal. The maximum improvement in the voltage profile, when all resources are considered, is in the order of 6.5%.

In order to better understand how the different populations contribute to the control action, Figure 4.25 shows the active power injected/absorbed by the SC array at bus 840 when the ESSs are the only controllable resources, as well as when TCL and SC are coordinated. Also, in this figure the aggregate active power of the elastic loads



(a) Base case and improved voltage profiles for Scenario I



(b) Base case and improved voltage profiles for Scenario II

Figure 4.21: Base case and improved 24hr network voltage profiles for two different scenarios of forecasting errors in the PV production.

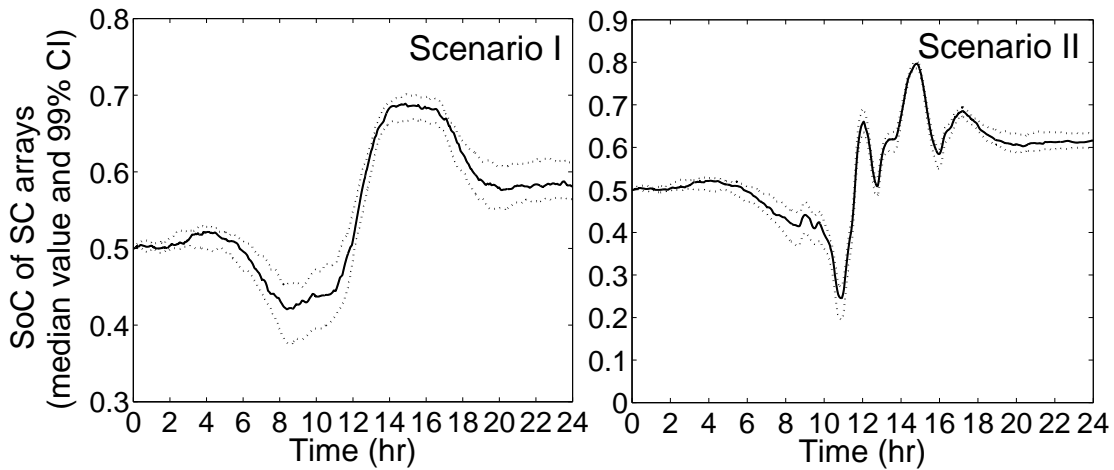


Figure 4.22: 24hr SoC of the SC arrays for two different scenarios of forecasting errors in the PV production.

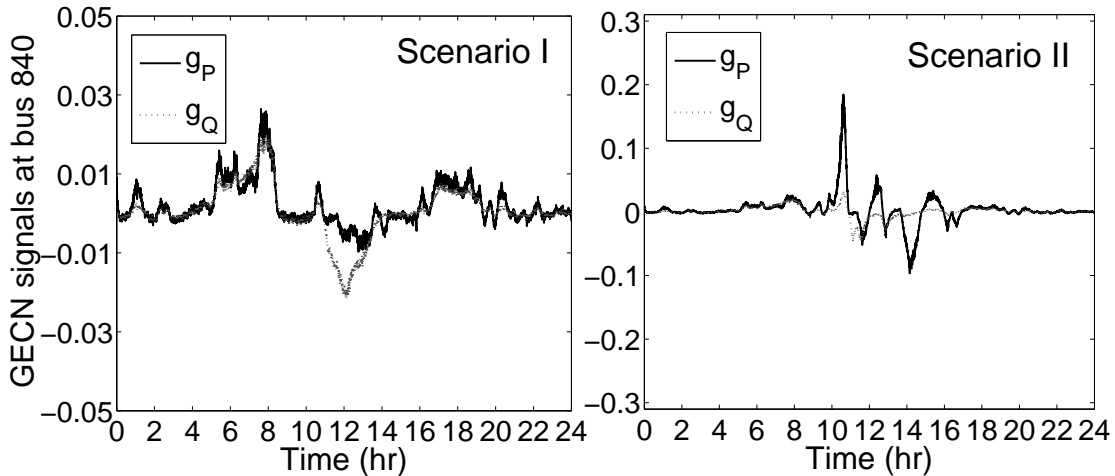


Figure 4.23: 24hr GECN signals sent to bus 840 for two different scenarios of forecasting errors in the PV production.

at bus 840 is depicted for the same cases.

In Figure 4.26, the median value SoC of the SC arrays is shown when only SC are controlled (solid line) and when both populations respond to the signals (dashed line). Overall, one can observe that when TCL are included in the control actions the response of the SC is smoothed, i.e., the SC are charged/discharged less when the TCL are also contributing to the voltage control. However, the amount of voltage profile improvement remains almost the same compared to the case of only ESS. This indicates that part of the power that was provided by the ESSs is now substituted by the TCL response. This result is due to the fact that the designed control mechanism requires a given amount of power/energy per bus, which can be provided by any

4.6. GECN Performance Evaluation and Application Examples: Primary Voltage Control via Demand Response and Distributed Storage Management

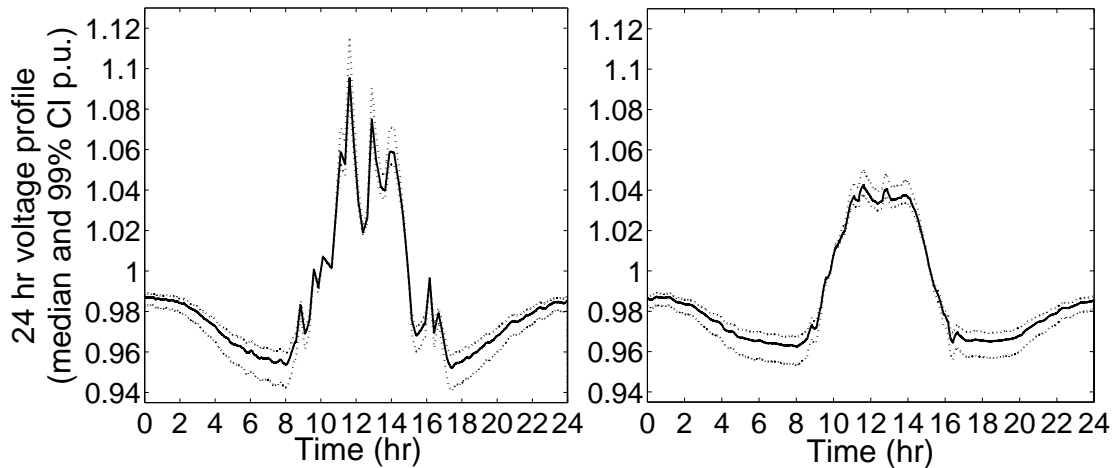


Figure 4.24: Base case and improved 24hr network voltage profiles when both SC and TCL respond to GECN.

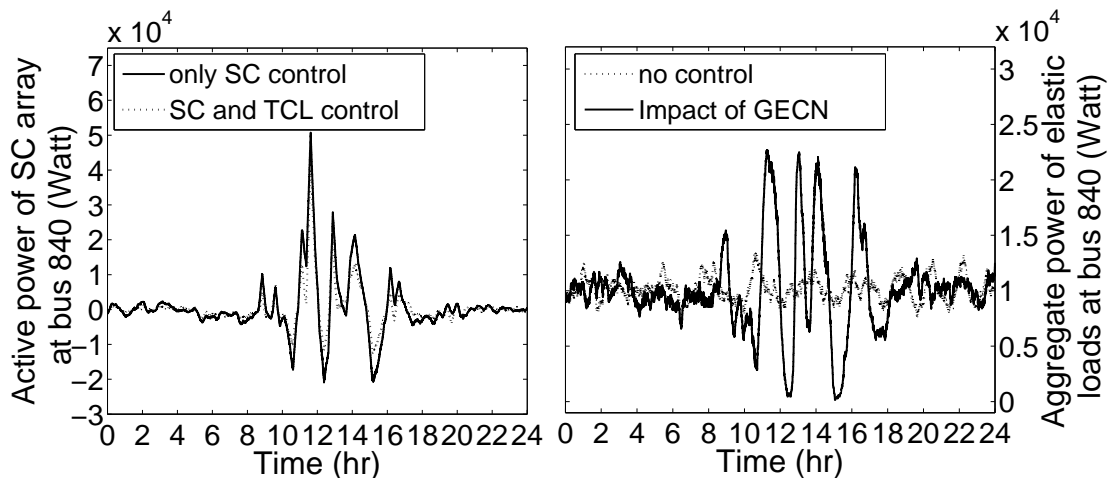


Figure 4.25: Active power of the SC array and the elastic appliances when only supercapacitors are controlled and when both populations respond to the GECN signals.

resource connected to the considered bus.

4.6.4 On the Adequacy of volt/var Control in ADNs

Traditionally, voltage control is related to reactive power control (e.g., static var compensators) [156]. This is true in the case of HV transmission networks or, in general, networks where the ratio of the longitudinal-line resistance versus reactance is small and the decoupling of the active and reactive power is a valid approximation. However, such an assumption is no longer applicable to distribution networks that, when performing voltage control, require to take into account active power injections in

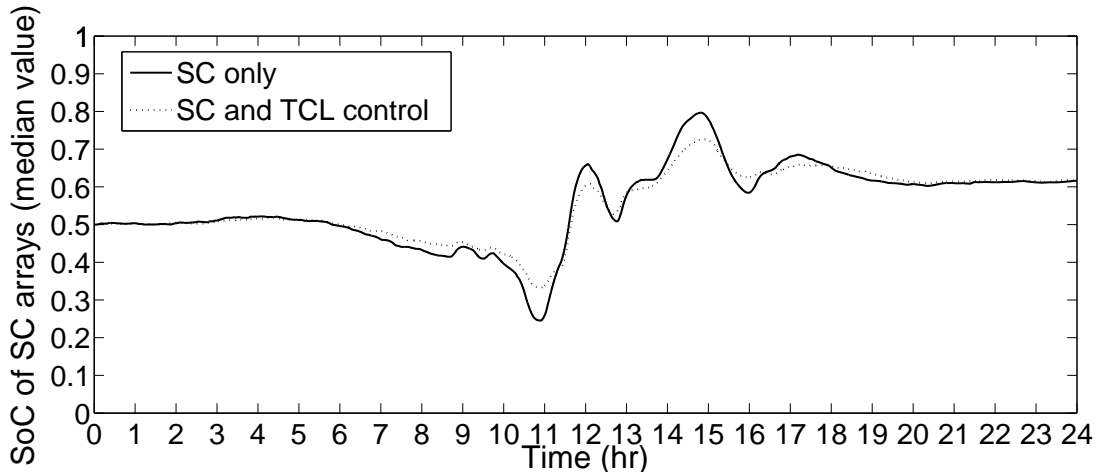


Figure 4.26: Median value of the 24hr SoC of the SC arrays when only SC are controlled and when SC and TCL are coordinated.

addition to reactive power injections.

In the following, we investigate the importance of active versus reactive power-support for voltage control in these specific networks. To this end, we vary the resistance of the lines and we observe the optimal ΔP^* and ΔQ^* that are required to improve the voltage profile. Figure 4.27 depicts the optimal active and reactive power adjustments for different values of the ratio R/X of the lines. Specifically, the line resistances are varied from 0.25 to 2.75 times their initial value while the line inductances are kept constant. The figure shows the values of the optimal active and reactive

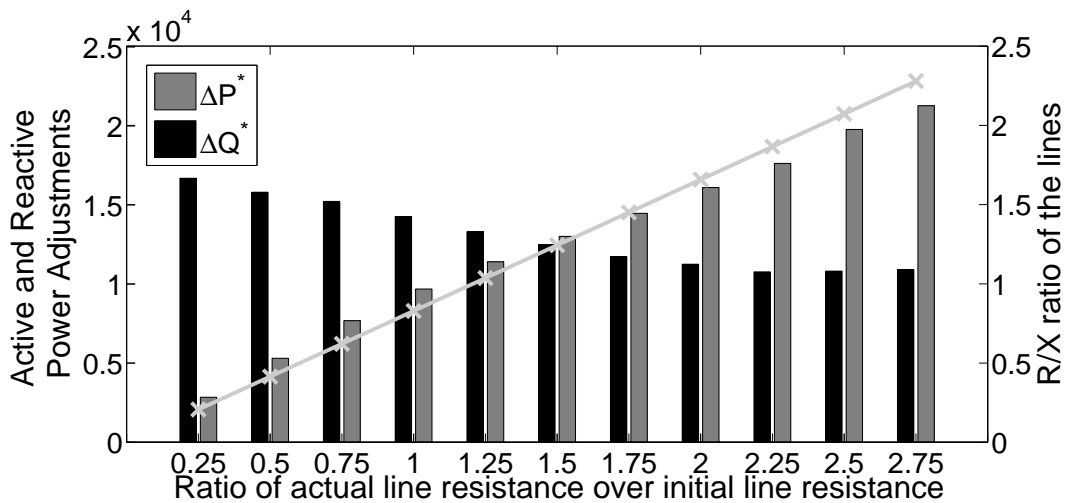


Figure 4.27: Optimal active and reactive power adjustments necessary to improve the voltage by 2% as a function of the line parameters.

4.6. GECN Performance Evaluation and Application Examples: Primary Voltage Control via Demand Response and Distributed Storage Management

power adjustments ΔP^* and ΔQ^* of bus 890 at a specific time-instant. These values are computed in order to improve the network voltage profile by 2%. In the same figure the light-gray line shows the actual R/X of the network lines. One can observe that as the value of the line resistance is increasing, i.e., when the ratio R/X of the lines is increasing, the optimal active power adjustments are linearly dependent on the R/X ratio, and become more important than the relevant reactive power adjustments.

This observation has two implications. First, as in distribution networks the ratio R/X ratio of the lines is, in general, not negligible, the active power support is necessary when performing primary voltage control. Thus, engaging demand response and ESS control mechanisms in the context of primary voltage control is important. Second, the network characteristics are directly impacting the sizing of the storage devices.

4.6.5 Application of GECN to Compensate Fast Voltage Variations: The Case of Load Inrush

In this section we show the capability of the proposed control scheme to cope with fast voltage variations originating from a large load inrush.

Figure 4.28 depicts one hour real measurements of active and reactive power originating from a real LV network in Switzerland that show the periodic inrush of a large load. During this hour one can observe that the phenomenon of load inrush is present both in the active, as well as in the reactive power profile. The data have been sampled each second by applying an average filtering of measured quantities.

In order to investigate the performances of the algorithm during voltage sags in the network caused by a load inrush, we apply the proposed voltage control mechanism to

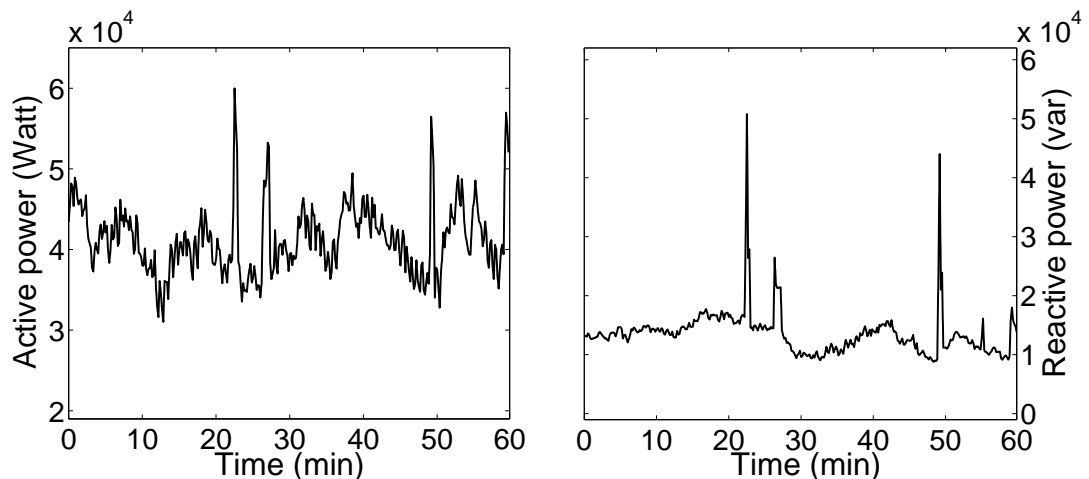


Figure 4.28: One hour measurements of active and reactive power showing the periodic inrush of a large load.

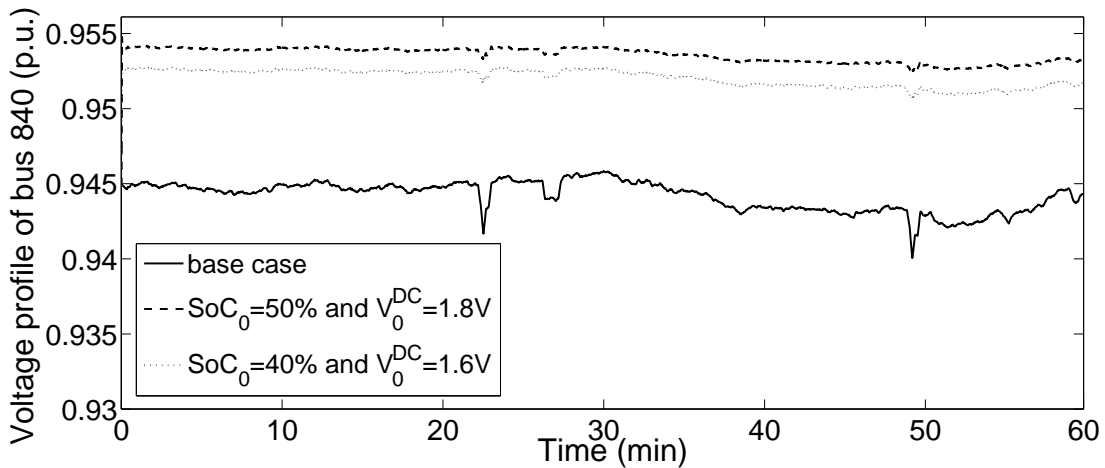


Figure 4.29: One hour voltage profile of bus 840 during a periodic inrush of a large load with and without GECN control.

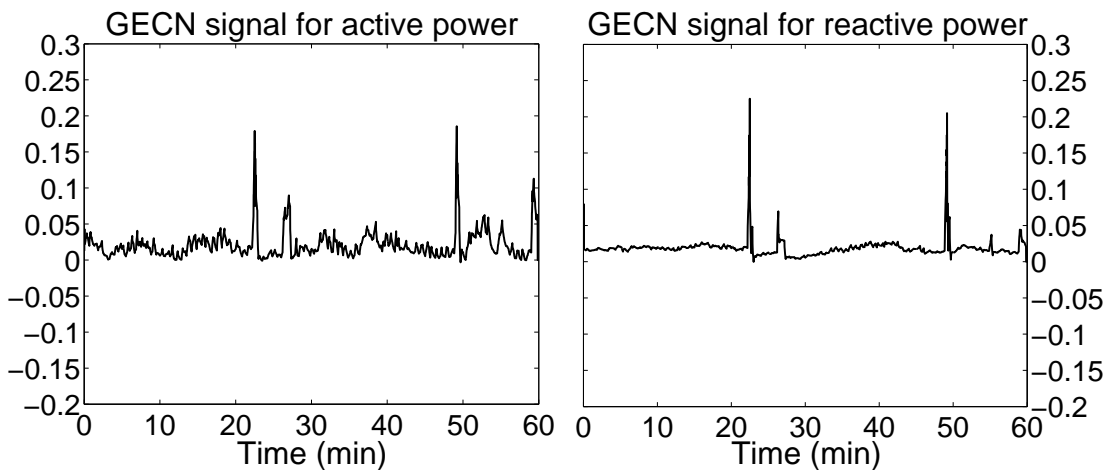


Figure 4.30: GECN signals sent to bus 840 during a periodic inrush of a large load.

control the SC arrays. In this scenario, the GECN signals are computed by the DNO and sent to the network buses every second. We consider Scenario I and we assume that the load inrush occurs at bus 840 in the most loaded period of the day (i.e., hour 7:15 to 8:15). Also, we consider 2 different cases. In the first, we assume that the SCs are in their initial state with $\text{SoC}=50\%$ and $V_{DC}=1.8\text{V}$. In the second case we assume that the SCs are already used up to this period of the day and we initialize their state to the state of this specific instant taken from the simulations presented in Section 4.6.2 ($\text{SoC}=40\%$ and $V_{DC}=1.6\text{V}$). The results are shown in Figure 4.29 where the improvement in the voltage profile is shown for both cases. We can observe that the voltage sags are significantly reduced and the voltage remains within the necessary limits for safe

4.7. Hardware-in-the-Loop Validation of the GECN Mechanism

operation. For the sake of completeness we provide in Figure 4.30 the signals used to achieve the improvement in the voltage profile in the second case, where the SCs arrays are already utilized the moment when the load inrush occurs. In this figure, one can observe how the signals adjust to the specific conditions in the network.

4.6.6 Computational Performances of the GECN Network Controller

In Eq. 4.1 the variation of the tap-changers' position Δn is a discrete variable. Therefore, when the DNO wishes to include the variation of the tap-changers, the problem becomes a mixed integer non linear programming (MINLP) one. In order to solve the optimization problem a MATLAB/GAMS interface is used [157]. In GAMS the KNITRO solver [158] is used to find the solution to both the MINLP, when the taps are included and the NLP, when the DNO disregards the presence of the tap-changers.

For the considered horizon of 24 hours the optimization problem is solved every 16 seconds resulting in 5400 execution times. In Table I the mean CPU times necessary to solve the MINLP, as well as the NLP, with reference to an Intel CORE i7, 2.80 GHz, 4GB RAM, running Windows 7, are presented. In the same table the relevant 95-th percentiles are also reported. It can be observed that the time required to solve the optimal control problem with a standard laptop is compatible with a real-time use of the proposed approach. Indeed, as shown in Table 5.10, for the selected time-step (16 seconds) the optimal problem is solved in the order of few hundreds of ms.

Table 4.5: CPU time necessary for solving the optimization problem in Eq. 4.1

	Mean (ms)	95-th Percentile (ms)
MINLP	181.2	194.7
NLP	168.2	186.8

4.7 Hardware-in-the-Loop Validation of the GECN Mechanism

Prior to the actual deployment of a new control mechanism in a real network, it is crucial to validate its behavior and performance. The reason is that the assessment of a control process in the real field is practically impossible. First, the true system state is hidden, therefore it is not possible to quantify the control performances. Second, emergency situations such as contingencies or disturbances that might occur in the grid can result in unpredictable control actions. To overcome these limitations, the control process operation can be validated in laboratory contexts using Real-Time Simulators (RTSs) and associated Hardware-in-the-Loop (HIL) setups.

In this direction, the goal of this section is the experimental validation of the GECN mechanism via a dedicated HIL setup. In order to perform the RT assessment of GECN, we design a dedicated HIL test platform described next. Using the HIL

setup and realistic high-frequency sampled time-series for solar panels injections and consumption, we validate the RT operation of GECN when applied to the case of thermostatically controlled loads for providing primary voltage control and we assess the time latencies of the control process.

4.7.1 HIL Setup and Experiment Design

The HIL setup that has been designed and implemented for the experimental validation of the GECN control scheme is shown in Figure 4.31. It consists of a RTS that communicates via the local Ethernet network with a workstation. In the RTS, we have developed specific models to represent the electrical network, the PMUs, the TCLs and the GECN load controllers. In addition to the controllable resources, non-dispatchable production coming from distributed solar panel units and non-controllable demand are also included in the RTS.

In the RTS, three-phase bus voltage and injected current signals, i.e., the true system state, are forwarded to the PMUs that are installed in some of the network buses. It is worth noting that the developed set-up corresponds to a real grid located in the Netherlands and the location of the PMUs corresponds to the real installation of these devices in the ADN. This location depends on installation constraints set by the DNO, as well as on the network observability. The PMUs estimate the synchrophasors of nodal voltages and injected/absorbed currents, encapsulate them according to the IEEE Std. C37.118.2-2011 and stream the relevant frames via Ethernet to the workstation. More details on the model of the RTS PMU can be found in [159].

In the workstation, a specific LabVIEW interface comprises a PDC, a RTSE, as well as the GECN network controller. The dataframes streamed by the PMUs are received first by the PDC where they are decapsulated, aggregated and time-aligned. Next, they

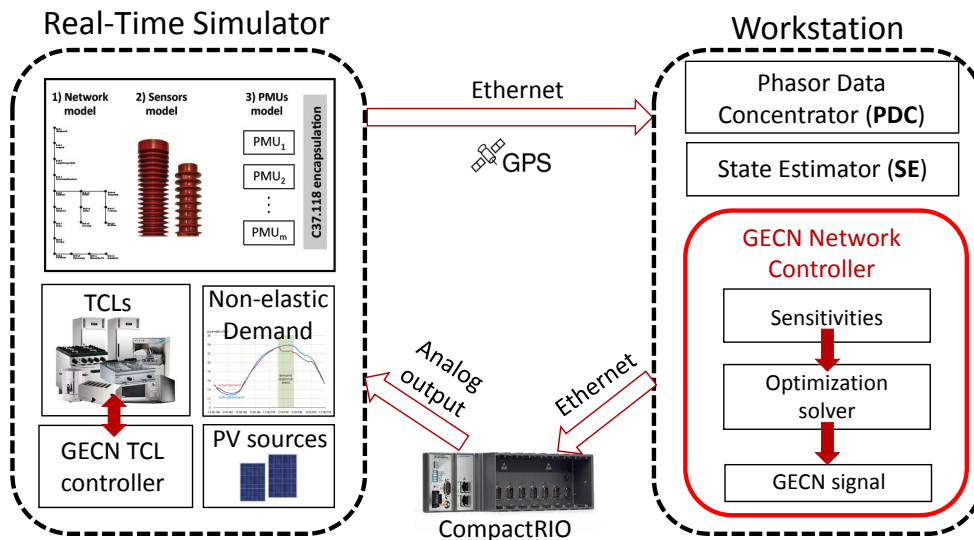


Figure 4.31: The proposed HIL setup for the validation of GECN.

4.7. Hardware-in-the-Loop Validation of the GECN Mechanism

are passed to a Kalman Filter (KF)-based SE. A detailed description of both the PDC and the RTSE process can be found in [160, 161]. Once the estimated state is available, it is received by the GECN network controller block, implemented also in LabVIEW, that uses this information to compute the broadcast control signals. To this end, first the voltage sensitivity coefficients are computed ([17]) and next, the optimal control problem in 4.1 is solved. Finally, the GECN broadcast control signal is computed. The operation of the GECN network controller is triggered every 16sec. In order to close the control loop, the GECN signal is sent via Ethernet to a micro-controller where it is transformed to an analog voltage signal and transmitted via dedicated analog outputs back to the network buses in the RTS. There, each signal is received by all the GECN load controllers that are connected to a single network bus. The local controllers change the state of the TCLs according to the received signal and, consequently, the state of the network.

The ADN model in the RTS is the BLM 2.10 feeder, namely a real 18-buses medium voltage feeder, part of the Alliander electrical distribution grid located in the Netherlands¹³. Its topology is shown in Figure 4.32(a). The voltage of the slack bus (bus 1) is equal to 10 kV RMS line-to-line. The network short-circuit power is equal to 300 MVA and $R_{cc}/X_{cc} = 0.1$. Figure 4.32(b) shows the physical area where the feeder of interest is located, as well as the PMU installation. Ten out of the network buses are equipped with PMUs. In particular buses 1, 3, 5, 6, 8, 10, 12, 13, 15 and 17 in Figure 4.32(a) that correspond to the blue squares locations shown in Figure 4.32(b). At each of the buses equipped with PMUs, apart from bus 1, we consider a population of 400 controllable refrigerators. The characteristics of the elastic appliances, as well as the TCL controller parameters are shown in Table 4.6. In addition to the controllable resources, real measurements of 24hr curves of consumption and production coming from distributed PV units are considered in each network bus. The aggregate active and reactive power injections profiles of all the network buses are shown in Figure 4.33¹⁴.

In what follows, we first verify that the RT implementation of GECN is the same as the off-line event-driven simulation in Matlab by performing a regression testing. Then we evaluate the performance of GECN in terms of voltage optimality and we characterize its time requirements using the network and power profiles presented in this section.

4.7.2 Regression Testing

In this section we want to verify that the implementation of the GECN control mechanism in real-time is identical to the off-line version in Matlab used for the simulations in the previous sections. For this purpose, the goal is to run the same test-case in Matlab off-line and in real-time and obtain identical resulting voltage profiles, as well

¹³The data of this feeder have been made available by Alliander within the context of the C-DAX FP7 EU project (<http://www.cdax.eu/>).

¹⁴These aggregate data come from measurements taken at a different feeder other than the BML 2.10.

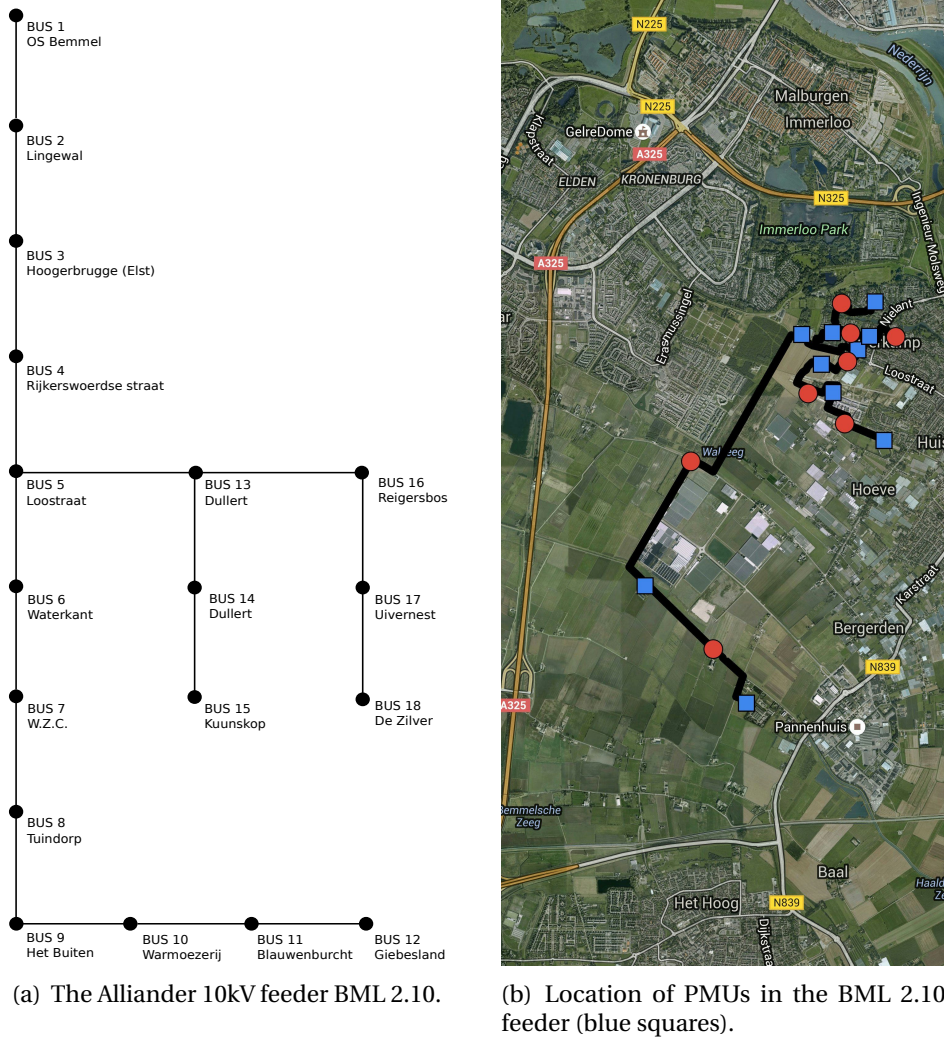


Figure 4.32: Topology and location of PMUs in the Alliander BML 2.10 feeder.

Table 4.6: Parameters of the elastic appliances and the load controller

Parameter	Value
Temperature deadband, $\Theta(^{\circ}C)$	[1,6]
Ambient temperature, $\theta_0(^{\circ}C)$	19
Thermal conductivity, $A(kW/^{\circ}C)$	10.563
Coefficient of performance, (η)	3
Rated power, P_r (Watt)	150
Time step, τ (sec)	1
Time constant, $T_c = m_c/A$ (hrs)	$\sim U(1.326, 2.778)$
Controller time counter, T_0 (sec)	480
Internal state parameter, ξ	0.4
Appliance power factor, $\cos \varphi$	0.85

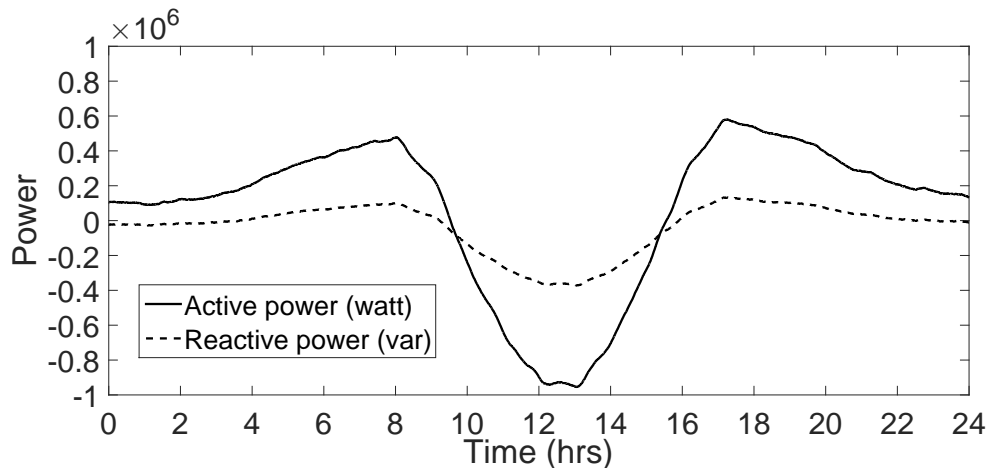


Figure 4.33: Aggregated non-controllable active and reactive power injections of all network buses.

as aggregated power of the controllable TCLs. However, there are several factors that render such a comparison difficult. In particular, the probabilistic nature of the GECN local controllers and the noise introduced by the analog signals do not allow to obtain a deterministic output of the controllable loads between different simulations. Furthermore, the finite integration time-step of the RTS involves truncation errors caused by the RTS solver that are different from the event-driven simulator developed in Matlab that, instead uses the power flow calculus. For all these reasons, we test and compare separately the operations of the GECN network controller and the load controllers.

For the validation of the GECN network controller, we perform the following test. We first run a 24hr off-line Matlab simulation and we store every second the network state, i.e., the nodal voltage phasors, the nodal power injections, as well as the computed GECN signals for each network bus. Then, we use the nodal voltage phasors and power injections as input to the LabVIEW implementation of the GECN network controller block shown in Figure 4.31. In this way, we can compare the 24hr GECN signals computed in Matlab with the ones obtained from the GECN network controller that is used in the experimental set-up. The results of this test are shown in Figures 4.34- 4.35. In these figures we plot the difference between the 24hr GECN signal computed off-line in Matlab and the one computed by the RT implementation in LabVIEW. For the sake of brevity we show only the signals sent to bus 3 (Hoogerbrugge-Elst), which is the controllable bus closest to the slack bus and bus 12 (Giebesland) which is the furthest one. As it can be observed, the difference between the GECN signals is negligible, in the order of 10^{-11} , which indicates that the implemented GECN network controller is behaving in RT as the event-driven one developed in Matlab.

For the validation of the local controllers of the TCLs we adopt a similar procedure. We run a 24hr off-line simulation in Matlab and we store the GECN signals sent to the

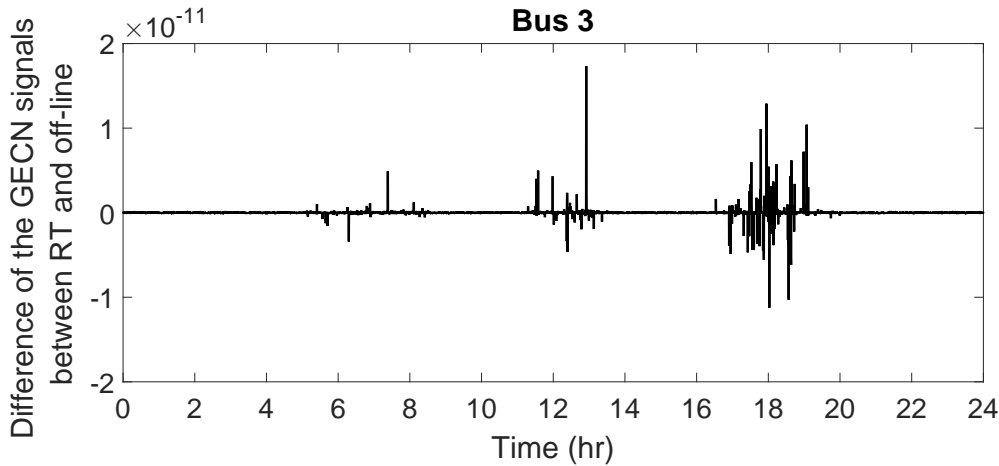


Figure 4.34: Difference between the 24hr GECN signals sent to bus 3 computed by the Matlab off-line and the LabVIEW RT implementation of the GECN network controller.

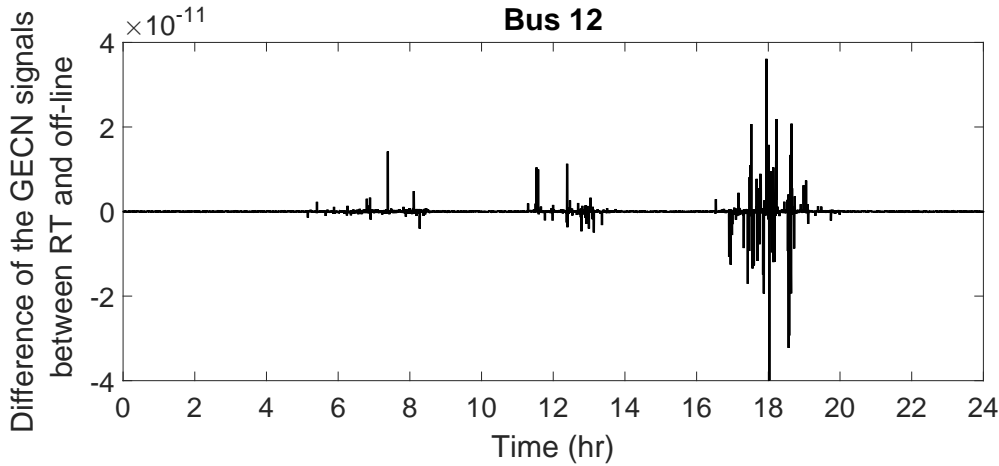


Figure 4.35: Difference between the 24hr GECN signals sent to bus 12 computed by the Matlab off-line and the LabVIEW RT implementation of the GECN network controller.

MV network buses, as well as the aggregate power of the controllable resources. Then we use the control signals as input to the RT TCL controller which is implemented in Simulink and we observe the aggregate TCL power at each MV bus. In both the RT and the off-line simulations we make sure to set the seed of the random number generator so that the same sequence of random numbers is produced in the two simulations. By doing so we are able to compare the two different implementations of the local resources controller in the two different software platforms. Figures 4.36 and 4.37 show the aggregate TCL power of bus 3 and 12 respectively computed in the off-line simulations (black squares) and in real-time (red line)¹⁵. As it can be observed in these figures the aggregate powers of the TCLs are exactly superposed, indicating that the TCL controller, as well as the TCL model are behaving in RT exactly as the ones in matlab.

¹⁵Note that in this case we do not show the differences between the aggregate powers computed in the two implementations as they are exactly zero for the whole 24hr period.

4.7. Hardware-in-the-Loop Validation of the GECN Mechanism

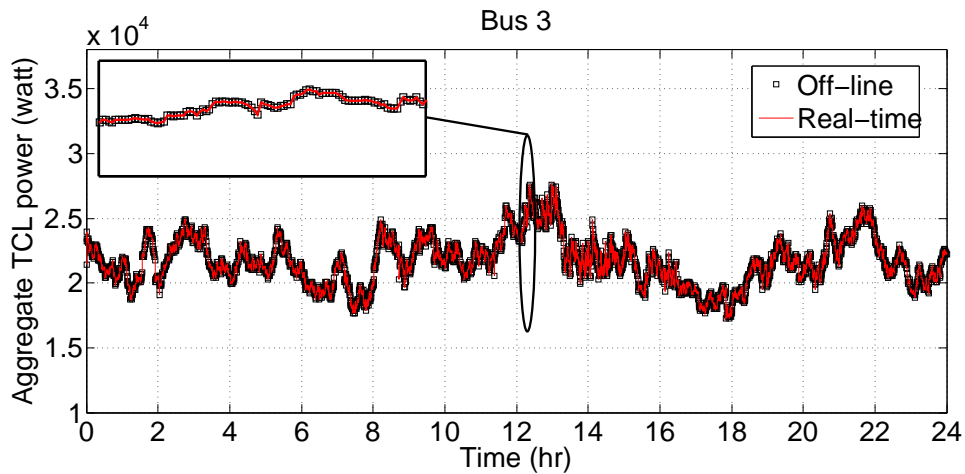


Figure 4.36: Aggregate power consumption of TCLs connected to bus 3 in Matlab off-line (black squares) and in RT simulation (red line).

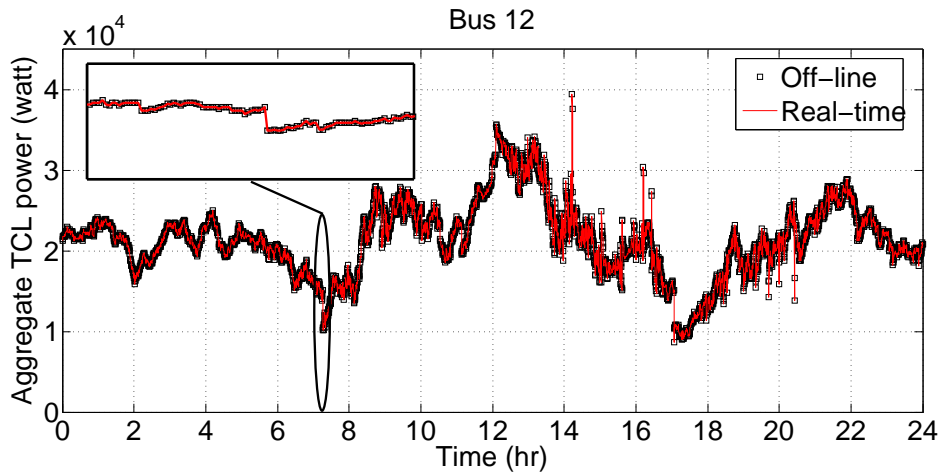


Figure 4.37: Aggregate power consumption of TCLs connected to bus 12 in Matlab off-line (black squares) and in RT simulation (red line).

4.7.3 Demonstration Example and Performance Assessment

In this section we evaluate the performances of GECN as a RT primary voltage controller in ADNs. To this end we use the real distribution feeder shown in Figure 4.32 and the HIL set-up described in detail in Section 4.7.1.

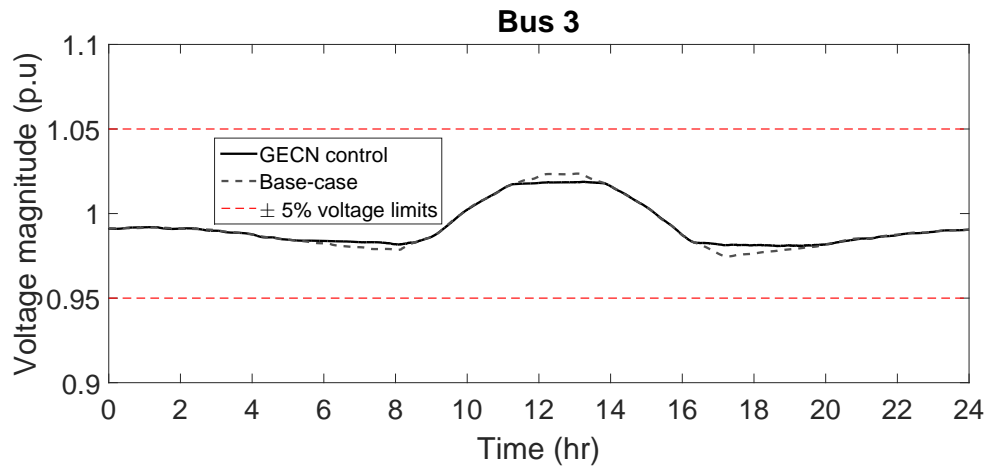
First, we run a 24hr RT simulation without enabling the GECN network controller in order to obtain the base-case voltage profile, as well as the uncontrolled aggregate consumption of the TCLs. The results of this simulation for the voltage are shown in the dashed gray lines in Figures 4.38(a)-4.39(a). For the sake of brevity, we show the network voltage profiles that exhibit the minimum and maximum voltage variations, namely the one of bus 3 and bus 12 that are the closest and the furthest away from the slack bus respectively. It is worth observing that for bus 12, the absence of a suitable control produces voltages below the allowed limit of 0.95p.u. in correspondence of the peak consumption periods, i.e., hours 7-8 and 17-18. Moreover, over-voltages above

1.05p.u. occur in the middle of the day during the peak production of the PV units, i.e. hours 12-13. In Figures 4.38(c)-4.39(c) the aggregate power of the refrigerators in buses 3 and 12 respectively are shown for the base-case in red.

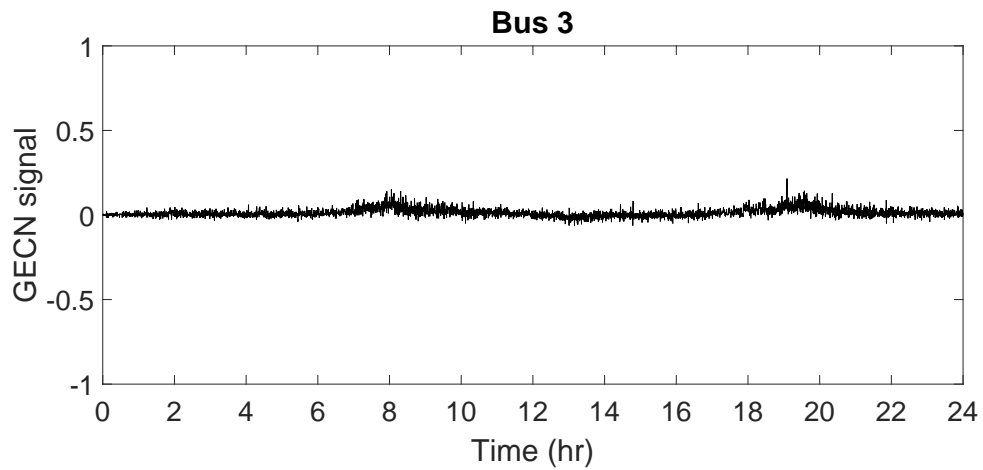
Next, we run a 24hr RT simulation where GECN control is enabled. The improvement in the voltage profile of buses 3 and 12 due to the application of GECN is shown in Figures 4.38(a)-4.39(a) (black curves). It is worth noting that the GECN is able to control in real-time the network voltage guaranteeing that the resulting profiles remain for the whole 24hr period within the allowed $\pm 5\%$ limits shown in the dashed red lines. The GECN signals that correspond to this improvement in the voltage profiles are shown in Figures 4.38(b)-4.39(b) for bus 3 and 12 respectively. As expected, the signal sent to bus 12 exhibits larger magnitudes caused by the larger voltage variations in this bus, whilst GECN signals are close to zero for bus 3. In fact, the three peaks of the signal observed in Figure 4.39(b) correspond to the time periods when under-voltages and over-voltages occur in Figure 4.39(a), i.e., hours 7-8, 12-13 and 17-18. The GECN signals cause variations of the aggregate TCL power of the controllable buses that can be observed in Figures 4.38(c)-4.39(c) in black. Compared to the base-case consumption (red curves) the TCLs consume less during hours 7-8 and 17-18, responding correctly to the positive GECN signal that dictates there is a peak in consumption that causes under-voltages. On the contrary, the TCLs consume more during hours 12-13 in order to locally compensate the peak in the PV power production and decrease the corresponding over-voltages. Overall, these results indicate that the GECN control mechanism is able to selectively control the aggregated demand per bus and successfully provide real-time primary voltage control in active distribution networks.

In addition to the performance evaluation of GECN in terms of voltage optimality, it is interesting to assess the time latencies of the control process. In Figure 4.40 we show the time required by the GECN network controller to solve the centralized optimization problem throughout the 24hr period. It is worth noting that even during the time-periods when voltage control is required in the network, the solution time of the optimization problem is in the order of few ms. Furthermore, Figure 4.41 shows the CDFs of the time required to solve the centralized optimization problem off-line, using the solver `fmincon` of Matlab and in RT, using the gradient descent method. It is worth noting the significant improvement of the adopted solution method in RT which is in the order of 10 times faster. In particular, the median value of the solution time is 1.12ms in RT with a corresponding 95-th percentile of 2.70ms, where as off-line these values are 17.37ms and 32.82ms respectively. In [161] the authors characterize the latency of the whole process from the moment the data is arrived to the PDC until the state is available from the RTSE for the case of the BML 2.10 feeder and they find that this latency is in the order of 20ms. Therefore, taking into account the time latencies shown in Figure 4.40, within roughly 35ms from the moment the data is available to the PDC we are able to solve the centralized optimization problem and compute the GECN signals. Overall, the timing performance shown here confirms the adequateness of GECN as a primary controller.

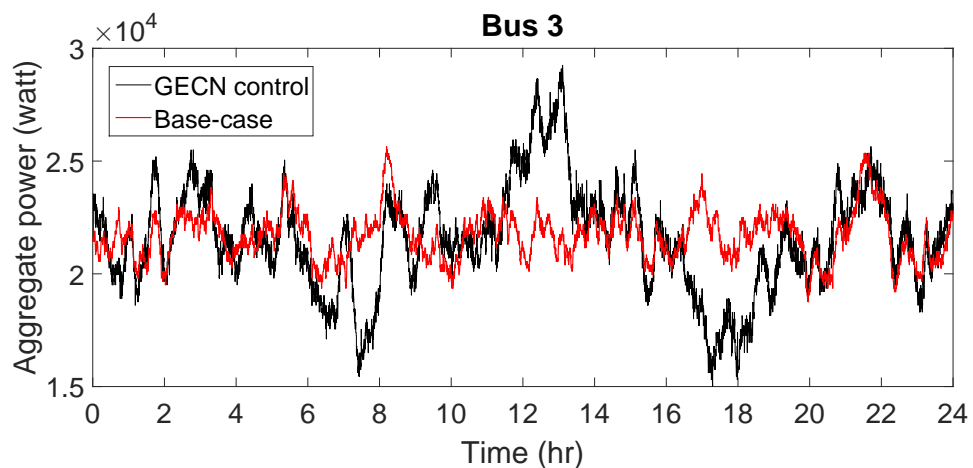
4.7. Hardware-in-the-Loop Validation of the GECN Mechanism



(a) 24hr voltage profile of bus 3 before (gray dashed line) and after (black line) the GECN control.

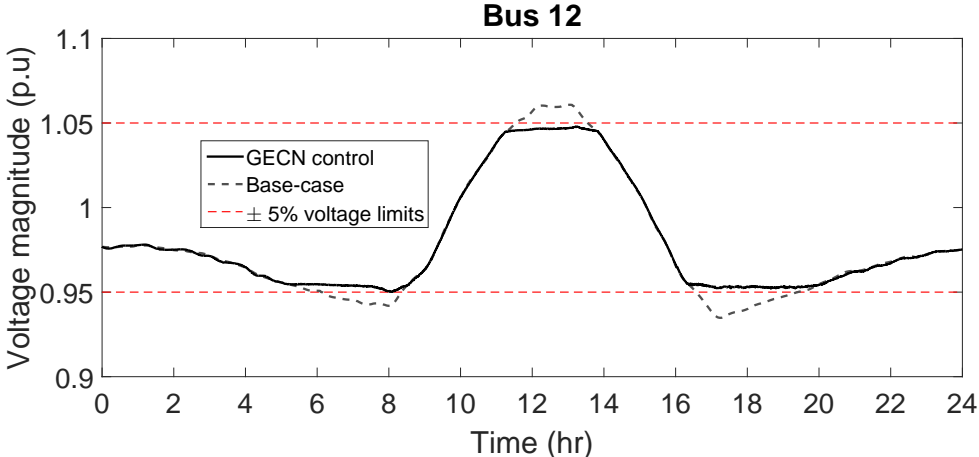


(b) 24hr GECN signal sent to bus 3.

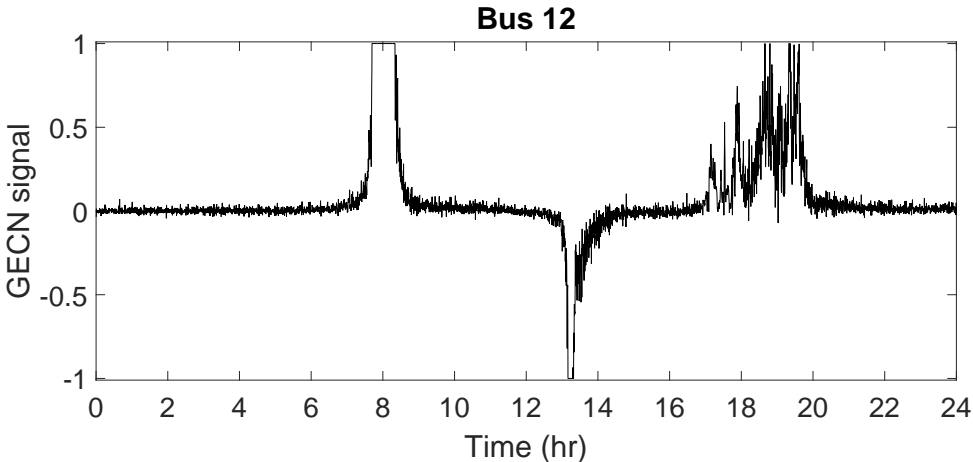


(c) 24hr aggregate power consumption of the TCLs connected to bus 3 before (red curve) and after (black curve) the GECN control.

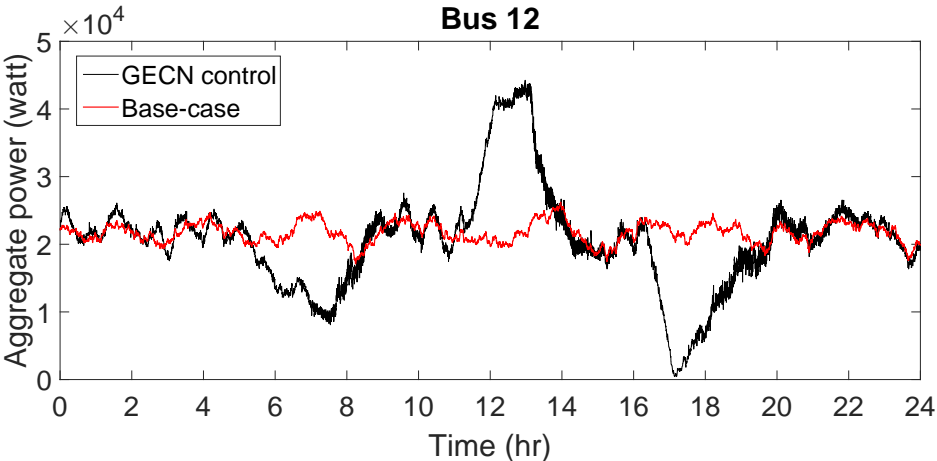
Figure 4.38: Voltage profile, GECN signal and aggregate TCL power of bus 3.



(a) 24hr voltage profile of bus 12 before (gray dashed line) and after (black line) the GECN control.



(b) 24hr GECN signal sent to bus 12.



(c) 24hr aggregate power consumption of the TCLs connected to bus 12 before (red curve) and after (black curve) the GECN control.

Figure 4.39: Voltage profile, GECN signal and aggregate TCL power of bus 12.

4.8. Discussion on the Applicability of GECN in a Real ADN Context and its Comparison with respect to Traditional Control Means

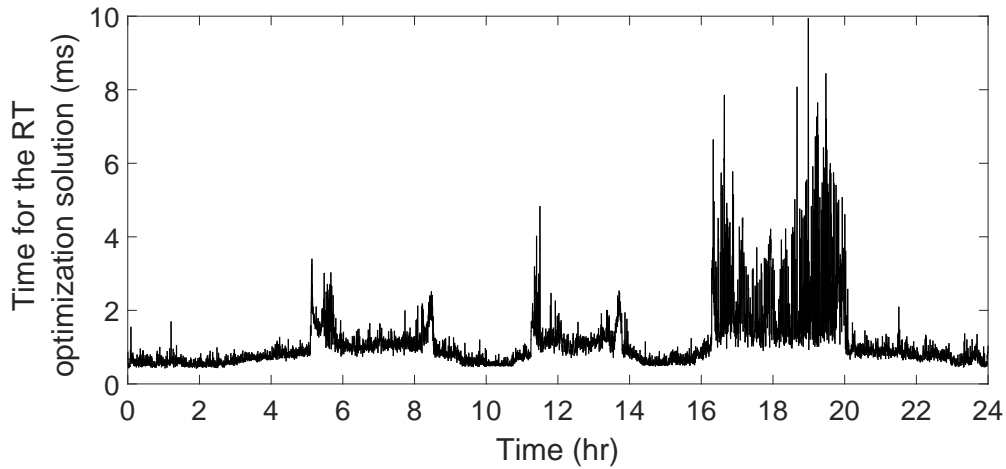


Figure 4.40: Time required for the solution of the optimization problem.

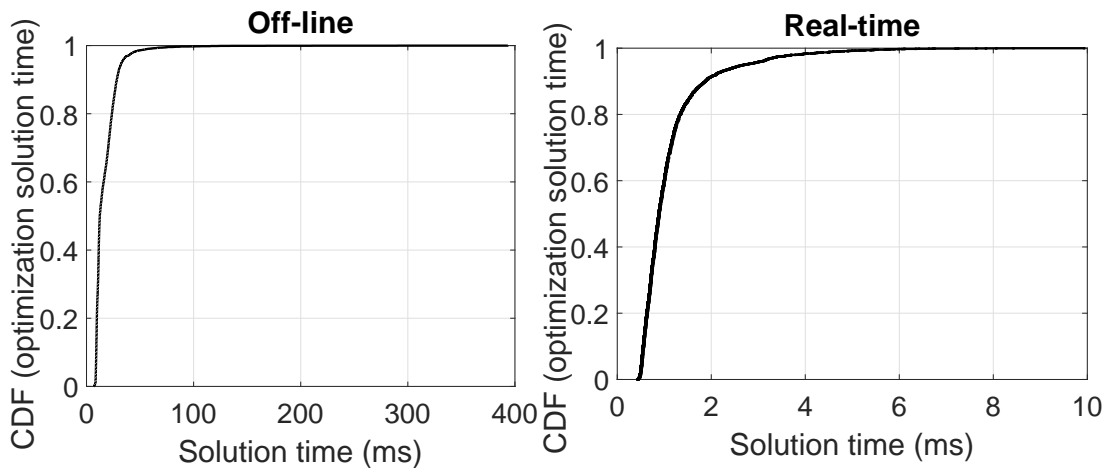


Figure 4.41: CDF of the time required to solve the optimal control problem, comparison between off-line and RT implementations.

4.8 Discussion on the Applicability of GECN in a Real ADN Context and its Comparison with respect to Traditional Control Means

In this section we discuss several aspects related to the adoption of GECN in a real ADN context. Furthermore, we provide a brief comparison between the performances of GECN and traditional approaches used for voltage control in distribution networks.

The proposed control mechanism has been compared to the use of traditional voltage control actuators composed by OLTCs and shunt capacitors. In particular, we

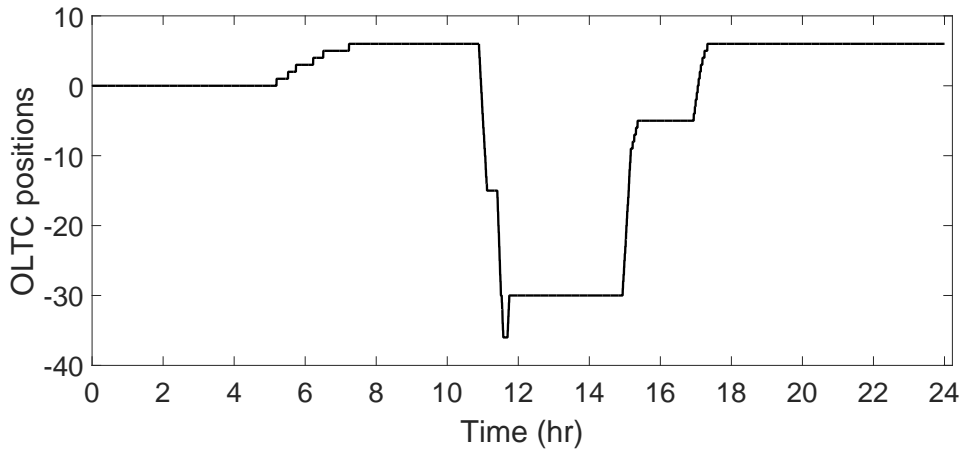


Figure 4.42: Tap-changers’ position when voltage control is performed using solely the OLTC of the primary substation’s transformer.

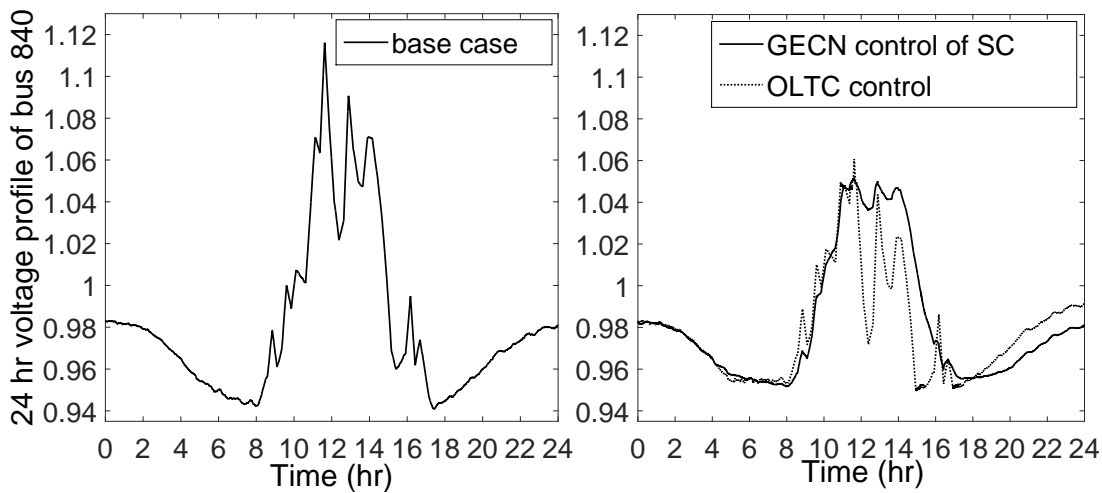


Figure 4.43: Voltage profile when voltage control is performed using solely the OLTC of the primary substation’s transformer.

have performed simulations assuming that voltage control is performed relying solely on the OLTCs placed in the primary substation and using static var compensators also placed in the primary substation. In the first scenario, where the voltage is controlled via the OLTC, one can observe in Figures 4.43 and 4.42 that the amount of tap changes necessary to achieve a voltage profile similar to the one obtained by the SC in Section 4.6.2 is prohibitive. This is due to the highly volatile nature of the PV. Also, we can observe that in such a case where the voltage reaches a high value (1.2p.u.) the maximum limit of the OLTC is reached in some periods and thus the voltage profile cannot be maintained between $\pm 5\%$ of the network rated value. Typical values for

4.8. Discussion on the Applicability of GECN in a Real ADN Context and its Comparison with respect to Traditional Control Means

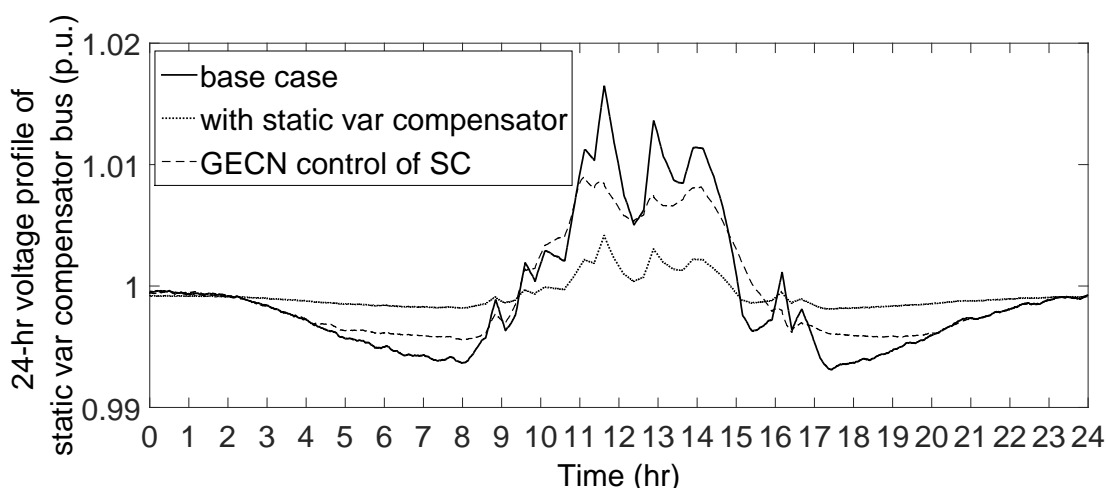


Figure 4.44: Voltage profile of the bus where the static var compensator is connected when voltage control is performed using static var compensation.

the average number of OLTC operations in distribution and transmission networks are in the order of 7000 manoeuvres (e.g., [162]). This implies that with few tens of manoeuvres per day this number will be reached within a year. As far as the static var compensator is concerned, we have assumed that it is scheduled such that the power factor in the slack bus is maintained close to 1. The effect on the voltage profile due to the presence of the static var compensator is local and the improvement of the voltage in buses that are far away from the primary substation is not substantial. To better highlight this we show in Figures 4.44 and 4.45 the voltage profiles of bus 840 which is the bus furthest from the slack bus (thus exhibiting the largest voltage variations) and the voltage profile of the bus where the static var compensator is placed (right after the primary substation). Overall, the simulation results have shown: (i) the non-effectiveness of shunt capacitors in the period of high PV production and, (ii) an increased daily use of OLTCs that causes these components to consume their typical life on a yearly basis (e.g., [162]).

Indeed, voltage regulators have not been designed for fast/primary voltage control in ADNs that inherently requires continuous control actions. On the contrary, OLTCs have been designed to control slow voltage variations due to the seasonal changes of the distribution networks conditions. For this reason, a new literature on the use of distributed storage systems for ADN ancillary services is emerging [129]. However, in case the DNO wishes to utilize traditional solutions, the GECN mechanism can be used to provide a further leverage to the network in addition to the DNO's own resources. That is why, the proposed GECN algorithm was initially conceived and designed to coexist with traditional solutions. In fact, the GECN algorithm allows a coordination of elastic appliances and OLTCs, where the OLTC daily operation are limited to account for their sensitive nature. Also, as mentioned earlier, reactive power compensators can

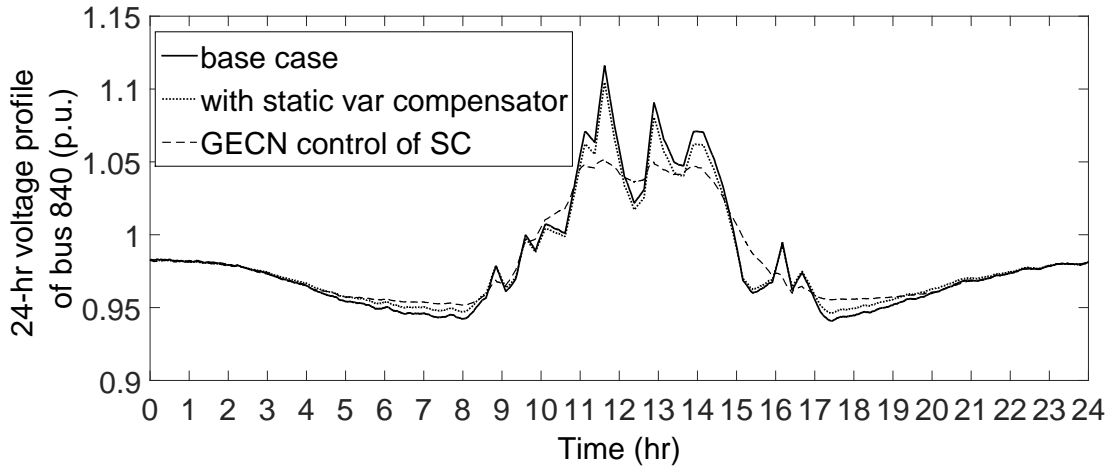


Figure 4.45: Voltage profile of bus 840 when voltage control is performed using static var compensation.

be directly accounted for in the proposed mechanism. Furthermore, it is important to note that even though the main purpose of GECN is voltage control, the algorithm is also penalizing deviations from the day-ahead scheduled consumption profiles in the network, indirectly performing a sort of power balance that reduces costs of importing energy from the external grid. This is an additional functionality for example that cannot be performed by the OLTC or the shunt capacitors.

In this chapter the ESSs are modelled as SC arrays. However, the development of the storage controller as described in Section 4.5.2 is not limiting as it is applicable to any type of electrochemical-based storage system. Furthermore, we have assumed that the SC arrays are connected to the MV network buses and are under the propriety of the DNO for the support of the voltage in the network. However, we expect that ESSs, due to their ability to cover a wide spectrum of applications, will be increasingly present in active distribution networks ranging from large units owned by the DNO or by individual operators to small distributed local storage units owned by the customers of the grid. In all cases, the proposed algorithm is designed in such a way that if the storage units are able to interpret GECN signals, i.e., are equipped with the storage controller, they can participate in the voltage control actions, as well as in the natural objective of ESSs, namely the local energy balance.

Finally, another contribution is the inherent flexibility of the proposed control scheme that is capable of achieving similar improvement in the network voltage profile by using solely SC or a combination of ESS and DR by sending in all cases a common signal to the resources attached to the network buses. In fact the control mechanism requires a given amount of power/energy per network bus that can be provided by any resource connected to the considered bus. What differs in the various scenarios

is the utilization of the different resources. This is supported for example by the fact that the SC are charged/discharged less in the presence of TCL than in the case when there is solely SC control as shown in Figure 4.26. Of course, the exact utilization of the different resources depends on several factors such as the availability of the different elastic resources in the network, the characteristics of the network itself and the loads/injections profiles. For example in distribution networks with higher R/X ratio active power management will play a significant role, hence contribution of elastic loads in the voltage control will be non-negligible and also larger ESSs in terms of energy capacity might be required. Furthermore, due to the design of GECN that prohibits operation of the elastic appliances in mini-cycles, it is expected that, in networks where highly volatile uncontrollable generation is present, ESSs will be contributing more to voltage support than the elastic loads. Finally, in cases where the availability of the elastic loads or ESSs is limited and the DNO does not wish to invest on building new infrastructure, centralized traditional resources can be incorporated in the GECN scheme, such as OLTCs or static var compensators (e.g., [120]).

In any case, it is advisable that the DNO performs offline studies prior to deploying the proposed scheme, in order to evaluate the availability of the distributed elastic resources in the network and the needs of the network in terms of voltage support. Then, in case the needs of the network are not satisfied, it is in the DNO's jurisdiction to decide whether to invest in new dedicated infrastructure, (e.g., ESSs) or to coordinate traditional resources with the broadcast signals.

4.9 Conclusions

In this chapter we have proposed GECN, a control protocol able to optimally exploit distributed energy storage, irrespectively of its nature (i.e., TCL and/or actual storage systems) for ADN primary voltage control. The proposed control architecture relies on a real-time state estimation process that allows for one-way communication between the DNO and the controllable DERs using broadcast signals.

The proposed control scheme is validated by making reference to typical IEEE 13- and IEEE 34-nodes distribution test feeders which are appropriately adapted in order to include a large population of heterogeneous household controllable loads, supercapacitor arrays along with non-elastic demand, as well as non-dispatchable power injections represented by photovoltaic arrays whose power injection profiles have been inferred from real measurements.

The results show that the proposed GECN control mechanism is able to successfully provide primary voltage control in distribution networks. The capability of GECN to control the voltage deviations via a coordinated control of TCLs and OLTCs is in the order of 1 – 2% when the uncontrolled voltage variations in the network are in the order of $\pm 6\%$. These results are achieved without severely impacting the end-users and the OLTCs operations, which are maintained in a reasonable amount per day (roughly 15). Furthermore, the use of elastic loads for voltage control is shown to mitigate the

use of other traditional voltage control systems like OLTC and, in fact, with 30% of elastic demand available no control action on OLTCs is required.

The capability of controlling the voltage deviations via distributed storage systems is up to 6% of the network's voltage rated value and large voltage variations due to the highly volatile PV production are significantly smoothed by the use of GECN. In addition, the results indicate that the same GECN control signals are able to sufficiently coordinate different energy resources, as long as the latter are equipped with local controllers. In fact, roughly the same improvement in the network voltage profile is achieved (6.5%) when controlling both TCLs and SCs or solely SCs, which indicates that GECN is able to control heterogeneous energy resources towards a common goal via the same broadcast signal.

Furthermore, the performance of GECN during a large load-inrush indicates that it is suitable to compensate unexpected sags in the voltage due to high time-varying loads/generators. This feature allows to positively verify the adequateness of GECN to be a primary controller even if it makes use of distributed information.

Finally, the HIL experimental validation of GECN, using a real MV feeder located in the Netherlands, has shown that it can successfully maintain the network voltage profile within acceptable limits for safe operation in a realistic setting. Additionally, the time required for the RT solution of the optimal control problem is in the order of few ms, which confirms the adoption of GECN as a primary control scheme. Finally, the RT implementation of the GECN network controller, as well as of the TCL controllers into dedicated equipment will, in principle, facilitate the actual deployment of the control process in the real field.

5 Centralized and Distributed AC OPF Algorithms

5.1 Introduction

In Chapters 3 and 4 we have focused on optimal control algorithms that rely on an approximation/linearization of the power flow equations by means of sensitivity coefficients. In this chapter we go one step further in the problem formulation and we cast the voltage control and lines congestion management problem as a non-approximated AC optimal power flow problem (OPF).

The category of optimal power-flow problems represents the main set of problems for the optimal operation of power systems. The first formulation of an OPF problem appeared in the early 1960s and has been well-defined ever since [163]. It consists in determining the operating point of controllable resources in an electric network in order to satisfy a specific network objective, such as minimization of losses or generation costs subject to a wide range of constraints including power-flow equations, capability curves of the controllable resources, as well as operational limits on the line power-flows and node voltages.

The AC-OPF problem is known to be non-convex, thus difficult to solve efficiently (e.g., [164, 165, 166]). Due to this non-convex nature of the problem, most of the proposed schemes either do not guarantee to yield an optimal solution or they are based on approximations that convexify the problem in order to guarantee convergence. These approximations, often, either lead to (i) misinterpretation of the system model [167] or (ii) solutions that, even though mathematically sound, might be far away from the real optimal solution, thus having little meaning for the grid operation [168].

In this respect, in the first part of this chapter, we briefly review several OPF algorithms that are based on approximations and assumptions in order to guarantee convergence. In particular, we focus on the branch-flow convexification of the OPF problem that has been recently proposed by Farivar and Low in [35, 36] and is claimed to be exact for the case of radial distribution systems under specific assumptions, despite the absence of apparent approximations. We show that this claim, in fact, does not hold, as it leads to an incorrect system model and therefore, there is a need to develop algorithms for the solution of the non-approximated OPF problem that

remains inherently non-convex. In detail, we show through practical examples that in [35, 36], on one hand, there is a misinterpretation of the physical network model related to the ampacity constraint of the lines' current flows and, on the other hand, the proof of the exactness of the proposed relaxation requires unrealistic assumptions related to the unboundedness of specific control variables.

To overcome the aforementioned limitations, we propose, in the second part of this chapter, an algorithm for the solution of the non-approximated non-convex AC OPF problem in radial networks. Our proposed solution uses an augmented Lagrangian approach and relies on the method of multipliers ([169, 170, 171]) and does not require that the problem be convex. In particular, as a first step we design a centralized OPF algorithm that is proven to converge to a local minimum of the original non-approximated OPF problem.

With respect to the case of controlling multiple dispersed energy resources, it is of interest to also define a distributed solution method that is formally equivalent to the centralized formulation. To this end, we investigate the application of the alternating method of multipliers (ADMM) for the distributed solution of the original non-approximated OPF problem. Even though ADMM requires the underlying problem to be convex in order to guarantee convergence, it was applied also to the case of non-convex AC OPF problems with promising convergence performance (e.g., [172, 173]). However, we show, through practical examples, cases for which the ADMM-based decomposition of the non-relaxed OPF problem fails to converge.

To overcome the identified limitations, we present a distributed version of the proposed algorithm that, unlike ADMM, is based on a primal decomposition [174] and does not require that the problem be convex. In this decentralized version of the algorithm, at each iteration, local agents, assigned to network buses and network lines, exchange messages with their neighbors using only local information. We prove that the distributed algorithm converges to the same solution as the centralized version. Finally, we present an asynchronous implementation of the distributed algorithm where the messages of the neighboring agents need not be synchronized.

The main contributions of this chapter can be summarized as follows. We show that the BFM-based convexification of the OPF problem proposed in [35, 36] that is claimed to be exact for the case of radial distribution systems under specific assumptions, despite no apparent approximations, is, in fact, not exact. We extend this approach to account for networks characterized by lines modeled accurately as π -equivalents. We show that even in the case where the system model is correctly represented, the BFM-based convexification of the OPF problem might provide physically infeasible solutions. Next, we investigate ADMM for the distributed solution of the OPF problem. We highlight specific cases for which the ADMM-based solution of the non-relaxed OPF problem fails to converge. We design a centralized algorithm for the solution of the non-approximated non-convex AC-OPF problem that is based on an augmented lagrangian approach. We use a primal decomposition framework to

extend the proposed algorithm to a fully decentralized asynchronous implementation. We assess the performances of the proposed centralized algorithm in all the cases where the BFM convexification and the ADMM-based solution failed and we show that convergence is achieved. Finally, we formulate the optimal voltage control and lines congestion management via scheduling of the injections of distributed photovoltaic units as an AC-OPF problem and we show using a typical IEEE 13-nodes test feeder that the proposed centralized and distributed algorithms converge to the same solution.

5.2 Related Work

The OPF problem is a well-known problem in the context of operation and planning of power systems. The first formulation of an OPF problem appeared in the early 1960s by Carpentier [163] and has been an active area of research ever since [175, 176, 177]. In general, the OPF is a non-linear constrained optimization problem that seeks to determine the operating point of controllable resources in an electric network in order to satisfy a specific network objective subject to a wide range of system constraints. Within this framework, there is an extremely wide variety of OPF formulations. Typical examples of OPF refer but are not limited to unit commitment, grid planning and reactive power dispatch problems and typical controllable resources considered in the relevant literature are generators, storage systems, on-load tap changers (OLTC), flexible AC transmission systems (FACTS) and loads (e.g., [178, 179, 180, 181, 182]). The system constraints include power-flow equations, capability curves of the controllable resources, as well as operational limits on the line power-flows and node voltages (e.g., [183]).

It is well-known that the OPF problem is a non-convex one, therefore difficult to solve efficiently (e.g., [164, 165, 166]). Since the problem was first formulated, several techniques have been used for its solution. Among others, non-linear and quadratic programming techniques, Newton-based methods, interior point methods in the earlier years, as well as heuristic approaches based on genetic algorithms, evolutionary programming, and particle-swarm optimization in recent years (e.g., [175, 176, 177]). This category of techniques, namely non-linear methods and heuristics, essentially seek to find a local optimum solution of the OPF. They cannot guarantee the identification of the global optimal solution and they are, often, characterized by high computational complexity.

In order to provide convergence guarantees, a large group of proposed schemes in the literature relies on approximations. In general, these approximations used in the formulation of an OPF problem can be categorized in two large groups: approximations of the physical network models and methods that relax the space of the solutions and/or control variables (e.g., convex relaxation).

In the first case, we can find OPF formulations that rely mainly on linearization of the AC power flow equations. Such attempts typically (i) consider the DC power flow, (ii) use the decoupled AC power flow or (iii) neglect the network losses and/or

the transverse parameters of the lines. Specifically, the concepts of the DC and the decoupled OPF have been extensively used in the literature (e.g., [184, 185, 186, 187]), as they approximate the OPF problem with linear programming problems and, therefore, enable its fast solution. Furthermore, the authors in [188] use the so-called Dist-Flow equations ([189]) to linearize the power flows and propose an ADMM-based OPF algorithm that neglects the real and reactive losses. Finally, several contributions rely on simplified network line-models that neglect the transverse parameters, resulting in inaccuracies of the physical system model (e.g., [190, 191, 192]).

In the second case, we can find OPF formulations where, typically, the constraints are relaxed in order to convexify the problem. In particular, a large number of contributions recently proposed a semi-definite programming (SDP) formulation of the OPF problem, where the rank-one constraint of a matrix is relaxed and the algorithm is claimed to yield zero-duality gap for radial distribution networks (e.g., [193, 194, 195]). Another relaxation is proposed in [192] where the OPF problem is cast as a second order cone programming (SOCP). A similar technique is used in [196], where the equality constraints of the branch flows are relaxed.

In both the aforementioned categories of approximations, the modified OPF formulations guarantee convergence of the proposed algorithms. The reached solutions, however, even though mathematically sound, are not always meaningful for the grid operation. The DC and the decoupled OPF work sufficiently well for transmission systems, nevertheless they can introduce large errors when used for solving the OPF in the case of distribution systems (e.g., [197]). As far as the semidefinite relaxation is concerned, its limitations have been recently investigated. The authors in [168] show through practical examples, that in the case of negative locational marginal prices or strict line-flow constraints it can lead to solutions that are not valid, namely for which the duality gap is not zero. Furthermore, in [198] the authors show the existence of multiple local optima of the OPF problem due to the feasible region being disconnected and due to the nonlinearities of the constraints; they show that the SDP formulation of the OPF problem fails to find the global optimum in cases where there are multiple local optima. In the same direction, a recent review ([191]) summarizes the semidefinite relaxations applied to the OPF problem and discusses their limitations.

Recently, another formulation of the OPF problem has been proposed ([199, 200, 35, 36, 201]). This formulation also belongs to the category of the semidefinite relaxations and uses the so-called branch-flow model (BFM) for describing the network. The BFM essentially describes the network flows using as variables the currents and the powers of the various network branches, instead of the nodal injections. In [35, 36] Farivar and Low propose an OPF formulation that relies on the BFM representation of the network and they present a two-step relaxation procedure that turns the problem into a second-order cone program (SOCP). The authors prove that under specific assumptions both relaxation steps are exact for the case of radial networks, hence a globally optimal OPF solution can be retrieved by solving the relaxed convex prob-

lem. However, in what follows, we show, on one hand, that the Farivar-Low model misinterprets the physical network model by imposing an ampacity constraint on a fictitious line-current flow that neglects the contribution of the shunt components of the line and that, on the other hand, the proof of the exactness of the proposed relaxation requires unrealistic assumptions related to the unboundedness of specific control variables.

Currently, the OPF problem is becoming more compelling due to the increasing penetration of embedded generation in distribution networks, essentially composed by renewable resources. The distributed nature of such resources, as well as their large number and stochasticity increase significantly the complexity of the OPF problem and bring about the need for distributed solutions. In this direction, several distributed algorithms have been proposed in the literature. In [202, 203] the authors design a dual-ascent algorithm for optimal reactive power-flow with power and voltage constraints. In [194, 195] dual decomposition is used as the basis for the distributed solution of the OPF problem. Finally, a significant number of contributions propose distributed formulations of the OPF problem that are based on the alternating direction method of multipliers (ADMM) (e.g., [204, 194, 172, 188, 205, 173]). ADMM requires the underlying problem to be convex in order to guarantee convergence, yet it has been applied also to the case of non-convex AC OPF problems with promising convergence performance (e.g., [172, 173]). As we show in this chapter, through practical examples, there are cases for which the ADMM-based decomposition of the non-relaxed OPF problem fails to converge.

5.3 Generic OPF Formulation

In the rest of the chapter, we consider a balanced radial network composed of buses (\mathcal{B}), lines (\mathcal{L}), generators (\mathcal{G}) and loads (\mathcal{C}). The network admittance matrix is denoted by Y . Several generators/loads can be connected to a bus $b \in \mathcal{B}$. We denote that a generator $g \in \mathcal{G}$ or a load $c \in \mathcal{C}$ is connected to a bus by “ $g \in b$ ” and “ $c \in b$ ”. A line $\ell \in \mathcal{L}$ is represented using a π -equivalent model and it has a receiving and a sending end denoted by ℓ^+ and ℓ^- . Each line is connected to two adjacent buses: $\beta(\ell^+)$ and $\beta(\ell^-)$, respectively.

The traditional formulation of the OPF problem consists in minimizing a specific network objective:

$$\min_{\bar{S}_g, \bar{S}_c, \bar{S}_\ell^+, \bar{S}_\ell^-, \bar{I}_\ell^+, \bar{I}_\ell^-, \bar{V}_b} \sum_{g \in \mathcal{G}} C_g(\bar{S}_g) + \sum_{c \in \mathcal{C}} C_c(\bar{S}_c) \quad (5.1)$$

The first term of the network objective (C_g) in (5.1) is typically a non-decreasing convex function accounting for the minimization of the generation costs or the network real power losses. The second term (C_c) is included in the objective when the cost of non-supplied load is taken into account.

The following set of constraints is considered:

$$\sum_{g \in b} \bar{S}_g - \sum_{c \in b} \bar{S}_c + \sum_{\beta(\ell^+) = b} \bar{S}_{\ell^+} + \sum_{\beta(\ell^-) = b} \bar{S}_{\ell^-} = 0, \quad \forall b \in \mathcal{B} \quad (5.2)$$

$$\bar{S}_{\ell^+} = \bar{V}_{\beta(\ell^+)} \bar{I}_{\ell^+}, \quad \bar{S}_{\ell^-} = \bar{V}_{\beta(\ell^-)} \bar{I}_{\ell^-}, \quad \forall \ell \in \mathcal{L} \quad (5.3)$$

$$\bar{I}_{\ell^+} = \bar{Y}_\ell (\bar{V}_{\beta(\ell^+)} - \bar{V}_{\beta(\ell^-)}) + \bar{Y}_{\ell_0^+} \bar{V}_{\beta(\ell^+)}, \quad \forall \ell \in \mathcal{L} \quad (5.4)$$

$$\bar{I}_{\ell^-} = \bar{Y}_\ell (\bar{V}_{\beta(\ell^-)} - \bar{V}_{\beta(\ell^+)}) + \bar{Y}_{\ell_0^-} \bar{V}_{\beta(\ell^-)}, \quad \forall \ell \in \mathcal{L} \quad (5.5)$$

$$V_{min} \leq |\bar{V}_b| \leq V_{max}, \quad \forall b \in \mathcal{B} \quad (5.6)$$

$$|\bar{S}_{\ell^+}| \leq S_{\ell_{max}}, \quad \text{or} \quad |\bar{I}_{\ell^+}| \leq I_{\ell_{max}}, \quad \forall \ell \in \mathcal{L} \quad (5.7)$$

$$|\bar{S}_{\ell^-}| \leq S_{\ell_{max}}, \quad \text{or} \quad |\bar{I}_{\ell^-}| \leq I_{\ell_{max}}, \quad \forall \ell \in \mathcal{L} \quad (5.8)$$

$$\bar{S}_g \in \mathcal{H}_g, \quad \forall g \in \mathcal{G} \quad \text{and} \quad \bar{S}_c \in \mathcal{H}_c, \quad \forall c \in \mathcal{C} \quad (5.9)$$

where, \bar{S} denotes the complex power¹, \bar{V}_b is the direct sequence phase-to-ground voltage of node b , \bar{I}_{ℓ^+} (\bar{I}_{ℓ^-}) is the current flow in the receiving (sending) end of line ℓ , \bar{Y}_ℓ is the longitudinal admittance of a line, $\bar{Y}_{\ell_0^+}$ ($\bar{Y}_{\ell_0^-}$) is the shunt capacitance at the receiving (sending) end of the line, and \mathcal{H}_g , \mathcal{H}_c are the capability curve of the generator g and the limits of the load c respectively². If a generator (load) is non-controllable then the set \mathcal{H}_g (\mathcal{H}_c) is limited to a single point.

The first constraint (5.2) corresponds to the power balance constraint at each network bus, whereas (5.3) is an alternative way to define the AC power flow equations. Constraints (5.6) and (5.7) are so-called node voltage and lines ampacity constraints, i.e., limits on node voltages and line power/current flows. The last constraints (5.9) represent the capability limits that each of the controllable devices should respect.

The equality constraints (5.3) render the OPF problem non-convex and, therefore, difficult to solve efficiently. The majority of the proposed algorithms in the literature rely on several approximations and/or convex relaxations and seek a solution to a modified OPF problem. In what follows, we describe and discuss the applicability and limitations of the BFM-based convexification of the OPF problem.

5.4 On the Limits of the Farivar-Low Approach for the Solution of the OPF Problem

5.4.1 The Farivar-Low Formulation of the OPF Problem

We assume the same objective function as in Eq. 5.1 and again consider that the network lines are represented using a π -model. Contrary to the formulation in (5.2)-(5.9), we reformulate the constraints of the OPF problem by using the branch power

¹We use the convention that positive values represent power injection and negative power consumption.

²Note that different types of controllable generators or loads can be accounted for via their corresponding capability curves/limits.

5.4. On the Limits of the Farivar-Low Approach for the Solution of the OPF Problem

and current flows as variables, similarly to [35]. To this end, we denote by \bar{S}_ℓ and \bar{I}_ℓ the power and the current that flow across the longitudinal elements of a network line ℓ from the receiving toward the sending end, for which it holds that

$$\bar{I}_\ell = \bar{Y}_\ell(\bar{V}_{\beta(\ell^+)} - \bar{V}_{\beta(\ell^-)}), \quad \forall \ell \in \mathcal{L} \quad (5.10)$$

$$\bar{S}_\ell = \bar{V}_{\beta(\ell^+)} \bar{I}_\ell, \quad \forall \ell \in \mathcal{L} \quad (5.11)$$

The power and current flows along the shunt elements of the lines are taken into account in the bus power balance constraints as nodal injections. In this direction, we denote by \bar{Y}_{b_0} the sum of all the shunt elements of the lines that are adjacent to bus b . Hence, the constraints of the OPF problem are reformulated as follows by Farivar and Low:

$$\sum_{g \in b} \bar{S}_g - \sum_{c \in b} \bar{S}_c = \sum_{\beta(\ell^+)=b} \bar{S}_\ell - \sum_{\beta(\ell^-)=b} (\bar{S}_\ell - \bar{Y}_\ell^{-1} |\bar{I}_\ell|^2) - \bar{Y}_{b_0} |\bar{V}_b|^2, \quad \forall b \in \mathcal{B} \quad (5.12)$$

$$|\bar{I}_\ell|^2 = \frac{|\bar{S}_\ell|^2}{|\bar{V}_{\beta(\ell^+)}|^2}, \quad \forall \ell \in \mathcal{L} \quad (5.13)$$

$$|\bar{V}_{\beta(\ell^-)}|^2 = |\bar{V}_{\beta(\ell^+)}|^2 + |\bar{Y}_\ell^{-1}|^2 |\bar{I}_\ell|^2 - (\bar{Y}_\ell^{-1} \bar{S}_\ell + \bar{Y}_\ell^{-1} \bar{S}_\ell), \quad \forall \ell \in \mathcal{L} \quad (5.14)$$

$$V_{min}^2 \leq |\bar{V}_b|^2 \leq V_{max}^2, \quad \forall b \in \mathcal{B} \quad (5.15)$$

$$|\bar{I}_\ell|^2 \leq I_{\ell_{max}}^2, \quad \forall \ell \in \mathcal{L} \quad (5.16)$$

$$Re(\bar{S}_g) \in [P_{g_{min}}, P_{g_{max}}], \quad Im(\bar{S}_g) \in [Q_{g_{min}}, Q_{g_{max}}], \quad \forall g \in \mathcal{G} \quad (5.17)$$

$$Re(\bar{S}_c) \in [P_{c_{min}}, P_{c_{max}}], \quad Im(\bar{S}_c) \in [Q_{c_{min}}, Q_{c_{max}}], \quad \forall c \in \mathcal{C} \quad (5.18)$$

Note that in the Farivar-Low formulation of the OPF problem, the capability curves of the controllable loads and generators, i.e., constraints (5.17), (5.18) on the nodal powers \bar{S} are limited to rectangular regions. This is essential for the conic relaxation proposed in [35, 36].

Starting from this formulation, Farivar and Low relax the equality constraints in (5.13) to inequalities and cast the aforementioned problem as a second-order cone program (SOCP). They also prove that for radial networks a global solution of the original OPF problem can be recovered from the solution of the relaxed problem if there are no upper bounds on the loads. In other words, Farivar and Low solve (5.12)-(5.18) by setting $P_{c_{max}} = \infty$ and $Q_{c_{max}} = \infty$ in constraint (5.18).

We show, in what follows, that this formulation is not equivalent to (5.1)-(5.9). In particular, constraint (5.16) (constraint (9) in [35]) is only an approximation of the ampacity constraints and, moreover, the assumptions on the controllability and bounds of the energy resources in the network are unrealistic.

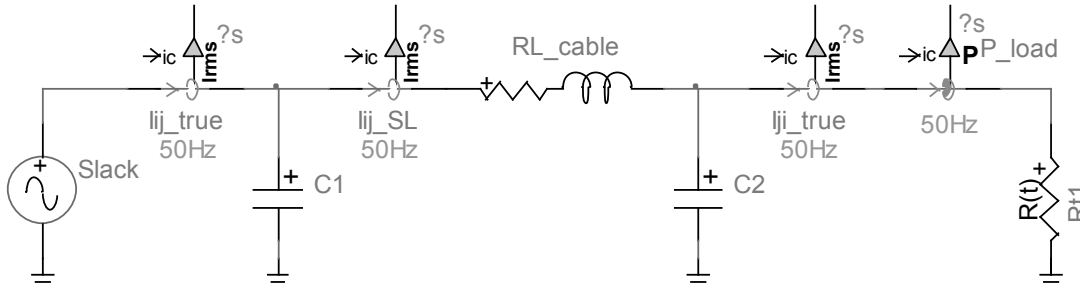


Figure 5.1: The test network used for the numerical comparison of the current flows at the sending/receiving end of the lines and the current flow along the longitudinal line impedance.

Table 5.1: Parameters of the test network in Figure 5.1

Parameter	Value
Network rated voltage, V (kV)	15
Line parameters, R (Ohms), L (H), C (uF)	(1,0.003,0.54)

5.4.2 Misinterpretation of the Physical Network Model in the Farivar-Low OPF Formulation

The branch-flow model has been often used in load-flow studies (e.g., [206, 207]) and constitutes an accurate representation of the network model. The first problem with the Farivar-Low formulation in (5.12)-(5.18) is that it misinterprets the physical network model when constraining the line flows in the network. Even though the power-flow equations in (5.12)-(5.14) are exact when the shunt capacitances are considered as nodal injections, the constraint (5.16) is imposed on a fictitious current flow across the longitudinal component of the lines, thus *does not* account for the current flow toward the shunt elements. Therefore, the optimum of problem (5.12)-(5.18) can be such that the line ampacity constraint is violated.

To better clarify why this occurs, we use a single-branch toy network, as shown in Figure 5.1. The line parameters, as well as the base values of the system are given in Table 5.1. A purely resistive load is connected to bus 2 that we vary linearly in the range of [100 – 10000]Ohms in order to numerically quantify the mismatch between those quantities. We measure the current flows at the two ends of the line, as well as the flow along the longitudinal impedance of the line. Figure 5.2 shows the measured quantities as a function of the load. It can be observed that the current flowing across the longitudinal impedance of the line under-estimates the actual current flow in the receiving end of the line.

As a consequence, in the Farivar-Low formulation setting the limit on the longitudinal current flow below the line ampacity does not guarantee that the actual line

5.4. On the Limits of the Farivar-Low Approach for the Solution of the OPF Problem

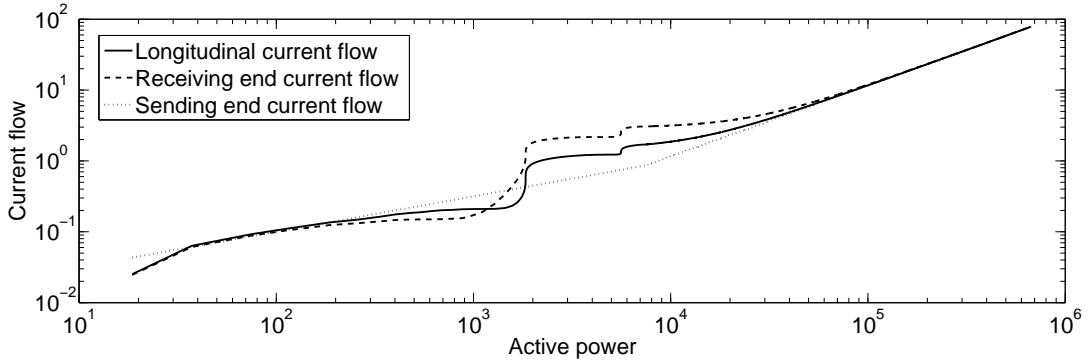


Figure 5.2: Current flows at the sending/receiving end of the line and along the longitudinal line impedance (log-log scale).

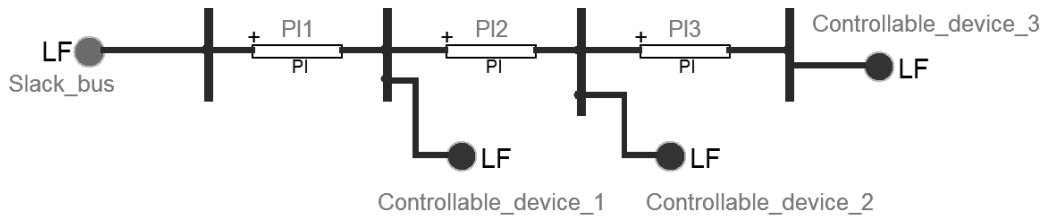


Figure 5.3: Network used in the study of the Farivar-Low OPF formulation.

current will respect this limit. In order to illustrate such a scenario, we consider yet another simple test network shown in Figure 5.3. All the network lines are built by using the same values of resistance, reactance and capacitance per km, but by assuming different values of their length³. We assume a first test case where the controllable device connected to bus 4 is a generator, whereas controllable loads are connected to buses 2 and 3. The network characteristics, the base values, the capability limits of the controllable resources⁴, and the voltage and ampacity bounds are provided in Table 5.2. We assume that the controllable generation operates at a unity power factor. The problem in (5.12)-(5.18) is formulated and solved in Matlab. The objective function accounts for resistive losses minimization, as well as utility maximization of the controllable generation units:

$$\min_{\bar{S}_g, \bar{S}_\ell, |\bar{V}_b|, |\bar{I}_\ell|} - \sum_{g \in \mathcal{G}} \text{Re}(\bar{S}_g) + \sum_{\ell \in \mathcal{L}} \text{Re}(\bar{Y}_\ell) |\bar{I}_\ell|^2 \quad (5.19)$$

In order to investigate the order of magnitude of the violation of the ampacity constraint, we solve the OPF problem for various line lengths and network voltage-rated values. In particular, we assume that the line lengths are uniformly multiplied by a factor in the range [1.25 – 7.5] (while keeping the network voltage rated value to

³Typical values of MV underground cables are considered for the resistance, reactance and shunt capacitances of the lines [208].

⁴The upper bounds of the active and reactive power of the loads are considered to be infinite, as required in the Farivar-Low formulation.

Table 5.2: Parameters of the test network in Figure 5.3 used for the investigation of the line ampacity limit violation

Parameter	Value
Network rated voltage and base power, V (kV), S (MVA)	24.9,5
Line parameters, R (Ohms/km), L (mH/km), C (uF/km)	(0.193,0.38,0.24)
$[P_{gmin}, P_{gmax}]$ (MW)	[0, 2]
P_{cmin} (MW) (bus2, bus3)	(0.05, 0.06)
Q_{cmin} (Mvar) (bus2, bus3)	(0.03, 0.027)
$[V_{min}, V_{max}]$ (p.u)	[0.9, 1.1]
I_{max} (A)	80

Table 5.3: Parameters of the test network in Figure 5.3 used for the investigation of the network operating point on the line ampacity limit violation

Parameter	Value
$[P_{gmin}, P_{gmax}]$ (MW) (bus 2)	[0, 0.01]
$[P_{gmin}, P_{gmax}]$ (MW) (bus 3)	[0, 0.012]
(P_{cmin}, Q_{cmin}) (MW, Mvar) (bus 4)	0.3, 0.15

its nominal value) and the network voltage rated value varies in the range $[15 - 45]kV$ (while keeping the line lengths to their nominal values). Once the optimal solution is computed in each case, we calculate the actual current flows in the sending/receiving end of the lines and we compute the maximum constraint violation. The results are shown in Figure 5.4. As the line length increases, the current flowing toward the shunt capacitors increases, thus neglecting its contribution to the line flow leads to significant violations of the ampacity limit. At 7.5 times the initial line length, the violation reaches a value of 18.4%. The effect of the network voltage-rated value is similar, with a maximum constraint violation of 25% when the voltage value is 45kV.

In addition to the effect of the line lengths and the network voltage-rated value, we study the effect of the network operating point on the ampacity violation. To this end, we consider a second test case where the controllable device connected to bus 4 is a load and generators are connected to buses 2 and 3. The capability limits of the controllable resources are provided in Table 5.3. For this setting, Figure 5.5 shows the solution of the Farivar-Low OPF problem, namely current flows at the receiving/sending end of the network lines, as well as across the longitudinal impedance. We can observe that the maximum violation of the ampacity constraint is in the order of 40%.

In order to avoid current flows that exceed the lines' ampacity limits, i.e., in order to use the BFM in an accurate way, the Farivar-Low formulation should either consider the actual current flows in the receiving/sending ends of the lines as optimization variables, or should add the contribution of the current flows toward the shunt elements of the lines to the longitudinal current flow in the inequality constraint (5.16). In this

5.4. On the Limits of the Farivar-Low Approach for the Solution of the OPF Problem

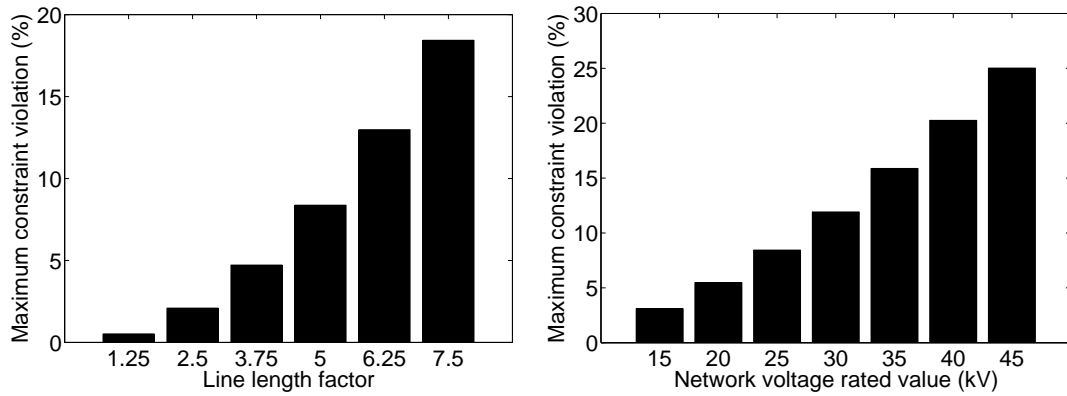


Figure 5.4: Maximum ampacity constraint violation as a function of the line lengths and the network voltage rated value.

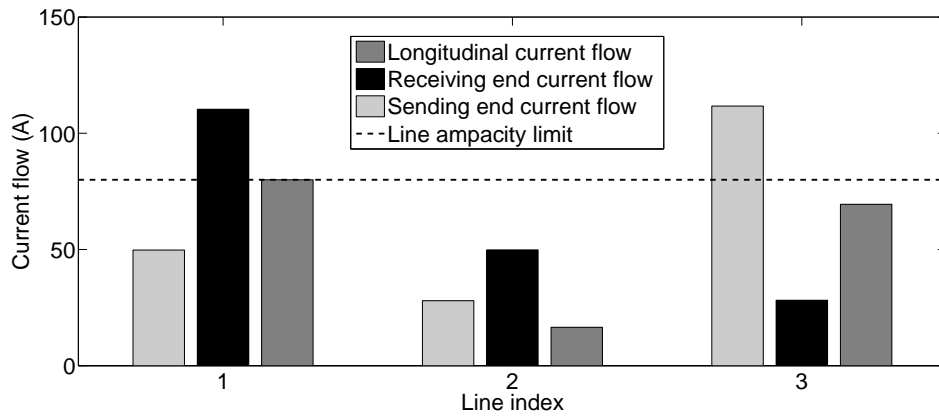


Figure 5.5: Farivar-Low OPF solution for the current flows at the sending/receiving end of the network lines and across the longitudinal line impedance under heavy consumption and light generation conditions.

case, however, (5.12)-(5.18) can no longer be solved efficiently as proposed in [35, 36]. Therefore, the generic OPF problem cannot be convexified by using Farivar-Low's approach.

5.4.3 On the Assumptions Required for the Exactness of the Farivar-Low Relaxation

In addition to the aforementioned fundamental problem, which is related to the physical network model, Farivar and Low require specific assumptions to hold in order to prove the exactness of the proposed relaxations. Several of these assumptions are too strong and not realistic.

To begin with, the OPF formulation in [35, 36] assumes controllability of both loads and generators in the network buses and, in particular, assumes rectangular bounds on the powers of loads/generators. This is quite a strong assumption, as usually the DNO

Table 5.4: Parameters of the test network in Figure 5.3 used for the investigation of the unboundedness of the consumption

Parameter	Value
$[P_{gmin}, P_{gmax}]$ (MW)	[0, 1.2]
(P_{cmin}, Q_{cmin}) (MW, Mvar) (buses 2,3)	(0.0125, 0.0026)

has very few specific control points available in the network with capability curves that are typically more complex and that account, among others, for capabilities of power electronics and limitations of machinery. An even more serious limitation is that the Farivar-Low model considers no upper bounds on the controllable loads in order to prove the exactness of the proposed relaxation. This implies that in cases where excessive production of the generators causes violations of the voltage or line-flows limits, local demand is invoked to compensate for the increased generation. In order to illustrate such a setting and to show that the result of the OPF problem can result in unrealistic values for demand, we consider the same network in Figure 5.3 and we assume that there is high penetration of distributed generation and a low demand. The values of loads and generation, as well as the corresponding limits are shown in Table 5.4. Solving the optimization problem and considering infinite upper bounds on the demand results in load values that are significantly increased, compared to the minimum values shown in Table 5.4. The resulting optimal power points are shown in Figure 5.6. We show in black the initial values for active and reactive power of loads and generation (corresponding to the values of Table 5.4), and in gray the results of the OPF solution (when not accounting for upper bounds on loads). It is worth observing that the optimal active power consumption of bus 3 is increased 23.6 times and the reactive power consumption at buses 2 and 3 is increased 85.3 and 92 times, respectively. In a realistic setting, even if part of the demand in the network is controllable, the amount of available demand response is limited and such an increase in the consumption is most likely not possible. Therefore, in such a case, the congestion and voltage problems should be solved by properly controlling the generator within its capability limits. In addition to this, typically, the active and reactive power consumption should be linked via the corresponding power factor. We observe, however, that the OPF solution in this scenario results in very large values for the reactive power consumption and, in particular, the power factor of bus 2 is 0.03 after the OPF solution, whereas initially its value was 0.98. In an attempt to relax this assumption, Farivar and Low claim that the infinite upper bound on the loads, when not applicable, can be replaced by equivalent conditions [201]. However, not only are these conditions unrealistic, they are also not applicable in our context as they require no upper bound on the voltage magnitudes. This is in contradiction with the actual problem we target to solve, i.e., voltage rise due to high penetration of renewable energy resources.

5.4. On the Limits of the Farivar-Low Approach for the Solution of the OPF Problem

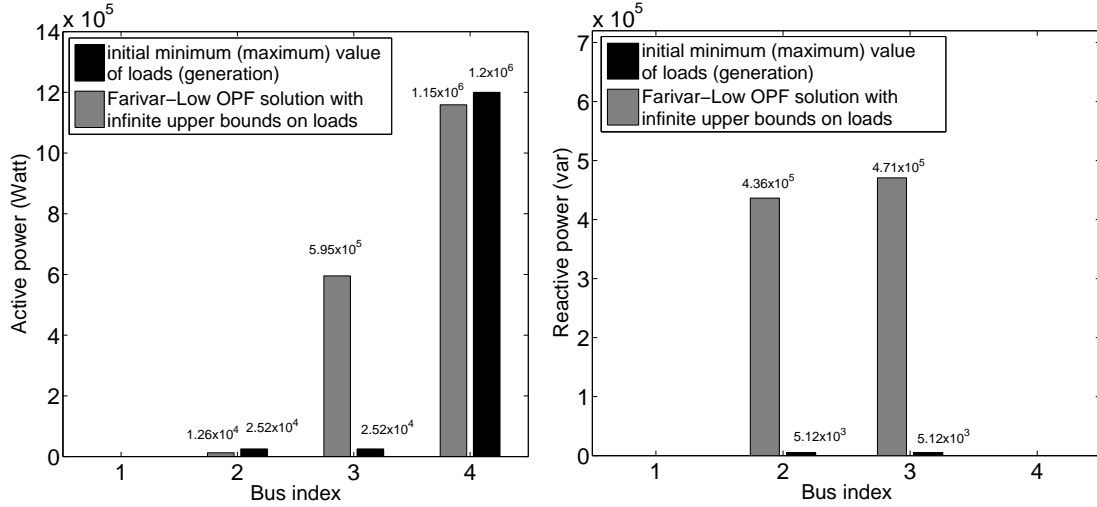


Figure 5.6: Optimal solution of the Farivar-Low OPF formulation for the active and reactive power set-points when upper bounds on loads are infinite.

5.4.4 On the Extension of the SOCP Relaxation to Networks with Lines Modeled as π -equivalents

In this section, we discuss a possible approach that can be used to extend the initial formulation in (5.12)-(5.18) in order to account for the shunt elements of the lines. We show through concrete examples that extending the Farivar-Low approach to a system model that is correctly represented cannot guarantee the exactness of the SOCP relaxation and, thus, the retrieval of a feasible OPF solution.

A straightforward way to account for the line ampacity constraints in (5.16) is to re-write a new set of line constraints for the case of π -model lines, while keeping the same branch flow variables. In this case, the line constraints are reformulated as follows:

$$|\bar{I}_\ell|^2 + |\bar{Y}_{\ell_0^+}|^2 |\bar{V}_{\beta(\ell^+)}|^2 + 2\text{Re}(\bar{Y}_{\ell_0^+} \bar{S}_\ell) \leq I_{\ell_{max}}^2, \forall \ell \in \mathcal{L} \quad (5.20)$$

$$|\bar{I}_\ell|^2 + |\bar{Y}_{\ell_0^-}|^2 |\bar{V}_{\beta(\ell^-)}|^2 + 2\text{Re}(\bar{Y}_{\ell_0^-} (\bar{Y}_\ell^{-1} |\bar{I}_\ell|^2 - \bar{S}_\ell)) \leq I_{\ell_{max}}^2, \forall \ell \in \mathcal{L} \quad (5.21)$$

It is worth noting that these new constraints, that account also for the line flows towards the shunt elements, are convex and can be added to Farivar and Lows' OPF formulation. However, this doesn't mean that the optimal solution of the relaxed SOCP problem is guaranteed to be a physically feasible one, in other words, the theorem in [35] does not hold here.

To support this claim, let us consider the following simple example. We use once again the same simple test network shown in Figure 5.3. We assume a test case where the controllable device connected to bus 4 is a load, whereas controllable generators are connected to buses 2 and 3. The network characteristics, the base values, the

Table 5.5: Parameters of the test network in Figure 5.3

Parameter	Value
Network rated voltage and base power, V (kV), S (MVA)	24.9,5
Line parameters, R (Ohms/km), L (mH/km), C (uF/km)	(0.193,0.38,0.24)
P_{gmax} (bus2, bus3)(MW)	(1, 1.2)
P_{cmin} (MW) (bus4)	0.1
Q_{cmin} (Mvar) (bus4)	0.05
$[V_{min}, V_{max}]$ (p.u)	[0.9, 1.1]
I_{max} (A)	80

Table 5.6: SOCP inequalities in (5.13)

Line	Value
1 – 2	$1.7E - 16$
2 – 3	-0.0461
3 – 4	$1.3E - 16$

capability limits of the controllable resources, and the voltage and ampacity bounds are provided in Table 5.5. We assume that the controllable generators operate at a unity power factor. Note that the upper bounds for the loads are considered infinite as required in the original formulation of Farivar and Low.

We solve the problem in Matlab and the resulting values for the SOCP inequalities for each network line are shown in Table. 5.6. In this case, after the solution of the OPF problem not all the inequalities in (5.13) are satisfied with equality, namely the SOCP relaxation is inexact, therefore, the obtained solution has no physical meaning and a physically feasible solution cannot be recovered.

Overall, the examples shown in this section indicate that the proposed Farivar-Low relaxation cannot be trivially extended to lines represented as π -model equivalents even with convex constraints applied to the line exact π -model. Overall, the fundamental problems with the Farivar-Low approach, as well as with the several additional assumptions, prohibit its application to the generic OPF problem. As a consequence, there is a need to design algorithms that target the original non-approximated OPF problem that remains inherently non-convex. Recent trends are in favor of using ADMM for the solution of the OPF problem. Even though ADMM requires the underlying problem to be convex in order to guarantee convergence, it has been applied also to the case of non-convex AC OPF problems with promising convergence performance (e.g., [172, 173]). In what follows we first present the ADMM solution of the problem in (5.1)-(5.9) and then we highlight specific scenarios for which ADMM fails to converge when applied to the non-approximated OPF problem.

5.5 On the Application of ADMM for the Solution of the OPF Problem

5.5.1 ADMM-based Solution of the OPF Problem

The ADMM-based solution of the OPF problem requires that the control variables are split into two separate groups and that the objective function is separable across this splitting [209]. To this end, we introduce additional slack variables, \bar{z} , for the devices' and loads' power injections and for the line power flows and we reformulate the OPF problem as follows⁵:

$$\min_{\substack{\bar{S}_g, \bar{z}_g, \bar{S}_c, \bar{z}_c, \bar{S}_{\ell^+}, \bar{z}_{\ell^+}, \bar{S}_{\ell^-}, \bar{z}_{\ell^-} \\ \bar{E}_{\ell^+}, \bar{E}_{\ell^-}, \bar{I}_{\ell^+}, \bar{I}_{\ell^-}, \bar{V}_b}} - \sum_g U_g(\text{Re}(\bar{S}_g)) + \sum_b J_V(|\bar{V}_b|) + \quad (5.22)$$

$$\sum_{\ell} J_I(|\bar{I}_{\ell^+}|, |\bar{I}_{\ell^-}|) + \sum_b \phi\left(\sum_{g \in b} \bar{z}_g - \sum_{c \in b} \bar{z}_c + \sum_{\beta(\ell^+)=b} \bar{z}_{\ell^+} + \sum_{\beta(\ell^-)=b} \bar{z}_{\ell^-}\right)$$

$$\text{subject to: } \bar{S}_g = \bar{z}_g, \forall g \in \mathcal{G}, \quad \text{and} \quad \bar{S}_c = \bar{z}_c, \forall c \in \mathcal{C} \quad (5.23)$$

$$\bar{S}_{\ell^+} = \bar{z}_{\ell^+}, \quad \text{and} \quad \bar{S}_{\ell^-} = \bar{z}_{\ell^-}, \forall \ell \in \mathcal{L} \quad (5.24)$$

$$\bar{E}_{\ell^+} = \bar{V}_{\beta(\ell^+)}, \quad \text{and} \quad \bar{E}_{\ell^-} = \bar{V}_{\beta(\ell^-)}, \forall \ell \in \mathcal{L} \quad (5.25)$$

where ϕ is the characteristic function of the set $\{\bar{x} \in \mathbb{C} : \bar{x} = 0\}$, J_V is a penalty function with value 0 if $V_{min} \leq |\bar{V}_b| \leq V_{max}$ and ∞ otherwise and J_I is a penalty function with value 0 if $\max(|\bar{I}_{\ell^+}|, |\bar{I}_{\ell^-}|) \leq I_{\ell_{max}}$ and ∞ otherwise.

The augmented Lagrangian for this problem is as follows:

$$\begin{aligned} L_{\omega}(\bar{S}_g, \bar{S}_c, \bar{S}_{\ell^+}, \bar{S}_{\ell^-}, \bar{E}_{\ell^+}, \bar{E}_{\ell^-}, \bar{I}_{\ell^+}, \bar{I}_{\ell^-}, \bar{z}_g, \bar{z}_c, \bar{z}_{\ell^+}, \bar{z}_{\ell^-}, \bar{V}_b, \bar{\mu}, \bar{\nu}, \bar{\lambda}) \\ = - \sum_g U_g(\text{Re}(\bar{S}_g)) + \sum_b J_V(|\bar{V}_b|) + \sum_{\ell} J_I(|\bar{I}_{\ell^+}|, |\bar{I}_{\ell^-}|) \\ + \sum_b \phi\left(\sum_{g \in b} \bar{z}_g - \sum_{c \in b} \bar{z}_c + \sum_{\beta(\ell^+)=b} \bar{z}_{\ell^+} + \sum_{\beta(\ell^-)=b} \bar{z}_{\ell^-}\right) \\ + \frac{\omega}{2} \left\{ \sum_{\ell} |\bar{E}_{\ell^+} - \bar{V}_{\beta(\ell^+)} + \bar{\mu}_{\ell}|^2 + \sum_{\ell} |\bar{E}_{\ell^-} - \bar{V}_{\beta(\ell^-)} + \bar{\nu}_{\ell}|^2 \right. \\ \left. + \sum_g |\bar{S}_g - \bar{z}_g + \bar{\lambda}_g|^2 + \sum_c |\bar{S}_c - \bar{z}_c + \bar{\lambda}_c|^2 \right. \\ \left. + \sum_{\ell} |\bar{S}_{\ell^+} - \bar{z}_{\ell^+} + \bar{\lambda}_{\ell^+}|^2 + \sum_{\ell} |\bar{S}_{\ell^-} - \bar{z}_{\ell^-} + \bar{\lambda}_{\ell^-}|^2 \right\} \quad (5.26) \end{aligned}$$

where $\bar{\mu}, \bar{\nu}, \bar{\lambda}$ are the lagrange multipliers associated with the equality constraints (5.23)-(5.25).

The ADMM algorithm at the k -th iteration consists of the following steps:

⁵In what follows we assume that demand is non-controllable. Also, as in [204], the constraints (5.3), (5.9) are considered internal constraints of the lines and devices respectively and $\bar{I}_{\ell^+}, \bar{I}_{\ell^-}$ are internal variables of the lines.

1. First, all the devices, loads and lines update in parallel the primary variables, and their internal variables, i.e., $(\bar{S}_g, \bar{S}_c, \bar{S}_{\ell^+}, \bar{S}_{\ell^-}, \bar{E}_{\ell^+}, \bar{E}_{\ell^-}, \bar{I}_{\ell^+}, \bar{I}_{\ell^-})$ with the secondary variables, and the dual variables fixed ⁶:

For each network line ℓ :

$$\begin{aligned} & (\bar{S}_{\ell^+}^{k+1}, \bar{S}_{\ell^-}^{k+1}, \bar{E}_{\ell^+}^{k+1}, \bar{E}_{\ell^-}^{k+1}, \bar{I}_{\ell^+}^{k+1}, \bar{I}_{\ell^-}^{k+1}) = \\ & \underset{\bar{S}_{\ell^+}, \bar{S}_{\ell^-}, \bar{E}_{\ell^+}, \bar{E}_{\ell^-}, \bar{I}_{\ell^+}, \bar{I}_{\ell^-}}{\operatorname{argmin}} J_I(|\bar{I}_{\ell^+}^+|, |\bar{I}_{\ell^-}^-|) + \\ & \frac{\omega}{2} (|\bar{E}_{\ell^+} - \bar{V}_{\beta(\ell^+)}^k + \bar{\mu}_{\ell}^k|^2 + |\bar{E}_{\ell^-} - \bar{V}_{\beta(\ell^-)}^k + \bar{\nu}_{\ell}^k|^2 \\ & + |\bar{S}_{\ell^+} - \bar{z}_{\ell^+}^k + \bar{\lambda}_{\ell^+}^k|^2 + |\bar{S}_{\ell^-} - \bar{z}_{\ell^-}^k + \bar{\lambda}_{\ell^-}^k|^2) \end{aligned} \quad (5.27)$$

$$\text{subject to: } \bar{S}_{\ell^+} = \bar{E}_{\ell^+} \underline{I}_{\ell^+} \quad \text{and} \quad \bar{S}_{\ell^-} = \bar{E}_{\ell^-} \underline{I}_{\ell^-} \quad (5.28)$$

$$\bar{I}_{\ell^+} = \bar{Y}_{\ell}(\bar{E}_{\ell^+} - \bar{E}_{\ell^-}) + \bar{Y}_{\ell_0^+} \bar{E}_{\ell^+} \quad (5.29)$$

$$\bar{I}_{\ell^-} = \bar{Y}_{\ell}(\bar{E}_{\ell^-} - \bar{E}_{\ell^+}) + \bar{Y}_{\ell_0^-} \bar{E}_{\ell^-} \quad (5.30)$$

$$\text{For each device } g: \quad (5.31)$$

$$\bar{S}_g^{k+1} = \underset{\bar{S}_g}{\operatorname{argmin}} -U_g(\operatorname{Re}(\bar{S}_g)) + \frac{\omega}{2} (|\bar{S}_g - \bar{z}_g^k + \bar{\lambda}_g^k|^2)$$

$$\text{subject to: } \bar{S}_g \in \mathcal{H}_g$$

$$\text{For each load } c: \bar{S}_c^{k+1} = \bar{S}_c \quad (5.32)$$

2. Then, by using the updated primary variables, the secondary variables are updated, i.e., (\bar{z}, \bar{V}_b) , on a bus level. We denote by \bar{z}_b the vector of complex powers of all the devices, loads and lines that are connected to bus b , i.e., $\bar{z}_b \triangleq (\bar{z}_{g:g \in b}, \bar{z}_{c:c \in b}, \bar{z}_{\ell^+:\beta(\ell^+)=b}, \bar{z}_{\ell^-:\beta(\ell^-)=b})$:

$$\bar{z}_b^{k+1} = \underset{\bar{z}_b}{\operatorname{argmin}} (\phi(\sum_{g \in b} \bar{z}_g - \sum_{c \in b} \bar{z}_c + \sum_{\beta(\ell^+)=b} \bar{z}_{\ell^+} + \sum_{\beta(\ell^-)=b} \bar{z}_{\ell^-})) \quad (5.33)$$

$$\begin{aligned} & + \frac{\omega}{2} \{ \sum_{g \in b} |\bar{S}_g^{k+1} - \bar{z}_g + \bar{\lambda}_g^k|^2 + \sum_{c \in b} |\bar{S}_c^{k+1} - \bar{z}_c + \bar{\lambda}_c^k|^2 \\ & + \sum_{\beta(\ell^+)=b} |\bar{S}_{\ell^+}^{k+1} - \bar{z}_{\ell^+} + \bar{\lambda}_{\ell^+}^k|^2 + \sum_{\beta(\ell^-)=b} |\bar{S}_{\ell^-}^{k+1} - \bar{z}_{\ell^-} + \bar{\lambda}_{\ell^-}^k|^2 \} \\ \bar{V}_b^{k+1} & = \underset{\bar{V}_b}{\operatorname{argmin}} (J(\bar{V}_b) + \frac{\omega}{2} \{ \sum_{\beta(\ell^+)=b} |\bar{E}_{\ell^+}^{k+1} - \bar{V}_b + \bar{\mu}_{\ell}^k|^2 \\ & + \sum_{\beta(\ell^-)=b} |\bar{E}_{\ell^-}^{k+1} - \bar{V}_b + \bar{\nu}_{\ell}^k|^2 \}) \end{aligned} \quad (5.34)$$

⁶Note that demand is not controllable, hence the loads do not require the solution of an optimization problem to update their power consumption.

5.5. On the Application of ADMM for the Solution of the OPF Problem

Table 5.7: Parameters of the test network in Figure 5.3 used for the ADMM-based solution of the OPF problem

Parameter	Value
Generators' power, $ \bar{S}_{i_{gmax}} , i = 2, 3, 4$ (MVA)	0.40, 0.39, 0.46
Generators' power factor, $\cos\phi_{i_g}, i = 2, 3, 4$	0.9
Loads' active power, $P_{i_c}, i = 2, 3, 4$ (MW)	2.76, 2.16, 2.46
Loads' reactive power, $Q_{i_c}, i = 2, 3, 4$ (MW)	1.38, 1.08, 1.23
Shunt capacitor (bus 2), case I and II (uF)	(239, 859)
Penalty term gain, ω	1
Tolerance and maximum number of iterations	$10^{-4}, 10^4$

3. Finally, dual variables, i.e., $\bar{\mu}, \bar{\nu}, \bar{\lambda}$ are updated:

$$\bar{\mu}_\ell^{k+1} = \bar{\mu}_\ell^k + (\bar{E}_{\ell^+}^{k+1} - \bar{V}_{\beta(\ell^+)}^{k+1}) \quad (5.35)$$

$$\bar{\nu}_\ell^{k+1} = \bar{\nu}_\ell^k + (\bar{E}_{\ell^-}^{k+1} - \bar{V}_{\beta(\ell^-)}^{k+1}) \quad (5.36)$$

$$\bar{\lambda}_g^{k+1} = \bar{\lambda}_g^k + (\bar{S}_g^{k+1} - \bar{z}_g^{k+1}) \quad (5.37)$$

$$\bar{\lambda}_c^{k+1} = \bar{\lambda}_c^k + (\bar{S}_c^{k+1} - \bar{z}_c^{k+1}) \quad (5.38)$$

$$\bar{\lambda}_{\ell^+}^{k+1} = \bar{\lambda}_{\ell^+}^k + (\bar{S}_{\ell^+}^{k+1} - \bar{z}_{\ell^+}^{k+1}) \quad (5.39)$$

$$\bar{\lambda}_{\ell^-}^{k+1} = \bar{\lambda}_{\ell^-}^k + (\bar{S}_{\ell^-}^{k+1} - \bar{z}_{\ell^-}^{k+1}) \quad (5.40)$$

The stopping criterion for this algorithm is that the primal and dual residuals (defined as in [209]) are less than a small predefined tolerance or that a maximum number of iterations has been reached.

In what follows, we show specific scenarios where the ADMM algorithm fails to converge to a solution.

5.5.2 Investigation of the Convergence of the ADMM-based Solution of the OPF Problem

We consider the same network as in Figure 5.3. Each network bus, apart from the slack bus, has a load and a generator connected to it. The demand in the network is assumed to be non-controllable, whereas the generators are assumed to be distributed solar panels with typical PV-type capability constraints. For this scenario, the capability limits and the values of loads and generation are given in Table 5.7. In addition to the loads and generation, we consider that a shunt capacitor is connected to bus 2. In order to model this shunt capacitor, we consider that it is part of the first network line. In particular, we consider that the shunt capacitance on the sending end of the π -model of the line connecting buses 1 and 2 is modified accordingly to account for the shunt capacitor.

We implement and solve the ADMM algorithm in Matlab for two different cases

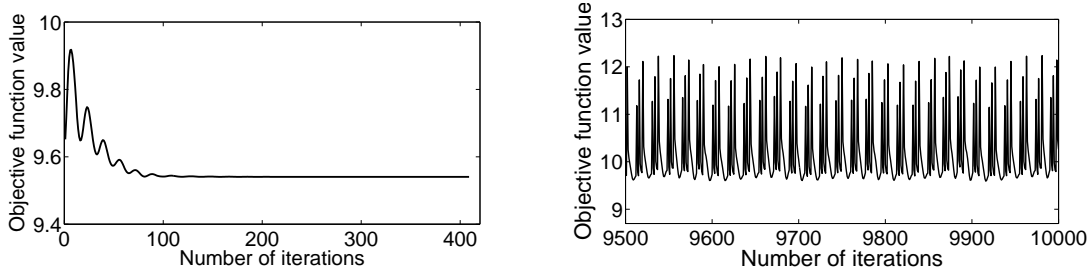


Figure 5.7: Objective function value for case I and II (last 500 iterations).

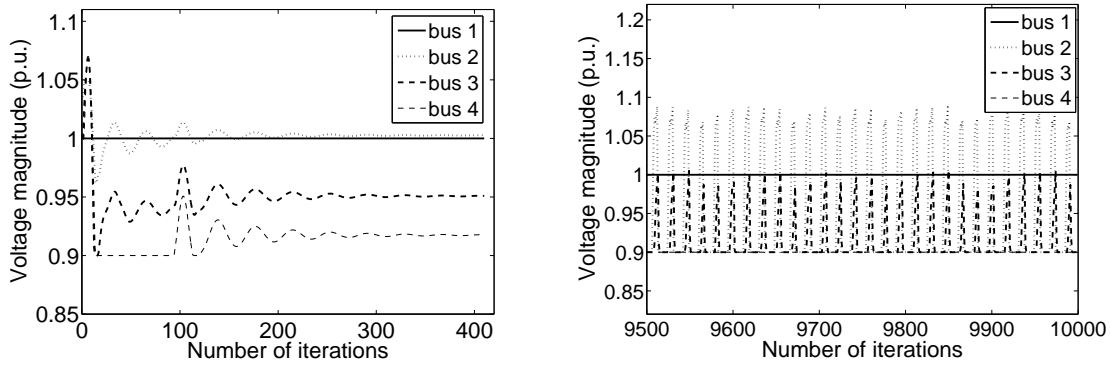


Figure 5.8: Voltage magnitude evolution for cases I and II (last 500 iterations).

that correspond to two different values of the size of the shunt capacitor (see Table 5.7). In Case I, even though the OPF problem solved is the non-approximated non-convex one, ADMM converges, within the predefined tolerance, in 411 iterations. The left figure in Figure 5.7 shows the objective function value as a function of the number of iterations of ADMM. The left figure in Figure 5.8 shows the convergence of the buses' voltage magnitudes and Figure 5.9 shows how the primal and dual residuals evolve with the iterations. On the contrary, in Case II, ADMM fails to converge to a solution and reaches the maximum number of iterations. This is shown in Figure 5.7 (right), 5.8 (right) and 5.10 where the objective function, as well as the residuals and bus voltages are plotted for the last five hundred iterations until the maximum number of iterations is reached; we can observe that they exhibit oscillations.

In what follows we analyze why the ADMM algorithm converges in Case I but fails in Case II. To begin with, the first network line has the peculiarity that the voltage at its receiving end $\bar{E}_{\ell+}$ (i.e., the slack bus voltage) is fixed⁷. As a consequence, the first equality constraint in (5.28) becomes linear in the real and imaginary part of the voltage $\bar{E}_{\ell-}$, whereas the second equality constraint in (5.28) becomes quadratic on the real and imaginary part of the voltage $\bar{E}_{\ell-}$. In fact, the coefficients of the quadratic terms in the latter constraint are $Re(\bar{Y}_{\ell})$ and $-Im(\bar{Y}_{\ell}) - Im(\bar{Y}_{\ell_0^-})$ for the real and imaginary parts, respectively. Due to the physics of the network, $Re(\bar{Y}_{\ell})$ and $Im(\bar{Y}_{\ell_0^-})$ are positive for a

⁷This holds for all the lines that are connected to the slack bus.

5.5. On the Application of ADMM for the Solution of the OPF Problem

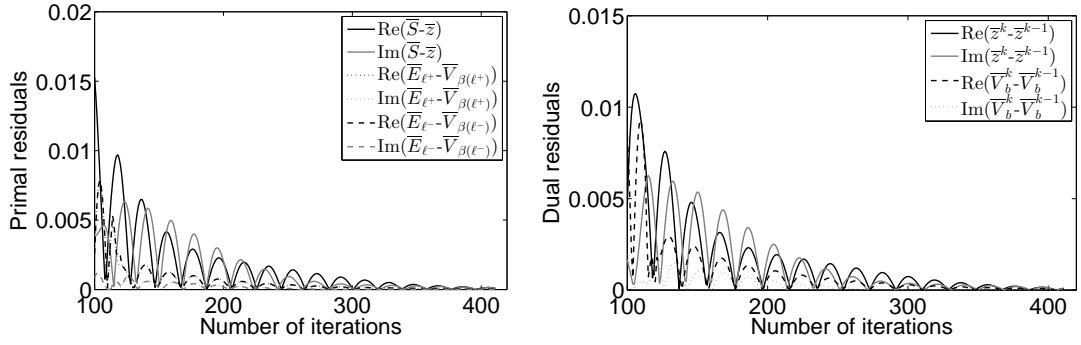


Figure 5.9: Norm of the primal/dual residuals for case I (last 311 iterations).

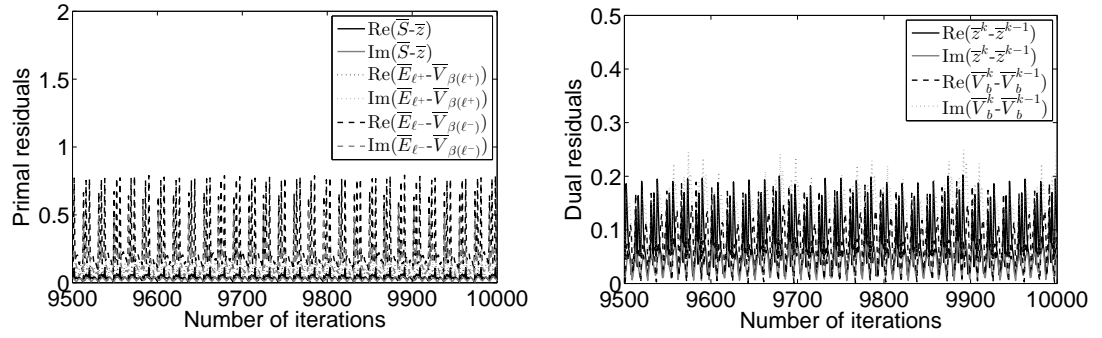


Figure 5.10: Norm of the primal/dual residuals for case II (last 500 iterations).

network line and $Im(\bar{Y}_\ell)$ is negative. Furthermore, typically, the longitudinal reactance $Im(\bar{Y}_\ell)$ is much larger than the shunt capacitance $Im(\bar{Y}_{\ell_0^-})$ of a network line. Therefore, typically the coefficients of both quadratic terms are positive, and the line problem in (5.27) is convex for the lines that are connected to the slack bus. This is the case for the Case I. However, in Case II the size of the shunt capacitor, connected to bus 2, is such that $Im(\bar{Y}_{\ell_0^-}) > -Im(\bar{Y}_\ell)$, thus the coefficient of the aforementioned quadratic term in (5.28) is no longer positive and the corresponding line problem becomes non-convex.

Apart from the aforementioned case of the shunt capacitor, the ADMM algorithm also fails to converge to a solution when on-load tap changers (OLTCs) are included in the OPF formulation. In fact, the effect of the OLTCs is similar to that of the shunt capacitors, in the sense that the line problem in (5.27) becomes once again non-convex for those lines that are connected to regulating transformers. To better understand why this occurs, let us consider a transformer with OLTC capabilities between buses 1 and 2 in the network and let us denote the ideal transformer admittance by Y_t and the OLTC ratio by α . Then based on the OLTC model in [210], the longitudinal admittance of the first network line equals αY_t and the shunt elements of the receiving and sending ends of the same line are $\alpha(\alpha - 1)Y_t$ and $(1 - \alpha)Y_t$ respectively. Hence, there is an additional control variable, namely the ratio α , that appears in the equality constraints (5.28) of the first network line problem, and both these constraints become quadratic in \bar{E}_{ℓ^-} and α and non-convex.

5.6 AC OPF in Radial Distribution Systems

As a solution to the limitations identified above, we propose here both a centralized and a distributed algorithm for the solution of the non-convex AC-OPF problem in radial networks. We first write the AC OPF problem presented in Section 5.3 in an equivalent form, and then we provide a centralized, as well as a distributed algorithm for its solution.

We make the following assumptions about the grid model:

- A1. We consider a direct sequence representation of the grid;
- A2. Any two-port component (e.g., lines, transformers etc.) is represented as a π -equivalent;
- A3. We assume a perfect knowledge of the system parameters, i.e., the network admittance matrix is known;
- A4. The nodal-power injections are voltage-independent;
- A5. The control variables are composed by the nodal power injections/absorptions.

5.6.1 The Proposed Centralized OPF Algorithm

We are interested in maximizing the social welfare of the economic agents that use the grid, while maintaining an acceptable network voltage profile and respecting the line ampacity limits. Specifically, we tune the line ampacities and the network voltage profiles by controlling the (P, Q) -injections of distributed controllable devices \mathcal{G} (e.g., renewable generators) in a “fair” way: Each controllable device $g \in \mathcal{G}$ has a certain utility function $U_g(\cdot)$, and the sum of these utility functions is maximized subject to the satisfaction of the network operation constraints (voltage and ampacity). The resulting set-point is thus Pareto-optimal, i.e., no single device can increase its utility without hurting the utility of some other device, and locally-“fair”, i.e., the resulting set-point is a local maximizer of the sum of the device utilities lying on the Pareto boundary of feasible set-points.

For each network line, we introduce two auxiliary variables $\bar{E}_{\ell+}$ and $\bar{E}_{\ell-}$ representing the complex voltage at the two ends of the line. Assumptions A1-A3 allow us to express the corresponding injected currents and powers at the two ends of line ℓ :

$$\bar{I}_{\ell+} = \bar{I}_{\ell+}(\bar{E}_{\ell+}, \bar{E}_{\ell-}) = (\bar{Y}_{\ell} + \bar{Y}_{\ell_0^+})\bar{E}_{\ell+} - \bar{Y}_{\ell}\bar{E}_{\ell-} \quad (5.41)$$

$$\bar{I}_{\ell-} = \bar{I}_{\ell-}(\bar{E}_{\ell+}, \bar{E}_{\ell-}) = (\bar{Y}_{\ell} + \bar{Y}_{\ell_0^-})\bar{E}_{\ell-} - \bar{Y}_{\ell}\bar{E}_{\ell+} \quad (5.42)$$

$$\bar{S}_{\ell+} = \bar{S}_{\ell+}(\bar{E}_{\ell+}, \bar{E}_{\ell-}) = \bar{E}_{\ell+}\bar{I}_{\ell+} \quad (5.43)$$

$$\bar{S}_{\ell-} = \bar{S}_{\ell-}(\bar{E}_{\ell+}, \bar{E}_{\ell-}) = \bar{E}_{\ell-}\bar{I}_{\ell-} \quad (5.44)$$

In the remainder of this chapter, unless otherwise stated, the complex line currents and powers expressed above are always computed according to equations (5.41)-(5.44).

5.6. AC OPF in Radial Distribution Systems

They are thus all functions of $\bar{E}_{\ell+}$ and $\bar{E}_{\ell-}$ *exclusively*, although the arguments are often omitted for the sake of brevity. All quantities are expressed in per-unit, unless otherwise specified.

For the sake of readability, we denote the vector formed by the real and imaginary parts of variables $(\bar{E}_{\ell+}, \bar{E}_{\ell-})_{\ell}$ by $y \in \mathbb{R}^{4L}$, where $L = |\mathcal{L}|$ is the number of lines. Note that for a given value of y , the corresponding currents and powers do not necessarily satisfy Kirchhoff's law.

We call y feasible if it satisfies voltage consistency and per-bus power-balance. Voltage consistency means that the voltages of all the lines incident to a specific bus $b \in \mathcal{B}$ are identical, i.e., have the same amplitude V_b and the same argument φ_b :

$$|\bar{E}_{\ell+}| = V_{\beta(\ell+)}, \quad |\bar{E}_{\ell-}| = V_{\beta(\ell-)} \quad (5.45)$$

$$\arg(\bar{E}_{\ell+}) = \varphi_{\beta(\ell+)}, \quad \arg(\bar{E}_{\ell-}) = \varphi_{\beta(\ell-)}, \quad \forall \ell \in \mathcal{L}. \quad (5.46)$$

At each bus $b \in \mathcal{B}$, power-balance is satisfied if and only if

$$\sum_{\beta(\ell+)=b} \bar{S}_{\ell+} + \sum_{\beta(\ell-)=b} \bar{S}_{\ell-} = - \sum_{g \in b} \bar{S}_g - \bar{S}(b), \quad \forall b \in \mathcal{B}, \quad (5.47)$$

where S_g is the controlled generated power of device g found at bus b , $\bar{S}(b)$ denotes the non-controllable power injection at bus b , and $\bar{S}_{\ell+}, \bar{S}_{\ell-}$ are obtained via (5.43)-(5.44).

If y is feasible, it is important to note that equations (5.41)-(5.44) describe the exact AC power-flow equations. Hence, we use a non-approximated model of the grid.

We write the OPF formulation (Section 5.3) equivalently:⁸

$$\max_{\substack{\bar{S}_g, V_b, \varphi_b \\ \bar{E}_{\ell+}, \bar{E}_{\ell-}}} \sum_{g \in \mathcal{G}} W_g(\bar{S}_g) \quad \text{subject to:} \quad (5.48)$$

Feasibility constraints (5.45), (5.46), (5.47)

$$|\bar{I}_{\ell+}| \leq I_{\ell, \max} \quad \text{and} \quad |\bar{I}_{\ell-}| \leq I_{\ell, \max}, \quad \forall \ell \in \mathcal{L} \quad (5.49)$$

$$V_{\min} \leq V_b \leq V_{\max}, \quad \forall b \in \mathcal{B} \quad (5.50)$$

$$\bar{S}_g \in \mathcal{H}_g, \quad \forall g \in \mathcal{G} \quad (5.51)$$

As previously stated, the objective function is the sum of the welfare of the controllable devices W_g . In the above formulation, we denote by \mathcal{G} the set of controllable devices and by $\bar{S}_g = P_g + jQ_g$ the controllable injected power by device g , subject to the capability constraint (5.51). The set \mathcal{G} can contain both generators and consumers. However, for the sake of presentation clarity, we consider that \mathcal{G} contains uniquely PV generators. This is not a limiting assumption, as our results apply to any device with controllable power injections (including controllable loads). Non-controllable loads

⁸Unlike in Section 5.3, we consider without loss of generality that there are two types of connected devices: they either have controllable power injection \bar{S}_g or impose an overall fixed power injection $\bar{S}(b)$ in bus b .

do not appear in the objective function, that expresses the utility of PV generators (a concave increasing function $U(\cdot)$ of active power injection) and the losses of the power converter:

$$W_g(\bar{S}_g) = U_g(P_g) - \eta(P_g^2 + Q_g^2), \forall g \in \mathcal{G}. \quad (5.52)$$

We consider typical capability curves of PV power inverters:

$$\mathcal{H}_g = \{\bar{S}_g : |\bar{S}_g| \leq S_{g,\max}, |\arg(\bar{S}_g)| \leq \phi_{g,\max}\}. \quad (5.53)$$

In order to solve the problem (5.48)-(5.51), we convert the inequality constraints (5.49) to equality constraints by introducing slack variables $i_{\ell+}$ and $i_{\ell-}$ as follows:

$$|\bar{I}_{\ell+}| + i_{\ell+} = I_{\ell,\max} \text{ and } |\bar{I}_{\ell-}| + i_{\ell-} = I_{\ell,\max}, \forall \ell \in \mathcal{L} \quad (5.54)$$

$$i_{\ell+}, i_{\ell-} \geq 0, \quad \forall \ell \in \mathcal{L} \quad (5.55)$$

We denote by x the real vector of variables formed by the artificial control variables $(V_b, \varphi_b)_{b \in \mathcal{B}}$, $(i_{\ell+}, i_{\ell-})_{\ell \in \mathcal{L}}$, and the device controllable injected power $(P_g, Q_g)_{g \in \mathcal{G}}$.

Notice that all the equality constraints above, (5.45), (5.46), (5.47), and (5.54) can be summarized as $g(y) + Ax + b = 0$, where $g(\cdot)$ is a smooth non-convex function that can be derived from equations (5.41)-(5.46), and A is a positive definite matrix. Similarly, the inequality constraints, (5.50), (5.51), and (5.55), can be expressed as $h(x) \geq 0$, where $h(x)$ is a convex function that can be derived from equations (5.50), (5.55), and (5.53). We denote the objective by $f(x)$, where f is concave.

We can thus write our problem in the more compact form:

$$\max_{x,y} f(x) \quad (5.56)$$

$$\text{subject to } g(y) + Ax + b = 0 \quad (5.57)$$

$$h(x) \geq 0. \quad (5.58)$$

We write its augmented Lagrangian ([169, 170, 171]):

$$\begin{aligned} \mathcal{L}_\rho(x, y; \lambda) = & f(x) + \lambda'(g(y) + Ax + b) \\ & - \frac{\rho}{2} \|g(y) + Ax + b\|^2, \end{aligned} \quad (5.59)$$

where ρ is the weight of the quadratic penalty term added to the classic Lagrangian function, and λ is the vector of Lagrange multipliers associated with the equality constraints (5.57).

Our centralized iterative algorithm for solving the OPF is based on the method of multipliers ([169, §4.2]). This method was first introduced for solving iteratively non-linear equality constrained problems. It is shown to converge under more general

Algorithm 3 Centralized algorithm for the OPF (5.56)-(5.58)

- Set $k=0$ and initialize control variables x and y :
 $\bar{S}_g^0 = 0, \bar{E}_{\ell^+}^0 = \bar{E}_{\ell^-}^0 = 1, V_b^0 = 1, \varphi_b^0 = 0, i_{\ell^+}^0 = i_{\ell^-}^0 = 0$ (per-unit), Lagrange multipliers $\lambda^0 = 0$, increasing gain sequence $(\rho^k)_k, \rho^k \rightarrow \infty$.
 - 1: **repeat**
 - 2: Maximize the augmented Lagrangian for fixed $\lambda = \lambda^k$:

$$(x^{k+1}, y^{k+1}) = \arg \max_{x, y: h(x) \geq 0} L_{\rho^k}(x, y; \lambda^k). \quad (5.60)$$
 - 3: Update the Lagrange multipliers:

$$\lambda^{k+1} = \Pi_{[-\bar{\lambda}, \bar{\lambda}]} \left\{ \lambda^k + \rho^k \left[g(y^{k+1}) + Ax^{k+1} + b \right] \right\} \quad (5.61)$$
 - 4: $k \leftarrow k+1$
 - 5: **until** the maximum number of iterations has been reached **or** the change in the Lagrange multipliers between two consecutive iterations is less than a tolerance $\delta > 0$
-

conditions than dual ascent [209]. Algorithm 3 summarizes the proposed centralized algorithm, and Theorem 2 characterizes its convergence.

The main advantage of the method of multipliers is that there exists a finite value $\bar{\rho}$ such that the problem (5.60) is locally convex for all $\rho^k > \bar{\rho}$. Note also that the algorithm bounds the value of λ at each iteration. The next vector of multiplier estimates λ is obtained after a projection on the set $[-\bar{\lambda}, \bar{\lambda}]$ defined as $[-\bar{\lambda}_1, \bar{\lambda}_1] \times [-\bar{\lambda}_2, \bar{\lambda}_2] \times \dots$; the constant vector $\bar{\lambda}$ is chosen such that the sought optimal vector of Lagrange multipliers λ^* lies in $[-\bar{\lambda}, \bar{\lambda}]$ (see [211, §2.2.2]).

Theorem 2. *For smooth objective function $f \in \mathcal{C}^2$ and suitably chosen $\bar{\lambda}$ such that the optimal vector of Lagrange multipliers λ^* satisfies $\lambda^* \in [-\bar{\lambda}, \bar{\lambda}]$, Algorithm 3 converges to a local minimum of the nonlinear program (5.56)-(5.58).*

Proof. By [211, Proposition 1.23], our problem satisfies assumption (S) from [211, §2.2], since the equality constraint is a \mathcal{C}^2 function of y , and the objective function is chosen to be \mathcal{C}^2 . Proposition 2.7 from the same reference guarantees the desired convergence, if the iterates (x^k, y^k, λ^k) reach the set D from Proposition 2.4 of [211], i.e., if there exists a \bar{k} such that $(x^{\bar{k}}, y^{\bar{k}}, \lambda^{\bar{k}}) \in D$ (for all the following indices $k > \bar{k}$, the iterates stay in D , and convergence ensues). The existence of such a \bar{k} follows from the choice of the divergent increasing sequence of gains (ρ^k) and from the boundedness of the sequence (λ^k) . \square

Due to the quadratic terms in the expression of the augmented Lagrangian (5.59),

the optimization problem in (5.60) does not decouple across the network and, therefore, cannot be solved in a distributed manner. In the following section, we reformulate this problem in an equivalent way that leads to a distributed algorithm for its resolution.

5.6.2 Distributed Solution of the OPF Problem

We adopt a primal decomposition method [174] that gives an iterative algorithm for the minimization of the problem in *Step 2* of Algorithm 3. In (5.59) the line voltages $y = (\bar{E}_{\ell+}, \bar{E}_{\ell-})$ are “coupling” variables. If these variables are fixed to a specific value, then problem (5.60) decouples in smaller, easier (convex) problems, that can be solved by local agents.

Specifically, to solve (5.60) iteratively for fixed values of the Lagrange multiplier estimates $\hat{\lambda}$ and fixed gain $\hat{\rho}$ we take the following approach: At the n -th iteration, the value of the coupling variables $y^n = (\bar{E}_{\ell+}^n, \bar{E}_{\ell-}^n)$ is assumed fixed. The x variables, *i.e.*, the power set-points of the controllable devices (\bar{S}_g), the bus voltages (\bar{V}_b), and the slack variables $i_{\ell+}, i_{\ell-}$, are computed by solving the following constrained convex optimization problem:

$$x^{n+1} = \arg \max_{x: h(x) \geq 0} L_{\hat{\rho}}(x, y^n, \hat{\lambda}). \quad (5.62)$$

Next, the coupling variables y are updated as follows:

$$y^{n+1} = y^n + \alpha^n (\nabla_y L_{\hat{\rho}})(x^{n+1}, y^n, \hat{\lambda}), \quad (5.63)$$

where α^n is a positive step-size sequence of the gradient descent. The choice of the step-size is related to the topology of the network and the parameters of the lines (*i.e.*, the network admittance matrix). For example, a large constant step-size might not allow the algorithm to converge, whereas a small constant step-size could cause slow convergence⁹.

The algorithm stops when the norm of the update in the y variables is less than some small positive tolerance ε , *i.e.*, when $\|\nabla_y L_{\hat{\rho}}(x^{n+1}, y^n, \hat{\lambda})\| \leq \varepsilon$.

Theorem 3. *The algorithm (5.62)-(5.63) with tolerance ε in the stopping criterion converges to a vicinity $\mathcal{B}((x^*, y^*), \delta)$ of a local optimum (x^*, y^*) of problem (5.60). If (5.60) is strongly locally convex in y in a vicinity of (x^*, y^*) , then $\delta = \Theta(\varepsilon^2)$.*

Proof. (Sketch) Denote $v(y) = \max_{x: h(x) \geq 0} L_{\hat{\rho}}(x, y, \hat{\lambda})$ and $x^*(y)$ the value of x that achieves this maximum (5.62). Theorem 2.1 of [212] says that the optimum $(x^*(y^*), y^*)$

⁹In order to properly tune this parameter, a dedicated off-line study can be performed before deployment of the proposed algorithm.

of $\max_y v(y)$ coincides with the one of (5.60). Moreover, a δ -optimal solution $(x^*(y_\delta), y_\delta)$ of $\max_y v(y)$ (that is, $v(y_\delta) \geq v(y^*) - \delta$) is also δ -optimal for (5.60).

We now show that it holds that $\nabla_y v(y) = (\nabla_y L_{\hat{\rho}})(x^*(y), y, \hat{\lambda})$, or equivalently, $\frac{Dx^*(y)}{Dy}(\nabla_x L_{\hat{\rho}})(x^*(\bar{y}), \bar{y}, \hat{\lambda}) = 0$. If we can show this, then the algorithm (5.62)-(5.63) is equivalent to a gradient ascent in y on $v(y)$. It is easy to show that the function $v(y)$ is “smooth” (C^2). By the strong local convexity around (x^*, y^*) of the augmented Lagrangian, [169, Exercise 1.2.10] allows us to conclude that $\delta = \Theta(\varepsilon^2)$.

Note that problem (5.62) is convex. Consider the optimal multipliers μ^* corresponding to the constraints $h(x) \geq 0$. They satisfy the KKT conditions:

$$\begin{aligned} (\nabla_x L_{\hat{\rho}})(x^*(y), y, \hat{\lambda}) &= \sum_i \mu_i^*(y) \nabla_x h_i(x^*(y)) \\ \mu_i^*(y) h_i(x^*(y)) &= 0; \quad \mu_i^* \geq 0. \end{aligned}$$

Define the following functions: $\psi_i(y) := h_i(x^*(y))$. Since $x^*(y)$ is always feasible, it means that $\psi_i(y) \geq 0$. Consider the set of indices $\mathcal{I}_0(y) := \{i : h_i(x^*(y)) = 0\}$. Take some $i \in \mathcal{I}_0(y)$. In this case the function $\psi_i(y)$ has an extremal point in y , which implies that $\nabla_y \psi_i(y) = 0$, or again that $\frac{Dx^*(y)}{Dy} \nabla_x h_i(x^*(y)) = 0$. For all $i \notin \mathcal{I}_0(y)$, by KKT we have $\mu_i^*(y) = 0$. By the above arguments,

$$\begin{aligned} &\frac{Dx^*(y)}{Dy}(\nabla_x L_{\hat{\rho}})(x^*(y), y, \hat{\lambda}) \\ &= \sum_i \mu_i^*(y) \frac{Dx^*(y)}{Dy} \nabla_x h_i(x^*(y)) = 0. \end{aligned}$$

□

Thanks to its separability property, problem (5.62) can be solved in a distributed manner. Bus agents can be responsible for updating the power set-points of the controllable devices (\bar{S}_g) that are connected to them, as well as their voltages (\bar{V}_b) in parallel, and lines can be responsible for updating the slack variables (i_{ℓ^+}, i_{ℓ^-}). Specifically, the power set-points (\bar{S}_g^{n+1}) of devices in bus b are obtained by solving the following convex problem:

$$\begin{aligned} (\bar{S}_g^{n+1}) &= \arg \max_{\bar{S}_g \in \mathcal{H}_g} \sum_{g \in b} W_g(\bar{S}_g) \\ &\quad - \frac{\hat{\rho}}{2} \left| \sum_{g \in b} \bar{S}_g + \bar{S}(b) + \sum_{\beta(\ell^+)=b} \bar{S}_{\ell^+}^n + \sum_{\beta(\ell^-)=b} \bar{S}_{\ell^-}^n - \frac{\hat{\lambda}_b}{\hat{\rho}} \right|^2, \end{aligned}$$

where $\hat{\lambda}_b$ is the given multiplier corresponding to the constraint (5.47) of bus b . The other problems (for the other x variables) have simpler expressions that we do not reproduce for brevity sake.

Similarly, (5.63) can be decomposed across the different network lines: line-agents

Algorithm 4 Distributed algorithm for the OPF (5.56)-(5.58)

- Set $k=0$ and initialize control variables x and y :
 $\bar{S}_g^0 = 0, \bar{E}_{\ell^+}^0 = \bar{E}_{\ell^-}^0 = 1, V_b^0 = 1, \varphi_b^0 = 0, i_{\ell^+}^0 = i_{\ell^-}^0 = 0$ (per-unit), Lagrange multipliers $\lambda^0 = 0$, increasing diverging gain sequence $(\rho^k)_k, \rho^k \rightarrow \infty$, decreasing tolerance sequence $(\varepsilon^k \geq 0)_k, \varepsilon^k \rightarrow 0$.
- 1: **repeat**
 - 2: $n \leftarrow 0; \tilde{x}^0 \leftarrow x^k; \tilde{y}^0 \leftarrow y^k$
 - 3: **repeat**
 - 4: $\tilde{x}^{n+1} = \arg \max_{x: h(x) \geq 0} L_{\rho^k}(x, \tilde{y}^n, \lambda^k)$
 - 5: $\tilde{y}^{n+1} = \tilde{y}^n + \alpha^n (\nabla_y L_{\rho^k})(\tilde{x}^{n+1}, \tilde{y}^n, \lambda^k)$
 - 6: $n \leftarrow n+1$
 - 7: **until** $\|\nabla_y L_{\rho^k}(\tilde{x}^{n+1}, \tilde{y}^n, \lambda^k)\| \leq \varepsilon^k$
 - 8: $x^{k+1} \leftarrow \tilde{x}^{n+1}; y^{k+1} \leftarrow \tilde{y}^{n+1}$
 - 9: $\lambda^{k+1} = \Pi_{[-\bar{\lambda}, \bar{\lambda}]} \{ \lambda^k + \rho^k [g(y^{k+1}) + Ax^{k+1} + b] \}$
 - 10: $k \leftarrow k+1$
 - 11: **until** the maximum number of iterations has been reached **or** the change in the Lagrange multipliers between two consecutive iterations is less than a tolerance $\delta > 0$
-

can update the voltages at their two ends in parallel. In terms of required information, each bus agent needs to know only the voltage values of the lines that are incident to it, the constraints of the devices, and the state of the loads that are connected to it. Finally, in order to compute the partial derivatives of (5.63) with respect to its voltages, each line requires solely the information of the power balance and the voltage values of its two adjacent buses. The actual implementation of the distributed synchronous OPF algorithm is summarized below in Algorithm 4.

Theorem 4. *For smooth objective function $f \in \mathcal{C}^2$ and suitably chosen $\bar{\lambda}$ such that the optimal vector of Lagrange multipliers λ^* satisfies $\lambda^* \in [-\bar{\lambda}, \bar{\lambda}]$, Algorithm 4 converges to a local minimum of the nonlinear program (5.56).*

Proof. The proof is similar to the one of Theorem 2. It uses Proposition 2.16 of [211] for convergence, which only requires at each iteration a δ^k -optimal solution for (5.60) with $\delta^k \rightarrow 0$. By Theorem 3 we can conclude. \square

In a realistic setting, in order to take full advantage of the distributed formulation of the OPF algorithm, as described above and to avoid the overhead cost of coordination between agents, the updates should be performed in an asynchronous fashion. Contrary to ADMM-based algorithms, which require a synchronized implementation of the updates, the proposed algorithm can be implemented in an asynchronous manner. In this direction, we assume that each of the bus and line agents has its own two local poisson clocks with different rates. The clock with the lower rate ($C1$) triggers

5.7. Performance Evaluation of the Centralized OPF Algorithm

the multiplier update (5.61) and the clock with the higher rate ($C2$) triggers the events described in steps (5.62)-(5.63).

In detail, all the control variables and the Lagrange multipliers are first initialized. Then, every time the $C2$ clock of a bus ticks, this bus performs local update operations by using the most recent stored values for the voltages of its incident lines and for the associated Lagrange multipliers. Once the bus updates its power and voltage values, it informs the incident lines of the changes. Similarly, when the $C2$ clock of a line ticks, the line agent updates the variables $(i_{\ell+}, i_{\ell-})$ by taking into account the most recent values of the line current flows and associated Lagrange multipliers. In addition to this update, the updates of the voltages of its two end-points are triggered. In order to compute the new values, the line uses the most recent stored values for the adjacent buses' powers and voltages, and once the updates are completed the line communicates this information to its neighboring buses. Now, when the $C1$ clock of a bus or a line ticks, then the corresponding agent updates the Lagrange multipliers (5.61). It is worth noting, that we no longer have a serial implementation of the various updates like the ones presented in Algorithm 4. On the contrary, the different rates of the clocks are chosen in such a way to ensure that, on average, a sufficient number of the updates occurs before an update of the corresponding Lagrange multiplier takes place.

5.7 Performance Evaluation of the Centralized OPF Algorithm

In this section, we investigate the performances and convergence properties of the centralized OPF Algorithm 3 in several different scenarios. In particular, we consider the cases presented in Sections 5.4 and 5.5, where the BFM convexification leads to an incorrect solution of the OPF problem and ADMM fails to converge to a solution. Additionally, we investigate the performances of the proposed centralized algorithm under different initial conditions of the electrical-network state. In order to do so, we consider the same 4-bus test network as in Figure 5.3. We assume a first test case where the controllable device connected to bus 4 is a generator, whereas controllable loads are connected to buses 2 and 3. The network characteristics, the base values, the capability limits of the controllable resources, and the voltage and ampacity limits are given in Figure 5.3 and Table 5.2. In what follows, the objective function accounts for the minimization of the network losses, as well as for the utility of the generating units, namely:

$$\min_{\bar{S}_g, \bar{S}_\ell, V_b, \varphi_b, |\bar{I}_\ell|} - \sum_{g \in \mathcal{G}} \text{Re}(\bar{S}_g) + \sum_{\ell \in \mathcal{L}} \text{Re}(\bar{Y}_\ell) |\bar{I}_\ell|^2 \quad (5.64)$$

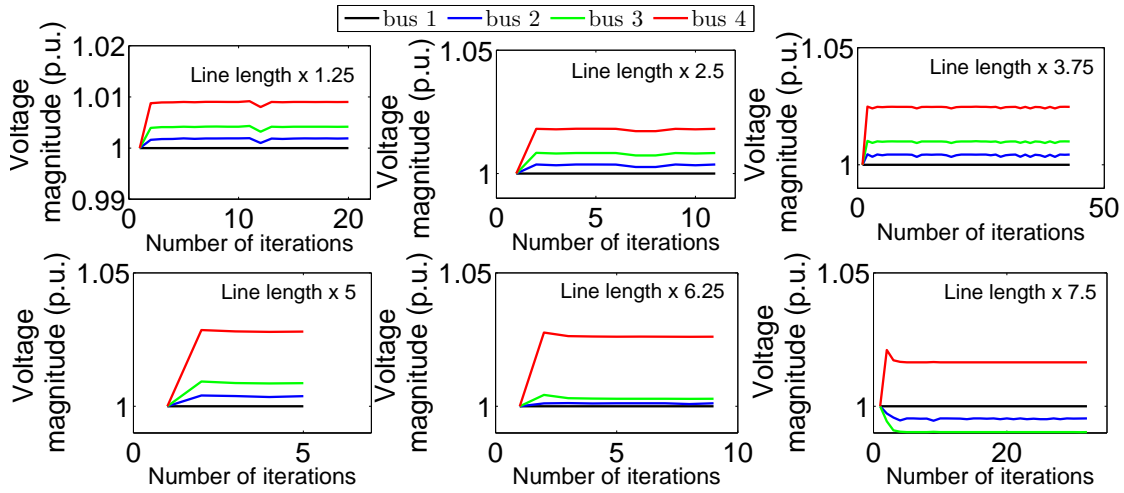


Figure 5.11: Evolution of the magnitude of network voltages for various line lengths.

5.7.1 Effect of the Line Length, Network Rated Value and Network State on the Convergence of the Centralized OPF Algorithm

In order to compare the performances of the proposed algorithm with the OPF algorithm proposed in [35, 36], we solve the OPF problem for various line lengths and network voltage rated values as in Section 5.4.2. In particular, we assume that the line lengths are uniformly multiplied by a factor in the range $[1.25 - 7.5]$ (while keeping the network voltage rated value to its nominal value) and the network voltage rated value varies in the range $[15 - 40]kV$ (while keeping the line lengths to their nominal values). The evolution of the bus voltages, the line-current flows, as well as the active and reactive powers, are shown in Figures 5.11-5.16. It is worth noting that in all the cases the proposed algorithm converges in few iterations. Furthermore, we observe from Figure 5.12 and Figure 5.15 that the line-current flows satisfy the line ampacity limit, once the algorithm has converged, in all cases. In particular, in Figure 5.12 it is worth observing that as the line length increases the receiving and sending-end current flows of the same line become significantly different. The behavior of the current flows as the voltage rated value increases is similar (Figure 5.15). This effect is due to the increasing contribution of the current flow toward the shunt elements of the lines. In fact, we show, in Figures 5.17 and 5.18, the amount of reactive power produced by the shunt elements of the lines for the various values of the line lengths and the network voltage rated values. We observe that as the line length increases or the rated value of the voltage increases the reactive power produced by the shunt elements of the line increases as well.

We investigate, in addition to the effect of the line lengths and the network voltage rated value, the performance of the proposed algorithm under a different network operating point. To this end, we consider a second test-case where the controllable device connected to bus 4 is a controllable load and generators are connected to buses 2 and 3. In this respect, we consider an extra term in the objective function, which

5.7. Performance Evaluation of the Centralized OPF Algorithm

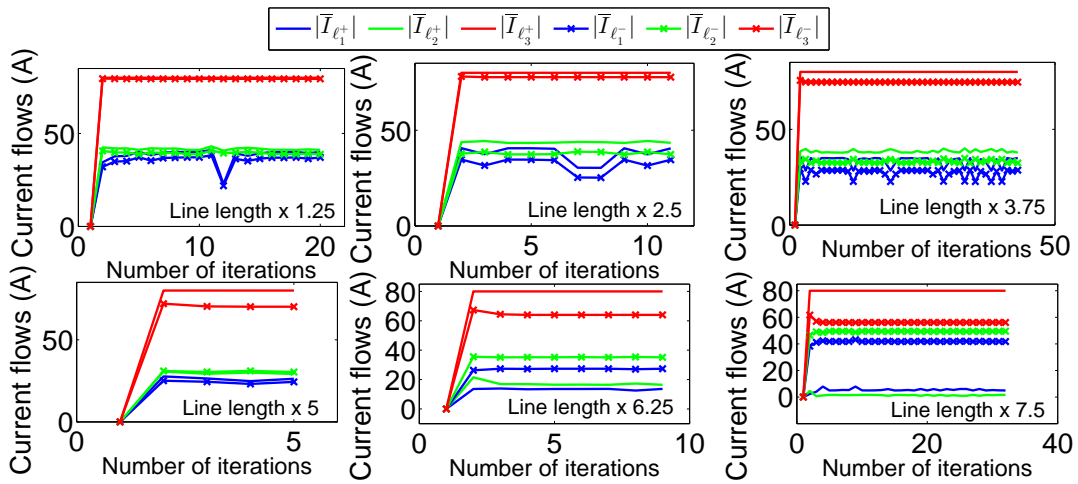


Figure 5.12: Evolution of the line current flows for various line lengths.

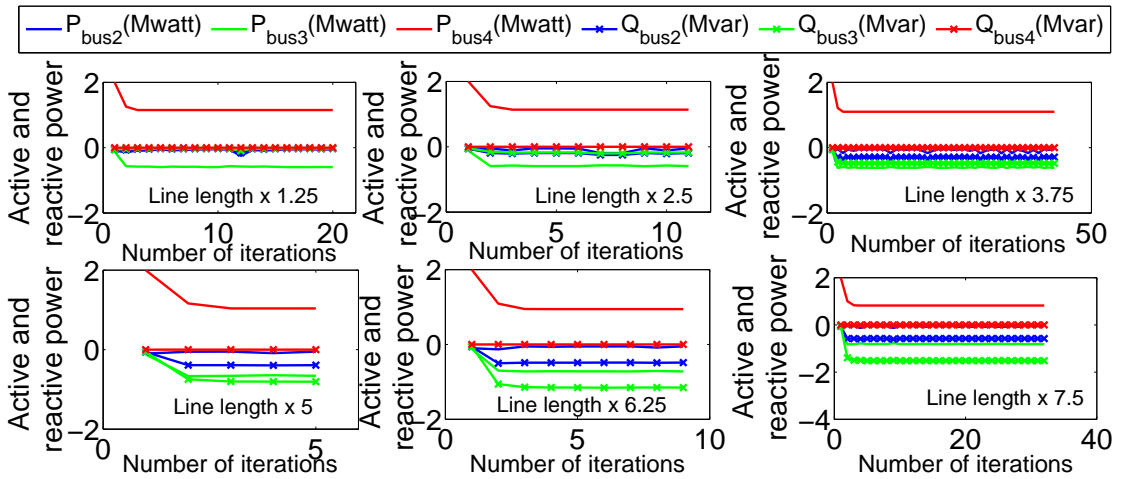


Figure 5.13: Evolution of the active and reactive power of the controllable devices for various line lengths.

represents the utility associated with the controllable load and is given by $(P_L - P_o)^2$, where P_o represents a constant amount of load that has to be served. The capability limits of the controllable resources are shown in Table 5.8. The convergence of the voltages, current flows, as well as active and reactive powers are shown in Figure 5.19. For the sake of brevity, we only show the evolution of the active and reactive power of the controllable load of bus 4, as the controllable generators are small and reach their maximum value upon convergence.

5.7.2 Performance Evaluation of the Proposed Algorithm in the Presence of Shunt Capacitors in the Network

In what follows, we consider the same network adopted in the previous section and a case where each network bus, apart from the slack, has a load and a generator con-

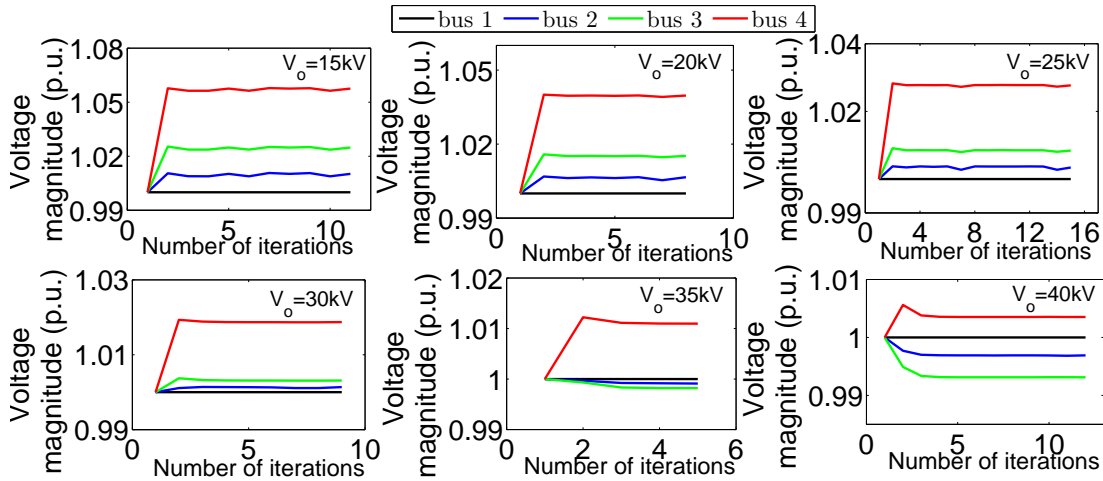


Figure 5.14: Evolution of the magnitude of network voltages for various values of the network rated voltage.

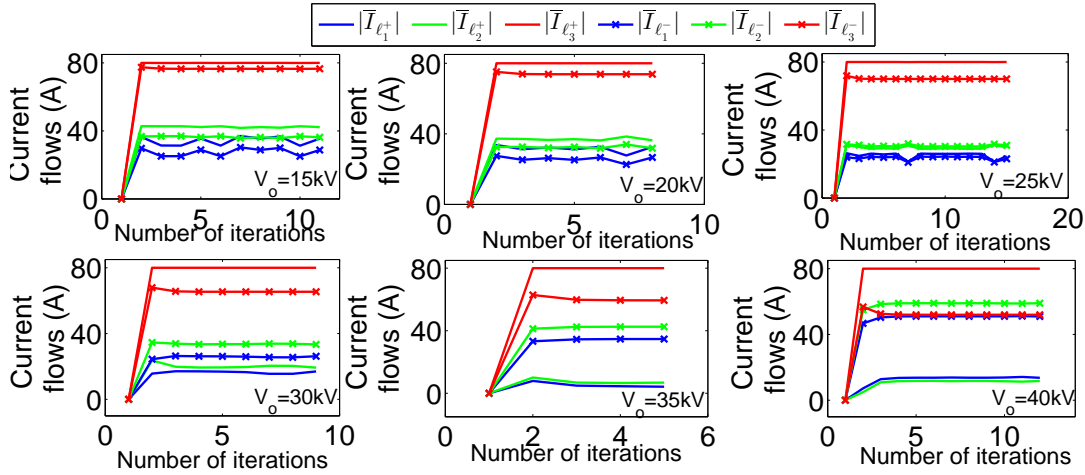


Figure 5.15: Evolution of the line current flows for various values of the network rated voltage.

nected to it. The demand in the network is assumed to be non-controllable, whereas the generators are assumed to be distributed solar panels with typical PV-type capability constraints given by (5.53). For this scenario, the capability limits and the values of loads and generation are shown in Table 5.9. In addition to the loads and generation, we consider that a shunt capacitor is connected to bus 2. In order to model this shunt capacitor, we consider that it is part of the first line. In particular, we consider that the shunt capacitance on the sending end of the π -model of the line that connects buses 1 and 2 is modified accordingly, to account for the shunt capacitor. For this particular test case, it is worth noting that ADMM exhibits oscillations and fails to converge to a solution (see Figures 5.7-5.10).

The results for this specific test-case, for the voltage magnitudes and the active and reactive power of the buses, are shown in Figure 5.20. It is worth observing that

5.7. Performance Evaluation of the Centralized OPF Algorithm

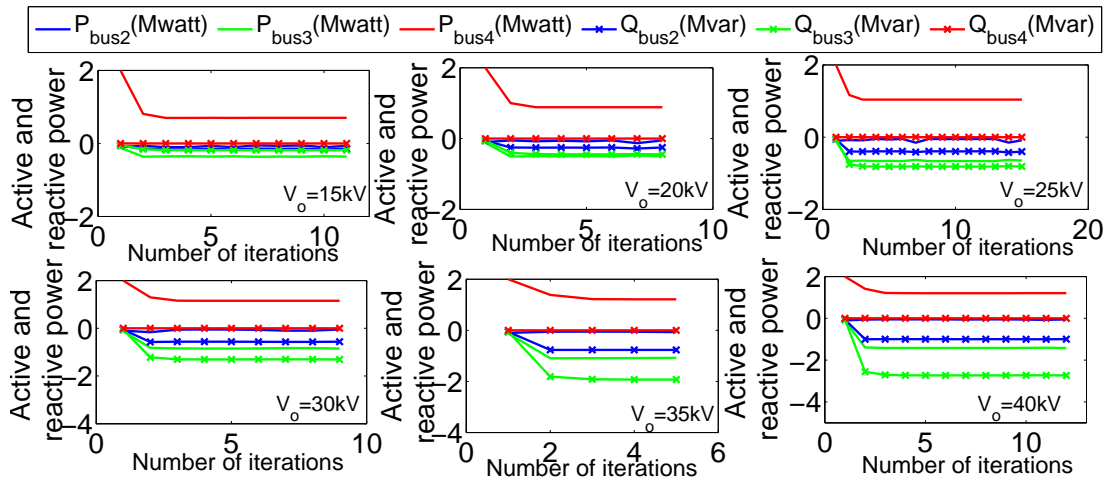


Figure 5.16: Evolution of the magnitude of active and reactive power of the controllable devices for various values of the network rated voltage.

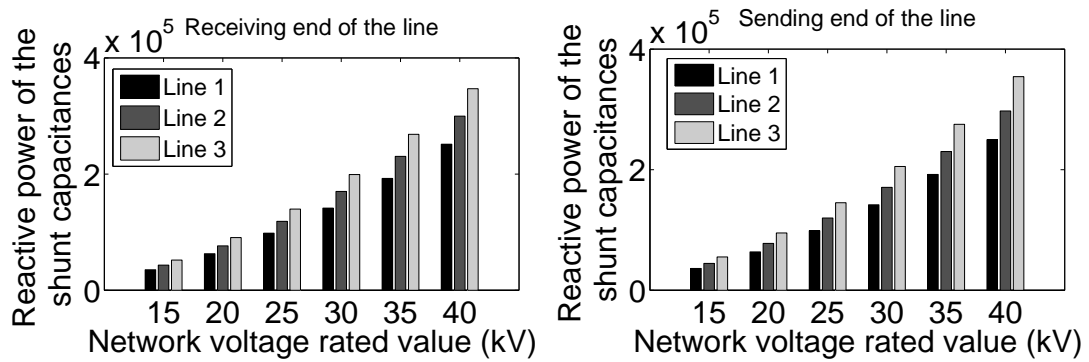


Figure 5.17: Reactive power produced by the shunt elements of the lines for various values of the network voltage rated value.

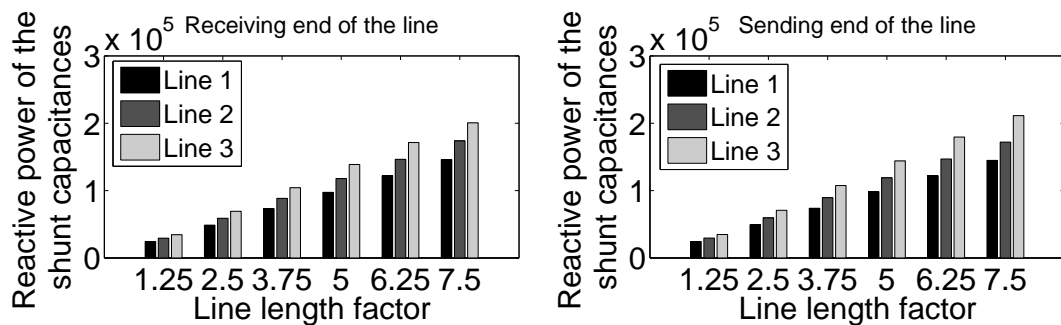


Figure 5.18: Reactive power produced by the shunt elements of the lines for various line lengths.

the proposed algorithm converges to a solution within a few tens of iterations; which is contrary to the ADMM-based solution of the OPF problem.

Table 5.8: Parameters of the test network used for the investigation of the performance of the proposed OPF algorithm under a different operating point

Parameter	value
$[P_{gmin}, P_{gmax}]$ (bus 2) (MW)	[0, 0.01]
$[P_{gmin}, P_{gmax}]$ (bus 3) (MW)	[0, 0.012]
(P_{cmin}, Q_{cmin}) (MW,Mvar) (bus 4)	0.3, 0.15
P_o (MW) (bus 4)	1

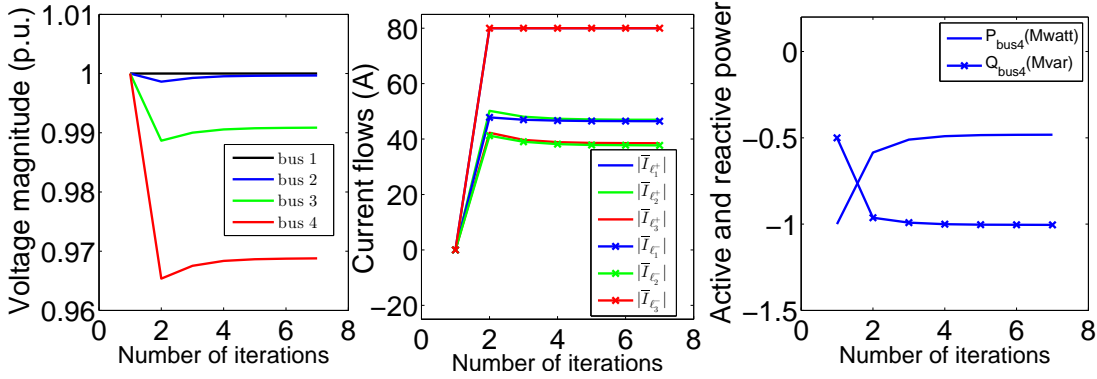


Figure 5.19: Evolution of the magnitude of network voltages, current flows, as well as active and reactive power of the controllable load at bus 4 for the case of low generation and high load in the network.

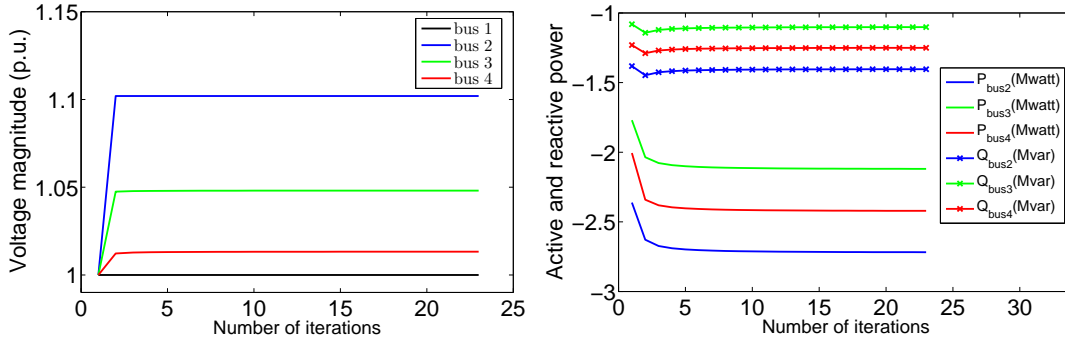


Figure 5.20: Evolution of the active and reactive power, as well as the voltages of the buses when a shunt capacitor is connected to bus 2.

5.7.3 Performance Evaluation of the Proposed Algorithm under Different Initial Conditions of the Network State

Finally, we investigate the performances of the proposed algorithm under different initial conditions of the network state variables. In order to do so, we initialize the magnitude of the control variables $\bar{E}_{\ell+}^0, \bar{E}_{\ell-}^0, V_b^0$ in Algorithm 3 in the range $[0.9, 1.1]$ and their angle in the range $[-\pi/6, \pi/6]$, totaling 121 different cases. For each combination, we solve the centralized OPF problem for the same network adopted in Figure 5.3. In all the cases the algorithm converges to the same solution within a few tens of iterations.

5.8. Performance Evaluation of the Proposed Distributed Asynchronous OPF Algorithm

Table 5.9: Parameters of the test network used for the evaluation of Algorithm 1 in the presence of shunt capacitors in the network

Parameter	Value
Generators' power, $ \bar{S}_{i_{gmax}} , i = 2, 3, 4$ (MVA)	0.40, 0.39, 0.46
Generators' power factor, $\cos\phi_{i_g}, i = 2, 3, 4$	0.9
Loads' active power, $P_{i_c}, i = 2, 3, 4$ (MW)	2.76, 2.16, 2.46
Loads' reactive power, $Q_{i_c}, i = 2, 3, 4$ (MW)	1.38, 1.08, 1.23
Shunt capacitor (bus 2)(uF)	859
Penalty term gain, ρ	10^4
Tolerance and maximum number of iterations	$10^{-4}, 10^4$
$[V_{min}, V_{max}]$ (p.u)	$[0.9, 1.1]$

Table 5.10: Number of iterations for the solution of the OPF problem (Algorithm 3)

	Mean number of iterations	95-th Percentile
Algorithm 3	18.21	46.45

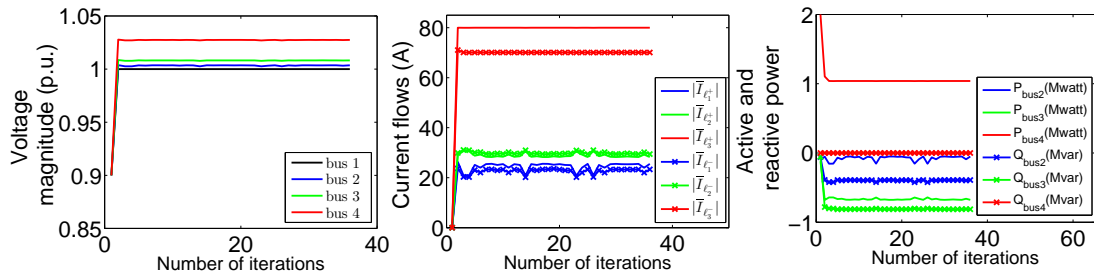


Figure 5.21: Evolution of the magnitude of network voltages, line current flows and active and reactive power of the controllable devices when the initial voltage magnitudes are set to 0.9 and the voltage angles to $-\pi/6$.

In Table 5.10, the mean value of the number of iterations, as well as the 95-th percentile are shown. For the sake of brevity, we show in Figures 5.21-5.22 the convergence results for the voltage, as well as for the current flows and the active and reactive power profiles for the two extreme cases, specifically when the voltage magnitude is set to 0.9 (1.1) and the voltage angle is set to $-\pi/6$ ($\pi/6$).

5.8 Performance Evaluation of the Proposed Distributed Asynchronous OPF Algorithm

In this section, we assess the performance of the proposed algorithm with respect to a realistic grid represented by a modified IEEE 13-nodes test feeder ([109]). The modifications are (i) balanced lines, (ii) inclusion of secondary substations where

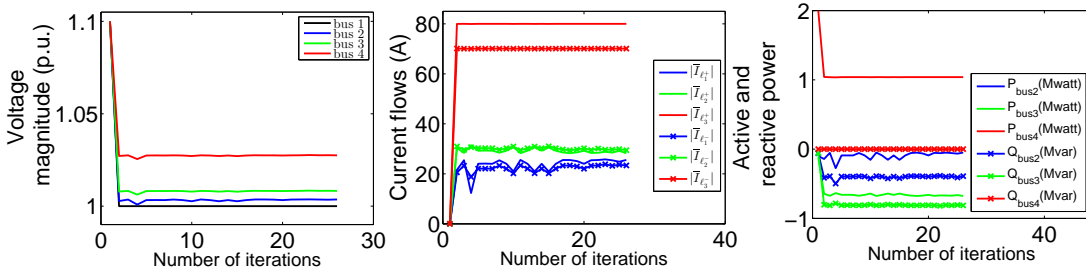


Figure 5.22: Evolution of the magnitude of network voltages, line current flows and active and reactive power of the controllable devices when the initial voltage magnitudes are set to 1.1 and the voltage angles to $\pi/6$.

voltage independent PQ-injections are placed, and (iii) lines ten times longer. We use this benchmark to assess the behavior of the proposed distributed asynchronous OPF

Table 5.11: Capability limits and values of loads and generation for the evaluation of Algorithm 4

Bus	$S_{g_{max}}$ (MVA)	$P_c(MW)/$ $Q_c(Mvar)$	Bus	$S_{g_{max}}$ (MVA)	$P_c(MW)/$ $Q_c(Mvar)$
2	0.0437	0.0025 / 0.0011	8	0.0347	0.0031 / 0.0014
3	0.0480	0.0029 / 0.0012	9	0.0403	0.0031 / 0.0013
4	0.0506	0.0032 / 0.0013	10	0.0373	0.0031 / 0.0013
5	0.0367	0.0029 / 0.0012	11	0.0482	0.0024 / 0.0010
6	0.0443	0.0029 / 0.0012	12	0.0399	0.0030 / 0.0013
7	0.0426	0.0025 / 0.0010	13	0.0436	0.0029 / 0.0012

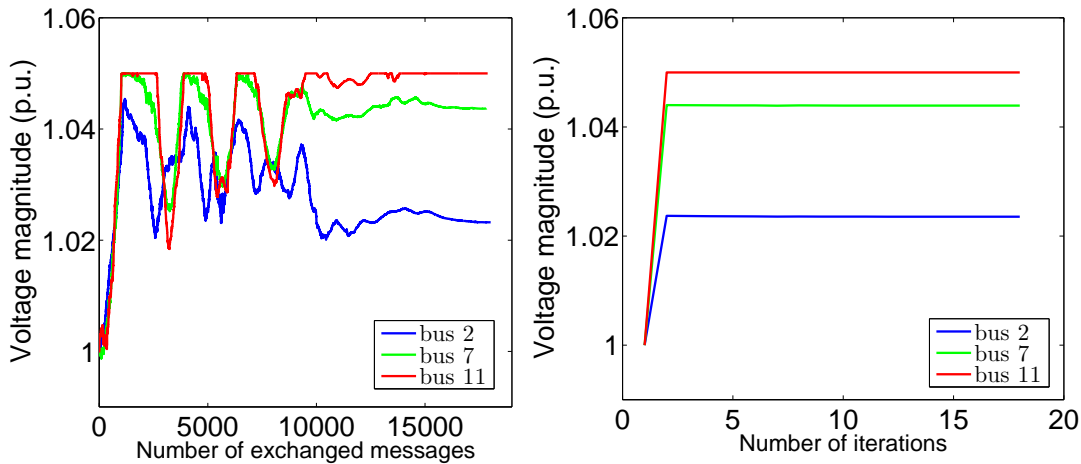


Figure 5.23: Evolution of the voltage magnitude for the distributed asynchronous algorithm as a function of the number of messages exchanged (left) and for Algorithm 1 as a function of the number of iterations (right).

5.8. Performance Evaluation of the Proposed Distributed Asynchronous OPF Algorithm

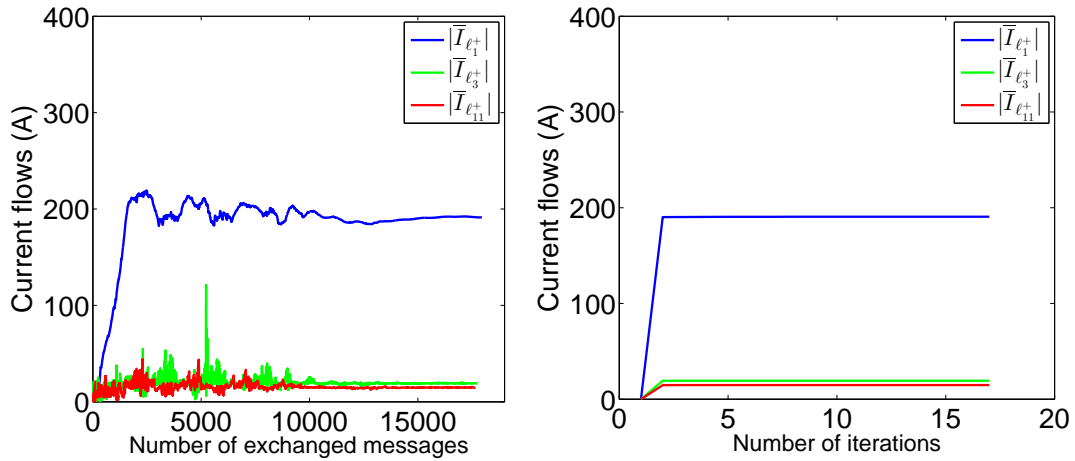


Figure 5.24: Evolution of the current flows for the distributed asynchronous algorithm as a function of the number of messages exchanged (left) and for Algorithm 1 as a function of the number of iterations (right).

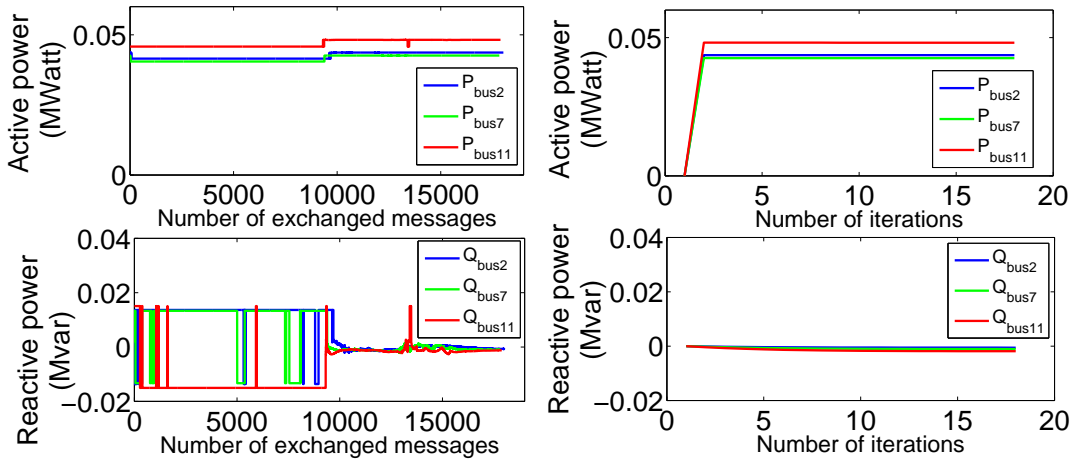


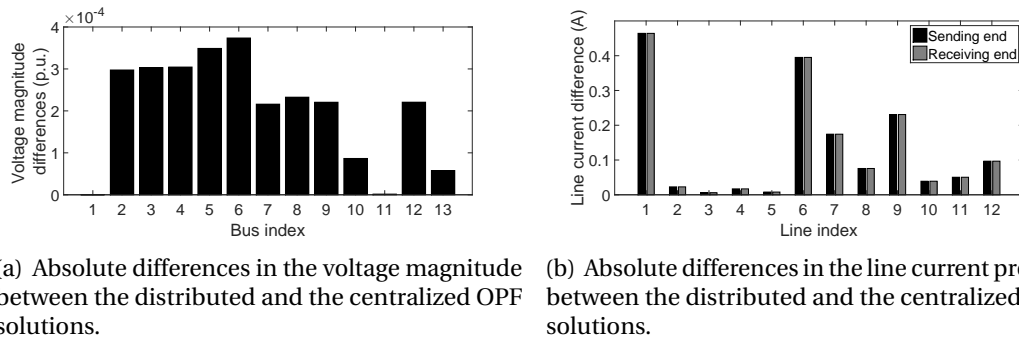
Figure 5.25: Evolution of the active and reactive power for the distributed asynchronous algorithm as a function of the number of messages exchanged (left) and for Algorithm 1 as a function of the number of iterations (right).

algorithm. Also, we compare the solution and convergence of the distributed version of the algorithm to the centralized one.

We consider a test case where each network bus, apart from the slack bus, has a load and a generator connected to it. The demand in the network is assumed to be non-controllable, whereas the generators are assumed to be distributed solar panels with typical PV-type capability constraints. For this test case, the capability limits and the values of loads and generation are shown in Table 5.11.

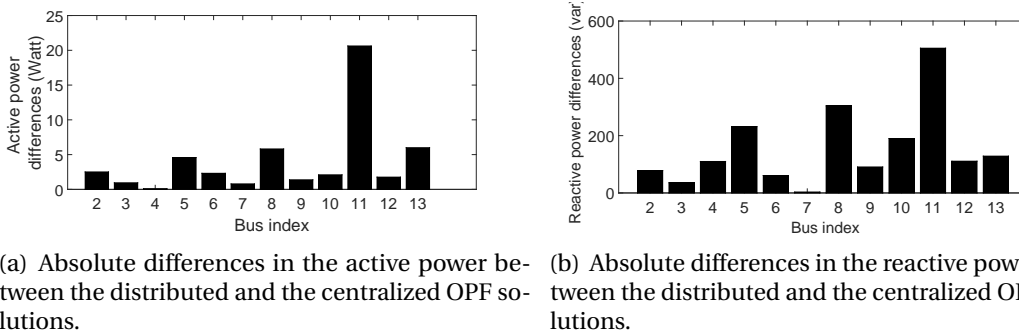
We solve the OPF problem in (5.48)-(5.53) using Algorithm 3, as well as the asynchronous implementation of Algorithm 4. The results are shown in Figures 5.23- 5.25. For the sake of brevity, we plot only the evolution of the magnitudes of the minimum

Chapter 5. Centralized and Distributed AC OPF Algorithms



(a) Absolute differences in the voltage magnitude between the distributed and the centralized OPF solutions. (b) Absolute differences in the line current profiles between the distributed and the centralized OPF solutions.

Figure 5.26: Difference in the solutions of the centralized and distributed OPF solutions for the network voltage and current profiles.



(a) Absolute differences in the active power between the distributed and the centralized OPF solutions. (b) Absolute differences in the reactive power between the distributed and the centralized OPF solutions.

Figure 5.27: Difference in the solutions of the centralized and distributed OPF solutions for the active and reactive power of the controllable resources.

voltage, the maximum voltage and the median value of the voltage. We plot also the evolution of the minimum, maximum and median values of the current flows on the receiving-end of the line and the evolution of the active and reactive powers. It is worth observing that Algorithm 3 converges to the optimal solution within few iterations and also that the distributed asynchronous implementation of Algorithm 4 converges to the same solution as its centralized counterpart. To support this claim, we show in Figures 5.26-5.27 the absolute differences in the solutions of the centralized and distributed OPF algorithms in terms of voltage magnitude, line currents, as well as active and reactive power injections of the controllable resources.

5.9 Comparison of the OPF Algorithms and the Linearized Control Algorithms

In this section we compare the performances of the proposed centralized OPF algorithm, presented in this chapter, to the linearized controls, presented in the previous chapters, that rely on state estimation and computation of sensitivity coefficients.

5.9. Comparison of the OPF Algorithms and the Linearized Control Algorithms

Table 5.12: Capability limits and values of loads and generation for the evaluation of Algorithm 4

Bus	$S_{g_{max}}$ (MVA)	$P_c(MW)/$ $Q_c(Mvar)$	Bus	$S_{g_{max}}$ (MVA)	$P_c(MW)/$ $Q_c(Mvar)$
2	0.0675	0.0051 / 0.0022	8	0.0537	0.0065 / 0.0027
3	0.0742	0.0059 / 0.0025	9	0.0624	0.0062 / 0.0026
4	0.0783	0.0063 / 0.0027	10	0.0577	0.0061 / 0.0026
5	0.0568	0.0059 / 0.0025	11	0.0746	0.0049 / 0.0021
6	0.0686	0.0058 / 0.0025	12	0.0617	0.0059 / 0.0025
7	0.0659	0.0050 / 0.0021	13	0.0675	0.0058 / 0.0025

To this end, first, we translate the control problem described in Section 5.6.1 into its linearized counterpart as follows:

$$\min_{\bar{S}_g} \sum_{g \in \mathcal{G}} U_g(P_g) - \eta(P_g^2 + Q_g^2) \quad (5.65)$$

$$\text{subject to: } V_{min} \leq |\bar{V}_b| + (\mathbf{K}_{\mathbf{P}_g, \mathbf{Q}_g} \Delta(\mathbf{P}_g, \mathbf{Q}_g))_b \leq V_{max}, \quad \forall b \in \mathcal{B} \quad (5.66)$$

$$|\bar{I}_{\ell^+} + (\mathbf{H}_{\mathbf{P}_g, \mathbf{Q}_g} \Delta(\mathbf{P}_g, \mathbf{Q}_g))_{\ell^+}| \leq I_{\ell_{max}}, \quad \forall \ell \in \mathcal{L} \quad (5.67)$$

$$|\bar{I}_{\ell^-} + (\mathbf{H}_{\mathbf{P}_g, \mathbf{Q}_g} \Delta(\mathbf{P}_g, \mathbf{Q}_g))_{\ell^-}| \leq I_{\ell_{max}}, \quad \forall \ell \in \mathcal{L} \quad (5.68)$$

$$\bar{S}_g \in \mathcal{H}_g, \quad \forall g \in \mathcal{G} \quad \text{and} \quad \bar{S}_c \in \mathcal{H}_c, \quad \forall c \in \mathcal{C} \quad (5.69)$$

where $\mathbf{K}_{\mathbf{P}_g, \mathbf{Q}_g}$, $\mathbf{H}_{\mathbf{P}_g, \mathbf{Q}_g}$ are the voltage and current sensitivity coefficients with respect to the buses where controllable resources are connected¹⁰. Using this formulation the sole control variables are the nodal power injections of the PVs.

In what follows, we compare the solutions, the convergence and the timing performances of the non-convex OPF and of the linearized problem in (5.65)-(5.69).

For the performance assessment of the control algorithms we consider the IEEE 13-nodes test feeder modified with balanced lines, ten times longer to render the network weaker. We consider a test case where each network bus, apart from the slack bus, has a load and a generator connected to it. As in the previous section, the demand in the network is assumed to be non-controllable, whereas the generators are assumed to be distributed PVs. For this test case, the capability limits and the values of loads and generation are shown in Table 5.12¹¹.

The voltage limits are set to $\pm 5\%$ of the network rated value and the ampacity limits are set to 300A for the network lines. The uncontrolled voltage and line currents profiles are shown in Figures 5.28. As it can be observed, the base case voltage is above the allowed limit of 1.05p.u., whereas the current flows are within the ampacity limits. We

¹⁰Note that the shunt elements of the lines are included in the current sensitivities computation.

¹¹Note that these values are inferred from real measurements.

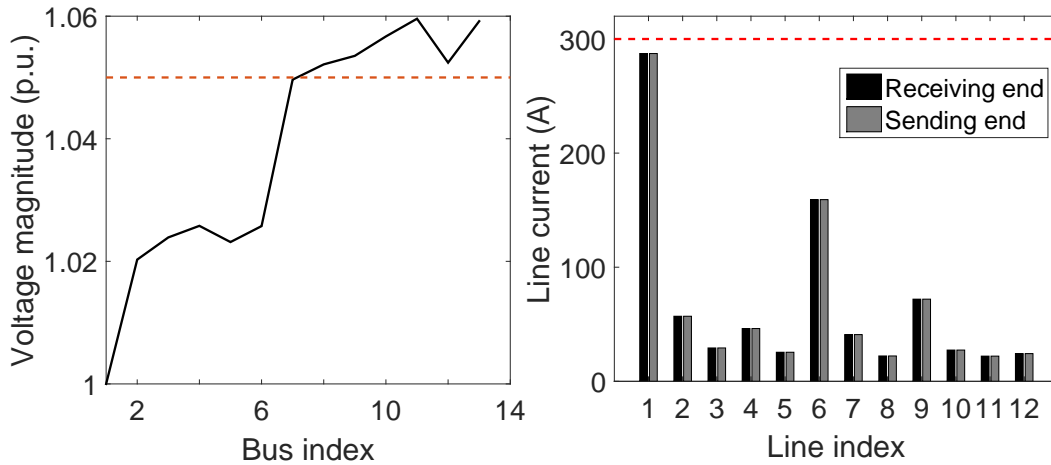


Figure 5.28: Uncontrolled network voltage profile and line current flows.

solve both the OPF problem using the centralized algorithm and its linearized version and we compare the obtained solutions. Figures 5.29-5.33 show the optimal solutions, as well as the resulting differences in the optimal solutions of the two algorithms in terms of voltage magnitude profiles, line current flows and nodal active and reactive power injections. Both algorithms are able to find an optimal solution that satisfies the voltage constraints and, in fact, the resulting optimal solutions are almost identical. In terms of optimality of the solution, the difference in the objective function value is also negligible. In particular, the OPF solution has a smaller objective value than the linearized problem but the actual difference is in the order of $3.04E - 5$. The last aspect that we compare is the time required for the solution of the optimal control problem with the two algorithms. To this end, we run each algorithm 100 times and store the CPU time required for the solution of each optimization problem. In Table 5.13 the mean value of the CPU time required for each algorithm is shown, as well as the corresponding 95-th percentile. As expected, the OPF algorithm is computationally heavier.

Table 5.13: Comparison of CPU time required to solve the centralized OPF problem and its linearized counterpart

	Mean (sec)	95-th Percentile (sec)
Centralized OPF	71.260	176.467
Linearized Algorithm	0.143	0.196

5.10 Conclusions

In this chapter we investigate the limits of the branch flow convexification proposed by Farivar-Low in [35, 36] and of the ADMM-based solution of the OPF problem. In

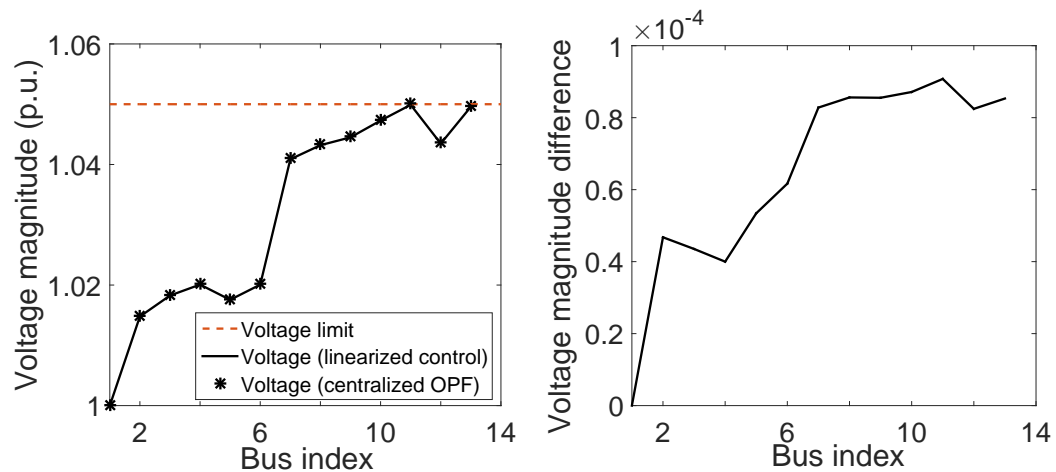


Figure 5.29: Optimal voltage profile of the centralized OPF algorithm and its linearized version, as well as the difference in the obtained solutions.

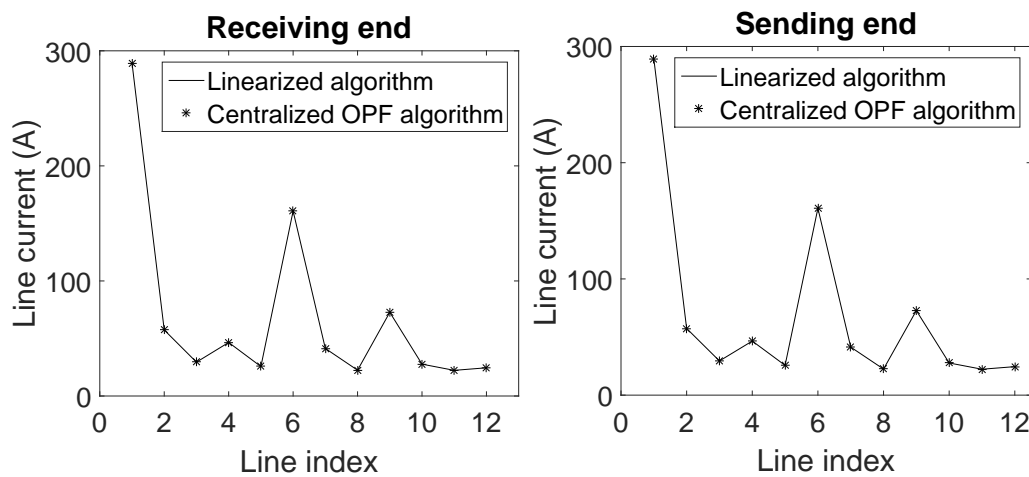


Figure 5.30: Line current flows for the two control algorithms, namely the centralized OPF and its linearized version.

particular, we discuss the misinterpretation of the physical model in the Farival-Low formulation of the OPF problem and the unrealistic assumptions therein. We show that the BFM-convexification of the OPF problem can result in solutions that violate the line ampacity constraints up to 30 – 40% depending on the network configuration (i.e., line parameters, line length, rated voltage value, operating point). Additionally, we show that the unboundedness of the consumption required for the exactness of the SOCP relaxation can result in solutions where the demand increases to unrealistic levels (up to hundreds of times) to ensure convergence to a feasible solution. In an effort to extend the BFM-based OPF formulation to account for lines correctly modeled as physically correct π -equivalents, we find that the theorem of exactness in [35, 36] does no longer hold and exactness may not be guaranteed. Furthermore, we provide the ADMM-based decomposition of the OPF problem and we show that, depending on the network parameters, there are cases for which the ADMM-based solution of the

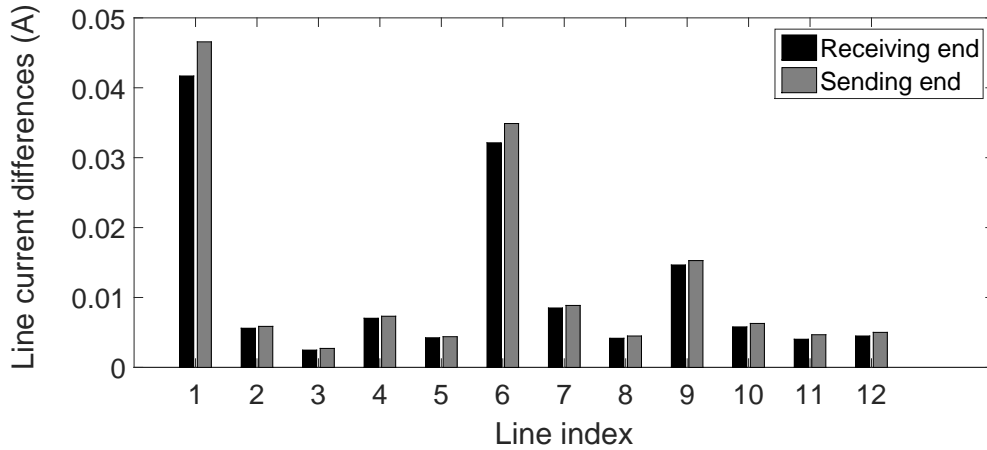


Figure 5.31: Difference in the line current flows obtained from solving the OPF problem and its approximated linearized version.

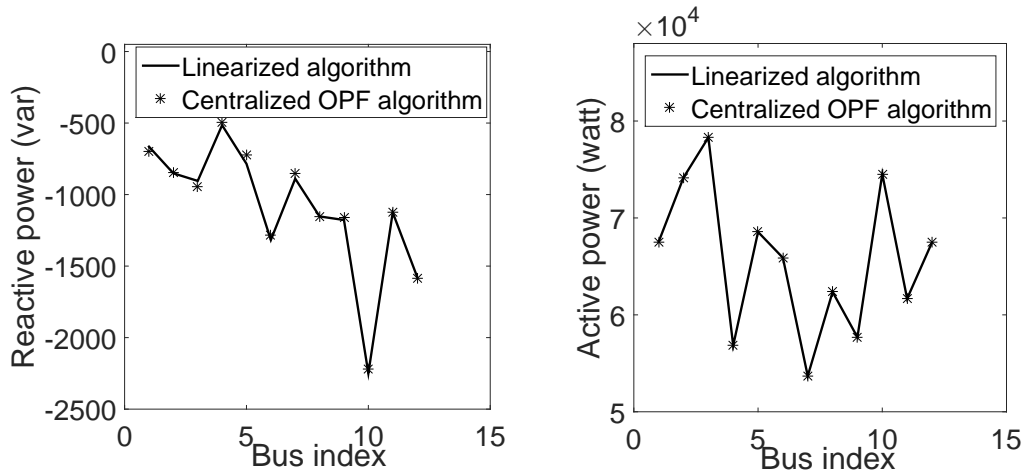


Figure 5.32: Nodal power set-points of the controllable DERs for the two control algorithms, namely the centralized OPF and its linearized version.

non-relaxed OPF problem fails to converge.

To overcome the limitations of existing OPF solutions we propose specific algorithms for the solution of the AC non-convex OPF problem in radial networks that are proven to converge to a local minimum of the original problem. These algorithms use an augmented Lagrangian approach and rely on the method of multipliers for the OPF solution. The two algorithms solve the centralized and decentralized (asynchronous) formulation of the targeted OPF. We show the robustness of the centralized version with respect to the following parameters: (i) line lengths, (ii) network-rated voltage values and (ii) network operating points (cases where the BFM convexification leads to an incorrect solution), (iii) presence of lumped shunt capacitors in the grid (where ADMM failed to converge to a solution) and (iv) initial conditions of the electrical network state. In all cases the proposed centralized algorithm converges to a solu-

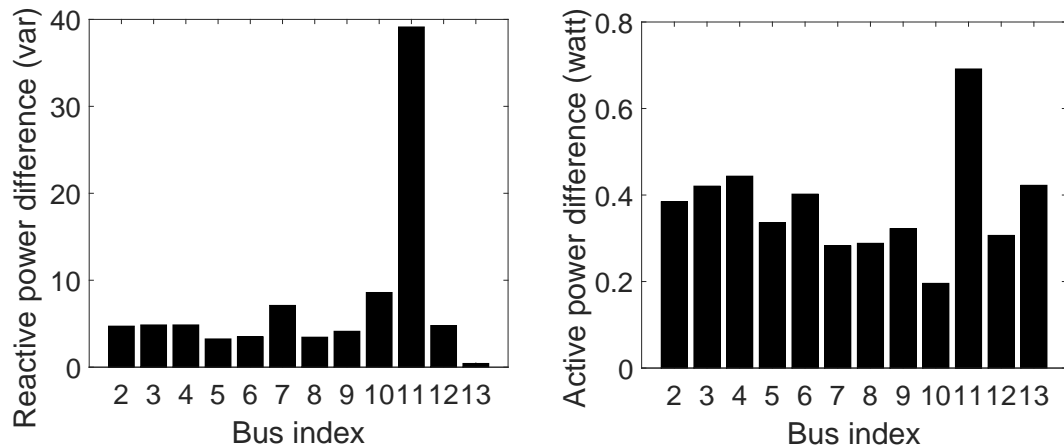


Figure 5.33: Absolute difference in the nodal power set-points of the controllable DERs for the two control algorithms, namely the centralized OPF and its linearized version.

tion that always satisfies the line ampacity constraints within few tens of iterations. Finally, we verify the equivalence of the two proposed algorithms for the case of the IEEE 13-nodes test distribution feeder where realistic operating conditions have been considered. Both algorithms are found to converge to the same solution (i.e., nodal voltages, nodal powers and line current flows). In the case of the centralized algorithm, also for this benchmark network, convergence is achieved in few tens of iterations. The distributed version of the OPF algorithm requires a non-negligible amount of exchanged messages between neighboring bus- and line-agents but each iteration entails simpler operations than one iteration of the centralized algorithm. As far as future work is concerned, we plan to focus on the improvement of the convergence behavior and scalability of the proposed distributed algorithm.

6 Conclusions

In this thesis we design real-time optimal control schemes for active distribution networks. In particular, we focus on voltage control and lines congestion management as these are identified as the two major operational challenges within the context of ADNs.

In order to design control algorithms tailored to the characteristics of distribution networks, that will allow their evolution to active systems, a number of technical challenges related to the ADNs operation have been taken into account. In particular, the significant short-term volatility of non-dispatchable renewable energy resources in combination with the low inertia and higher dynamics that characterize distribution networks require optimal controls that meet stringent time constraints. Additionally, with the view that the increasing penetration of DERs can become an opportunity for the DNO rather than a problem, it is essential to optimally control network participants, i.e., demand and generation, in addition to the traditional control of passive network elements (e.g., OLTCs). Furthermore, the coordination of numerous DERs in ADNs, in combination with their small individual impact and diverse nature calls for unified scalable and/or distributed control mechanisms.

In this thesis, we design and propose a set of control algorithms, ranging from fully centralized to fully decentralized solutions. Furthermore, we investigate the potential of a variety of DERs, expected to be present in ADNs, such as distributed generation units, energy storage systems and elastic demand, for providing ADNs ancillary services. In particular, in terms of control strategies, we have focused on the following design approaches:

- Centralized control schemes that rely on sensitivity coefficients and use a point-to-point communication between the DNO and the controllable DERs;
- Decentralized control mechanisms that rely on sensitivity coefficients, use broadcast signals to control large populations of DERs and rely on state estimation for the feedback channel;
- Centralized and distributed non-convex AC-OPF control algorithms.

Chapter 6. Conclusions

First we investigate the voltage control and lines congestion management problem in distribution networks as a centralized linearized problem relying on voltage and current sensitivity coefficients, similar to approaches used in HV transmission system. To this end, we assume that the network admittance matrix is known and that a monitoring infrastructure and a state estimation process are available that allow the DNO to observe the grid state at frequent time-intervals. In order to extend traditional HV approaches to the inherent multi-phase unbalanced configuration of distribution networks and to increase its computational efficiency we provide a formal analytical derivation of node-voltages and line-currents sensitivities as a function of the power injections and transformers' tap-changers positions. The derivation of the sensitivities allows us to propose a dedicated control scheme where each of the three phases of the controllable resources can be scheduled independently of the others. Using the same centralized control architecture, we investigate the design of algorithms that do not rely on the knowledge of the network model and we present results indicating that the accurate knowledge of the network admittance matrix, which is a key assumption in the control process, can be relaxed. In the case where the network admittance matrix is known with uncertainty and in particular when the DNO has available nominal values along with uncertainty bounds for the feeder parameters we propose a robust optimization framework for the solution of the voltage control problem. In the case where the network admittance matrix is not available at all we rely on a monitoring infrastructure that provides measurements of voltage magnitudes and power injections only and we propose a method to compute voltage sensitivity coefficients using solely measured quantities.

Second, with respect to the case of controlling energy resources that are numerous and diverse, we extend the proposed centralized linearized controller to design GECN, a primary voltage control mechanism that is unified and scalable. GECN still relies on the knowledge of the system model and on availability of both a monitoring infrastructure and a state estimation process. The goal of GECN is to perform primary voltage control in ADNs on an aggregate level relying on state estimation for the feedback channel and without micro-managing each DER which would require the specific knowledge of each resource's internal state. This goal is achieved via low bit-rate broadcast control signals sent to large populations of distributed energy resources in order to manage the variations of the aggregate nodal power injections in the network buses. These signals are computed by a centralized network controller that solves an optimization problem to obtain optimal active and reactive nodal power set-points that lead to the desired operating point for voltage control and they are continuously adjusted as a function of the observed power variations in the network buses. From the controllable DERs perspective, all the resources connected to a specific network bus, irrespectively of their nature, receive a common GECN signal. The local controller of each controllable resource is designed in a way that it decides the system's response to the received signal according to each device's internal state, constraints and capabilities. Overall, GECN is conceived either to operate stand-alone as a primary controller

or it can be deployed by the DNO as a further leverage in coordination with traditional control resources, such as the OLTCs.

Both the aforementioned approaches rely on linearization of the link between nodal voltages/line current flows (controlled quantities) and nodal power injections (control variables) by means of sensitivity coefficients. In the last part of the thesis we express the voltage control and lines congestion management problem without approximation of the power flow equations, resulting in a control problem that belongs to the category of AC-OPF problems. In particular we formulate the problem of optimally scheduling the injections of distributed photovoltaic units for voltage control and lines congestion management purposes as a non-linear non-convex AC-OPF problem. For the solution of the control problem, first, we review existing centralized and distributed OPF algorithms. In particular, we focus on the BFM-based SOCP convexification of the OPF problem and on the application of ADMM to the non-convex AC-OPF problem. Both approaches exhibit serious limitations as we show through practical examples. The BFM-based solution leads to an incorrect system model and can result in unrealistic solutions as it requires the unboundedness of specific control variables, whereas ADMM, in specific cases, exhibits oscillations and is not able to converge to a solution. To overcome the identified limitations, we propose a centralized algorithm for the solution of the non-approximated non-convex AC OPF problem in radial networks that is proven to converge to a local minimum of the original problem. It uses an augmented Lagrangian approach and relies on the method of multipliers and does not require that the problem be convex. In an effort to solve the OPF problem in a distributed way, we exploit the structure of the optimization problem and we apply a primal decomposition method on the proposed centralized algorithm. In the resulting distributed version of the algorithm, at each iteration, local agents, assigned to network buses and network lines, exchange messages with their neighbors and solve simple optimization problems using only local information. We present an asynchronous implementation of the distributed algorithm where the messages of the neighboring agents need not be synchronized. Finally, we show that the distributed algorithm converges to the same solution as the centralized version.

All the control algorithms proposed in this thesis are validated using several benchmark networks, ranging from small-scale systems, where typical values of MV underground cables taken from manufacturers' data are considered for the line parameters, to larger balanced and unbalanced IEEE distribution test feeders. The test networks are appropriately adapted in order to include controllable DERs, as well as non-controllable demand and non-dispatchable power injections represented by photovoltaic arrays. The considered DERs are modeled using realistic capability curves or their corresponding circuit-representation where applicable. The loads and generation profiles are inferred, in all the cases, from real measurements originally taken from distribution feeders and actual PV installations in Switzerland and Italy.

The performance evaluation of the developed algorithms, through an extensive

Chapter 6. Conclusions

set of simulations, shows that they are able to successfully provide primary voltage control and lines congestion management in distribution networks. In particular, significant improvement in the network voltage profile (up to 6% of the network's voltage rated value) is achieved and increased voltage variations due to the highly volatile PV production are significantly smoothed by the use of the proposed algorithms. Moreover, unexpected sags in the voltage due to high time-varying loads are compensated. Additionally, unbalanced control of the network voltage and line-current profiles can be achieved using the proposed methods and is shown to be more effective than the 3-phase balanced control of the DERs' output in cases where large imbalances exist in the network. Furthermore, the use of storage systems, demand response, conventional and renewable distributed generation units is shown, first, to successfully contribute to primary voltage control and lines congestion management and, second, to mitigate the use of other traditional control systems like OLTC and static var compensators. Within the context of GECN, heterogeneous DERs are shown to be successfully coordinated towards a common control objective responding to the same broadcast signal. Finally, the non-approximated non-convex AC-OPF formulation of the voltage control and lines congestion management problem can be solved in a centralized or a fully decentralized, asynchronous way and is shown to successfully converge to an optimal solution that satisfies voltage constraints and line ampacity limits.

Bibliography

- [1] N. Hatziargyriou *et al.*, “CIGRE WG "Network of the Future", electricity supply systems of the future,” *Electra*, vol. 256, pp. 42–49, 2011.
- [2] European Network of Transmission System Operators for Electricity (ENTSO-E), “Draft network code on demand connection,” December 5, 2012.
- [3] F. Pilo, S. Jupe, F. Silvestro, K. El Bakari, C. Abbey, G. Celli, J. Taylor, A. Baitech, and C. Carter-Brown, “Planning and optimisation of active distribution systems—an overview of cigre working group c6. 19 activities,” in *Integration of Renewables into the Distribution Grid, CIRED 2012 Workshop*. IET, 2012, pp. 1–4.
- [4] M. Delfanti, M. Merlo, G. Monfredini, V. Olivieri, M. Pozzi, and A. Silvestri, “Hosting dispersed generation on italian MV networks: Towards smart grids,” in *Harmonics and Quality of Power (ICHQP), 2010 14th International Conference on*, Sept 2010, pp. 1–6.
- [5] E. Coster, J. Myrzik, B. Kruimer, and W. Kling, “Integration issues of distributed generation in distribution grids,” *Proceedings of the IEEE*, vol. 99, no. 1, pp. 28–39, Jan 2011.
- [6] N. Singh, E. Kliokys, H. Feldmann, R. Kussel, R. Chrustowski, and C. Joborowicz, “Power system modelling and analysis in a mixed energy management and distribution management system,” *IEEE Trans. Power Systems*, vol. 13, no. 3, pp. 1143–1149, 1998.
- [7] N. Jenkins, R. Allan, P. Crossley, D. Kirschen, and G. Strbac, *Embedded generation*, A. T. Johns and D. F. Warne, Eds. IET, 2000, vol. 9, no. 3.
- [8] N.-G. James, *Control and Automation of Electrical Power Systems*. Hoboken, NJ: CRC Press, 2006.
- [9] A. Borghetti, M. Bosetti, S. Grillo, S. Massucco, C. Nucci, M. Paolone, and F. Silvestro, “Short-term scheduling and control of active distribution systems with high penetration of renewable resources,” *IEEE Systems Journal*, vol. 4, no. 3, pp. 313–322, 2010.

Bibliography

- [10] Q. Zhou and J. Bialek, "Generation curtailment to manage voltage constraints in distribution networks," *IET, Generation, Transmission & Distribution*, vol. 1, no. 3, pp. 492–498, 2007.
- [11] T. Senjyu, Y. Miyazato, A. Yona, N. Urasaki, and T. Funabashi, "Optimal distribution voltage control and coordination with distributed generation," *IEEE Trans. Power Delivery*, vol. 23, no. 2, pp. 1236–1242, 2008.
- [12] P. Romano and M. Paolone, "Enhanced interpolated-DFT for synchrophasor estimation in FPGAs: Theory, implementation, and validation of a PMU prototype," *IEEE Trans. Instrumentation and Measurement*, vol. 63, no. 12, pp. 2824–2836, Dec 2014.
- [13] A. G. Phadke and J. S. Thorp, *Synchronized phasor measurements and their applications*. Springer Science & Business Media, 2008.
- [14] M. Pignati, M. Popovic, S. Barreto Andrade, R. Cherkaoui, D. Flores, J.-Y. Le Boudec, M. M. Maaz, M. Paolone, P. Romano, S. Sarri *et al.*, "Real-time state estimation of the EPFL-campus medium-voltage grid by using PMUs," in *The Sixth Conference on Innovative Smart Grid Technologies (ISGT2015)*, no. EPFL-CONF-203775, 2014.
- [15] T. Van Cutsem and C. Vournas, *Voltage stability of electric power systems*. Springer Science & Business Media, 1998, vol. 441.
- [16] K. Christakou, D.-C. Tomozei, M. Bahramipanah, J.-Y. Le Boudec, and M. Paolone, "Primary voltage control in active distribution networks via broadcast signals: The case of distributed storage," *IEEE Trans. Smart Grid*, vol. 5, no. 5, pp. 2314–2325, Sept 2014.
- [17] K. Christakou, J. LeBoudec, M. Paolone, and D.-C. Tomozei, "Efficient computation of sensitivity coefficients of node voltages and line currents in unbalanced radial electrical distribution networks," *IEEE Trans. Smart Grid*, vol. 4, no. 2, pp. 741–750, 2013.
- [18] L. Czarnecki and Z. Staroszczyk, "On-line measurement of equivalent parameters for harmonic frequencies of a power distribution system and load," *IEEE Trans. Instrumentation and Measurement*, vol. 45, no. 2, pp. 467–472, 1996.
- [19] A. K. Deb, *Powerline ampacity system: theory, modeling and applications*. CRC Press, 2000.
- [20] M. T. Schilling, R. Billinton, and M. G. dos Santos, "Bibliography on power systems probabilistic security analysis 1968-2008," *International Journal of Emerging Electric Power Systems*, vol. 10, no. 3, 2009.

-
- [21] I. Dobson, B. A. Carreras, and D. E. Newman, "A loading-dependent model of probabilistic cascading failure," *Probability in the Engineering and Informational Sciences*, vol. 19, no. 01, pp. 15–32, 2005.
- [22] J. Chen, J. S. Thorp, and I. Dobson, "Cascading dynamics and mitigation assessment in power system disturbances via a hidden failure model," *International Journal of Electrical Power & Energy Systems*, vol. 27, no. 4, pp. 318–326, 2005.
- [23] S. Mei, A. Xue, and X. Zhang, "On power system blackout modeling and analysis based on self-organized criticality," *Science in China Series E: Technological Sciences*, vol. 51, no. 2, pp. 209–219, 2008.
- [24] B. Carreras, D. Newman, I. Dobson, and A. Poole, "Evidence for self-organized criticality in a time series of electric power system blackouts," *IEEE Trans. Circuits and Systems I: Regular Papers*, vol. 51, no. 9, pp. 1733–1740, Sept 2004.
- [25] D. Newman, B. Carreras, V. Lynch, and I. Dobson, "Exploring complex systems aspects of blackout risk and mitigation," *IEEE Trans. Reliability*, vol. 60, no. 1, pp. 134–143, March 2011.
- [26] . COMMISSION REGULATION (EU), "Guideline on capacity allocation and congestion management," 24 July 2015.
- [27] S. Singh and A. David, "Optimal location of facts devices for congestion management," *Electric Power Systems Research*, vol. 58, no. 2, pp. 71–79, 2001.
- [28] G. Granelli, M. Montagna, F. Zanellini, P. Bresesti, R. Vailati, and M. Innorta, "Optimal network reconfiguration for congestion management by deterministic and genetic algorithms," *Electric power systems research*, vol. 76, no. 6, pp. 549–556, 2006.
- [29] R. Fang and A. David, "Transmission congestion management in an electricity market," *IEEE Trans. Power Systems*, vol. 14, no. 3, pp. 877–883, Aug 1999.
- [30] P. Rao and K. Rao, "An efficient load shedding algorithm for radial systems," in *Conference on Convergent Technologies for the Asia-Pacific Region, TENCON*, vol. 2, Oct 2003, pp. 771–774.
- [31] B. Talukdar, A. Sinha, S. Mukhopadhyay, and A. Bose, "A computationally simple method for cost-efficient generation rescheduling and load shedding for congestion management," *International Journal of Electrical Power & Energy Systems*, vol. 27, no. 5–6, pp. 379 – 388, 2005. [Online]. Available: <http://www.sciencedirect.com/science/article/pii/S014206150500030X>
- [32] D. Burke and M. O'Malley, "Factors influencing wind energy curtailment," *IEEE Trans. Sustainable Energy*, vol. 2, no. 2, pp. 185–193, April 2011.

Bibliography

- [33] Y. Gu and L. Xie, "Fast sensitivity analysis approach to assessing congestion induced wind curtailment," *IEEE Trans. Power Systems*, vol. 29, no. 1, pp. 101–110, Jan 2014.
- [34] D. Torregrossa, J.-Y. Le Boudec, and M. Paolone, "Model-free computation of ultra short-term prediction intervals of solar irradiance," *IEEE Trans. Smart Grid*, *under review*, 2015.
- [35] M. Farivar and S. H. Low, "Branch flow model: Relaxations and convexification - part I," *IEEE Trans. on Power Systems*, vol. 28, no. 3, pp. 2554–2564, 2013.
- [36] M. Farivar and S. Low, "Branch flow model: Relaxations and convexification - part II," *IEEE Trans. on Power Systems*, vol. 28, no. 3, pp. 2565–2572, Aug 2013.
- [37] P. UNION, "Directive 2009/28/ec of the european parliament and of the council of 23âapril 2009 on the promotion of the use of energy from renewable sources and amending and subsequently repealing directives 2001/77/ec andâ2003/30/ec," 2009.
- [38] "Database of state incentives for renewables and efficiency, <http://www.dsireusa.org/>," 2009.
- [39] I. E. Agency, "Combined heat and power, evaluating the benefits of greater global investment," 2008.
- [40] M. H. Bollen and F. Hassan, *Integration of distributed generation in the power system*. John wiley & sons, 2011, vol. 80.
- [41] J. Lopes, N. Hatziargyriou, J. Mutale, P. Djapic, and N. Jenkins, "Integrating distributed generation into electric power systems: A review of drivers, challenges and opportunities," *Electric Power Systems Research*, vol. 77, no. 9, pp. 1189–1203, 2007.
- [42] G. Pepermans, J. Driesen, D. Haeseldonckx, R. Belmans, and W. D'haeseleer, "Distributed generation: definition, benefits and issues," *Energy Policy*, vol. 33, no. 6, pp. 787 – 798, 2005. [Online]. Available: <http://www.sciencedirect.com/science/article/pii/S0301421503003069>
- [43] J. Schlabbach, D. Blume, and T. Stephanblome, *Voltage quality in electrical power systems*. IET, 2001, no. 36.
- [44] P. Q. A. Guide, "Voltage disturbances," *Standard EN*, vol. 50160, 2005.
- [45] "Din vde 0100-100 (vde 0100 part 100): 2002-08."
- [46] "Ieee recommended practice for monitoring electric power quality," *IEEE Std 1159-2009 (Revision of IEEE Std 1159-1995)*, pp. c1–81, June 2009.

- [47] S. A. P. Q. Standard, "Nrs 048-2: 1996," 1996.
- [48] H. Knutson and B. B. Miles, "Cable derating parameters and their effects," *IEEE paper, no. PCIC-77-5*, 1977.
- [49] "Ieee recommended practice for industrial and commercial power systems analysis," *IEEE Std 399-1997*.
- [50] "National electrical code (nec)," *NFPA 70-1996*.
- [51] "Standard power cable ampacity tables," *IEEE Std 835-1994*.
- [52] "Electric cables - calculation of the current rating," *IEC Std 60287*, 2006.
- [53] A. Guerrisi, "Thermal analysis of power lines: Methodologies and applications," Ph.D. dissertation, Politecnico di Torino, 2013.
- [54] P. P. Barker and R. W. De Mello, "Determining the impact of distributed generation on power systems. i. radial distribution systems," in *Power Engineering Society Summer Meeting, 2000. IEEE*, vol. 3. IEEE, 2000, pp. 1645–1656.
- [55] J. Peas Lopes, "Integration of dispersed generation on distribution networks-impact studies," in *Power Engineering Society Winter Meeting, 2002. IEEE*, vol. 1, 2002, pp. 323–328 vol.1.
- [56] S. Conti, S. Raiti, G. Tina, and U. Vagliasindi, "Distributed generation in lv distribution networks: voltage and thermal constraints," in *Power Tech Conference Proceedings, 2003 IEEE Bologna*, vol. 2. IEEE, 2003, pp. 6–pp.
- [57] P. Djapic, C. Ramsay, D. Pudjianto, G. Strbac, J. Mutale, N. Jenkins, and R. Allan, "Taking an active approach," *Power and Energy Magazine, IEEE*, vol. 5, no. 4, pp. 68–77, July 2007.
- [58] S. A. Papathanassiou, "A technical evaluation framework for the connection of {DG} to the distribution network," *Electric Power Systems Research*, vol. 77, no. 1, pp. 24 – 34, 2007. [Online]. Available: <http://www.sciencedirect.com/science/article/pii/S0378779606000241>
- [59] S. Liew and G. Strbac, "Maximising penetration of wind generation in existing distribution networks," in *Generation, Transmission and Distribution, IEE Proceedings-*, vol. 149, no. 3. IET, 2002, pp. 256–262.
- [60] R. Tonkoski, L. A. Lopes, and T. H. El-Fouly, "Coordinated active power curtailment of grid connected pv inverters for overvoltage prevention," *IEEE Trans. Sustainable Energy*, vol. 2, no. 2, pp. 139–147, 2011.
- [61] D. Pudjianto, P. Djapic, M. Aunedi, C. K. Gan, G. Strbac, S. Huang, and D. Infield, "Smart control for minimizing distribution network reinforcement cost due to electrification," *Energy Policy*, vol. 52, pp. 76–84, 2013.

Bibliography

- [62] V. F. Martins and C. L. Borges, "Active distribution network integrated planning incorporating distributed generation and load response uncertainties," *IEEE Trans. Power Systems*, vol. 26, no. 4, pp. 2164–2172, 2011.
- [63] S. Corsi, "The secondary voltage regulation in italy," in *Power Engineering Society Summer Meeting, 2000. IEEE*, vol. 1, 2000, pp. 296–304 vol. 1.
- [64] S. Corsi, M. Pozzi, C. Sabelli, and A. Serrani, "The coordinated automatic voltage control of the italian transmission grid-part i: reasons of the choice and overview of the consolidated hierarchical system," *IEEE Trans. Power Systems*, vol. 19, no. 4, pp. 1723–1732, Nov 2004.
- [65] H. Lefebvre, D. Fragnier, J. Boussion, P. Mallet, and M. Bulot, "Secondary coordinated voltage control system: feedback of edf," in *Power Engineering Society Summer Meeting, 2000. IEEE*, vol. 1, 2000, pp. 290–295 vol. 1.
- [66] J. Paul, J. Leost, and J. Tesson, "Survey of the secondary voltage control in france : Present realization and investigations," *IEEE Trans. Power Systems*, vol. 2, no. 2, pp. 505–511, May 1987.
- [67] J. Sancha, J. Fernandez, A. Cortes, and J. Abarca, "Secondary voltage control: analysis, solutions and simulation results for the spanish transmission system," *IEEE Trans. Power Systems*, vol. 11, no. 2, pp. 630–638, May 1996.
- [68] J. Paul, C. Corroyer, P. Jeannel, J. Tesson, F. Maury, and A. Torra, "Improvements in the organization of secondary voltage control in france," *CIGRE Session Paris*, pp. 39–03, 1990.
- [69] Y. G. Rebours, D. S. Kirschen, M. Trotignon, and S. Rossignol, "A survey of frequency and voltage control ancillary services—part i: Technical features," *IEEE Trans. Power Systems*, vol. 22, no. 1, pp. 350–357, 2007.
- [70] M. Nick, O. Alizadeh-Mousavi, R. Cherkaoui, and M. Paolone, "Security constrained unit commitment with dynamic thermal line rating," *IEEE Trans. Power Systems*, vol. PP, no. 99, pp. 1–12, 2015.
- [71] A. Bersani, A. Borghetti, C. Bossi, L. De Biase, O. Lamquet, S. Massucco, A. Morini, C. A. Nucci, M. Paolone, S. Quaia *et al.*, "Management of low voltage grids with high penetration of distributed generation: concepts, implementations and experiments," in *Cigré 2006 Session*, no. EPFL-CONF-180111, 2006.
- [72] A. Borghetti, M. Bosetti, S. Grillo, M. Paolone, and F. Silvestro, "Short-term scheduling of active distribution systems," in *PowerTech, 2009 IEEE Bucharest*. IEEE, 2009, pp. 1–7.
- [73] A. Borghetti, M. Bosetti, S. Grillo, A. Morini, M. Paolone, and F. Silvestro, "A two-stage scheduler of distributed energy resources," in *Power Tech, 2007 IEEE Lausanne*. IEEE, 2007, pp. 2168–2173.

-
- [74] A. Borghetti, M. Bosetti, C. A. Nucci, M. Paolone, S. Massucco, F. Silvestro, and S. Scalari, "A procedure for the automatic scheduling of distributed energy resources in medium voltage networks," in *CIREN 20th International Conference on Electricity Distribution*, 2009.
- [75] J. Peschon, D. Piercy, W. Tinney, and O. Tveit, "Sensitivity in power systems," *IEEE Trans. Power Apparatus and Systems*, no. 8, pp. 1687–1696, 1968.
- [76] D. Shirmohammadi, H. Hong, A. Semlyen, and G. Luo, "A compensation-based power flow method for weakly meshed distribution and transmission networks," *IEEE Trans. Power Systems*, vol. 3, no. 2, pp. 753–762, 1988.
- [77] A. Wood and B. Wollenberg, *Power generation, operation, and control*. Wiley New York, 1996, vol. 2.
- [78] R. Marconato, "Electric power systems, vol. 2," *CEI, Italian Electrotechnical Committee, Milano, Italy*, 2002.
- [79] M. Begovic and A. Phadke, "Control of voltage stability using sensitivity analysis," *IEEE Trans. Power Systems*, vol. 7, no. 1, pp. 114–123, 1992.
- [80] D.-H. Choi and L. Xie, "Impact analysis of locational marginal price subject to power system topology errors," in *Smart Grid Communications (SmartGrid-Comm), 2013 IEEE International Conference on*, Oct 2013, pp. 55–60.
- [81] K. Clements and P. Davis, "Detection and identification of topology errors in electric power systems," *IEEE Trans. Power Systems*, vol. 3, no. 4, pp. 1748–1753, Nov 1988.
- [82] S. Frank, J. Sexauer, and S. Mohagheghi, "Temperature-dependent power flow," *IEEE Trans. Power Systems*, vol. 28, no. 4, pp. 4007–4018, Nov 2013.
- [83] A. Ben-Tal, L. El Ghaoui, and A. Nemirovski, *Robust optimization*. Princeton University Press, 2009.
- [84] D. Bertsimas and M. Sim, "The price of robustness," *Operations research*, vol. 52, no. 1, pp. 35–53, 2004.
- [85] S. Conti, S. Raiti, and G. Vagliasindi, "Voltage sensitivity analysis in radial mv distribution networks using constant current models," in *IEEE International Symposium on Industrial Electronics (ISIE)*. IEEE, 2010, pp. 2548–2554.
- [86] D. Khatod, V. Pant, and J. Sharma, "A novel approach for sensitivity calculations in the radial distribution system," *IEEE Trans. Power Delivery*, vol. 21, no. 4, pp. 2048–2057, 2006.

Bibliography

- [87] Q. Zhou and J. Bialek, "Simplified calculation of voltage and loss sensitivity factors in distribution networks," in *Proc. of the 16th Power Systems Computation Conference (PSCC2008), Glasgow, Scotland, 2008*.
- [88] J. Bandler and M. El-Kady, "A unified approach to power system sensitivity analysis and planning, part i: Family of adjoint systems," in *Proc. IEEE Int. Symp. Circuits Syst*, 1980, pp. 681–687.
- [89] —, "A new method for computerized solution of power flow equations," *IEEE Trans. Power Apparatus and Systems*, no. 1, pp. 1–10, 1982.
- [90] —, "A unified approach to power system sensitivity analysis and planning, part ii: Special class of adjoint systems," in *Proc. IEEE Int. Symp. Circuits Syst*, 1980, p. 688.
- [91] L. Ferreira, "Tellegen's theorem and power systems—new load flow equations, new solution methods," *IEEE Trans. Circuits and Systems*, vol. 37, no. 4, pp. 519–526, 1990.
- [92] R. Gurram and B. Subramanyam, "Sensitivity analysis of radial distribution network—adjoint network method," *International Journal of Electrical Power & Energy Systems*, vol. 21, no. 5, pp. 323–326, 1999.
- [93] Y. Chen, A. Dominguez-Garcia, and P. Sauer, "A sparse representation approach to online estimation of power system distribution factors," *IEEE Trans. Power Systems*, vol. PP, no. 99, pp. 1–12, 2014.
- [94] —, "Measurement-based estimation of linear sensitivity distribution factors and applications," *IEEE Trans. Power Systems*, vol. 29, no. 3, pp. 1372–1382, May 2014.
- [95] S. Weckx, R. D'Hulst, and J. Driesen, "Voltage sensitivity analysis of a laboratory distribution grid with incomplete data," *IEEE Trans. Smart Grid*, vol. 6, no. 3, pp. 1271–1280, May 2015.
- [96] D. Bertsimas, E. Litvinov, X. A. Sun, J. Zhao, and T. Zheng, "Adaptive robust optimization for the security constrained unit commitment problem," *IEEE Trans. Power Systems*, vol. 28, no. 1, pp. 52–63, 2013.
- [97] S. A. Malcolm and S. A. Zenios, "Robust optimization for power systems capacity expansion under uncertainty," *Journal of the operational research society*, pp. 1040–1049, 1994.
- [98] K. Y. Lee, X. Bai, and Y.-M. Park, "Optimization method for reactive power planning by using a modified simple genetic algorithm," *IEEE Trans. Power Systems*, vol. 10, no. 4, pp. 1843–1850, 1995.

-
- [99] A. J. Conejo, J. M. Morales, and L. Baringo, "Real-time demand response model," *IEEE Trans. Smart Grid*, vol. 1, no. 3, pp. 236–242, 2010.
- [100] S. Sarri, M. Paolone, R. Cherkaoui, A. Borghetti, F. Napolitano, and C. Nucci, "State Estimation of Active Distribution Networks: Comparison Between WLS and Iterated Kalman-Filter Algorithm Integrating PMUs," in *3rd IEEE PES Innovative Smart Grid Technologies (ISGT) Europe Conference*, 2012.
- [101] P. Pegoraro, J. Tang, J. Liu, F. Ponci, A. Monti, and C. Muscas, "Pmu and smart metering deployment for state estimation in active distribution grids," in *Energy Conference and Exhibition (ENERGYCON), 2012 IEEE International*, Sept 2012, pp. 873–878.
- [102] G. De Carne, M. Liserre, K. Christakou, and M. Paolone, "Integrated voltage control and line congestion management in active distribution networks by means of smart transformers," in *Industrial Electronics (ISIE), 2014 IEEE 23rd International Symposium on*, June 2014, pp. 2613–2619.
- [103] J. Arrillaga, D. Bradley, and P. Bodger, "Power system harmonics, 1985."
- [104] H. Chiang and M. Baran, "On the existence and uniqueness of load flow solution for radial distribution power networks," *IEEE Trans. Circuits and Systems*, vol. 37, no. 3, pp. 410–416, 1990.
- [105] A. Abur and A. Exposito, *Power system state estimation: theory and implementation*. CRC, 2004, vol. 24.
- [106] J. Mahseredjian, S. Lefebvre, and X. Do, "A new method for time domain modelling of nonlinear circuits in large linear networks," in *Proc. of 11th Power Systems Computation Conference PSCC*, 1993.
- [107] J. Mahseredjian, "Simulation des transitoires électromagnétiques dans les réseaux électriques," *Édition Les Techniques de l'Ingénieur*, 2008.
- [108] J. Mahseredjian, S. Denetière, L. Dubé, B. Khodabakhchian, and L. Gérin-Lajoie, "On a new approach for the simulation of transients in power systems," *Electric power systems research*, vol. 77, no. 11, pp. 1514–1520, 2007.
- [109] W. Kersting, "Radial distribution test feeders," in *Power Engineering Society Winter Meeting, 2001. IEEE*, vol. 2, 2001, pp. 908–912 vol.2.
- [110] A. Ellis, R. Nelson, E. Von Engeln, R. Walling, J. McDowell, L. Casey, E. Seymor, W. Peter, C. Barker, and B. Kirby, "Reactive power interconnection requirements for PV and wind plants - recommendations to NERC," Sandia Report, Tech. Rep., 2012.
- [111] D. Bertsimas and M. Sim, "Robust discrete optimization and network flows," *Mathematical programming*, vol. 98, no. 1, pp. 49–71, 2003.

Bibliography

- [112] D. Bertsimas, D. B. Brown, and C. Caramanis, "Theory and applications of robust optimization," *SIAM review*, vol. 53, no. 3, pp. 464–501, 2011.
- [113] A. L. Soyster, "Technical note-convex programming with set-inclusive constraints and applications to inexact linear programming," *Operations research*, vol. 21, no. 5, pp. 1154–1157, 1973.
- [114] A. Ben-Tal and A. Nemirovski, "Robust solutions of linear programming problems contaminated with uncertain data," *Mathematical programming*, vol. 88, no. 3, pp. 411–424, 2000.
- [115] D. L. Mills, "Internet time synchronization: the network time protocol," *IEEE Trans. Communications*, vol. 39, no. 10, pp. 1482–1493, 1991.
- [116] H. E. Z. Farag and E. F. El-Saadany, "A novel cooperative protocol for distributed voltage control in active distribution systems," *IEEE Trans. Power Systems*, vol. PP, no. 99, pp. 1–1.
- [117] H. Farag, E. El-Saadany, and R. Seethapathy, "A two ways communication-based distributed control for voltage regulation in smart distribution feeders," *IEEE Trans. Smart Grid*, vol. 3, no. 1, pp. 271–281, March.
- [118] K. Turitsyn, N. Sinitsyn, S. Backhaus, and M. Chertkov, "Robust broadcast-communication control of electric vehicle charging," in *Smart Grid Communications (SmartGridComm), 2010 First IEEE International Conference on*, Oct., pp. 203–207.
- [119] S. Bashash and H. Fathy, "Robust demand-side plug-in electric vehicle load control for renewable energy management," in *American Control Conference (ACC), 2011*, 29 2011-July 1, pp. 929–934.
- [120] K. Christakou, D.-C. Tomozei, J.-Y. Le Boudec, and M. Paolone, "GECN: Primary voltage control for active distribution networks via real-time demand-response," *IEEE Trans. Smart Grid*, vol. 5, no. 2, pp. 622–631, March 2014.
- [121] K. Ramakrishnan, S. Floyd, and D. Black, "The Addition of Explicit Congestion Notification (ECN) to IP, September 2001. Internet Engineering Task Force (IETF)," RFC 3168, Tech. Rep.
- [122] J. Taneja, D. Culler, and P. Dutta, "Towards cooperative grids: Sensor/actuator networks for renewables integration," in *First IEEE International Conference on Smart Grid Communications (SmartGridComm)*. IEEE, 2010, pp. 531–536.
- [123] S. Koch, J. Mathieu, and D. Callaway, "Modeling and control of aggregated heterogeneous thermostatically controlled loads for ancillary services," in *Proc. 17th Power Syst. Comput. Conf. (PSCC2011), Stockholm, Sweden*, 2011, pp. 1–7.

- [124] S. Backhaus, N. Sinityn, S. Kundu, and I. Hiskens, "Modeling and control of thermostatically controlled loads," Los Alamos National Laboratory (LANL), Tech. Rep., 2011.
- [125] Q. Zhou and J. Bialek, "Energy storage is a key smart grid element," in *Proc. of Cigré Symposium, The Electric Power System of the Future, Sept. 13-15, Bologna, Italy*, 2011.
- [126] A. Oudalov, T. Buehler, and D. Chartouni, "Utility scale applications of energy storage," in *Energy 2030 Conference, 2008. ENERGY 2008. IEEE*, Nov 2008, pp. 1–7.
- [127] A. Oudalov, D. Chartouni, C. Ohler, and G. Linhofer, "Value analysis of battery energy storage applications in power systems," in *Power Systems Conference and Exposition, 2006. PSCE '06. 2006 IEEE PES*, Oct 2006, pp. 2206–2211.
- [128] M. Nick, M. Hohmann, R. Cherkaoui, and M. Paolone, "On the optimal placement of distributed storage systems for voltage control in active distribution networks," in *Innovative Smart Grid Technologies (ISGT Europe), 2012 3rd IEEE PES International Conference and Exhibition*, Oct., pp. 1–6.
- [129] "Electric energy storage systems," *Cigré Technical Brochure Working Group C6.15*, April 2011.
- [130] N. Saker, M. Petit, and J. Coullon, "Demand side management of electrical water heaters and evaluation of the cold load pick-up characteristics (clpu)," in *PowerTech, Trondheim. IEEE*, 2011, pp. 1–8.
- [131] M. Arnold and G. Andersson, "Model predictive control of energy storage including uncertain forecasts," in *Proc. PSCC*, 2011.
- [132] S. Koch, F. Barcenas, and G. Andersson, "Using controllable thermal household appliances for wind forecast error reduction," in *IFAC Conference on Control Methodologies and Technology for Energy Efficiency. Citeseer*, 2010.
- [133] M. Albadi and E. El-Saadany, "A summary of demand response in electricity markets," *Electric Power Systems Research*, vol. 78, no. 11, pp. 1989–1996, 2008.
- [134] J. Mathieu, M. Dyson, and D. Callaway, "Using residential electric loads for fast demand response: The potential resource and revenues, the costs, and policy recommendations," in *Proceedings of the ACEEE Summer Study on Buildings, Pacific Grove, CA, Aug.*, 2012.
- [135] T. Keep, F. Sifuentes, D. Auslander, and D. Callaway, "Using load switches to control aggregated electricity demand for load following and regulation," in *Power and Energy Society General Meeting. IEEE*, 2011, pp. 1–7.

Bibliography

- [136] T. Vandoorn, B. Renders, L. Degroote, B. Meersman, and L. Vandevelde, "Active load control in islanded microgrids based on the grid voltage," *IEEE Trans. Smart Grid*, vol. 2, no. 1, pp. 139–151, 2011.
- [137] J. Wu, J. Ekanayake, and K. Samarakoon, "Frequency response from electric vehicles," in *ENERGY 2011, The First International Conference on Smart Grids, Green Communications and IT Energy-aware Technologies*, 2011, pp. 148–152.
- [138] K. Samarakoon, J. Ekanayake, and N. Jenkins, "Investigation of Domestic Load Control to Provide Primary Frequency Response Using Smart Meters," *IEEE Trans. Smart Grid*, vol. 3, no. 1, pp. 282–292, 2012.
- [139] X. Liu, A. Aichhorn, L. Liu, and H. Li, "Coordinated control of distributed energy storage system with tap changer transformers for voltage rise mitigation under high photovoltaic penetration," *Smart Grid, IEEE Transactions on*, vol. 3, no. 2, pp. 897–906, June 2012.
- [140] R. G. Valle and J. A. P. Lopes, *Electric vehicle integration into modern power networks*. Springer, 2012, vol. 2.
- [141] T. Voice, P. Vytelingum, S. Ramchurn, A. Rogers, and N. Jennings, "Decentralised control of micro-storage in the smart grid," in *Twenty-Fifth AAAI Conference on Artificial Intelligence*, 2011.
- [142] N. Lu and D. Chassin, "A state-queueing model of thermostatically controlled appliances," *IEEE Trans. Power Systems*, vol. 19, no. 3, pp. 1666–1673, 2004.
- [143] P. Constantopoulos, F. Schweppe, and R. Larson, "ESTIA: A real-time consumer control scheme for space conditioning usage under spot electricity pricing," *Computers & operations research*, vol. 18, no. 8, pp. 751–765, 1991.
- [144] S. Piller, M. Perrin, and A. Jossen, "Methods for state-of-charge determination and their applications," *Journal of power sources*, vol. 96, no. 1, pp. 113–120, 2001.
- [145] B. Belvedere, M. Bianchi, A. Borghetti, C. Nucci, M. Paolone, and A. Peretto, "A microcontroller-based power management system for standalone microgrids with hybrid power supply," *IEEE Trans. Sustainable Energy*, vol. 3, no. 3, pp. 422–431, July.
- [146] V. Pop, H. J. Bergveld, P. Notten, and P. P. Regtien, "State-of-the-art of battery state-of-charge determination," *Measurement Science and Technology*, vol. 16, no. 12, p. R93, 2005.
- [147] I. Papic, "Simulation model for discharging a lead-acid battery energy storage system for load leveling," *IEEE Trans. Energy Conversion*, vol. 21, no. 2, pp. 608–615, 2006.

-
- [148] M. Coleman, C. K. Lee, C. Zhu, and W. G. Hurley, "State-of-charge determination from emf voltage estimation: Using impedance, terminal voltage, and current for lead-acid and lithium-ion batteries," *IEEE Trans. Industrial Electronics*, vol. 54, no. 5, pp. 2550–2557, 2007.
- [149] B. Yann Liaw, G. Nagasubramanian, R. G. Jungst, and D. H. Doughty, "Modeling of lithium ion cells a simple equivalent-circuit model approach," *Solid state ionics*, vol. 175, no. 1, pp. 835–839, 2004.
- [150] S. R. Nelatury and P. Singh, "Equivalent circuit parameters of nickel/metal hydride batteries from sparse impedance measurements," *Journal of power sources*, vol. 132, no. 1, pp. 309–314, 2004.
- [151] A. J. Salkind, P. Singh, A. Cannone, T. Atwater, X. Wang, and D. Reisner, "Impedance modeling of intermediate size lead-acid batteries," *Journal of power sources*, vol. 116, no. 1, pp. 174–184, 2003.
- [152] T. B. Reddy, *Linden's Handbook of Batteries*. McGraw-Hill, 2011, vol. 4.
- [153] L. Zubieta and R. Bonert, "Characterization of double-layer capacitors for power electronics applications," *IEEE Trans. Industry Applications*, vol. 36, no. 1, pp. 199–205, 2000.
- [154] D. Torregrossa, M. Bahramipanah, E. Namor, R. Cherkaoui, and M. Paolone, "Improvement of dynamic modeling of supercapacitor by residual charge effects estimation," *IEEE Trans. Industrial Electronics*, vol. PP, no. 99, pp. 1–1, 2013.
- [155] M. Stadler, W. Krause, M. Sonnenschein, and U. Vogel, "Modelling and evaluation of control schemes for enhancing load shift of electricity demand for cooling devices," *Environmental Modelling & Software*, vol. 24, no. 2, pp. 285–295, 2009.
- [156] M. Eremia and M. Shahidehpour, *Handbook of Electrical Power System Dynamics: Modeling, Stability, and Control*. Wiley-IEEE Press, 2013, vol. 92.
- [157] M. C. Ferris, "Matlab and gams: Interfacing optimization and visualization software," *Mathematical Programming Technical Report*, no. 98-19, p. 21, 1998.
- [158] R. H. Byrd, J. Nocedal, and R. A. Waltz, "Knitro: An integrated package for nonlinear optimization," in *Large-scale nonlinear optimization*. Springer, 2006, pp. 35–59.
- [159] P. Romano, M. Pignati, and M. Paolone, "Integration of an iee std. c37. 118 compliant pmu into a real-time simulator," in *PowerTech, 2015 IEEE Eindhoven*. IEEE, 2015, pp. 1–6.
- [160] L. Zanni, S. Sarri, M. Pignati, R. Cherkaoui, and M. Paolone, "Probabilistic assessment of the process-noise covariance matrix of discrete kalman filter state

Bibliography

- estimation of active distribution networks,” in *Probabilistic Methods Applied to Power Systems (PMAPS), 2014 International Conference on*. IEEE, 2014, pp. 1–6.
- [161] S. Sarri, M. Pignati, P. Romano, L. Zanni, and M. Paolone, “A hardware-in-the-loop test platform for the performance assessment of a pmu-based real-time state estimator for active distribution networks,” in *the 2015 IEEE PowerTech Conference (accepted for presentation)*, 2015.
- [162] C. H. K. W. S. Virayavanich and A. Seiler, “Reliability of on-load tap changers with special consideration of experience with delta connected transformer windings and tropical environmental conditions,” *Cigré, paper*, pp. 12–103, 1996.
- [163] J. Carpentier, “Contribution to the economic dispatch problem,” *Bulletin de la Société Française des Electriciens*, vol. 3, no. 8, pp. 431–447, 1962.
- [164] B. C. Lesieutre, I. Hiskens *et al.*, “Convexity of the set of feasible injections and revenue adequacy in FTR markets,” *IEEE Trans. on Power Systems*, vol. 20, no. 4, pp. 1790–1798.
- [165] I. A. Hiskens and R. J. Davy, “Exploring the power flow solution space boundary,” *IEEE Trans. on Power Systems*, vol. 16, no. 3, pp. 389–395, 2001.
- [166] Y. Makarov, Z.-Y. Dong, and D. Hill, “On convexity of power flow feasibility boundary,” *IEEE Trans. on Power Systems*, vol. 23, no. 2, pp. 811–813, May 2008.
- [167] A. G. Bakirtzis and P. N. Biskas, “A decentralized solution to the DC-OPF of interconnected power systems,” *IEEE Trans. on Power Systems*, vol. 18, no. 3, pp. 1007–1013, 2003.
- [168] B. Lesieutre, D. Molzahn, A. Borden, and C. Demarco, “Examining the limits of the application of semidefinite programming to power flow problems,” in *2011 49th Annual Allerton Conference on Communication, Control, and Computing (Allerton)*, Sept 2011, pp. 1492–1499.
- [169] D. P. Bertsekas, *Nonlinear Programming*, 2nd ed. Athena Scientific, Sep. 1999.
- [170] M. J. Powell, “Algorithms for nonlinear constraints that use lagrangian functions,” *Mathematical programming*, vol. 14, no. 1, pp. 224–248, 1978.
- [171] M. R. Hestenes, “Multiplier and gradient methods,” *Journal of optimization theory and applications*, vol. 4, no. 5, pp. 303–320, 1969.
- [172] A. X. Sun, D. T. Phan, and S. Ghosh, “Fully decentralized AC optimal power flow algorithms,” in *Power and Energy Society General Meeting (PES)*. IEEE, 2013, pp. 1–5.
- [173] T. Erseghe, “Distributed optimal power flow using ADMM,” *IEEE Trans. on Power Systems*, vol. 29, no. 5, pp. 2370–2380, Sept 2014.

- [174] D. P. Palomar and M. Chiang, "A tutorial on decomposition methods for network utility maximization," *IEEE Journal on Selected Areas in Communications*, vol. 24, no. 8, pp. 1439–1451, 2006.
- [175] J. A. Momoh, M. El-Hawary, and R. Adapa, "A review of selected optimal power flow literature to 1993. part I: Nonlinear and quadratic programming approaches," *IEEE Trans. on Power Systems*, vol. 14, no. 1, pp. 96–104, 1999.
- [176] —, "A review of selected optimal power flow literature to 1993. part II: Newton, linear programming and interior point methods," *IEEE Trans. on Power Systems*, vol. 14, no. 1, pp. 105–111, 1999.
- [177] Z. Qiu, G. Deconinck, and R. Belmans, "A literature survey of optimal power flow problems in the electricity market context," in *Power Systems Conference and Exposition, PSCE. IEEE/PES*. IEEE, 2009, pp. 1–6.
- [178] D. Sun, B. Ashley, B. Brewer, A. Hughes, and W. F. Tinney, "Optimal power flow by newton approach," *IEEE Trans. on Power Apparatus and Systems*, vol. PAS-103, no. 10, pp. 2864–2880, Oct 1984.
- [179] D. Gayme and U. Topcu, "Optimal power flow with large-scale storage integration," *IEEE Trans. on Power Systems*, vol. 28, no. 2, pp. 709–717, May 2013.
- [180] M. Adibi, R. Polyak, I. Griva, L. Mili, and S. Ammari, "Optimal transformer tap selection using modified barrier-augmented lagrangian method," *IEEE Trans. on Power Systems*, vol. 18, no. 1, pp. 251–257, Feb 2003.
- [181] C. Lehmkoetter, "Security constrained optimal power flow for an economical operation of FACTS-devices in liberalized energy markets," *IEEE Trans. on Power Delivery*, vol. 17, no. 2, pp. 603–608, Apr 2002.
- [182] B. Hayes, I. Hernando-Gil, A. Collin, G. Harrison, and S. Djokić, "Optimal power flow for maximizing network benefits from demand-side management," *IEEE Trans. on Power Systems*, vol. 29, no. 4, pp. 1739–1747, July 2014.
- [183] R. Jabr, "Optimal power flow using an extended conic quadratic formulation," *IEEE Trans. on Power Systems*, vol. 23, no. 3, pp. 1000–1008, Aug 2008.
- [184] A. J. Conejo and J. A. Aguado, "Multi-area coordinated decentralized DC optimal power flow," *IEEE Trans. on Power Systems*, vol. 13, no. 4, pp. 1272–1278, 1998.
- [185] P. N. Biskas, A. G. Bakirtzis, N. I. Macheras, and N. K. Pasialis, "A decentralized implementation of DC optimal power flow on a network of computers," *IEEE Trans. on Power Systems*, vol. 20, no. 1, pp. 25–33, 2005.
- [186] O. Alsac, J. Bright, M. Prais, and B. Stott, "Further developments in LP-based optimal power flow," *IEEE Trans. on Power Systems*, vol. 5, no. 3, pp. 697–711, 1990.

Bibliography

- [187] B. Stott and O. Alsac, "Fast decoupled load flow," *IEEE Trans. on Power Apparatus and Systems*, no. 3, pp. 859–869, 1974.
- [188] P. Sulc, S. Backhaus, and M. Chertkov, "Optimal distributed control of reactive power via the alternating direction method of multipliers," *IEEE Trans. on Energy Conversion*, vol. 29, no. 4, pp. 968–977, Dec 2014.
- [189] M. Baran and F. Wu, "Optimal sizing of capacitors placed on a radial distribution system," *IEEE Trans. on Power Delivery*, vol. 4, no. 1, pp. 735–743, Jan 1989.
- [190] S. Bose, D. F. Gayme, K. M. Chandy, and S. H. Low, "Quadratically constrained quadratic programs on acyclic graphs with application to power flow," *arXiv preprint arXiv:1203.5599*, 2012.
- [191] L. Gan and S. Low, "Convexification of AC optimal power flow," *PSCC*, Aug 2014.
- [192] R. A. Jabr, "Radial distribution load flow using conic programming," *IEEE Trans. on Power Systems*, vol. 21, no. 3, pp. 1458–1459, 2006.
- [193] J. Lavaei and S. Low, "Zero duality gap in optimal power flow problem," *IEEE Trans. on Power Systems*, vol. 27, no. 1, pp. 92–107, Feb 2012.
- [194] E. Dall'Anese, H. Zhu, and G. B. Giannakis, "Distributed optimal power flow for smart microgrids," *IEEE Trans. on Smart Grid*, vol. 4, no. 3, pp. 1464–1475, 2013.
- [195] B. Zhang, A. Lam, A. Dominguez-Garcia, and D. Tse, "An optimal and distributed method for voltage regulation in power distribution systems," *IEEE Trans. on Power Systems*, vol. PP, no. 99, pp. 1–13, 2014.
- [196] M. Farivar, C. R. Clarke, S. H. Low, and K. M. Chandy, "Inverter VAR control for distribution systems with renewables," in *International Conference on Smart Grid Communications (SmartGridComm)*. IEEE, 2011, pp. 457–462.
- [197] B. Stott, J. Jardim, and O. Alsac, "DC power flow revisited," *IEEE Trans. on Power Systems*, vol. 24, no. 3, pp. 1290–1300, 2009.
- [198] W. Bukhsh, A. Grothey, K. McKinnon, and P. Trodden, "Local solutions of the optimal power flow problem," *IEEE Trans. on Power Systems*, vol. 28, no. 4, pp. 4780–4788, Nov 2013.
- [199] M. Farivar and S. H. Low, "Branch flow model: Relaxations and convexification." in *CDC*, 2012, pp. 3672–3679.
- [200] N. Li, L. Chen, and S. H. Low, "Exact convex relaxation of OPF for radial networks using branch flow model." in *SmartGridComm*. Citeseer, 2012, pp. 7–12.
- [201] L. Gan, N. Li, U. Topcu, and S. Low, "Branch flow model for radial networks: convex relaxation," in *Proceedings of the 51st IEEE Conference on Decision and Control*, 2012.

-
- [202] S. Bolognani, R. Carli, G. Cavraro, and S. Zampieri, "A distributed control strategy for optimal reactive power flow with power constraints," in *52nd Annual Conference on Decision and Control (CDC)*. IEEE, 2013, pp. 4644–4649.
- [203] —, "A distributed control strategy for optimal reactive power flow with power and voltage constraints," in *IEEE International Conference on Smart Grid Communications (SmartGridComm)*, Oct 2013, pp. 115–120.
- [204] M. Kraning, E. Chu, J. Lavaei, and S. Boyd, "Dynamic network energy management via proximal message passing," *Foundations and Trends in Optimization*, vol. 1, no. 2, pp. 70–122, 2013.
- [205] Q. Peng and S. H. Low, "Distributed algorithm for optimal power flow on a radial network," *arXiv preprint arXiv:1404.0700*, 2014.
- [206] R. Cespedes, "New method for the analysis of distribution networks," *IEEE Trans. on Power Delivery*, vol. 5, no. 1, pp. 391–396, Jan 1990.
- [207] H.-D. Chiang and M. Baran, "On the existence and uniqueness of load flow solution for radial distribution power networks," *IEEE Trans. on Circuits and Systems*, vol. 37, no. 3, pp. 410–416, Mar 1990.
- [208] Nexans, "Câbles de réseau basse tension et câbles moyenne tension," *Catalogue*, available online.
- [209] S. Boyd, N. Parikh, E. Chu, B. Peleato, and J. Eckstein, "Distributed optimization and statistical learning via the alternating direction method of multipliers," *Foundations and Trends® in Machine Learning*, vol. 3, no. 1, pp. 1–122, 2011.
- [210] W. D. Stevenson and J. J. Grainger, "Power system analysis," *New York: McGraw-Hill International Editions*, pp. 141–190, 1994.
- [211] D. Bertsekas, *Constrained Optimization and Lagrange Multiplier Methods*, ser. Athena scientific series in optimization and neural computation. Athena Scientific, 1996. [Online]. Available: <http://books.google.ch/books?id=-UQZAQAIAAJ>
- [212] A. Geoffrion, "Generalized benders decomposition," *Journal of Optimization Theory and Applications*, vol. 10, no. 4, pp. 237–260, 1972. [Online]. Available: <http://dx.doi.org/10.1007/BF00934810>

École Polytechnique Fédérale de Lausanne (EPFL)
 Laboratory for Computer Communications and Applications (LCA2)
 BC 204, Station 14, CH-1015 Lausanne, Switzerland
 Tel: +41 21 69 35610, +41 78 90 93 407
 Email: konstantina.christakou@epfl.ch
 Website: <http://people.epfl.ch/konstantina.christakou>

- EDUCATION**
- EPFL - École Polytechnique Fédérale de Lausanne, Switzerland** 2011 Sep - present
 PhD. Candidate, Computer Communications and Applications Laboratory 2,
 Distributed Electrical Systems Laboratory
 Thesis title: “*Real-Time Optimal Controls for Active Distribution Networks: From Concepts to Applications*”
 Advisors: Prof. J.-Y. Le Boudec, Prof. M. Paolone
- NTUA - National Technical University of Athens, Greece** 2004 Sep - 2010 Jun
 Diploma of Engineering, Electrical and Computer Engineering **(9.22/10.00)**
Major: Telecommunications and Networking *Top 3 % of my class*
Minor: Electronics and Circuits, Operation Management
 Thesis title: “*Design of a Routing Algorithm Based on a Markovian Decision Process for Wireless Mesh Networks that Operate under Fading Conditions*”
 Advisor: Prof. P. G. Cottis
- RESEARCH AREAS**
- Real-time control of active distribution networks
 - Grid ancillary services in active distribution networks (voltage control, lines congestion management)
 - Demand-side management and storage applications for active distribution networks
 - Design of distributed control algorithms for power systems
- PUBLICATIONS**
- K. Christakou, M. Pignati, R. Rudnik, S. Sarri, J.-Y. Le Boudec and M. Paolone, “*Hardware-in-the-loop Validation of the Grid Explicit Congestion Notification Mechanism for Primary Voltage Control in Active Distribution Networks*”, submitted to the 19th Power Systems Computation Conference (PSCC 2016) (under review)
 - C. Mugnier, K. Christakou, J. Jaton, M. De Vivo, M. Carpita and M. Paolone, “*Model-less/Measurement-based Computation of Voltage Sensitivities in Unbalanced Electrical Distribution Networks*”, submitted to the 19th Power Systems Computation Conference (PSCC 2016) (under review)
 - K. Christakou, M. Paolone and A. Abur, “*Voltage Control in Active Distribution Networks Under Uncertainty in the System Model: A Robust Optimization Approach*”, submitted to IEEE Transactions on Power Systems, 2015 (under review)
 - K. Christakou, “*A Unified Control Strategy for Active Distribution Networks via Demand Response and Distributed Energy Storage Systems*”, submitted to Sustainable Energy, Grids and Networks Journal, Elsevier, 2015 (under review)
 - K. Christakou, D.-C. Tomozei, J.-Y. Le Boudec, M. Paolone, “*AC OPF in Radial Distribution Networks-Parts I, II*”, arXiv preprint arXiv:1503.06809, August 2015, (under review)

- K. Christakou, D.-C. Tomozei, M. Bahramipanah, J.-Y. Le Boudec, M. Paolone, “*Primary Voltage Control in Active Distribution Networks via Broadcast Signals: The Case of Distributed Storage*”, IEEE Transactions on Smart Grid, August 2014
- G. De Carne, M. Liserre, K. Christakou, M. Paolone, “*Voltage Control and Current Congestion Management in Distribution Grids by means of Smart Transformers*, IEEE International Symposium on Industrial Electronics, pp.2613-2619, 1-4 June 2014
- K. Christakou, D.-C. Tomozei, J.-Y. Le Boudec, M. Paolone, “*GEEN: Primary Voltage Control for Active Distribution Networks via Real-Time Demand-Response*”, IEEE Transactions on Smart Grid, vol.5, no.2, pp.622-631, March 2014
- K. Christakou, J.-Y. Le Boudec, M. Paolone, D.-C. Tomozei, “*Efficient Computation of Sensitivity Coefficients of Node Voltages and Line Currents in Unbalanced Radial Electrical Distribution Networks*”, IEEE Transactions on Smart Grid, vol.4, no.2, pp.741-750, June 2013

INVITED TALKS

- “*Model-less Optimal Voltage Control of Unbalanced Distribution Networks*”, SCCER-FURIES Annual Conference November 25th, 2015 (co-presentation with Prof. Mauro Carpita, HES-SO)
- “*Voltage and Power Flows Control in Active Distribution Networks*”, Center for Ultra-Wide-Area Resilient Electric Energy Transmission Networks (CURENT), SLC web-seminar for Northeastern University, October, 2014
- “*GEEN: Voltage Control in Active Distribution Networks via Real-Time Demand Response and Distributed Storage Control*”, University of Kiel - Christian-Albrechts-Universität zu Kiel (CAU), May 2014
- “*GEEN: Voltage Control in Active Distribution Networks via Real-Time Demand Response and Distributed Storage Control*”, Electricité de France S.A. (EDF), January 2014

HONORS & AWARDS

- *Best Poster Award*, Nano-Tera Annual Plenary Meeting, May, 2014
- *Fellowship*, EPFL, 2011-2012
- *Scholarship*, Greek State Scholarship Foundation, for being admitted 9th to the ECE department of the National Technical University of Athens, 2004
- *Scholarship*, Eurobank EFG and Greek Ministry of National Education and Religious Affairs, for achieving the highest GPA in the national exams in Piraeus, Greece, 2004-2005
- *Prize* (trip to Rome, Italy), Greek Ministry of National Education and Religious Affairs, for achieving the highest GPA in the national exams in Piraeus, Greece, 2002-2003

RESEARCH ACTIVITIES

- **Visiting scholar**, Prof. Ali Abur’s Power Systems Group, College of Electrical Engineering, Northeastern University, August 2014-December 2015
 - Voltage control in Active Distribution Networks under uncertainty: A robust optimization approach
- Development of a computationally efficient method for the analytical derivation of voltages and currents sensitivity coefficients as a function of the nodal power injections and transformers on-load tap changers’ position
- Design of a low-overhead decentralized demand-response control mechanism based on broadcast signals for the primary voltage control of active distribution networks

- Design of smart local controllers for thermostatically controlled loads and electrochemical-based storage systems for the interpretation of the broadcast signals and the participation to voltage control of active distribution networks
- Development of centralized and fully decentralized OPF algorithms for fair scheduling of distributed generation units
- **Supervised projects:**
 - Primary voltage control for active distribution networks via real-time demand-response: A hardware-in-the-loop test platform for the GECN, 2015, Internship Project, Roman Rudnik, (EPFL LCA2 internship student)
 - Applications of robust optimization to voltage control in power systems, 2015, spring semester project, Vidak Kazic, (EPFL master student)
 - Model development and real time simulation of GECN enabled loads: The case of thermostatically controlled loads, 2015, spring semester project, Lydie Magnone, (EPFL master student)
 - Implementation of a test-bed for the deployment of the GECN voltage control mechanism on a microgrid, 2014, spring semester project, François Chareyron, (EPFL bachelor student)
 - Voltage control and lines congestion management via real-time storage control in distribution networks with increased wind penetration, 2013, master thesis, Giovanni De Carne, (now PhD. in Kiel Germany)
- **Collaborations:**
 - “SMILE: The theoretical and application Study on a Metering and Intelligent tool for Low Voltage grid control Enhancement”, 2014 January - 2016 July
Project partners: EPFL Distributed Electrical Systems laboratory, DEPSYS Power Electronic Systems, IESE Institute for Energy and Electrical Systems of the HEIG-VD, Romande Energie
 - “Station de transfert d’énergie par pompage et turbinage à Arbaz: étude de l’installation, de l’intégration et de la gestion optimale du réseau”, 2013 February - 2014 May
Project partners: EPFL Distributed Electrical Systems laboratory, EPFL Hydraulic Machines laboratory, HES SO Valais, Centre de Recherches Energétiques et Municipales, CIMARK

TEACHING EXPERIENCE

- *Performance Evaluation of Computer and Communication Systems*, Graduate class, EPFL, 2015
- *Smart Grid Technologies*, Graduate class, EPFL, 2014 and 2015
- *Information Theory*, Undergraduate class, EPFL, 2014
- *TCP/IP Networking*, Graduate class, EPFL, 2012 and 2013

PEER REVIEWS

- *Reviewer*, IET Generation, Transmission and Distribution, since 2015
- *Reviewer*, IEEE Transactions on Smart Grid, since 2015
- *Reviewer*, IEEE Transactions on Industrial Informatics, since 2014
- *Reviewer*, IEEE Journal of Photovoltaics, since 2014
- *Reviewer*, IEEE Transactions on Power Systems, since 2013
- *Reviewer*, Elsevier Sustainable Energy, Grids and Networks Journal, since 2014

- *Reviewer*, Elsevier International Journal of Electrical Power and Energy Systems, since 2013
- *External reviewer*, 18th Power Systems Computation Conference (PSCC), 2014
- *External reviewer*, 5th International Conference on Future Energy Systems (ACM e-Energy), 2014
- *External reviewer*, 3rd IEEE International Conference on Smart Grid Communications (Smart-GridComm), 2012

IT SKILLS

Programming & Software : Matlab, EMTP-RV, GAMS, Simulink, Microsoft Visio, GNS3, PHP, Java, Python
Operating systems: Microsoft Windows, Linux

(Presented in descending order of expertise-current familiarity)

LANGUAGE SKILLS

Greek: Native
English: Fluent (CPE)
French: Fluent (Sorbonne II)
German: Intermediate (B1)

WORK EXPERIENCE

Greek Ministry of Economy, Competitiveness and Shipping 2010 Sep - 2011 May
“Operational Program: Digital Convergence”: Evaluation and funding of projects related to the information and telecommunications sector of Greece. Collaborated with a team of 5 people and supervised the shifts of the team.

Teaching Assistant for high school students 2005 Sep - 2007 Jun
 Organized Math, Physics and Chemistry tutoring lessons, for the preparation of senior students for the national exams.

ACTIVITIES & INTERESTS

- IEEE Power and Energy Society
- IEEE Society of Women in Engineering
- Board of European Students of Technology, 2008
- Volunteer in Athens Marathon, 2004-2006
- Books, theater, foreign languages, road-trips and travelling, pilates